



RETRIEVING FOREST CHARACTERISTICS
FROM HIGH-RESOLUTION AIRBORNE
S-BAND RADAR DATA

Thesis submitted for the degree of
Doctor of Philosophy
at the University of Leicester

by

Ramesh Kumar Ningthoujam MSc
Department of Geography
University of Leicester

2016

RETRIEVING FOREST CHARACTERISTICS FROM HIGH-RESOLUTION AIRBORNE S-BAND RADAR DATA

Ramesh Kumar Ningthoujam

Abstract

Synthetic Aperture Radar (SAR) data are utilized for improved mapping of forest cover and biophysical retrieval due to its sensitivity to forest canopy and structure. It is important to study the forest structure and biophysical parameters because it constitutes the major forest aboveground biomass (AGB). The S-band SAR frequency has not been consistently investigated for forest monitoring due to the lack of long-term data. Using the recent AirSAR campaign (2010-2014) over Savernake Forest and Wytham Woods in southern England, this thesis presents methods for analysing S-band SAR data for soil and forest canopies using the radiative transfer Michigan Microwave Canopy Scattering (MIMICS-I) model. The first result chapter shows that dominant scattering behaviour of S-band frequency arises from ground/trunk interactions with little direct crown scattering across all polarisations and incidence angles. The S-band backscatter shows significant sensitivity to both soil moisture content and surface roughness. Simulation experiments related to forest degradation show low co-polarisation backscatter due to reduced canopy component and tree density at S-band. Using the above information, the second result chapter shows that S-band HH- and VV-backscatter and Radar Forest Degradation Index (RFDI) data produces forest/non-forest classification map at 6 m resolution with 70% overall accuracy (kappa coefficient, $\kappa = 0.41$) while 63% overall accuracy (kappa coefficient, $\kappa = 0.27$) for the 20 m resolution map in a Maximum Likelihood algorithm. S-band data is also useful for mapping various non-forest cover types and monitoring forest cover changes over time due to the loss of volume scattering when forest canopies are removed. Using the field measured forest biomass, the third result chapter reveals that S-band radar backscatter correlates well with forest AGB. A consistent S-band backscatter/ biomass relationship is found, suggesting increasing backscatter sensitivity to forest AGB up to 100 t/ha with least error varying 90.46 - 98.65 t/ha at 25 m resolution (stand level) in low to medium incidence angles. The implications of these results are that S-band SAR data like the longer L-band SAR is highly suitable for mapping forest cover and monitoring cover changes and be able to retrieve low biomass stands below 100 t/ha.

Declaration of Authorship

This thesis is presented in accordance with the regulations for the degree of Doctor of Philosophy.

This thesis has not been previously submitted nor accepted for any degree at the University of Leicester and any other university. To the best of my knowledge, the work presented in the thesis holds entirely my own and with appropriate acknowledgement in the form of references and other sources.

This thesis is also a reflection of few papers presented in international academic conferences before the submission, which are listed below.

Conference Proceedings

- **Ningthoujam, R.K.**, Balzter, H., Tansey, K., 2015. Airborne SAR Campaign 2014 in Savernake forest, UK. SAR Workshop & RSPSoc Research Conversazione, Durham University, Durham, 20th March 2015, Oral presentation.
- **Ningthoujam, R.K.**, Rodríguez-Veiga, P., Spies, B., Brown, S., Lamb, A., Tansey, K., Balzter, H., 2013. A concept for monitoring forest with high-resolution S-band SAR, a case study of Savernake Forest, UK. DMC & NovaSAR International Conference Council Chamber, The IET: Savoy Place, London, 6-7th March 2013, Oral presentation.

In review for peer-reviewed publications

- **Ningthoujam, R.K.**, Tansey, K., Balzter, H., Morrison, K., Johnson, S.C.M., Gerard, F., George, C., Burbidge, G., Doody, S., Veck, N., Llewellyn, G.M. and Blythe, T., Mapping forest cover and forest cover change with airborne S-band radar.
- **Ningthoujam, R.K.**, Balzter, H., Tansey, K., Morrison, K., Johnson, S.C.M., Gerard, F., George, C., Malhi, Y., Burbidge, G., Doody, S., Veck, N., Llewellyn, G.M., Blythe, T., Rodriguez- Veiga, P., Van Beijma, S., Spies, B., Barnes, C., Padilla, M., Wheeler, J., Louis, V., Potter, T., Smith, A.E. and Polo Bermejo, J., Retrieval of forest biophysical variables in temperate mixed forest with airborne S-band radar.

Signed:

Date:

Acknowledgements

A number of individuals and organisations have supported and contributed me towards producing this thesis, for which I wish to express my gratitude whole-heartedly.

Through many critical discussions and support from my supervisors, has enabled me to write this thesis which I hope is a useful contribution to the microwave remote sensing in particular to the least explored S-band SAR backscatter interactions with vegetation.

Firstly, I would like to express my sincere and unreserved gratitude towards my primary supervisor Professor Heiko Balzter for his valuable and helpful discussions on radar remote sensing. Secondly, I am also extremely grateful to Professor Kevin Tansey for his expertise and critical advice on backscatter interaction with vegetation target.

Theoretical knowledge of radar backscatter interaction with forest canopy is equally important where Michigan Microwave Canopy Scattering model (MIMICS) plays an important component of this thesis and thanks to Professor Kevin for his constant encouragement and invaluable support to MIMICS simulations. MIMICS simulation was performed using FORTRAN compiler on ALICE High Performance Computing Facility at the University of Leicester.

My examiners Professor Iain Hector Woodhouse (School of Geoscience, University of Edinburgh) and Dr Juan Carlos (Geography, University of Leicester) do reserved a special place in this thesis whose comments/ feedbacks really improved the final thesis. A warm thanks to Professor Leland Pierce from the Radiation Lab, The University of Michigan (United States of America) for providing the code and tips on MIMICS-I.

The second part of this thesis relates to the airborne S-band SAR data acquired during two AirSAR Campaigns-2010 and 2014 (jointly collaboration with Airbus, NERC ARSF and Satellite Applications Catapult) over Savernake and Wytham Woods within Project Code: AS 14/24. These valuable datasets provides the necessary data for analysing the MIMICS-I predictions in context to S-band derived forest cover mapping and biophysical retrieval. My humble gratitude to the Airbus Defence and Space, UK for providing these airborne datasets, in particular Geoff Burbridge and Sam Doody (Airbus), Dr. Sarah Johnson (presently at University of Leicester), Dr. Gary Llewellyn

(NERC ARSF) and Professor Nick Veck (Satellite Applications Catapult) for their support on SAR data processing and technical knowledge throughout the pre- and post-campaigns.

A better understanding of forest canopy interaction with S-band backscatter depends on the improved modelling as future airborne and satellite data can complement but not substitute field data. The valuable field data supported by Forestry Commission (FC), Savernake and Bristol (Marlborough) and Environmental Change Network (ECN), Centre for Ecology and Hydrology provides opportunity to parametrise MIMICS-I model and verification of forest/non-forest cover maps. In person, Thomas Blythe and Lorna Sherrin are highly appreciated for their invaluable support in sharing FC GIS and ECN plot database.

My special appreciation goes to the big team of 10 researchers (Heiko Balzter, Pedro Rodriguez- Veiga, Bernard Spies, James Wheeler, Valentin Louis, Marc Padilla-Parellada, Thomas Potter and Chloe Barnes) at the Centre for Landscape and Climate Research (CLCR) and Alexander Edwards-Smith and Jaime Polo Bermejo (Cranfield University) for their support in the tree measurements during field trip to Savernake in summer 2012 and 2015. Colleagues at the CLCR, University of Leicester serves to be an important asset to this research. Thanks to Dr Virginia Nicolás-Perea (CLCR Research Development Manager) for providing facilities to undertake this research.

Our parents and family members have been a constant source of support and encouragement, for which I would like to express my deepest sense of gratitude to Noren Ningthoujam, Ibemhal O. Ningthoujam, Priyokumar Khumanthem, Manihanbi O. Khumanthem, Bagin Oinam, Ranita O. Oinam (with Ryan and Bebecha Oinam) and late Roni Ningthoujam and late TampakLeima O. Naorem for their blessings from the Far-East across Europe. Finally, I would like to appreciate my wife Anandini Khumanthem for her constant support and a source of strength in my research during these three years of amazing journey. Since 31 August 2013, our little Ms. Gianna Ningthoujam has always been a constant source of joy and happiness especially during dead-locks in research and during the final phase of thesis submission.

Lastly, THANK YOU ALL for making this journey a success.

Table of contents

	Page
Abstract	i
Declaration of Authorship	ii
Acknowledgements	iii
Table of contents	v
List of Figures	ix
List of Tables	xv
Glossary and Abbreviations	xvii
1. Introduction	1
1.1. Global carbon cycle	1
1.2. Forest cover	2
1.3. Forest degradation	6
1.4. Forest aboveground biomass	7
1.5. Aims and Overview of Thesis	9
2. Review of the literature	11
2.1. Microwave remote sensing	11
2.1.1. RADAR	11
2.1.2. The Radar Equation	12
2.1.3. Synthetic Aperture Radar	13
2.1.4. Speckle	13
2.1.5. Radiometric SAR Calibration	14
2.2. SAR scattering in forest	14
2.3. NovaSAR-S Mission	16
2.4. Microwave Canopy Scattering Modelling	18
2.4.1. Water Cloud Model	22
2.4.2. Santa Barbara Canopy Backscatter Model	22
2.4.3. Michigan Microwave Canopy Scattering Model	23
2.4.4. Multi-MIMICS Model	24
2.4.5. Massachusetts Institute of Technology (MIT) Model	25
2.4.6. Karam Model	25
2.4.7. Cylinder Model	26

2.4.8. A 3-Dimensional Model	27
2.5. Mapping of forest/ non-forest cover	27
2.6. Identification of forest degradation, clear-cut and forest fire	34
2.7. Retrieval of forest structure and aboveground biomass	39
2.8. Current knowledge gaps and research needs	50
2.9. Research Questions	50
2.10. Research Objectives	51
2.11. Summary	51
3. Materials and methods	53
3.1. Test sites	53
3.1.1. Savernake forest	53
3.1.2. Wytham Woods	54
3.2. SAR Data	56
3.2.1. Airborne SAR Campaigns	56
3.2.2. The UK AirSAR Campaign	57
3.2.3. SAR data processing	58
3.2.3.1. Single Look Complex data	58
3.2.3.2. Multi-looking	58
3.2.3.3. Speckle filtering	59
3.2.3.4. Geometric correction	60
3.2.3.5. Backscatter sigma-nought (σ_0) derivation	61
3.3. Field data	63
3.3.1. Forestry Commission GIS	63
3.3.2. Sample plot data for Savernake Forest and Wytham Woods	64
3.4. Methodology	65
3.4.1. MIMICS-I simulation	66
3.4.2. Airborne S-band derived forest/non-forest and change detection maps	73
3.4.2.1. SAR data interpretation, land cover legend and classification	74
3.4.2.2. Spatial resolution simulation and change detection	79

3.4.3. S-band derived forest biophysical retrieval	81
3.5. Summary	84
4. Soil and forest backscattering with S-band SAR using MIMICS-I simulation	85
4.1. Introduction	85
4.2. Methods	86
4.3. Results and discussion	87
4.3.1. Ground scattering as a function of soil moisture and surface roughness	87
4.3.2. Deciduous crown layer with leaves and branches	89
4.3.3. Coniferous crown layer with needles and branches	103
4.3.4. S-band backscatter responses from soil against forest canopy	108
4.3.5. Reduced canopy components	109
4.3.6. Reduced tree density	112
4.4. Summary	114
5. Forest/ non-forest and change mapping using airborne S-band SAR backscatter	116
5.1. Introduction	116
5.2. Methods	117
5.3. Results and discussion	120
5.3.1. Mapping F/NF	120
5.3.2. Detailed land cover classification	121
5.3.3. Accuracy assessment	123
5.3.4. Forest cover change analysis	128
5.4. Summary	131
6. Airborne S-band SAR backscatter relationships to forest biophysical characteristics	133
6.1. Introduction	133
6.2. Methods	135
6.3. Results and discussion	135

6.3.1. Field data	135
6.3.2. S-band backscatter sensitivity to forest structure	139
6.3.3. S-band backscatter sensitivity to forest aboveground biomass	143
6.3.4. Estimation of forest aboveground biomass using S-band backscatter	145
6.3.5. Accuracy of S-band backscatter-biomass regression	147
6.3.6. Uncertainty analysis	148
6.4. Summary	153
7. Synthesis and Conclusions	154
7.1. Introduction	154
7.2. S-band backscatter from soil and forest canopy using MIMICS-I model	155
7.3. Forest degradation using MIMICS-I model	156
7.4. Mapping forest/non-forest and change using S-band and Maximum Likelihood Classification	158
7.5. Sensitivity of S-band backscatter to forest biophysical characteristics	160
7.6. Airborne demonstrator to space-borne NovaSAR perspectives	162
7.7. Limitations	165
7.8. Future work and recommendations	166
Appendices	168
Bibliography	189

List of Figures

		Page
Figure 1.1.	The graph shows recent monthly mean CO ₂ measured at Mauna Loa Observatory, Hawaii. The dashed red line represents the monthly mean values, centered on the middle of each month while black line represents the same, after correction for the average of 7 adjacent seasonal cycles.	1
Figure 1.2.	Percent tree cover map for the year 2000 in the southern England region from 30 m spatial Landsat data (Savernake forest: red polygon) (Insert: UK map with Granule: 60°N, 10°W frame) (Source: Global Forest Change 2000-2014 (Hansen et al. 2014)).	4
Figure 1.3.	Forest/ non-forest map for year 2010 in the southern England region from PALSAR mosaics at 25 m resolution (Savernake forest: red polygon) (Insert: UK map with Grid 15: N21°W0002° frame) (Source: PALSAR Global Forest / Non-forest Map "2010"(JapanAerospaceExplorationAgency 2014))	5
Figure 2.1.	Overview of MIMICS model structure with different interaction components (DG-direct ground, DC-direct crown, C-G-crown-ground, G-C-G- ground-crown-ground, GC-ground crown, G-T or T-G-ground-trunk) (Ulaby et al. 1990).	21
Figure 3.1.	6 m pixel spacing S-band data acquired over Savernake (top) and Wytham (bottom) in 2014 (False colour composite: red: HH, green: VV, blue: RFDI) with sampled compartments (cyan polygon), training plots (red dot in both Savernake and Wytham) and validation plots (white with black dot) (Savernake).	55
Figure 3.2.	Comparison of different adaptive filters at different kernels (2014 acquired HH-polarisation in Savernake forest)	60
Figure 3.3.	Calibration target location and orientation at Baginton (Coventry airport) in 2010 (top) and Twin Otter overflying calibration corner reflector near Staverton airfield in 2014 (below) (Source: Airbus (2013b)).	62

Figure 3.4.	Forest types (A) and stand age (B) in Savernake forest (Source: Forestry Commission sub-compartment GIS database supported by Thomas Blythe).	63
Figure 3.5.	Example of a circular plot (top) with plot selection- at least 100 m distance from pathway (middle) and tree measurements (bottom) in Savernake Forest during March 2015.	64
Figure 3.6.	Methodology flowchart for MIMICS-I modelling.	66
Figure 3.7.	Tree architectural characteristics of deciduous (without leaves) (A) and coniferous species (with needles) (B).	70
Figure 3.8.	Methodology flowchart for mapping forest/ non-forest and change detection. *MLC: maximum likelihood classification, RFDI: Radar Forest Degradation Index, FC- sub/ - anc: Forestry Commission sub-compartment/ ancient database.	74
Figure 3.9.	S-band cross-calibration for forest (2640 ancient tree points) class between re-scaled 2010 and 2014 SAR imageries.	76
Figure 3.10.	Field photos for forest (A) and non-forest (B-clear-felled, C-bare-ground and D-grassland) in Savernake site.	77
Figure 3.11.	Aerial photo (top) and 6 m S-band data acquired in 2010 (middle) and 2014 (bottom) over Savernake forest as HH, VV backscatter and RFDI data in red, green and blue channel (Source: Airbus 2013a).	80
Figure 3.12.	Methodology flowchart for forest biophysical retrieval * DBH: tree diameter at breast height, H: canopy height and σ_0 : backscatter sigma-nought.	82
Figure 4.1.	S-band ground backscatter vs. soil volumetric moisture (m^3 water/ m^3 soil) (top) and soil RMS height (cm) (bottom) for co-polarisation at 15° , 30° and 45° radar range.	88
Figure 4.2.	HH (a) and VV (b) polarisations crown transmissivity vs. scattering angle from 830 leaves per cubic meter and 4.1 branches per cubic meter, crown transmissivity vs. density of leaves at 30° scattering angle (c) and crown transmissivity vs. frequency for Birch for L-, S-, C- and X-bands (d).	90

Figure 4.3.	Total co- and cross-polarisations canopy backscatter vs. scattering angle from 830 leaves and 4.1 branch density Birch for L-, S-, C- and X-band.	92
Figure 4.4.	Total co- and cross-polarisations canopy backscatter vs. scattering angle from 4.1 branch density Birch at different branch levels for L-, S-, C- and X-band.	93
Figure 4.5.	S-band backscatter vs. canopy parts at 0.5 volumetric moisture (m^3 water/ m^3 canopy) across incidence angles (top) and at varying volumetric moisture (m^3 water/ m^3 canopy) at 30° radar range (bottom) where T- and B- represents trunk and branches respectively.	95
Figure 4.6.	Total co-and cross-polarisations canopy backscatter components vs. scattering angle from 830 leaves and 4.1 branch density Birch at primary branch level for L-, S-, C- and X-band.	96
Figure 4.7.	Total co-and cross-polarisations canopy backscatter components vs. scattering angle from 830 leaves and 4.1 branch density Birch at fourth branch levels for P-, L-, S-, C- and X-band.	99
Figure 4.8.	Total canopy backscatter vs. SAR wavelengths from 4.1 branches per cubic meter, primary branch diameter (1 cm, 3 cm, 5 cm) (A, C) with 830 leaves per cubic meter (B, D) Birch stand at 30° scattering angle for co- and cross-polarisations.	100
Figure 4.9.	Total co-and cross-polarisations canopy backscatter components vs. canopy stand height (m) from 830 leaves and 4.1 branch density Birch for L-, S-, C- and X-band at 30° incidence angle.	102
Figure 4.10.	Horizontal (a) and Vertical (b) polarisation crown transmissivity vs. scattering angle from 85,000 needles and 3.4 branches per cubic meter Norway spruce, needle density at 30° scattering angle (c) and versus frequency at 30° scattering angle for L-, S-, C- and X-band.	104
Figure 4.11.	Total co-polarisation (top, middle) and cross-polarisation (bottom) canopy backscatter vs. scattering angle from 85,000 needles and 3.4 branch density Norway spruce for L-, S-, C- and X-band.	105

Figure 4.12.	Total co-and cross-polarisations canopy backscatter components vs. scattering angle from needle-branch canopy layer 85,000 needles and 3.4 branch density Norway spruce for L-, S-, C- and X-band.	106
Figure 4.13.	Total canopy backscatter vs. frequency from 85,000 needles and 3.4 branch density per cubic meter at varying branch sizes (1 cm, 3 cm, 5 cm) for co- (A) and cross-polarisations (B) Norway spruce at 30° scattering angle.	108
Figure 4.14.	Simulated forest canopy (deciduous, conifers) and soil total backscatter relationship as a function of radar incidence range at S-band (modelled against SAR data).	109
Figure 4.15.	Simulated backscatter for forest degradation as a function of canopy structure for deciduous stand at 0.012 tree density, 16.18 m canopy height, 38 cm DBH and 342.43 t/ha AGB for L- (A) and S-band (B) for VV- and HV- polarisations (15° -45° incidence angles) where 4 B: fourth branches, SEC B: secondary branches, PRI B: primary branch, L: leaf, T: trunk, SD: smooth dry soil and RW: rough surface wet soil.	111
Figure 4.16.	Simulated backscatter for forest degradation as a function of tree density with varying canopy height, DBH and AGB for L- (A) and S-band (B) (15° -45° incidence angles).	113
Figure 5.1.	Field, FC GIS, ancient tree plot locations for 126 forest and 130 non-forest (training and validation plots) overlaid on 2014 acquired S-band FCC at 6 m (a) and 20 m (b) pixel resolutions for Savernake forest.	118
Figure 5.2.	Box-plots of scattering returns of S-band SAR backscatter in 105 (F- Forest) and 105 (NF- Non-forest) sample plots (a) and different non-forest types with 50 (CF- Cleared-felled), 45 (BG- Bare-ground) and 10 (G- Grassland) sample plots (b). The central box in each box plot shows the inter-quartile range and median; whiskers indicate the 10th and 90th percentiles.	119

Figure 5.3.	F/NF cover map of Savernake using S-band polarimetry and maximum likelihood algorithm at 6 m (a) and 20 m (b) resolutions.	120
Figure 5.4.	Forest and different non-forest cover map of Savernake using S-band polarimetry and maximum likelihood algorithm at 6 m (a) and 20 m (b) resolutions.	122
Figure 5.5.	F/NF cover map of Savernake produced by L-band PALSAR for 2009 (A) and 2010 (B) at 25 m pixel resolution (Source: (JapanAerospaceExplorationAgency 2014)).	127
Figure 5.6.	Change detection map showing areas undergoing changes from forest to non-forest (red) from 2010 to 2014 at 6 m resolution.	129
Figure 5.7.	Percent tree cover (2000) (A) and forest loss (2013-2014) (B) at 30 m Landsat data from Hansen et al. (2014).	130
Figure 6.1.	6 m resolution S-band data over Savernake in 2014 (FCC: red: HH, green: VV, blue: RFDI) with sampled compartments (cyan polygon) and 17 training plots (red dot) in 2012 and 16 validation plots (white with black dot) in 2015.	135
Figure 6.2.	Histogram distribution of the training plots measured AGB below 600 t/ha used to estimate (25 plots) the backscatter-AGB relationship.	136
Figure 6.3.	Biomass values for the field plots against basal area (A), average canopy height (B), Stem number density (C) and average tree diameter (D).	138
Figure 6.4.	Basal area relationship with S-band backscatter (σ_0) at 0.25 ha for 2010 (A) and 2014 (B).	139
Figure 6.5.	Average canopy height relationship with S-band backscatter (σ_0) at 0.25 ha for 2010 (A) and 2014 (B).	140
Figure 6.6.	Stand number density relationship with S-band backscatter (σ_0) at 0.25 ha for 2010 (A) and 2014 (B).	141
Figure 6.7.	Average tree diameter relationship with S-band backscatter (σ_0) at 0.25 ha for 2010 (A) and 2014 (B).	142
Figure 6.8.	Above-ground biomass relationship with S-band backscatter (σ_0) for 2010 (A) and 2014 (B).	144

Figure 6.9.	Predicted AGB maps using S-band HH backscatter at 0.25 ha scale for Savernake forest in 2010 (A) and 2014 (B) using field biomass estimates.	146
Figure 6.10.	Results of biomass estimation using S-band backscatter (σ_0) based on training stands (25 stands-black square) and validation stands (16 stands- red circle) for HH-polarisation at 0.25 ha for 2010 (A) and 2014 (B). Locations of training and validation stands for Savernake are shown in Figure 6.1.	149
Figure 6.11.	Results of biomass estimation using S-band backscatter (σ_0) based on training stands (25 stands-black square) and validation stands (16 stands- red circle) for VV-polarisation at 0.25 ha for 2010 (A) and 2014 (B). Locations of training and validation stands for Savernake are shown in Figure 6.1.	150
Figure 6.12.	Results of biomass estimation using S-band backscatter (σ_0) based on training stands (25 stands-black square) and validation stands (16 stands- red circle) for HV-polarisation at 0.25 ha for 2010 (A) and 2014 (B). Locations of training and validation stands for Savernake are shown in Figure 6.1.	151

List of Tables

	Page
Table 2.1. Different frequencies of space-borne SAR used by radar community (IEEE Standard 521-1984.	12
Table 2.2. NovaSAR-S specification.	17
Table 2.3. Operational modes in NovaSAR-S SAR.	17
Table 3.1. Summary of S-band AirSAR images used in this research.	57
Table 3.2. Numerical values of input parameters for MIMICS-I model: bold = estimated; normal = measured.	68
Table 3.3. Definition of Forest and Non-forest classes.	78
Table 3.4. Allometric equations used to estimate tree above-ground biomass.	83
Table 5.1. Area distribution of F/NF cover for Savernake forest.	121
Table 5.2. Area distribution of different non-forest classes for Savernake forest.	123
Table 5.3. Confusion matrix for forest/ non-forest cover classified map at 6 m resolution for Savernake forest against forest plot locations and ancient tree database. Overall accuracy = 69.9%, Kappa coefficient (κ) = 0.4.	125
Table 5.4. Confusion matrix for forest/non-forest cover classified map at 20 m resolution for Savernake forest against forest plot locations and ancient tree database. Overall accuracy = 63.67%, Kappa coefficient (κ) = 0.27.	125
Table 5.5. Confusion matrix for forest/clear-felled/grassland/bare-ground cover classified map at 6 m resolution for Savernake forest against forest plot locations and ancient tree database. Overall accuracy = 52.34%, Kappa coefficient (κ) = 0.31.	126
Table 5.6. Confusion matrix for forest/ clear-felled/grassland/bare-ground cover classified map at 20 resolution for Savernake forest against forest plot locations and ancient tree database. Overall accuracy = 36.72%, Kappa coefficient (κ) = 0.07.	126
Table 5.7. Area distribution of F/NF cover for Savernake forest between 2010 and 2014 at 6 m resolution.	131

Table 6.1.	Summary of field measured forest variables and S-band backscatter for 2014 and 2010 at 0.25 ha.	137
Table 6.2.	Statistical relationships between field calculated aboveground biomass to basal area, average canopy height, stem number density and average tree diameter.	138
Table 6.3.	Statistical relationships between S-band backscattering (σ_0) to basal area.	140
Table 6.4.	Statistical relationships between S-band backscatter (σ_0) to average canopy height.	140
Table 6.5.	Statistical relationships between S-band backscattering (σ_0) to stand number density.	141
Table 6.6.	Statistical relationships between S-band backscattering (σ_0) to average tree diameter.	142
Table 6.7.	Results from the regression models relating S-band backscatter (σ_0) acquired in 2010- 2014 to plot biomass from combined sites.	144
Table 6.8.	Results of biomass regression models using S-band backscatter (σ_0) in Savernake and Wytham at 0.25 ha resolution. R^2 is the coefficient of correlation and $RMSE_c$ is the root mean square error calculated using cross-validation of the training plots (25 stands) for 2010 and 2014. $RMSE_v$ is the error when applying the regression model to the validation plots (16 stands).	148

Glossary and Abbreviations

AIRSAR	-	Airborne Synthetic Aperture Radar (NASA- JPL)
AirSAR	-	Airborne Synthetic Aperture Radar Demonstrator Facility (Airbus)
ALOS	-	Advanced Land Observing Satellite
AGB	-	Aboveground biomass
ASAR	-	Advanced Synthetic Aperture Radar
AVHRR	-	Advanced Very High-Resolution Radiometer (United States)
BGB	-	Belowground biomass
C	-	Carbon
CO ₂	-	Carbon-dioxide
dB	-	Decibel
DESDynI-R	-	Deformation, Ecosystem Structure and Dynamics of Ice
DLR	-	German Aerospace Center
DMC	-	Disaster Monitoring Constellation
EnviSat	-	Environmental Satellite
ERS-1/2	-	European Remote Sensing satellites (-1, -2) (Europe)
ESA	-	European Space Agency
E-SAR	-	Airborne Experimental- Synthetic Aperture Radar
Gt C per yr	-	Total carbon flux
FAO	-	Food and Agriculture Organisation
FRA	-	Forest Resources Assessments
GHz	-	Gega Hertz
GLAS	-	Geoscience Laser Altimeter System
HJ-1C	-	Huan Jing -1 Constellation (Chinese Remote Sensing Satellite)
HUTSCAT	-	Helsinki University of Technology Scatterometer
JAXA	-	Japan Aerospace Exploration Agency
JERS-1	-	Japanese Earth Resources Satellite (Japanese)
ICESat	-	Ice, Cloud and Land Elevation Satellite
LAI	-	Leaf Area Index
LiDAR	-	Light Detection and Ranging
MCPFE	-	Ministerial Conference on the Protection of Forests in Europe
MERIS	-	Medium Resolution Imaging Spectrometer

MODIS	-	Moderate Resolution Imaging Spectrometer
MIMICS	-	Michigan Microwave Canopy Scattering Model
MIT	-	Massachusetts Institute of Technology Model
Multi-MIMICS-		Multiple Michigan Microwave Canopy Scattering Model
MHz	-	Mega Hertz
MRF	-	Markov Random Fields
NERC	-	Natural Environment Research Council
NISAR	-	NASA ISRO Synthetic Aperture Radar
NOAA	-	National Oceanic and Atmospheric Administration
NPP	-	Net primary productivity
PALSAR	-	Phased Arrayed L-band Synthetic Aperture Radar
PDF	-	probability density function
ppm	-	parts per million
QuickSCAT	-	Quick Scatterometer
RADAR	-	Radio Detection and Ranging
Radarsat-1/2	-	C-band SAR (Canadian Space Agency)
REDD	-	Reducing Emissions from Deforestation and forest Degradation
rms	-	Root mean square (Soil)
RMSE	-	Root mean square error
SAR	-	Synthetic Aperture Radar
SBCBM	-	Santa Barbara Canopy Backscatter Model
SRTM	-	Shuttle Radar Topography Mission
σ_0	-	Sigma nought (backscatter coefficient)
SPOT	-	Satellite Probatoired' Observation de la Terre
SSTL	-	Surrey Satellite Technology Limited
t/ha	-	Tonnes per hectare (Aboveground biomass)
WCM	-	Water Cloud Model

Chapter 1: Introduction

1.1. Global carbon cycle

The equation of the global budget for atmospheric carbon-dioxide (CO₂) is critically important for understanding the impacts of climate change. The concentration of atmospheric CO₂ has been unprecedentedly increased from around 277 parts per million (ppm) since 1750 (Joos and Spahni 2008) to 402.52 ppm in January 2016 (Dlugokencky and Tans 2014) (Figure 1.1). The majority of carbon (C) emissions come from fossil fuel burning, cement production and large-scale land-use change (Ciais et al. 2013, Prentice et al. 2001). Of the total amount of CO₂ emitted into the atmosphere, nearly half of it remains in the atmosphere while the other half is absorbed into the oceans and the terrestrial biosphere (Ciais et al. 1997). However, the shared partition between these two reservoirs of carbon has been the subject of considerable debate change (Prentice et al. 2001). Therefore, to better understand the present carbon cycle and future climate change projection for supporting future climate policies, accurate assessment of CO₂ emissions and their redistribution among the biosphere is critically important (Le Quéré et al. 2014).

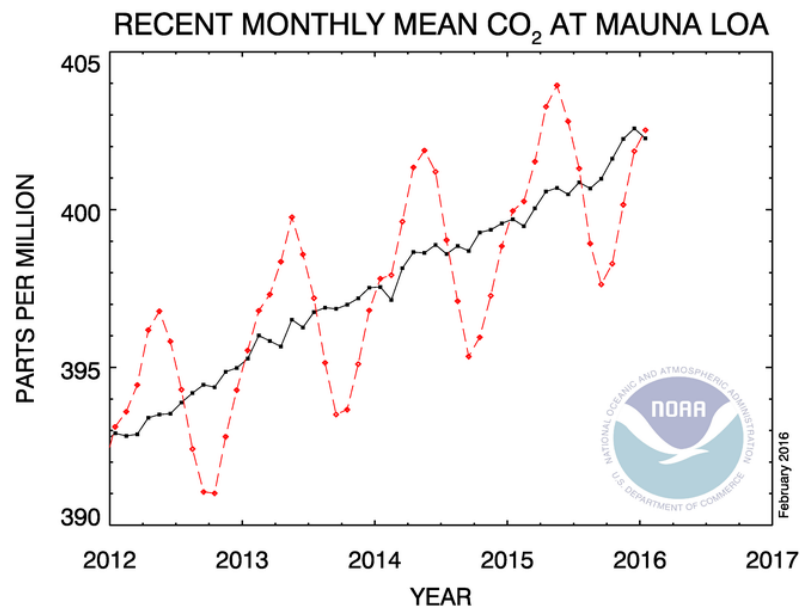


Figure 1.1. The graph shows recent monthly mean CO₂ measured at Mauna Loa Observatory, Hawaii. The dashed red line represents the monthly mean values, centered on the middle of each month while black line represents the same, after correction for the average of 7 adjacent seasonal cycles. Image reproduced with copyright permission from the Scripps Institution of Oceanography.

The terrestrial biosphere is currently either exchanging or absorbing atmospheric C particularly at the regional scale, for example in the Northern Hemisphere between 40°N to 70° N latitude. These changes in the Northern Hemisphere have been reported as a result of seasonal changes on terrestrial greenness based on vegetation growth trend analysis (Dixon et al. 1994, Kauppi et al. 1992), satellite remote sensing (Myneni et al. 2001, Nemani et al. 2003, Tucker et al. 2001), modelling (Lucht et al. 2002, Piao et al. 2015) and eddy covariance techniques (Valentini et al. 2000). On the contrary, it has been observed that land ecosystems may also become a source of large atmospheric CO₂ concentrations due to the changing climate system and intensive human activities (Cox et al. 2000), thus providing a positive feedback to a warming world towards the end of the twenty-first century (Friedlingstein et al. 2006).

Globally, seasonal variations of atmospheric CO₂ and dynamic climatic variables provide a complex and varying environment for different species of forest composition, structure, growth and its activity (for example, phenology and productivity). The climatic variables particularly air temperature, water availability and solar radiation along with the available atmospheric C acting as the resource responsible for the dynamic processes, structure, composition and functions in the forest ecosystem (Churkina and Running 1998, Churkina et al. 1999). For instance, air temperature and solar radiation together are responsible for forest growth covering around 60 % of the land ecosystem particularly in tropical forests (Nemani et al. 2003). On the other hand, the temperate forest ecosystem of North America and Eurasia in the northern latitudes is limited by cold winter temperatures with cloudy summers.

1.2. Forest cover

Globally, forest biome occupies an area of approximately 42 million km². These forests are concentrated in tropical, temperate and boreal lands occupying 30% of the land biosphere (Bonan 2008). They are amongst the most important natural ecosystems on earth (Potapov et al. 2008a, Potapov et al. 2008b) due to their importance as global timber stocks (MEA 2005), cultural values and responsible for global climate variability, evapo-transpiration (Avissar and Werth 2005) and bio-

geochemical fluxes at regional scales (Bojinski et al. 2014, Foley et al. 2005). Forest cover has also been used as a proxy for the assessment of threats to biodiversity and ecological integrity (Butchart et al. 2010) and estimation of terrestrial C emissions to atmospheric CO₂ concentrations (Miles and Kapos 2008). Emission of forest carbon is basically related to large-scale deforestation and clear-felled not lesser than a hectare area primarily concentrated in the tropical forests of South America, Africa and Southeast Asia (Rosenqvist et al. 2003).

Several studies have highlighted that human activities could alter the future of forest cover in terms of its composition, structure and function particularly in old growth forests of tropics. These anthropogenic activities are categorized as- physical (e.g. temperature, precipitation, radiation and climate change), chemical (e.g. atmospheric CO₂ concentrations, nutrient depositions) and biological (e.g. land-use change, wood extraction, hunting) (Lewis et al. 2004, Lewis et al. 2009, Wright 2005, Wright 2010) drivers. Therefore, The amount of forest cover and loss can be used as an input to management programmes related to different international strategic initiatives to protect its biodiversity (SCBD 2001), to reduce C emission from deforestation and degradation (Mollicone et al. 2007) and to stimulate use of sustainable forest management practices.

Recently, two satellite based forest and non-forest cover maps have been produced globally using both optical and Synthetic Aperture Radar (SAR) data. The optical data corresponds to finer spatial resolution Landsat data in assessing the forest cover (tree percent cover) and change (annual forest gain and loss) at global scale between 2000 and 2010 (Hansen et al. 2013). Figure 1.2 provides the percent tree cover map for the year 2000 in the southern England from Landsat data at 30 m resolution (Hansen et al. 2014). Due to the low solar illumination in the northern high latitudes, radar satellite have been utilised for a consistent wall-to-wall mapping of forest cover across the globe. The SAR based forest/non-forest cover map is related to the Phased Arrayed L-band Synthetic Aperture Radar (PALSAR) sensor from the Advanced Land Observing Satellite (ALOS). HV backscatter PALSAR data have demonstrated the capability of producing 25 m global F/NF cover maps from 2007 to 2010 achieving around 85% overall accuracy (Shimada et al. 2014) (Figure 1.3 for southern England region) (JapanAerospaceExplorationAgency 2014).

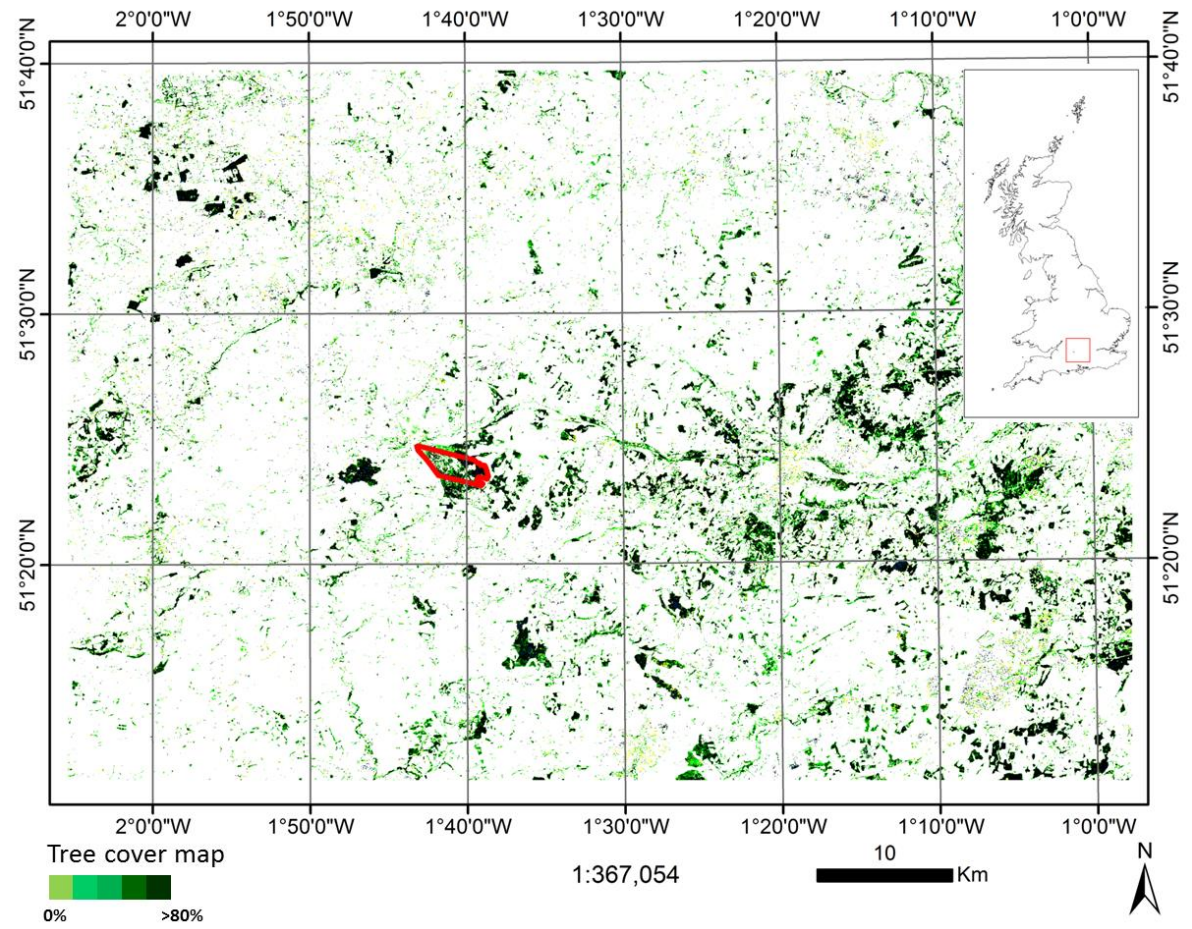


Figure 1.2. Percent tree cover map for the year 2000 in the southern England region from 30 m spatial Landsat data (Savernake forest: red polygon) (Insert: UK map with Granule: 60°N, 10°W frame) (Source: Global Forest Change 2000-2014 (Hansen et al. 2014)). Image reproduced with copyright permission from the Global Forest Change, University of Maryland.

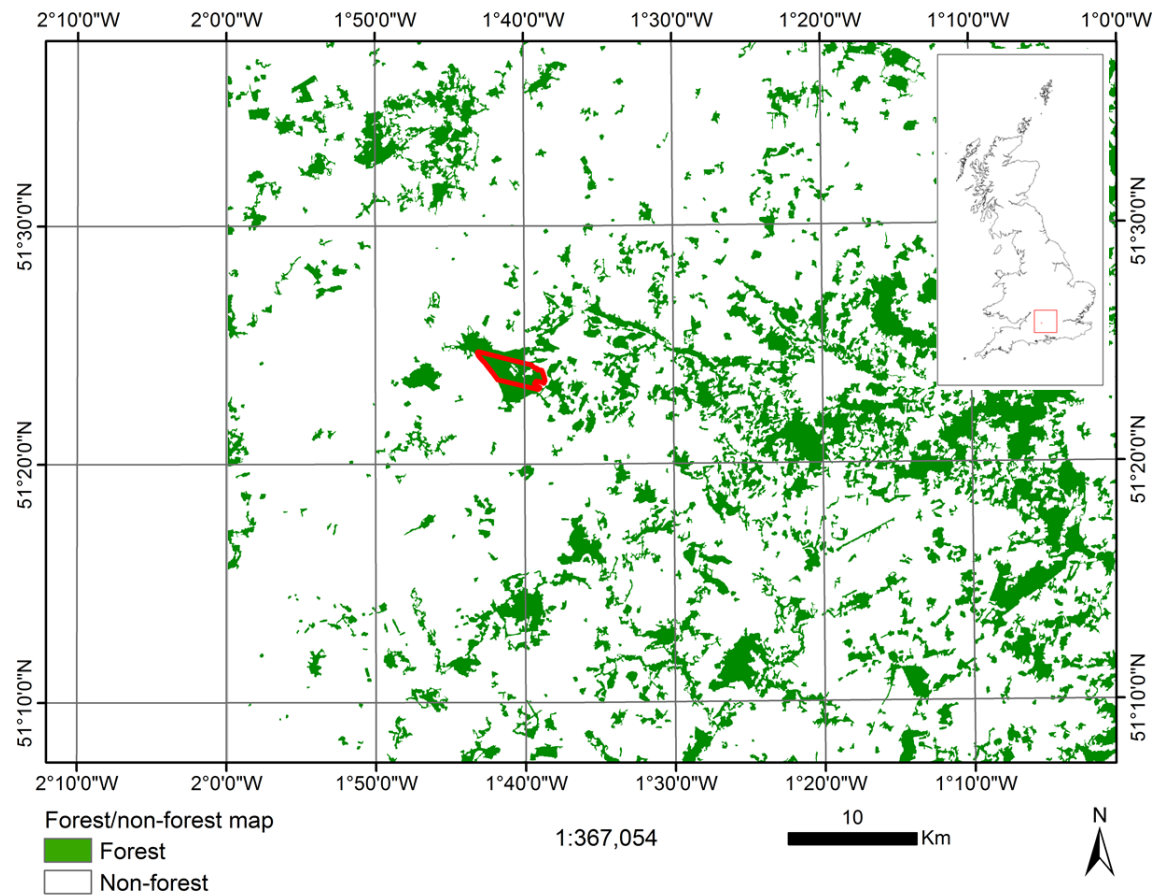


Figure 1.3. Forest/ non-forest map for year 2010 in the southern England region from PALSAR mosaics at 25 m resolution (Savernake forest: red polygon) (Insert: UK map with Grid 15: N21°W0002° frame) (Source: PALSAR Global Forest/ non-forest map "2010"(JapanAerospaceExplorationAgency 2014)). Image reproduced with copyright permission from the Japan Aerospace Exploration Agency.

1.3. Forest degradation

One of the largest uncertainties of terrestrial ecosystem and carbon cycle at regional to global scales is related to large-scale deforestation and degradation of forest.

Basically, deforestation and degradation of forest are too closely inter-related that they cannot be separated as individual processes. Deforestation is large-scale clear-cutting of existing forest and changing into other land-use such as agriculture and settlements. On the other hand, forest degradation can be put together as ‘change in crown cover and loss of biodiversity’ (Sitaula et al. 2005) due to ‘logging and forest fires’ which reduces the ‘carbon stock and productivity’ of the forest in a ‘long-term’ (Verolme and Moussa 1999). But the appropriate use of this definition applies to those areas where old growth forest lost their characteristics and values either by logging, wildfire or insect invasion (Putz and Redford 2010).

In the tropics, more than 20% of forests are affected by selective logging (Asner et al. 2009) due to canopy damage and fragmentation (Asner et al. 2006) and leaving forests highly susceptible to drought and fire (Cochrane 2003). They create forest with structure characterised by homogeneous canopy structure (Okuda et al. 2003), reduction in stem density (Slik et al. 2002) and total basal area (Bonnell et al. 2011) having a medium-sized tree stands (Bonnell et al. 2011) and reduced aboveground biomass (Blanc et al. 2009). Moreover, selectively logged areas are having more open canopy gaps with increased light intensities (Osazuwa-Peters et al. 2015). Models utilising the data from the Barro Colorado Island (BCI) 50 ha plot of Panama from unlogged plots predict that up to 70% carbon may be lost due to selectively logged forests (Bunker et al. 2005).

Over the last two decades, a net global C emission of 4.04 Gt CO₂ yr⁻¹ from deforestation and 0.8 Gt CO₂ yr⁻¹ from degradation has been estimated (Federici et al. 2015). However, the rates of degradation can be equivalent or more than the amount of deforestation at local scale (Zhuravleva et al. 2013). In fact, Margono et al. (2012) reported that almost 97% of new deforestation fronts do occur in previously disturbed or in different stages of degradation in Sumatra Island, Indonesia. Recently, van Lierop et al. (2015) found a strong relationship between degradation and net forest loss by region and climatic zone taking partial canopy cover reduction (at 250m spatial and 2000-2012 time frame of MODIS) as a proxy.

Moreover, forest degradation often begins at a very finer scale, NovaSAR 6m resolution data could provide a useful and better than other available datasets from Sentinel-1, ALOS-2 and other SAR sensors that provide global coverage.

Therefore, a robust and reliable method for estimating quantitatively undergoing forest degradation in time and space is critically important (UNFCCC 2008).

1.4. Forest aboveground biomass

Forests play a pivotal role in biophysical interactions and bio-geochemical exchanges (Foley et al. 1994) and constitute one of the principle and dynamic component of the global C cycle. For example, it has been estimated that on an annual basis, half of the atmospheric CO₂ is exchanged with the land biosphere through plant's photosynthesis (Ciais et al. 1997) and linking ~45% of terrestrial C to the land ecosystem Net Primary Productivity (NPP) in the form of forest aboveground biomass (AGB). The land ecosystem also regulates exchanges of energy, water and processes between atmosphere and land biosphere. Although at leaf level, all the direct processes and feedback on physiological processes have been well quantified, however, the impact of these processes at the ecosystem level remains unclear. This is important because the terrestrial ecosystem is main driver of global inter-annual atmospheric CO₂ variability (Peylin et al. 2005).

Several studies have shown that a major global C sink has been found in forest ecosystems (Ballantyne et al. 2012) particularly in old-growth forests (Luyssaert et al. 2008, Malhi and Phillips 2004). In forest ecosystem, terrestrial C is sequestered in the form of AGB as trunks, branches and leaves while soil carbon as belowground biomass (BGB) (Malhi et al. 2002). For instance, long-term monitoring plots in the forest ecosystems particularly in tropics have shown increased forest fragmentation and vulnerability to fires due to large-scale and rapid changes of forest biomass (Malhi and Phillips 2004). Moreover, forest biomass is also strongly associated with biodiversity (Bunker et al. 2005). Information related to forest canopy and biophysical characteristics such as tree height, density and AGB is important in modelling the state, condition and functioning of forest (Rosenqvist et al. 2003); useful as a means to mitigate the changing global climate and its uncertainties related to terrestrial ecosystem (Pagani et al. 2009).

Understanding the spatial and temporal patterns of AGB in forests is important for several reasons (Malhi and Phillips 2004). First, AGB information can provide insights into the possible drivers responsible for structural, process, functional and compositional changes of forest (Phillips and Lewis 2014). Second, biomass estimations can also provide information on emission factors for estimating carbon losses from processes related to deforestation and forest degradation (Willcock et al. 2012). Third, field AGB estimates can also assist in calibration and predictions of carbon utilising optical, microwave or LiDAR (Light Detection And Ranging) remote sensing techniques (Baccini et al. 2012, Saatchi et al. 2011a). Finally, biomass information can deliver data for parameterisation and validation of the large-scale ecosystem model predictions and their responses to a changing environment (Piao et al. 2013, Sitch et al. 2013). Hence, timely and accurate information on forest cover, its extent and AGB found in these forests is critically necessary to simulate the exchange of energy and carbon budget for present and future scenarios.

This thesis contributes to the knowledge about the monitoring of temperate forest using remote sensing technique for both mapping forest cover and relating with forest AGB. For this study, Synthetic Aperture Radar (SAR) data working on S-band frequency in forest ecosystem is being investigated utilising both SAR data and modelling. In particular, mapping of forest/ non-forest (F/NF) cover and relating to average tree diameter at breast height (DBH), canopy height (H) and forest AGB in mixed temperate forests of the United Kingdom (UK) are investigated. This research was conducted using high-resolution airborne S-band SAR data acquired during two AirSAR Campaigns (June 2010 and 2014), field data from test sites (Savernake Forest and Wytham Woods) and with spatial scales at pixel to stand levels. Although the present work is purely based on AirSAR campaign data and modelling approach, its applicability may be restricted to these particular data, time of acquisition, model type and test site. Yet, the findings and conclusions drawn have important implications that are applicable in a wider context particularly within the mixed deciduous temperate forest of the northern latitude.

1.5. Aims and Overview of Thesis

The mapping of forest cover and biophysical characteristics (structure and aboveground biomass) have been generated using robust, spatially resolved and systematic (repeated) remote sensing data particularly radar data at longer wavelengths (that is P- and L-band). In spite of the potential of SAR data, knowledge of the accurate radar wavelength and polarisation for a consistent monitoring of forest, its degradation and biophysical retrieval at local to global scale is still limited. Thus, there is a continued requirement for new experimental data and further improvement of the existing allometric models for biomass retrieval based on radar backscatter. This includes the forthcoming radar based P-band 'BIOMASS Mission' as part of ESA's Earth Explorer mission concept (Le Toan et al. 2011) and NASA's Decadal Survey Mission (previously called Deformation, Ecosystem Structure and Dynamics of Ice- DESDynI-R, now called NISAR) carrying an L-band SAR and a multi-beam LiDAR operating at 1064 nm (Hall et al. 2011).

From the UK perspectives, the concept of NovaSAR-S Mission is also under-developing which will carry S-band SAR sensor at low cost missions (Bird et al. 2013). However, the radiative nature of S-band radar wavelength is limitedly investigated over forest canopies related to forest cover, its degradation and biophysical characteristics in spite of the recently launched S-band Huan Jing (HJ) - 1C satellite from China in 2012 (OSCAR 2015). Therefore, the overall aim of this research is to explore S-band SAR backscatter sensitivity to forest ecosystem that whether this particular wavelength be useful for mapping forest cover, change analysis and structure retrieval.

The structure of thesis is outlined as follows:

Chapter 1 introduces the general background of the research related to importance of carbon cycle, forest cover, degradation and forest aboveground biomass across different ecosystem. Chapter 2 discusses radar remote sensing and different microwave canopy models for retrieving backscatter returns from forest canopies followed by detailed comprehensive literature review related to forest/non-forest cover mapping, forest degradation and biophysical characteristics focusing on boreal and temperate regions using radar data. This also includes the forthcoming NovaSAR-S Mission configurations related to this study.

Chapter 3 provides the full methodology related to different research questions addressed. This also includes the details of test sites (Savernake Forest and Wytham Woods), Michigan Microwave Canopy Scattering model (MIMICS-I) parameterisation and SAR-data processing chain. Finally, field data surveyed in 2012 and 2014 in Savernake, ancillary data from Forestry Commission for Savernake site and Environmental Change Network data for Wytham are also covered.

Chapter 4 presents the MIMICS-I simulation result of S-band signal interaction with soil moisture and surface roughness. This also includes forest canopy scattering as a function of different frequencies (X-, C-, S-, L-band), polarisations (co- and cross-) and radar look angles (15-45°) for both deciduous and conifers. Lastly, this chapter provides the radiative nature of S-band backscatter interaction with degraded forest.

Chapter 5 also presents the result of S-band SAR data in mapping forest/non-forest classes based on Maximum Likelihood Classification (MLC) algorithm in Savernake test site. The S-band derived forest/non-forest at StripMap and ScanSAR resolutions was validated using the PALSAR-based forest/non-forest at 25 m spatial resolution. This also includes the assessment of forest cover change detection between 2010 and 2014 over the same site and results are based on different simulations in line with NovaSAR-S configuration (StripMap, ScanSAR) in aid of Landsat based forest loss data.

Chapter 6 provides the results based on retrieval of forest biophysical characteristics (average tree diameter, canopy height and forest AGB) at S-band SAR backscatter and further prediction and cross-validation of forest biomass using regression equations for Savernake and Wytham sites, two years and at pixel to stand levels.

Chapter 7 brings together all the research findings from the previous chapters and synthesises them with individual conclusions for MIMICS experiments related to soil, forest canopy and degradation of forest; forest cover/ change mapping and forest biophysical parameter retrieval. General conclusions are provided specifically related to NovaSAR-S mission applicability and potential for forest/non-forest cover and biomass retrieval in future perspectives and limitations for this research.

Chapter 2: Review of the literature

2.1. Microwave remote sensing

For a consistent and systematic study on the global monitoring of forest ecosystem and its processes in space and time, satellite remote sensing technology offers efficient method in terms of larger area coverage and repetitive observations. Several studies have highlighted the potential of optical data utilising multi-temporal to acquire cloud-free imageries for studying forest ecosystem. However, operational monitoring for forest are often hampering particularly in tropics and in higher latitudes due to persistent cloud cover and low solar illumination respectively. For an operational system to monitor these forest in high spatial and temporal resolutions, microwave remote sensing technology is a complementary tool due to their advantages such as weather independent, cloud penetration and more sensitivity to forest structure and its biophysical parameters (Woodhouse 2006a).

Microwave based sensors used microwave radiation with wavelengths from about 1 centimetre to few tens of centimetres. Additionally, they can provide information related to sea wind and wave direction which cannot be possible by visible and infra-red sensors. Two types of microwave remote sensing exist: active and passive sensors. The active microwave sensors receives the microwave radiation (or pulse) being transmitted or scattered from target (e.g. forest canopy) which is incident while microwave radiation emitted from target is received by the passive microwave sensors. Examples of active sensors include Synthetic Aperture Radar (SAR), microwave scatterometers and radar altimeter while microwave radiometer is a passive microwave sensor.

2.1.1. RADAR

RADAR is an acronym for RADio Detection and Ranging. It is an active microwave remote sensing system using microwaves (or radio waves) and can operate day and night irrespective of weather conditions. Basically, the radar sensor (with antenna) is mounted on an aircraft which transmits microwave pulse in direction perpendicular

to the flight direction, hence called as Side-Looking Airborne Radar (SLAR) or Real Aperture Radar (RAR). Spatial resolution of radar imagery is basically determined by the transmitted wavelength, length of the antenna and distance between the target and sensor. This is feasible only for airborne systems where distance between the target and sensor/ platform are only up to few kilometre. On the contrary, space-borne systems are limited by long distances up to hundreds of kilometres and larger antenna size (to obtain high resolution data). Radar operates in a wide range of frequencies from a few MHz to hundreds of GHz. Table 2.1 gives the nomenclature used by radar community and examples for past, active and future radar missions.

Table 2.1. Different radar frequencies of space-borne used by radar community (IEEE Standard 521-1984).

Radar letter	Frequency	Wavelength (cm)	Examples of space-borne platform
UHF (P)	300-1000 MHz	100.0 - 68.0	BIOMASS
L	1-2 GHz	30.0 - 15.0	<u>JERS-1</u> , <u>ALOS PALSAR-1</u> , <u>ALOS PALSAR-2</u>
S	2-4 GHz	15.0 - 7.5	<u>Almaz-1</u> , <u>HJ-1C</u> , NovaSAR-S , NISAR
C	4-8 GHz	7.5 - 3.8	<u>Envisat- ASAR</u> , <u>Radarsat-1/2</u> , <u>Sentinel 1A</u> , <u>RISAT-1</u>
X	8-12 GHz	3.8 - 2.5	<u>TerraSAR-X</u> , <u>TanDEM-X</u>

*Underlined- Completed, Italics- Active and Bold- Future

2.1.2. The Radar Equation

There are two basic equations that govern the performance of a radar system- the Signal-to-Noise-Ratio (SNR) and the range resolution. The received microwave pulse to a sensor is a combination of target information with noise. This can be governed by the SNR as a function of the radar system, the range to the target and properties of the scattering target. Therefore, the SNR is defined as the ratio between the received power and the noise power. For a mono-static system using coherent integration during time t_{dwell} it is given by

$$SNR = \frac{P_{avg} \lambda^2 G^2 t_{dwell}}{(4\pi)^3 R^4 k_B T_S C_b L} \sigma$$

P_{avg} is the average transmitted power, λ is the wavelength of the transmitted wave, G is the gain of the antenna, R is the one-way distance (range) to the target, $k_B T_s$ gives the system noise power per unit bandwidth, C_b is a filter mismatch factor and L is a loss factor. Finally, σ is the radar cross section (RCS), with unit m^2 , which is a measure of the scattering strength of a target. A perfectly reflecting sphere has an RCS equal to its cross-sectional area. Thus, the RCS can be thought of as the cross-sectional area of a sphere which gives the same scattered power as the target. The return echo which is often RCS is called the radar backscatter which is a unit less variable. The backscattering coefficient is defined so that the average RCS from a distributed target with ground area A is $\sigma = A \cdot \sigma^0$.

2.1.3. Synthetic Aperture Radar

Unlike RAR system with large-sized and fixed antenna limitations, Synthetic Aperture Radar (SAR) is an active coherent side-looking radar system which transmits microwaves energy with known relative phases and synthesizes an antenna much larger than the physical antenna to produce high resolution imagery. This works with two approaches involving the Doppler beam sharpening and the principle of coherently combining a collection of low-resolution antennas in order to provide a greatly improved resolution. Using this technique, the Earth's features have been successfully imaged to a meter or below spatial resolution along the direction of the flight even from space-borne systems.

2.1.4. Speckle

In all types of coherence data including SAR imagery there is random interference (constructive and destructive) of the wavelets scattered by the target within one resolution pixel creating noise-like granulation called speckle (Woodhouse 2006a). Speckle is a noise-like scattering phenomenon embedded in the image itself possibly due to insufficient resolution of the sensor to resolve individual scatterers within an imaged pixel. For example, the received signals complex amplitude is the sum total of all the returns from all individual scatterers within a resolution cell. Thus, areas with strong backscatter will exhibit more variability than areas of weak backscatter. The presence of speckle in SAR data reduces the visibility of the imagery hence

decreasing the discrimination of the target. To minimise speckle effect in SAR imagery, incoherent averaging is performed. Basically, three main approaches are employed: First, using the Doppler phenomenon where several parts often called 'looks' are averaged incoherently termed to be 'multi-looking'. Second method involves averaging the neighbouring pixels using a windowing size function and third method utilizes averaging multiple SAR images over the same area provided a constant backscattering in the area of interest with dynamic speckle phenomena between image acquisitions (Woodhouse 2006a). However, there is a trade-off between the speckle minimisation and spatial resolution of the SAR image. Additionally to tackle the speckle problem prior to analysis, application of speckle reduction filters (Shupe and Marsh 2004, Shimabukuro et al. 2007) or aggregation of pixels (Kiage et al. 2005, Lang et al. 2008) are commonly employed approaches.

2.1.5. Radiometric SAR Calibration

The merits of SAR images in studies related to resource management can only be made provided the measurements of RCS (radiometric calibration) are met. Radiometric calibration may be achieved through internal or external calibration or using both. Internal calibration involves precise calibration of antenna and processor gains at transmit and receive antenna, radar look angles in elevation and azimuth direction. This also include Doppler tracking, elevation angle tracking, range cell migration correction, look extraction, slant-to-range conversion for precise calibration. Comparatively, it is easier to calibrate SAR imagery based on external target with known RCS characteristics. For example, a set of distributed targets or point target have been commonly used for calibration where corner reflectors are commonly employed for point target calibration (Dobson et al. 1986).

2.2. SAR scattering in forest

Theoretically, the received backscatter carries information related to forest characteristics (e.g. canopy structure, architecture and biophysical parameters) due to their interactions and scattering. Therefore, to derive these forest biophysical characteristics, it is critical to understand the different scattering theory of radar pulse. Secondly, microwaves are also electromagnetic waves, hence the scattering

mechanism for light governing the size, shape and material (its dielectric constant) of the canopy components in proportion to the incident wavelength is also applicable to microwave. Thus, it is highly recommended to avoid SAR data acquired during rainy days (or season) as they are very sensitive to dielectric constant (moisture content) of soil and forest being imaged and may lead to misinterpretation of the recorded backscatter.

In the microwave domain, there are three main interactions related to the size of the forest canopy (that is component and structure) and wavelength used termed to be Optical, Rayleigh and Mei types of scattering. First, optical scattering is related to very large canopy components (e.g. stem or trunk diameter) than the incident wavelength. It is also known as non-selective scattering as the scattering do not vary with wavelength. Second, Rayleigh scattering is related to very small components than the wavelength used where the scattering drops off very quickly with increasing wavelength. This may be related to size, shape and density of leaf and branches. Finally, Mei scattering refers to those scattering related with the size of the component between Rayleigh and Optical scattering where the effect of resonant occur. This implies that for a small change in the target size (leaf, branch) or wavelength used, a very sensitive type of scattering occurs. This effect of resonance is due to the coherent scattering from the different parts of the target's surface being imaged as a function wavelength size (Woodhouse 2006a).

The scattering behaviour in microwave domain has been largely addressed in the literature with specifically related to forest aboveground biomass through backscatter: biomass relationships with a level of saturation point (Imhoff 1995, Sandberg et al. 2011, Saatchi et al. 2011b, Baker et al. 1994, Le Toan et al. 1992). But, the underlying knowledge of these scatterings within different forest canopies, branching level and number stand density is poorly addressed. For instance, study by Woodhouse (2006b) have reported the dominance of a single-layer scattering between the two extremes of Rayleigh and optical to the changes in scatter number density rather than resonance effect via increasing canopy opacity. This study implies that the saturation level of radar backscatter to high forest canopies is also associated with low forest density having low growing stock/ biomass. In general,

the actual scattering from target depends on its physical size, shape, orientation including its building material (i.e., dielectric constant) and number density.

Applications of SAR data for studies on forest cover and biophysical retrieval have used X-, C-, L- and P-band data. However, current knowledge of the scattering behaviour of S-band SAR in forested areas is very limited. To date, S-band SAR data have not been easily available. The first S-band SAR observations from space were provided by the Russian Almaz-1 satellite, which carried a single-polarisation HH S-band SAR sensor operating between 1991 and 1992. The sensor look angle range is 20 to 70° with standard range of 32 to 50° and two experimental ranges of 20 to 32° and 50 to 70°. Very few studies of Almaz-1 data are available in the peer-reviewed literature, with a small number in oceanography (Ivanov and Litovchenko 1997), geology (Elizavetin and Paillou 1997) and forestry/ plantation (Fransson et al. 1999, Olsson et al. 1991, Rosenqvist 1996, Yatabe and Leckie 1995).

Since the Almaz-1 mission, innovative in radar technology has vastly improved in terms of radiometric quality, signal processing and data transmission. New interest in S-band SAR has led to the launch of the Environment and Disaster Monitoring Satellite HJ-1C from China with a single polarisation VV S-band (3.2 GHz) SAR instrument (Du et al. 2010) and the forthcoming NovaSAR-S satellite, which is the first in an intended constellation of low-cost radar satellite being manufactured in Britain (Bird et al. 2013).

2.3. NovaSAR-S Mission

The concept of NovaSAR-S comes from the Surrey Satellite Technology Limited's (SSTL) long-term expertise in making small satellite since the 1980s. For example, the Disaster Monitoring Constellation (DMC) operated by five nations could provide data with high spatial and temporal resolution in dealing with disaster monitoring and climate change. NovaSAR-S is being built by SSTL and Airbus Defence and Space (UK), designed as a small, light-weight S-band (3.1-3.3 GHz) SAR satellite at low cost missions (Bird et al. 2013). It will carry an active micro-strip patch phased array (3 x 1 m) on board the first S-band SAR satellite from the UK.

NovaSAR-S satellite is a complex payload with multi-mode having fully-polarimetry capabilities which can acquire data in both sun-synchronous and near equatorial orbits, the unique state-of-the-art covering pan-tropics and higher latitudes. NovaSAR-S will carry S-band SAR sensor with specifications listed in Table 2.2. The phase array antenna consisting of 18 phase centres can steer beam across track to collect data over 580 km using four operational modes under varying polarisations, swath, resolution, incidence angles and looks combinations as specified in Table 2.3. For example, in a sun-synchronous orbit, single NovaSAR satellite could achieve a 12.5 day repeat cycle in StripMap mode up to 2.2 day repeat cycle in equatorial orbit (15°). If three satellites were operated in constellation, then repeat-coverage in StripMap will be increased to every 3.5 days in sun-synchronous orbit or every day in equatorial orbit. Finally, the first NovaSAR-S is expected to get launch by 2016-2017 (Bird et al. 2013).

Table 2.2. NovaSAR-S specification.

Parameter	Specification
Orbit	Polar sun synchronous (10.30 LTAN) (dawn/dusk) Near equatorial(15°low inclination)
Altitude	580 km
Operating frequency	3.1- 3.3 GHz (S-band)
Ambiguity ratio	< -18 to -16dB
Sensitivity	StripMap (<-17.5dB), ScanSAR (<-18dB), Maritime (<-12dB) and ScanSAR wide (<-19dB)
Number of beams	18 strips
Repetitivity	14 to 3.5days (1-3 ScanSAR) in sun-synchronous 6.2 to 1 day (1-3 ScanSAR) in equatorial 15° 12.5 to 3.5 days (1-3 StripMap) in sun-synchronous 2.2 to 1 day (1-3 StripMap) in equatorial 15°

Table 2.3. Operational modes in NovaSAR-S SAR.

Imaging mode	Operating polarisation	Swath (km x km)	Resolution (m)	Incidence angles (°)	Number of looks
StripMap		20	6	16-25.4	4
		13-20		21.8- 31.2	
ScanSAR	Dual, tri or quad	100	20	15.8- 25.4	4
		50		25- 29.4	
Maritime ScanSAR		750	30	48.1- 73.1	1
Wide		140	30	14-27.4	4
		55		27.4- 32	

2.4. Microwave Canopy Scattering Modelling

For the past three decades, significant efforts in microwave remote sensing have been devoted to increase the forest classification accuracy and for estimating biophysical parameters particularly AGB retrieval. This is possible due to the polarimetric nature of SAR data by identifying the physical behaviour of the scattering mechanisms that contribute to the radar backscatter for both classification and biophysical purposes (Beaudoin et al. 1994). Furthermore, numerous studies have also revealed that longer wavelengths show greater sensitivity to forest biomass with HV-polarisation channel (Le Toan et al. 1992, Mermoz et al. 2015, Saatchi et al. 2007, Saatchi et al. 2011b, Sandberg et al. 2011). To validate these experimental results from SAR data analysis, understanding the relationships between SAR backscatter and forest parameters becomes critically important and necessary. For example, backscatter at P- or L- band utilising AIRSAR data is highly correlated to forest biophysical parameters (that is forest age, DBH, H and trunk biomass) of maritime pine forest (Le Toan et al. 1992).

In spite of the above observation, the sensitivity of backscatter to different canopy parts (leaves, branches and trunk) cannot be easily quantified due to the inter-relationship between forest parameters. Therefore, the radiative transfer based Massachusetts Institute of Technology (MIT) model (Yueh et al. 1992) was used to interpret the physical link between the backscatter and the biomass and found that VV- or HV- backscatter are affected by forest crown volume, canopy structure, moisture content and related to AGB (Beaudoin et al. 1994). Hence, several researchers have investigated the scattering mechanisms of forest parameters based on microwave canopy scattering models (Brolly and Woodhouse 2013, Brolly et al. 2012, Karam et al. 1995, Karam and Fung 1988, Liang et al. 2005, Sun and Ranson 1995, Sun et al. 1991, Ulaby et al. 1990, Wang et al. 1993a, Wang et al. 1993b, Wang and Imhoff 1993, Woodhouse 2006b).

Knowledge of S-band backscatter to crop and forest canopy classification (Guida et al. 2012, Natale et al. 2012) and AGB retrieval (Rosenqvist 1996) is very limited. A study on polarimetric radar from a single fir tree and group of young fir using Entropy (H)/ Alpha (α) decomposition techniques and time domain revealed main

scattering from the green needles and branches at S-band (Lopez-Sanchez et al. 2000). For the group of young fir, S-band backscatter has high penetration level than X- and C-band resulting to lower vegetation volume. Similarly, Lopez-Sanchez et al. (2006) also reported volume scattering to be the dominant mechanism with S-band backscatter due to uniform distribution over the whole maize plant using decomposition technique. Likewise, Sun et al. (2012) have reported that S-band backscatter is influenced by the dynamics of the canopy structure of wheat crop (in different growing stages) particularly from heading to milking stage at $\sim 40^\circ$ incidence angle. This study was carried out in wheat fields in northern China using ground measurements, tower-based S-band scatterometer and MIMICS model.

The sensitivity of soil component to the radiative nature of S-band frequency was investigated by Du et al. (2010) in preparation for HJ-1C launch. They found reasonable level of accuracy of $R^2 = 0.68$ (in soybean) and 0.71 (in corn) between observed and soil moisture retrieval at VV-polarisation channel. The algorithm works with S-band modeled backscatter from vegetation using first-order scattering model and soil scattering from the Advanced Integral Equation Method with simplification of a radar backscatter model for bare soil. To explore the radiative nature of S-band backscatter in terms of forest ecosystem, it is utmost important to understand the interaction mechanisms governing the S-band backscatter from forest canopy and its components. For this research study, the first order canopy scattering model of MIMICS (Ulaby et al. 1990) is used to examine the strength of S-band backscatter responses from forest canopy and to identify dominant scattering from different canopy parts (components). Specifically, the varying sensitivity of S-band backscatter responses from forest canopy against soil and identifying the dominant scattering from forest canopy parts will develop our understanding to draw further conclusions on forest cover mapping and forest parameters retrieval at S-band radar frequency.

Essentially, canopy scattering models help to understand the complex interaction of microwave backscatter with different components of the forest canopy and structure (leaves, needle, twigs and trunks) as a function of SAR system properties (wavelength, incidence angle and polarisations) (Liang et al. 2005, Sun and Ranson 1995, Ulaby et al. 1990, Wang and Imhoff 1993). In fact, modelling the effect of

forest canopy structure on microwave propagation is a difficult task due to the complex tree structure and their sensitivity to electromagnetic characteristics (Bosisio and Dechambre 2004). This involves solving the interactions of canopy components with microwave radiation from two perspectives: (1) Geometrically, forests can be modelled as a continuous random medium with discrete scatter (different shapes and sizes) embedded in a homogeneous volume. (2) Electromagnetically, these models can be classified as either to the wave theory or radiative transfer (RT) theory (Liang et al. 2005).

Model with wave theory works with modelling the canopy components as a set of dielectric cylinders and discs on the basis of Maxwell's equation. On the contrary, models based on radiative transfer theory works with propagation of energy and are more appropriate than the wave approach. Because canopy (leaves, needles and branches) have discrete configurations and dielectric constants much larger than that of air (Ulaby et al. 1990).

Generally, most models consist of two-layer canopy with upper canopy layer comprising of leaves, needles and branches while trunks as lower layer (Ulaby et al. 1990) (Figure 2.1). Structurally, the canopy is divided into three main regions as crown, trunk and underlying ground region. All the components of a tree canopy and ground are characterized by a set of dielectric models in terms of moisture content and microwave frequency. Different models account for different scattering mechanisms propagating through canopy, trunk interaction and backscattered from the ground surface. Some of the RT based microwave canopy scattering models have been described in next section:

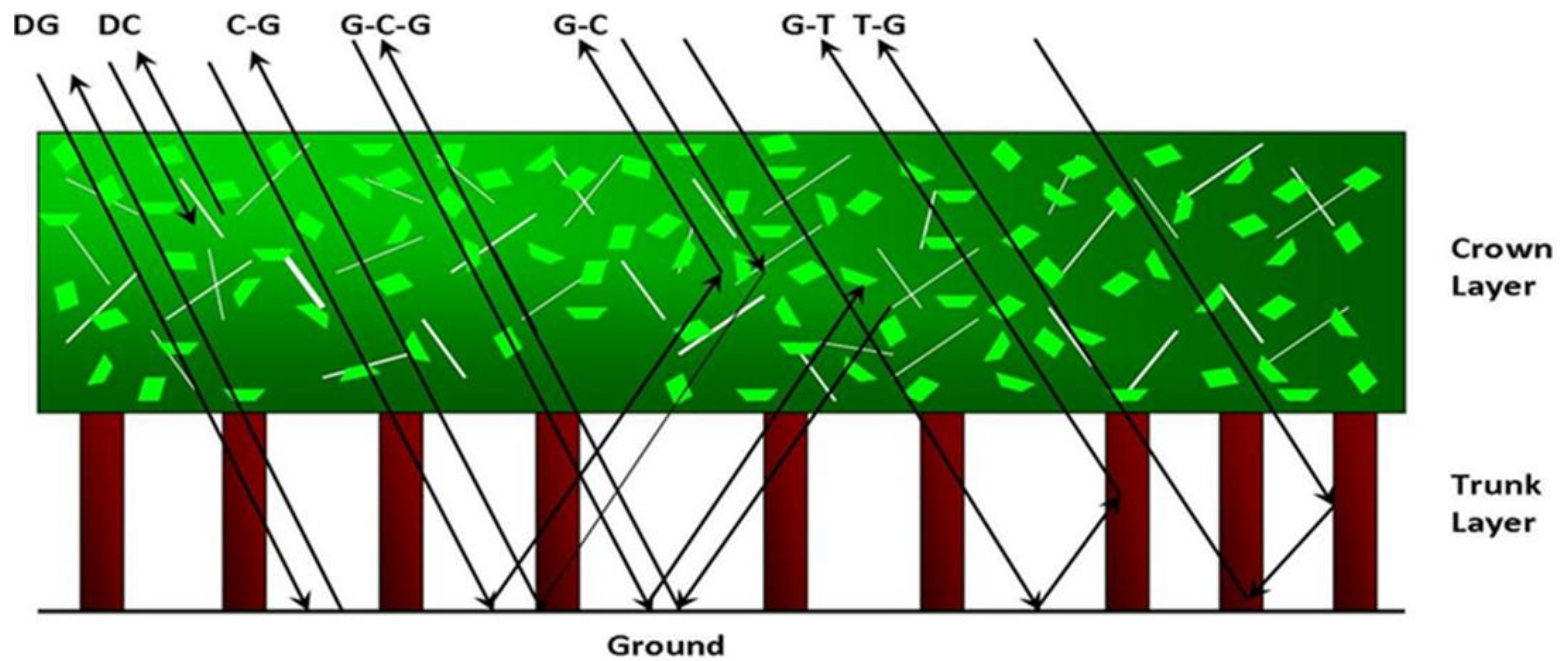


Figure 2.1. Overview of MIMICS model structure with different interaction components (DG-direct ground, DC-direct crown, C-G-crown-ground, G-C-G- ground-crown-ground, GC-ground crown, G-T or T-G-ground/trunk) from forest canopies (Ulaby et al. 1990). Image reproduced with copyright permission from the Radiation Laboratory, University of Michigan.

2.4.1. Water Cloud Model

The Water Cloud model (WCM) is based on single scattering mechanism that considers the canopy of vegetation as a cloud containing water droplets randomly distributed within the canopy (Attema and Ulaby 1978). Total backscatter returns are expressed as a function of the volumetric moisture content of the soil and vegetation. Generally, for a given polarisation the WCM simulation is expressed as:

$$\sigma_{0\text{ pp}} = \sigma_{0\text{veg}} + \sigma_{0\text{veg+soil}} + L^2 \sigma_{0\text{soil}} \quad (2.1)$$

where $\sigma_{0\text{ pp}}$ is the like-polarisation total backscatter coefficient, $\sigma_{0\text{veg}}$ is the backscatter contribution of the vegetation cover, $\sigma_{0\text{veg+soil}}$ is the multiple scattering involving vegetation elements and the soil surface, $\sigma_{0\text{soil}}$ is the backscatter contribution of the soil surface and L^2 is the two-way vegetation attenuation (Attema and Ulaby 1978). The second term in equation 2.1 represents the interaction of the incident radiation between the vegetation and the underlying soil. Additionally, WCM accounts for backscattering from surface and canopy only and ignore higher order of scattering interactions and scattering that might occur in the canopy gaps. WCM is simpler than any other models developed later as it requires fewer input parameters.

The WCM could predict a significant positive relationship with varying polarisations between 8 and 18 GHz frequency for four different crop types (alfalafa, corn, milo and wheat) having error between 1.1 to 2.6 dB. This model can also provide information related to attenuation from soil and vegetation layers to the backscatter.

2.4.2. Santa Barbara Canopy Backscatter Model

The canopy scattering model developed in the University of California at Santa Barbara (SBCBM) is related to discontinuous canopy layer by treating trees as discrete crowns (ellipsoids) and trunks (cylinders) located above a ground surface. Essentially, this model is more relevant to woodlands with low density tree stands and discrete crowns rather than a uniform layer (Sun et al. 1991). The model works on solving RT theory to a gap probability approach based on geometric-optical

canopy modelling. This approach allows modelling of sparsely wooded areas, and potentially the whole spectrum from nearly closed canopy forest to woodland. Finally, four scattering mechanisms are considered: surface backscattering, crown volume scattering, multipath crown-ground and ground/trunk interactions.

HH-polarisation backscatter is largely determined by the trunk/ground interaction at high incidence angles while crown scattering in VV-polarisation backscatter. Otherwise, three scattering mechanisms related to trunk/ground, crown-ground and direct ground are comparable in lower incidence angles for both polarisations. Comparatively, an increased but little contribution from crown scattering to the total backscatter has been observed at all polarisations with increasing incidence angles. For HV-polarisation channel, dominant scattering is largely determined by the crown and crown-ground mechanism to the total backscattering possibly due to inadequate backscatter from surface layer from sparse canopy cover (low density).

2.4.3. Michigan Microwave Canopy Scattering (MIMICS) Model

Michigan Microwave Canopy Scattering (MIMICS) model developed in University of Michigan is a two-layer canopy model with upper canopy layer consisting of leaves, needles, branches and trunks as lower layer which works on a first-order solution of the RT equations based on Foldy's method (function of height within the canopy) (Ulaby et al. 1988a) (see Figure 2.1). Structurally, MIMICS has three main regions in tree canopy- crown, trunk and underlying ground region. For an individual tree, the crown layer is assumed to be spheroidal in shape with height and diameter. It also contains branches and needles modelled as dielectric cylinders and characterised by a joint probability density function (pdf) in the case of coniferous species.

For deciduous type the crown section contains leaves modelled as flat rectangular discs and characterised by a joint pdf. The trunk section consists of an average height and average diameter with their orientation being characterised by the joint pdf. The underlying ground surface is characterised by its roughness as a function of root mean square (rms) height and a roughness correlation function of soil with different combination of soil types. All the components of a tree canopy including ground are characterized based on dielectric models in terms of moisture content, microwave frequency and physical temperature.

MIMICS model contain seven terms in the first-order solution which account for seven scattering mechanisms propagating through canopy, trunk interaction and backscattered from the ground surface. These terms includes (1) ground/trunk interaction component (2) total crown backscatter and (3) direct ground backscatter. The total crown backscatter consists of three main contributions resulting from (1) direct crown backscatter (2) ground and crown layer and (3) ground scattered directly back to the ground from crown layer and re-directed in the specular direction by the ground. MIMICS model has been developed into three generations: MIMICS- I (continuous or closed-crown geometries) (Ulaby et al. 1990); MIMICS-II (discontinuous or open-crown geometries) (McDonald and Ulaby 1993) and MIMICS -III (periodic row structured vegetation canopies) (Whitt and Ulaby 1994). Of the existing RT microwave based models, the MIMICS model is widely used in studies related to agriculture and vegetation (Lin 2009, Ulaby et al. 1990).

At L-band, MIMICS-I model has predicted the ground/trunk mechanism as the dominant across the incidence angles for HH-polarisation channel while at intermediate angular range for VV-polarisation channel from deciduous canopy. On the contrary, total-crown scattering dominates for both HH- and VV-polarisation channel at X-band due to lower penetration level.

2.4.4. Multi-MIMICS Model

To account for complex forest structure as a function of varying tree height, a multi-layered RT Multi-MIMICS model was developed in the University of Michigan (Liang et al. 2005). This model considered overlapped layers to account for mixtures of tall and short tree crowns with stands of mixed-species composition and age gradients. In this model, a tapered trunk model is introduced by cascading layers with increasing trunk radius instead of using a uniform stem.

At P-band, dominant scattering arises from interactions between trunks, large branches and ground surface. For example, a major scattering occurred largely due to ground and large branches interaction and also direct large branch scattering at VV- and HV-polarisation channels. At L-band, major scattering occurs from trunk/ground interactions at HH-polarisation channel while VV- and HV-channels contributions were largely mainly from the large branches. At C-band, scattering

from the small branches dominated in co-polarisation channel while HV-polarisation backscatter received scattering from both small and larger branches. The Multi-MIMICS model provides an improved backscatter/biomass relationship and showed better agreement with AIRSAR backscatter in forest ecosystems of Queensland in Australia (Liang et al. 2005).

2.4.5. Massachusetts Institute of Technology (MIT) Model

In the forest canopy, the structure of canopy also provide partially coherent scattering by different canopy components in the microwave domain. The RT model developed in the Massachusetts Institute of Technology (MIT) is based on clustered vegetation structures with reference to the relative phase information associated with structured scatterers (Yueh et al. 1992). This model involves calculation of scattering function of each scatterer by incorporating the phase interference of scattered field from each component/ parts.

At P-band, HH-polarisation channel has been mainly contributed from trunk/ground double bounce scattering where the backscatter is sensitive to trunk radius and density. VV- and HV-polarisation channels on the other hand, are being dominated by branch scattering from the crown. Backscatter prediction using MIT model has seen a good agreement with AIRSAR backscatter at P-band sensitivity to forest AGB in Landes pine forest of France (Beaudoin et al. 1994, Hsu et al. 1994). The strongest relationship of biomass/HV-backscatter in this maritime pine could possibly be due to the strong relationships between biomass in each canopy parts i.e., the crown, trunk and total AGB and branch diameter being the best predictor of the biomass of single branch or total canopy in this study site (Beaudoin et al. 1994).

2.4.6. Karam Model

The RT backscatter model developed by Karam et al. (1995) at the University of Texas, contains non-diagonal extinction matrices that account for the differences in propagation constants and the attenuation rates between the vertical and horizontal polarisations. This model was developed to simulate second-order radiative transfer equation for layered vegetation to account for the inner layer and inter-layer double-bounce scattering. The canopy layer can be represented up to three layers,

with the branches and leaves (or needles) within each layer being represented by randomly positioned finite-length dielectric cylinders. Different scatterer types with 20 maximum can be represented by randomly oriented distribution having different dielectric properties.

At P-band, HH- and VV-polarisation channel exhibit from the long branches and trunk/ground interaction particularly in young trees while only contribution from branch dominates in older trees. Only long branches seem to be dominant contributor to cross-polarisation channel for all ages. At L-band, scattering from twigs and branches are the main contributors to both co- and cross-polarisation channels. At C-band, both co- and cross-polarisation channels are dominantly arises from needles. Comparisons of the multi-frequency SAR backscatter against model predictions for both forest age and biomass from pine stands of Les Landes forest, France showed good agreements (Karam et al. 1995).

2.4.7. Cylinder Model

Cylinder model consists of a rough dielectric surface upon which a layer of trunks and branches are randomly distributed without the leaves, needles and twigs components (Durden et al. 1989). This model being developed for conifer species at L-band frequency assumed twigs and needles to be neglected due to their insensitivity to the polarisation signature at low- frequency. This model could construct the complete set of amplitude scattering matrix and Stokes matrix utilising the magnitude and phase at four polarisations.

The model indicates smaller backscatter from the trunks than total backscatter due to the other mechanisms for the selected forest type. This study also shows the strong dependence of the orientation of the cylinder to the backscatter return (in this case cylinder is oriented normal to the incident angle). At incidence angle ~ 45 to 50° , near vertical orientation of the standing trunk showed low backscatter returns with maximum scattering being directed towards the ground resulting to double-bounce scattering. On the contrary, backscatter from branches is much stronger than from trunks due to the varying orientation of the branches. Therefore, a dominant branch scattering or the double-bounce mechanisms may exhibit depending on the surface condition and tree density using this model and found good agreement against observed SAR data.

2.4.8. A 3- Dimensional Model

This model takes into account the spatial distribution of individual trees in a forest stand as a function of different canopy components comprising of crown and trunk. A layer of underlying forest floor represented by ground layer is modelled with gap component determined by the different shapes, sizes and orientation of individual trees. Five levels of backscatter returns were derived from crown, trunk and ground layers based on time interval of radar pulse.

Model simulations suggest that at longer wavelengths P- and L-band, strong backscatter arises from trunk/ground double-bounce backscatter due to the flat surface. However, the backscatter attenuation from canopy components (leaves, branches and twigs) increases from low to high frequency bands. VV-polarisation channel shows stronger backscatter than HH- and HV-polarisation channel resulting to weaker scattering from the lower part of the crown layer. Finally, comparison of the A 3- Dimensional model derived and AIRSAR backscatter reveal significant and positive results for all frequencies (P-, L- and C-band) and polarisations (highest for L-band) over the hemlock forest stand in Maine, USA (Sun and Ranson 1995).

From the above available literatures on different microwave canopy scattering models, there is a general reflection that low frequencies at P- and L-band exhibited a stronger scattering from forest canopy than high frequencies X- and C-band. The co-polarisation channel (HH- and VV-) exhibited stronger scattering than cross-polarisation channel in almost all the models. This strong scattering from both co- and cross polarisation channels are predominantly arises from interactions between trunks, large branches and ground surface across the incidence angles and from low to high frequencies. The radiative nature of S-band frequency in forest ecosystem is relatively mysterious due to low S-band data availability and conflicting results in few studies.

2.5. Mapping of forest/ non-forest cover

Approximately 47% of the Earth's land surface was assumed to be covered by closed forest about 8000 years ago based on numerous global and regional

biogeographic information (Billington et al. 1996). Following the Industrial Revolution, nearly 30 % of the world's land area is forested due to wildfires, drought, logging and large-scale deforestation particularly in the tropics (Shvidenko et al. 2005). Within this area, different forest types occur based on climatic (at global), soil, topography and disturbance factors at landscape level (Pan et al. 2013). They also constitute about 80 % of terrestrial AGB as a function of forest growth (e.g. regeneration) and mortality (e.g. logging, deforestation) (Shvidenko et al. 2005). The extent of losses in forest area and forest biomass (productivity) caused by human activities has been progressively substantial resulting to significant greenhouse gas emissions and regional to global climate changes and carbon budgets (UNEP et al. 2009). Therefore, accurate measurement of the forested areas and spatio-temporal variations in the biomass of these forests at local, national to global scales are needed. This includes development of accurate forest cover monitoring algorithm and data products essential for monitoring and management of forest (Hansen et al. 2008). However, the accuracies related to mapping forest types and density cover varies depending on the type of tools and methods used.

The United Nation's Food and Agriculture Organization (UN FAO), provides estimates of global forest cover at 5-10 year intervals since 1946 based on national statistics but complemented by remote sensing data (FAO 2012a, FAO 2012b). Remote sensing technology can provide a robust and continuous data on existing forest areas because of its synoptic observation having different sets of spectral, spatial and temporal information (Cihlar 2000, DeFries et al. 2007) given the cost and time of field inventory data. Additionally, the vegetation structure information retrieved by remotely sensed data can also be used as prospective inputs to ecosystem models for testing model predictions and to calibrate models (Hurtt et al. 2010). Therefore, in most of the maps showing areas of forest and non-forest (F/NF) at regional to global scale, use of optical remote sensing data is the primary source with reliable accuracy achieved but seems to be in-complete (GOFC-GOLD 2010).

Over the past decades, different forest cover maps at continental to global scales have been developed. In major global forest cover mapping programmes, different finer (e.g. Landsat, SPOT) to medium (e.g. MODerate Resolution Imaging Spectrometer: MODIS and Medium Resolution Imaging Spectrometer: MERIS) to

coarser (e.g. Advanced Very High Resolution Radiometer: AVHRR) spatial resolutions with optical sensors are widely used (Arino et al. 2008, Kim et al. 2014, Hansen et al. 2013, Bartholomé and Belward 2005, DeFries et al. 1998, Defries and Townshend 1994, Friedl et al. 2010, Loveland et al. 2000). Recently, two studies have demonstrated the feasibility of finer spatial resolution Landsat data in assessing the forest cover and change (annual forest gain and loss) at global scale between 2000 and 2010 (Hansen et al. 2013) and between 1990 and 2000 (Kim et al. 2014).

All the optical derived products are generated for a single year or period due to persistent cloud cover. Secondly, optical data are primarily sensitive to top-most layer of forest canopy due to shorter wavelength resulting to spectral reflectance, absorption and transmittance from leaves and canopy components. Despite its capabilities, optical data are basically sensitive to cloud cover, atmospheric aerosol and low solar illumination particularly in the tropics and higher latitudes respectively. Because of the spectral sensitivity to weather conditions and finer to coarse spatial with low to high temporal resolutions, the existing global F/NF data revealed considerable disagreements particularly between different forest types and in mixed vegetation classes (forest to herbaceous types) and uncertainties across spatial scales (Giri et al. 2005, Herold et al. 2008, Herold et al. 2006, Jung et al. 2006).

Microwave sensors such as SAR have emerged as a complementary tool for a reliable and more accurate mapping of forest cover and its changes due to their cloud penetration and weather independent (Lefsky and Cohen 2003). However, the utility of SAR data in forest cover are varied, and at times controversial. These includes: (1) lack of long-term SAR data from space-borne radar systems; (2) lack of appropriate methodology at different scales; (3) difficulty in interpreting radar backscatter data due to sensitivity to structural, geometric and volumetric scattering particularly at low frequencies (Simard et al. 2000). For instance, single polarisation X-band data show limitations in the separation of forest classes particularly in tropical secondary forest (Castro et al. 2003).

Studies utilizing TerraSAR-X data suggest that satisfactory results for land cover particularly forest classifications can be achieved using multiple polarisations. Therefore, polarimetric multi-temporal X-band SAR from TerraSAR-X have

achieved high accuracy in forest classification in the temperate forests of Germany (Breidenbach et al. 2009). Even, synergistic use of TeraSAR-X data with high resolution LiDAR data have achieved high accuracy reaching up to 90% in forest mapping in Austria (Perko et al. 2011). However, single polarisation X-band SAR based bistatic coherence from TanDEM-X have been investigated for mapping forests and other land cover classes in a tropical peat land area of Indonesia (Schlund et al. 2014). This study could also differentiate open from closed forest canopies where classification accuracy of 85% overall accuracy was achieved using coherence and textural information.

On the other hand, SAR sensor with low-frequency L-band is preferably utilised in mapping forested areas more accurately at regional to global scale. This is evident in international science application projects, for example the Global Rain Forest Mapping (GRFM) (Rosenqvist et al. 2000) in the tropical rainforest of South America, Africa, Asia and Australia; Global Boreal Forest Mapping (GBFM) (Rosenqvist et al. 2004) in Canada, Siberia, Europe and Central Africa Mosaic Project (CAMP) (Malingreau et al. 1997) in Africa etc.

In South American Amazon basin, Japanese Earth Resources Satellite (JERS-1) mosaic data acquired during dry and wet seasons with 100 m spatial resolution have successfully mapped 14 land cover types including mature and secondary forest based on mean backscatter and first order textural information achieving 78% accuracy level at 1 km scale (Saatchi et al. 2000). Seven first order textural features were computed and used to separate different classes based on a statistical distance with B-distance or the Jeffries-Matusita distance. They have used a two-stage classifier based on a posterior MLC technique and decision rules on both MLC and texture measures resulting to sensitivity to structure, biomass and moisture content (dry season) and inundated vegetation (wet season). Furthermore, Podest and Saatchi (2002) have demonstrated that 100 m mosaic JERS-1 backscatter and texture information can also be reliably suitable for mapping F/NF and the flooded vegetation with very high accuracy (>90%) level.

On a regional scale mapping, for example in the Central Africa of Gabon, Simard et al. (2000) have reported the potential of the JERS-1 data in discrimination of

different land cover classes particularly urban, swamp, temporarily/ permanent flooded vegetation, woody savanna, grass savanna, forest, open forest and raphia at an overall accuracy level of 80%. This study is based on decision tree classifier scheme utilizing multi-scale amplitude backscatter and textural information being extracted from JERS data. Amplitude backscatter data could classify different land cover such as savanna, forests and flooded vegetation while discrimination of different flooded vegetation classes such as permanent flooded vegetation, low mangroves and raphia are easily done using texture measures. The possibility of classifying the coastal vegetation is possible due to the explicit nature of temporal changes in the decision tree structure.

Likewise, using the similar methodology based on a decision tree classifier and the decision tree diagram, large scale mapping of flooded areas utilizing the combined L- and C-band data (Simard et al. 2002). This study could discriminate high and low mangroves and flooded forest in Gabon at 84% overall accuracy level against 66% (L-band) and 61% (C-band) alone. Similarly, fusion of 100 m mosaic L- and C-band from JERS-1 and ERS-1 having different incidence angles have demonstrated the potential mapping of lowland rain forest, permanently flooded forest and periodically flooded forest with 76.3% overall accuracy level (Mayaux et al. 2002).

The SAR data from the Phased Arrayed L-band Synthetic Aperture Radar (PALSAR) sensor from the Advanced Land Observing Satellite's (ALOS) is better than its predecessor JERS-1 for studying forest characteristics due to its similar wavelength with additional multiple polarisations, varying incidence angles and higher spatial resolutions. Additionally, L-band data having greater penetration level of forest canopies and weaker scattering from rough surfaces. For example, HV-backscatter PALSAR data have demonstrated the capability of producing 25 m global F/NF cover maps from 2007 to 2010 achieving around 85% overall accuracy (Shimada et al. 2014). This study used region-specific threshold values of HV backscatter coefficients as forest and non-forest have larger differences in HV gamma naught than those in the HH-channel. They found a stable temporal backscatter between 2006 and 2010 from F/NF in both HH and HV polarisations at global scale. Finally, it is estimated that forest cover during the study period decreased to 1.62 million hectare (around -0.042%) (Shimada et al. 2014).

At regional scale, in the Sumatra Island of Indonesia with varying topography, flat swampy lands and extensive tropical rain forests, Fine Beam Single (FBS) PALSAR data have demonstrated its capability in discrimination of forest cover from non-forest achieving around 79.34% overall accuracy and Kappa coefficient = 0.51 (Thapa et al. 2014). They utilized multi-resolution image segmentation (to minimise forest heterogeneity) and threshold (based on backscatter and object shape homogeneities) techniques. Having the threshold fitting with HV-polarisation at -11.5 dB has found good correspondence against reference data producing 65% (forest) and 86% (non-forest) producer's accuracy. Later, multi-temporal Fine Beam Dual polarisation (FBD) PALSAR data have also shown good discrimination of palm plantation against mature forest based on MLC algorithm with an accuracy level of 97% (Kappa coefficient of 0.64) (Morel et al. 2011). This study was conducted in the tropical forest and oil palm plantation in the Sabah province of Malaysia (Southeast Asia) where they found a significance decrease in the accuracy by adding a logged forest class to the classification.

Similarly, utilising 50 m ortho-rectified FBD PALSAR mosaic forest cover map of the year 2009 for Southeast Asia was generated (Dong et al. 2012). The methodology for forest cover map is based on HH, HV, HH/HV and HH-HV PALSAR threshold values and decision tree method attaining a high overall accuracy of 93.3% and a Kappa coefficient of 0.9 at 50 m resolution. Cross-validation against 300 m MERIS derived GlobCover, 500 m MODIS Land cover MCD 12Q1 data and FAO FRA calculations revealed closest spatial agreement to the FAO FRA 2010 estimates having detail and high spatial information with high accuracy (88% producer's accuracy and 95% user's accuracy) than Globcover and MCD12Q1 forest maps.

In addition to SAR backscatter, texture information was found to be most important useful property of SAR data at different wavelengths for classification of tropical primary forest (van der Sanden and Hoekman 1999). This study cover primary forest, selectively logged forest, secondary forest and other land cover classes of tropical forest in Guyana and Colombia where identification of primary forest required three C-, L-, P-band; secondary forests and logged forests with two C-, L-,

and/or P-band and non-forested areas using either single L- or P-band channel. Use of texture features in mapping different forest types have also been covered in Brazilian Amazon (Podest and Saatchi 2002, Saatchi et al. 2000) and Central Africa (Simard et al. 2000).

Studies have also shown that combination of optical and SAR data provides complete and complementary information which increases the accuracy level of land cover classification (Ban et al. 2010) as SAR derived forest maps would have some noise introduced by soil moisture and complex environment. For instance, in the large scale forested area of Brazilian Amazon, mapping of evergreen forest at 500 m spatial resolution is carried out by integrating L-band PALSAR and MODIS vegetation index data (Sheldon et al. 2012). In this, PALSAR based forest map is derived based on HH, HV and HH/HV ratio and decision tree framework with threshold while temporal profile analysis of Land Surface Water Index (LSWI) provides the MODIS derived forest map. The combined evergreen forest map based on spectral properties from MODIS and structural properties from PALSAR corresponds to approximately 96.7% agreement between PALSAR-derived and MODIS-derived forest maps.

Furthermore, to support Reducing Emissions from Deforestation and forest Degradation (REDD) over tropical forest of Southeast Asia, integration of high resolution 50 m mosaic PALSAR and MODIS NDVI at 250 m data have demonstrated the potential mapping F/NF cover at 50 m spatial resolution in large-scale areas of China reaching an overall accuracy of 96.2% and Kappa coefficient of 0.9 (Qin et al. 2015). This study utilizes similar methodology of Dong et al. (2012) working on decision tree classification algorithm using signatures from PALSAR backscatter data. The accuracy of this PALSAR-MODIS NDVI derived map shows a good linear relationship against forest maps of China National Forestry Inventory, Japan Aerospace Exploration Agency (JAXA) and Food and Agriculture Organisation's Forest Resources Assessments (FAO FRA).

While most of the SAR based forest mapping has used X-, C-, L- and P-band data, current knowledge about the suitability of S-band for mapping forest cover is very limited. For example, few recent studies have investigated S-band SAR data

acquired by Airborne demonstrator on vegetated areas in the UK test sites. This includes the study conducted by Guida et al. (2012) who demonstrated good classification of six different crop canopies using S-band data and H/ α and Pauli's polarimetric decomposition techniques. This study was conducted in the agriculture crop areas of Marlborough near Savernake forest in southern England. Similarly, S-band backscatter appears to have high sensitivity to forested areas using H/ α and Pauli's polarimetric decompositions than the X-band backscatter (Natale et al. 2012). The test site is located in the forested areas of Baginton site of southern England. Using the Pauli's decomposition technique, S-band backscatter appears to produce larger volume scattering from the forest canopy than the surrounding non-vegetated areas in comparison to X-band backscatter.

Additionally, study by van Beijma et al. (2014) have demonstrated the capability of airborne X- and S-band SAR data in mapping detailed salt marsh vegetation habitats in combination with elevation and optical data. This study was conducted in the Loughor Estuary of the Gower Peninsula in Wales where a mixture of different vegetation occurs in different zonations. The methodology consists of analysing 30 spatial variables including X- and S-based different polarimetric decompositions in a Random Forest classifier. This study shows that the differentiation of different vegetation habitats was better with S-band (overall accuracy of 78.2%, Kappa coefficient = 0.71) while X-band provided the best vegetation extent information (overall accuracy of 91.55%, Kappa coefficient = 0.83). Yet, there have been no studies on the capability of S-band SAR backscatter in mapping forest cover and changes in the temperate region of wider European region including the UK sites.

2.6. Identification of forest degradation, clear-cut and forest fire

Remote sensing as a tool can be used for a consistent monitoring of degradation inside forest due to larger area coverage and as frequently as possible even in inaccessible areas with time and cost effective. However, remotely sensed data can only be effective provided ground based information related to degradation of forest is supported. This is because identification of degradation in terms of size (small) and rate (gradual) is not easy using remote sensing data alone but often requires contemporary field data (Rosenqvist et al. 2003). Also, information related to C

emissions from forest degradation is even more challenging than the extent of degraded areas (Souza Jr et al. 2005) because forest biomass cannot be directly measured from space through remote sensing techniques (Woodhouse et al. 2012).

In spite of the above limitations, several studies have reported identification of forest degradation. For example, study with X-band single-pass utilizing TanDEM-X satellite can discriminate open forest (as a proxy of degraded) from closed undisturbed forest and have achieved an overall accuracy of 85% and Kappa coefficient of 0.84 (Schlund et al. 2014). It was carried out in the peat swamp forest in Central Kalimantan, Indonesia where areas of open to closed canopy forest, grassland, shrub land and wetlands exist. This level of accuracy was achieved using bistatic system based on interferometric coherence and textural information with feature selection process in comparison to both monostatic acquisition and bistatic scattering coefficients. The bistatic coherence was primarily due to volume decorrelation of forest canopy constituents and closely related to the canopy structure information in comparison to bistatic scattering coefficients.

In the Tapajos region of Brazilian Amazon, single JERS-1 imagery have been reported to detect primary forest and disturb areas (non-forest, regenerating forest) with 91.4% and 73% accuracy level for both disturbances (Grover et al. 1999). The site is a primary forest having many cleared land and different age class regenerating forest. This study uses different techniques of speckle reduction where simulated annealing has reported to be best algorithm for JERS data and could discriminate areas of forest disturbance from primary forest by their lower backscatter. This result is being supported with model predictions using MIMICS-I model. Similarly, monitoring of primary forest, secondary forest, pasture-crops and deforestation in Brazilian Amazon have been conducted based on supervised Bayesian algorithm with the Shuttle Imaging Radar-C (SIR-C)/X-SAR satellite data (Saatchi et al. 1997). This classification has achieved around 72% overall accuracy level with increased up to 87% when only three land cover classes are taken in account particularly regrowth-disturbed forest areas.

SAR backscatter relationship with plantation has also been investigated utilizing multi-temporal JERS-1 data (1992-1997) (Takeuchi et al. 2000). This study has found the multi-temporal L-band data in monitoring the process of plantation (initial

stage of development up to maturity) as a function of dynamic variability of backscatter changes. They observed decreased backscatter intensity around -4 to -6 dB corresponding to early stage of plantation while post fire or deforestation producing a strong and increased 4-6 dB due to single-bounce scattering from felled trees (e.g. trunks). This result was cross-validated using optical high resolution SPOT data. The site is a tropical primary forest with swamp forest and plantation accompanied by burnt felled trees in the southern Sumatra Island of Indonesia.

Using the AIRSAR L- and P-band SAR data with Cloude-pottier decomposition technique have demonstrated the possibility of detecting forest degradation levels (Trisasonko 2010). This study works on the premises that intact forests having high Entropy value due to strong volume scattering mechanism while low Entropy values due to increasing single random scattering mechanism from degraded landscape having dead stands without leaves or branches. The site is a dense tropical forest of Indonesia covering diverse ecosystem with valuable timber species and mangroves in the coastal areas. The study used Support Vector Machine supervised classification technique for generating land cover map depicting intact forest and levels of degradation on the basis of Entropy values being decomposed by Cloude-Pottier technique.

For discriminating forest and deforested areas, multi-temporal JERS-1 with segmentation process was utilized through comparing post-classification (imageries separately) against pre-classification (all imageries) techniques (Thiel et al. 2006). This study was carried out in five different test sites of temperate (Germany, UK and Sweden) and boreal (Russia) with different management practices of clear-cutting in all sites except Germany with thinning operation. The pre-classification method outperformed with an accuracy level of 90% for both forest cover and logging operations. Using the advanced L-band PALSAR sensor in bi-temporal FBD mode have detected the clear-cuts of forest achieving 90% accuracy with RMSE<10% particularly around the edges of the clear cuts (Pantze et al. 2014). This study uses polynomial based histogram matching for radiometric normalization, initial change detection with amplitude ratio thresholding iteratively and Markov random field (spatial, spectral) based change detection in an automatic unsupervised change detection approach. It was carried out in two clear-cut areas of hemi-boreal and boreal forest of Sweden with known recent clear-cuts using SPOT data.

In the central Mozambique region of African ecosystem dominated by miombo woodland, mapping of carbon flux due to small-scale deforestation and forest degradation using FBD mode PALSAR backscatter combined with 90 m Shuttle Radar Topography Mission (SRTM) elevation data have been investigated (Ryan et al. 2012). This study utilizes a methodology where PALSAR backscatter being regressed and bootstrapped based on 96 field plots with threshold to generate temporal AGB maps (carbon). They reported a reduction in forest biomass from 2007 to 2010 from forest degradation contributing 67% but at high uncertainty level.

Other studies utilising the synergy of PALSAR and optical data have also reported promising results. For instance, FBD PALSAR and Landsat data between 2007 and 2010 have demonstrated mapping of deforestation and degradation with an accuracy level of 88% and 89.3% respectively (Reiche et al. 2013). It was carried out in the rich tropical forest having high deforestation and degradation in Central Guyana. The study works on detecting forest degradation at sub-pixel level using Landsat while classifying forest and deforestation with PALSAR data based on decision tree algorithm and feature threshold using normalized Jeffries-Matusita distance.

In Lucas et al. (2006), the integration of AIRSAR L-band and Landsat-derived foliage projected cover data by simple thresholds showed possible mapping of woody regrowth. This study was conducted near Injune in Central Queensland (Australia) where areas of forest cover, agricultural clearings and woody regrowth dominated by *Acacia harpophylla* exists. However, the discrimination of woody regrowth using individual Landsat or SAR data was not possible. Additionally, study was carried out in differentiation of early-staged regrowth from mature forest using PALSAR backscatter and Landsat-derived foliage projective cover data (Lucas et al. 2014). This study was conducted in the Brigalow Belt Bioregion of Queensland, Australia where different stages of growth exists dominated by brigalow (*Acacia* species). User's and producers' accuracies for early regrowth corresponds to 81% and 69% while combined mature to intermediate stage forests with lower accuracy achieving 71% and 89%.

Fire eliminates vegetation cover, its component and also reduces moisture content due to damaged foliage and canopy components. Radar backscatter intensity is sensitive to structure, scattering components and moisture condition of the vegetation

canopy. Because of the changes in vegetation canopy components and moisture condition due to fire, this in turn, results in changes in both backscatter intensity and phase. For example, the dominant volume scattering from typical healthy vegetation canopy decreases as a result of randomly single and surface scattering from the open canopy and exposed ground surface. Therefore, the moisture condition and roughness of the ground surface will play an important contributor to the backscatter return. Studies have shown that longer wavelengths are sensitive to variations in the moisture and surface roughness of soil (Shi et al. 1997) and vary as a function of incidence angle (Rahman et al. 2008). For example, SAR backscatter increases with increasing soil moisture ranging between 0 and 40% (Baghdadi et al. 2007) following a logarithmic function (Ulaby et al. 1986).

Several studies have reported the dynamic backscatter changes due to fire-affected forested areas utilising multi-temporal SAR data. The study conducted by French et al. (1996) have found backscatter from recent forest fire to be influenced by the canopy damage, moisture condition of soil and regrowth status in post-fire. They reported strong changes in the backscatter of 3-6 dB with C-band SAR from ERS-1 from burnt scars in Alaska boreal forests that relates to the moisture condition of the soil. Additionally, using the multi-temporal ERS-1 data acquired before, during and after fire season in East Kalimantan, Indonesia (1997-98), Siegert and Ruecker (2000) found a decrease of 2-4 dB in backscatter due to fire under dry condition in comparison to unburned areas. Because significant backscatter intensity differences between burned and unburned areas was observed in dry weather conditions. In this, significant decrease of backscatter up to 5.5 dB was recorded after fire from non-forest and plantation areas due to maximum soil exposure with scattering from the unburnt canopy structure in comparison to fire affected forested areas.

In the Mediterranean region, few studies have attempted to establish radar backscatter relationship with fire disturbances. For example, comparison of X-, C- and L-band with burn severity estimates derived from Landsat data and field measurements have been investigated (Tanase et al. 2010). The study highlighted the co-polarisation backscatter increased with burn severity for shorter wavelength while opposite for L-band backscatter to higher soil moisture condition, resulting to distinguish between unburned and highly burned forest at X- and C-band. They found that cross-polarisation backscatter showed better relationship with burn

severity estimation for both C- and L-band data. From the modelling perspective, the radiative nature of the C-band backscatter from burned pine canopy was investigated utilising a discrete scattering model (Kalogirou et al. 2014). The predicted backscatter changes was found to be highly related to the changes in soil moisture, increased exposure of surface and canopy damage by fire. Therefore, the impacts of fire in forest appears to be mainly governed by the reduction in the canopy components (leaves, twigs, branches) from the imaging microwave perspectives (Kalogirou et al. 2014, Tanase et al. 2010).

Detection of forest degradation, clear-cut or fire scar using S-band SAR sensor is very uncertain due to limited radiative knowledge of S-band backscatter to forest canopy. Even the S-band backscatter responses to varying levels of processes involved in degradation, clear-cut or intermediate is very limited and may provide high ambiguity. Few studies have highlighted positive results utilising S-band SAR from Russian Almaz-1 satellite to be superior to ERS-1 data in discrimination of clear felled against forested areas (Yatabe and Leckie 1995). This study was conducted in mixed coniferous and broad-leaved forests of Ontario in Canada. In the same way, multi-temporal Almaz-1 have also highlighted higher capability in identifying clear felled against forested areas based on segmentation of homogenous areas using SPOT data (Fransson et al. 1999). The test site is carried out in a boreal conifer belt of northern Sweden where 32 ha of recently clear felled with 464 ha of forested areas. This study has correctly classified clear felled areas ~61.4% using mean textural features derived from first order histogram. Nevertheless, there have been any studies on investigating the S-band SAR backscatter in detection of forest degradation, clear-felled or logged in the temperate forest of the UK region in comparison to other SAR wavelengths.

2.7. Retrieval of forest structure and aboveground biomass

Forest aboveground biomass (AGB) is defined as the sum total of the biomass located in trunks and branches as the main component in a particular stand. On a broader sense, it is a by-product of several ecological and biological processes regulated with climate, soil and disturbance in forest ecosystem. Hence, evaluation of forest AGB is useful as a means to reduce errors in the estimation of global carbon cycle and its fluxes. On a local scale, the stock of forest AGB is usually derived from

ground census through harvesting or tree biometric measurements using sampling plots and empirical allometric model (Brown 1997).

Individual tree AGB is the product of its aboveground volume (m^3) and its average mass density (kg m^{-3}). Individual tree AGB measurements by direct harvesting are expensive and laborious job. Instead, biomass can be reliably estimated using indirect allometry approach. This method works with deriving the allometric equations, i.e., equations relating to field measurements to AGB due to the inter-relationship between the different parameters of a tree (DBH, H, tree species and age). At plot level, AGB refers to the sum of all the individual tree aboveground biomass related to the product of aggregated individual timber volume and average volumetric density in the plot. In fact, allometry based biomass derivation using tree physical properties are not representative of the actual forest biomass (Clark and Kellner 2012).

Aboveground biomass estimation on tree level allometric equations are often associated with errors due to up-scaling to larger areas (Chen et al. 2015), hence larger plot sizes greater than 0.25 ha is required to represent the normal biomass distribution with reduced coefficient variation below 20% (in the case of tropical forest) (Saatchi et al. 2011b). Forest biomass and structural information required are contiguous in regional to global scale; hence direct measurements of forest structure and biomass are far too expensive to be practical. Rather, an approach based on satellite remote sensing to produce spatially contiguous forest structure and biomass maps at finer spatial resolution through extrapolating the ground measurements at the tree level to regional to global scales is required.

Remote sensing is a promising technology to map forest biophysical characteristics at varying scales from landscape, national and continental scales (DeFries et al. 2007, GOFC-GOLD 2010, UNFCCC 2008). For instance, forest stand height has some relationships with SAR backscatter acquired at longer wavelengths for conifers (Le Toan et al. 1992) but this trend is less clear particularly with deciduous stands (Sader 1987). With the shorter wavelength, weak relationship of backscatter to stand height may be primarily governed by the lesser penetration into the canopy due to the crown closure (Sieber and Noack 1986), rather the backscatter is more closely related to the

patterns of the canopy envelope. Moreover, the backscatter intensity is strongly sensitive to the properties of terrain (slope, aspect) and may not be useful for height estimation. Towards this, SAR interferometry (interferometric phase) (Balzter 2001) and high-resolution radar based stand profiling (Hyypä et al. 2000) provides alternative methods for height estimation at X-/C-band.

Forest AGB cannot be directly measured from space, but the biomass estimates based on ground measurements can be calibrated and predictions of biomass using optical reflectance or SAR backscatter can be made (Dong et al. 2003, Woodhouse et al. 2012). A number of techniques and new methodologies for estimating forest AGB based on remotely sensed data have been proposed but is particularly challenging due to complex forest structure (Lu 2005, Steininger 2000). Furthermore, validation of model predicted AGB involves uncertainty and large error being propagated from trees to plots and pixels level (Chen et al. 2015). This is because the ground measured biomass used to calibrate the remote sensing based models are rarely measured directly (Clark and Kellner 2012). Instead, tree physical properties are being used through allometric models.

Despite wide use of optical data for forest characterisation, information on forest 3-D structure and biophysical characteristics are limited. For example, optical data derived Leaf Area Index (LAI) from AVHRR sensors have generated biomass changes in northern forest indicating larger C sink on decadal time scale due to distinct seasonality (Myneni et al. 2001). In the optical data, the dominant scattering behaviour is predominantly governed by spectral reflectance, absorption and transmittance properties of canopy components (upper layer) particularly leaf material, chlorophyll content etc. Because of these properties, optical data are quickly saturated with the complex forest structure and increased growing stock volume/ biomass content. On the contrary, scattering in the microwave domain is mainly controlled by the size, shape, texture and orientation of the larger scattering components in the canopy structure, e.g. branches, twigs and soil roughness as a function of longer wavelength than optical data. Hence, SAR data seems to be an alternative and more promising tool for supporting studies related to forest structure and biophysical parameters retrieval due to more scattering from the canopy components through deeper penetration level in the forest canopy (Imhoff 1995, Lucas et al. 2010).

The SAR backscatter from forest is not solely determined by the forest biological parameters, e.g. biomass but fundamentally dependent on dielectric properties (in particular moisture content) of canopy components and forest structure (size and orientation of leaves, branches, height, stand density) (Imhoff 1995, Lucas et al. 2010, Rosenqvist et al. 2007, Woodhouse et al. 2012). Moreover, the backscatter to biomass relationship and level of saturation is also dependent on the structure and nature of the forest (density and size) under observation and vary across environmental conditions (Woodhouse et al. 2012). For example, Lucas et al. (2010) has revealed better estimation of PALSAR derived AGB from forest and woodland during minimal surface moisture content due to highest backscatter dynamic range within large-sized and stem density in Queensland, Australia. On the contrary, study conducted in the primary and degraded tropical forests of Central Kalimantan, Indonesia, Enghart et al. (2011) have misrepresented relationship of AGB up to 600 t/ha using combined multi-temporal TerraSAR-X and PALSAR data. However, this result draws special attention from a wider SAR community (Woodhouse et al. 2012) supported by modelling perspectives (Woodhouse 2006b, Broly et al. 2012).

Recently, two biomass maps focusing on tropical forest of South America, Africa and Southeast Asia have been published at 500 m (Baccini et al. 2012) and 1 km (Saatchi et al. 2011a) resolutions utilising LiDAR data from the Ice, Cloud and Land Elevation Satellite (ICESat) Geoscience Laser Altimeter System (GLAS) with MODIS and Quick Scatterometer (QuickSCAT) radar data respectively. Comparing these biomass maps revealed substantial differences particularly in areas with limited field data (Mitchard et al. 2013). Large differences are found in forested areas at country level while, greater agreement at regional to biome level.

To further validate these biomass maps at regional scale, a large independent field data from the tropical forests of the Amazon basin was utilized and found significant spatial variations in forest structure and biomass with over- or under-estimated by > 25% at basin level (Mitchard et al. 2014). This study has highlighted that remotely sensed data cannot reliably measure woody density or species assemblages. On the contrary, Saatchi et al. (2015) have claimed that estimation of regional biomass variation based on random and limited ground-based forest inventories can be unrepresentative, yet regional biomass estimation can be achieved by spatially resolved, systematic and repeated measurements of forest structure via remote

sensing techniques with ground data. These studies have highlighted the importance and lack of data integration from multiple sources.

There are many regression based studies in which the relationship between forest biophysical characteristics and SAR backscatter at varying wavelengths and polarisations has been investigated. For this research, only those studies conducted in boreal and temperate sites are covered.

Shorter wavelength X-band data in interferometric mode (InSAR) have been found to relate with mean stand height and stand top height with high accuracy of 2.5 m and 2.9 to 4.1 m respectively (Balzter et al. 2007a). From the InSAR data, scattering phase centre height is being estimated using elevation terrain model and surface model while stand top height is estimated from the yield class models of the Forestry Commission. The site is a temperate pine managed forests of Thetford Forest, UK. Additionally, Balzter et al. (2007b) have presented forest canopy height mapping based on dual-wavelength InSAR at X- and L-band achieving an accuracy of 3.49 m error against LiDAR height model. In this study, the terrain elevation model is derived using L-band interferometry while the surface height model is derived using X-band interferometry based on the different scattering phase centres. This site is deciduous woodland of Monks Wood Nature Reserve in the UK comprising of different vegetation type and density.

In recent times, researchers are also focusing on forest canopy profiles for stand height estimation utilising very high resolution active scatterometer. For instance, Hyyppä and Hallikainen (1993) used the Helsinki University of Technology Scatterometer (HUTSCAT) mounted on a helicopter to measure the forest canopy profiles based on the range difference between maximum backscattered power as a function of distance to the sensor (along the flight line). This study was carried out in the pine and spruce forests of Finnish Forest Research Institute in Helsinki. They found a significant correlation of $R^2 = 0.9$ and 1 m Standard deviation for both Lorey's mean and dominant tree height of 100 tallest trees particularly pine with C-band frequency. Later, retrieval of forest stand mean height and stem volume was compared based on various remote sensing data estimates (Landsat, SPOT, hyperspectral AISA, ERS-1/2 Tandem and HUTSCAT) (Hyyppä et al. 2000). This study found that radar-derived stand profiles at C-band frequency based on

HUTSCAT obtained with 100 m spacing was the most appropriate data to mean height ($R^2 = 0.77$, Standard error of 2.97 m) and stem volume ($R^2 = 0.68$, Standard error of 55.7 m³/ha) retrieval.

Similarly, using the same methodology, prediction of mean height with improved accuracy of 1.6 m ($R^2 = 0.88$) and stem volume of 31 m³/ha ($R^2 = 0.85$) at stand level was achieved based on C- and X-band derived stand profiles (Hyyppä et al. 1997). This study also reported that stand profile at X-band appears to be highly significant to mean height due to higher attenuation at X-band through low penetration capability relative to C-band data. Furthermore, in the southern Finland, TerraSAR-X stereo SAR data have been used to predict plot stem volume up to 400m³/ha and RMSE = 34%. This result is based on forest variables calculated with 109 circular sample plots where average H and DBH were also correlated with RMSE equivalent to 14% and 19.7% respectively (Karjalainen et al. 2012).

Multi-temporal C-band from ASAR sensor have highlighted an improvement in the retrieval of growing stock volume up to 300 m³/ha and RMSE between 34.2% and 48.1% at 1 km scale in boreal forest (Santoro et al. 2011). This study was performed in the boreal forest of Central Siberia (Russia), Sweden and Quèbèc (Canada) utilising coarse resolution ScanSAR mode at 100 m and 1 km resolution based on BIOMASAR retrieval algorithm being calibrated with Water Cloud Model. Recently, using the similar methodology with hyper-temporal ASAR data, estimation of forest growing stock volume in the wider region of the northern hemisphere has been conducted at 1 Km resolution (Santoro et al. 2015). A least uncertainty in the boreal and temperate forest while sub-tropical forest having the largest is being recorded particularly in regions with very high stock volume and fragmented forest landscapes having an average RMSE 29%.

There are some studies utilising the coherence data acquired by ERS-1/2 and in combination with JERS-1 data. For example, Drezet and Quegan (2007) have estimated the forest AGB as a function of forest age structure predicted by C-band ERS Tandem coherence. In this, C-band coherence data is calibrated using the forest age GIS data of Britain and Water Cloud Model predictions at forest stand level. This study provides radar-derived forest age structure of Britain covering nearly 3 million

hectares of forest with age and biomass information at individual forest stands level. During the period of investigation in 1995, forest carbon uptake was predicted three times higher than the national inventory estimates.

In the boreal region, Wagner et al. (2003) have investigated mosaics of C-band ERS-1/2 Tandem coherence and L-band JERS-1 to determine the growing stock volume of Siberian boreal forest. They have developed an adaptive empirical model calibrated using forest inventory data from 38 sites to classify growing stock volume classes based on coherence and backscatter data. The classification algorithm for volume interval classes was made on the basis of the ecological and commercial attributes of the Russian Forestry Services. The forest classes identified were open or ≤ 20 m³/ha (early re-growth), 21-50 m³/ha (forest re-growth), 51-80 m³/ha (forest re-growth) and >80 m³/ha (commercial mature forest). This calculated stock volume classes were classified using MLC algorithm and used as input for an iterated contextual classifier. The algorithm has achieved up to 80 m³/ha accuracy level of stock volume at 50 m spatial resolution in boreal forest having volume ranging from 150 m³/ha in the middle taiga to 250 m³/ha in the southern taiga. The classification accuracy is 86% overall accuracy and Kappa coefficient of 0.72 in Siberia site.

Further validation of the algorithm was carried out in temperate pine forest plantation (Thetford Forest, UK), semi-natural boreal forest (Siggerfora, Sweden) and tropical rainforest of Amazon (Rondonia, Brazil) (Tansey et al. 2004). The classification accuracies for forest growing stock volume achieved an average of 70% overall accuracy and Kappa coefficient 0.22 to 0.43 in Siggerfora and Thetford forest respectively.

In the Central Alaska, studies have also demonstrated low moisture content to be important environmental factor responsible for high sensitivity to biomass. For example, Harrell et al. (1995) have demonstrated the sensitivity of SAR backscatter from ERS-1 and JERS-1 data to density, height and total biomass ($R^2 = 0.25$ for ERS-1 and 0.66 for JERS-1). This study was conducted in the 32 boreal forest sites of Alaska where different ABG levels of Black Spruce and White Spruce stand grow. Furthermore, Harrell et al. (1997) have found L-band from SIR-C sensor to be sensitive to the AGB retrieval particularly with HV-polarisation backscatter. This

study being conducted in the pine forests of southern United States has shown that SAR data acquired during dry season achieved better relationship with lowest RMSE for all AGB levels. Combining multi-temporal JERS with Landsat data have shown high sensitivity achieving $R^2 = 0.79$ and improved the saturation level of forest volume in the boreal forest of south-eastern Finland (Rauste 2005). This result was achieved based on the imageries acquired over summer season during the peak phenological growth in boreal forest. Using the JERS data only, a stable and consistent strong relationship (R^2 between 0.4 and 0.66) from over the summer growing season is also evident.

There are also studies using the low frequency SAR data at P-band and L-band acquired by both airborne (e.g. NASA-JPL AIRSAR) and satellite data (ALOS). For instance, in 29 forest sites of boreal forest in Alaska, a strong positive logarithmic relationship was found with the FBD PALSAR backscatter against the forest AGB (Suzuki et al. 2013). This corresponds to a strong relationship of $R^2 = 0.76$ and 0.64 for HV- and HH-polarisations respectively and the sensitivity of HV-polarisation to the forest AGB up to 120.7 t/ha. Similarly, a positive relationship also exists in the HV-polarisation to tree density, height and DBH. Furthermore, in the northern forest of Maine, United States with hardwood-boreal transitional forest having varying levels of forest biomass, SAR data acquired by airborne AIRSAR and space-borne SIR-C/X-band were compared (Ranson and Sun 1997). The results from AIRSAR data were quite better in mapping different broad-leaved forest stands while coniferous stands with SIR-C/X-SAR. Both the SAR data showed a close agreement for biomass estimation where an average biomass densities of 9.7 kg/m² and 9.0 kg/m² being predicted using AIRSAR and SIR-C respectively.

In the northeast United States, Cartus et al. (2012) have estimated accurate AGB based on PALSAR backscatter against Forest Inventory and Analysis county statistics achieving higher correlation with HV polarisation at $R^2 = 0.86$ and lower RMSE of 12.9 t/ha. This study was carried out exploiting the synergy of optical and SAR data to calibrate the semi-empirical model.

In Rauste et al. (1994), AIRSAR and HUTSCAT data collected from the temperate conifer at Freiburg and Helsinki test sites in south-western Germany and Finland respectively were analysed for forest stock volume and biomass. They found the

highest correlation with P-band (HV-polarisation: $R^2 = 0.75$) backscatter and forest volume/ AGB. On the other hand, a strong inverse relationship exists between pine biomass and X-band VV-polarisation in the Finnish test site. In the Flevoland forest region of Netherlands, the AIRSAR data with modelling have shown potential for growing stock volume estimation particularly at longer wavelengths (Israelsson et al. 1994). This site is broad-leaved and mixed species with poplar, ash, oak, maple, willow and beech as the main species. Using AIRSAR data, L- and P-band exhibited a strong sensitivity to stand volume up to 100-200 m³/ha and >200 m³/ha respectively while insignificant with C-band data. At P-band, a strong scattering from the ground/trunk interactions from HH-polarisation channel while direct crown with ground-crown interaction from both VV- and HV-polarisation channels has been predicted using model simulations.

In Baker et al. (1994), radar backscatter from P- and L-band in particular HV- and HH-polarisation channels have shown sensitivity to conifer growing stock volume and stand age at Thetford forest. This site is a managed productive forest with even-aged stands dominated by Corsican pine having timber volumes up to 500 m³/ha (approximately 185 t/ha biomass). The highest correlation coefficient of $R^2 = 0.71$ and 0.65 for P- and L-band respectively (both HV- and HH-polarisation channels) were observed to stand volume.

In Beaudoin et al. (1994) and Le Toan et al. (1992) the sensitivity of the AIRSAR and modelled backscatter on forest AGB in Landes forest in south-western France have been investigated. This site is a large homogenous conifer plantation stand dominated by maritime pine where they have reported the best sensitivity of AGB with the P-band having an estimated biomass error of around 20% than L- and C-band. This result from Landes forest was compared with AIRSAR data from loblolly pine at Duke University Research Forest in North Carolina, United States (Dobson et al. 1992) and found similar results with forest AGB at L- and P-band. In the study by Rignot et al. (1995), the results from Landes and Duke sites were compared from boreal broad-leaved Bonanza Creek experimental forest in Alaska and tropical rainforest Manu National Park in Peru utilising the AIRSAR data and reported 14 to 30% error rates of AGB estimation for these two sites. Finally, Imhoff (1995) have compared the coniferous forest of Landes and Duke against broad-leaved evergreen

of Hawaii utilising AIRSAR data and reported that the sensitivity of forest biomass at C-, L- and P-band were around 20 t/ha, 40 t/ha and 100 t/ha respectively.

The study by Sandberg et al. (2011) have demonstrated better sensitivity of P- and L-band backscatter acquired by the German Aerospace Centre's (DLR) airborne Experimental-SAR (E-SAR) system against forest AGB achieving higher accuracy with least error. This site is a hemi-boreal forest with Norway spruce, Scots pine and Birch tree species in Remningstorp region of southern Sweden. In this study, field sample plot data and high density LiDAR data are being used to obtain reference biomass estimates at 0.5 ha stand level. For L-band, the RMSE were between 31 and 46% and R^2 between 0.4 and 0.6 for HV-polarisation channel. For P-band data, higher accuracy between 18-27% RMSE and R^2 between 0.7 and 0.8 for HH- or HV-polarisation channel was achieved. This finding was further investigated by Soja et al. (2013) who developed a new biomass retrieval model for P-band SAR focussing on varying moisture condition and topographic terrain variations in northern and southern Sweden. This particular study reported the sensitivity of P-band backscatter to forest AGB with much lower RMSE of 22-30% mean biomass using HV and HH/VV ratio backscatter. The sensitivity of model due to topographic variability using SAR data in both sites revealed inconclusive. The P-band SAR based biomass level up to 200 t/ha was predicted with good agreement against LiDAR based in fairly flat Remningstorp site while underestimation of biomass larger than 100 t/ha was found in strong undulating topography Krycklan, north of Sweden.

In most of these studies, HV-polarisation backscatter have found stronger dependence on forest volume and biomass across different wavelength bands primarily due to the largest dynamic range and more level of pulse penetration. This is because scattering elements that change the polarisation of the incoming radar pulse through complex three-dimensional forest structure is easily detected. Although SAR data is often used as the best tool relating to AGB with some level of signal saturation point (Imhoff 1995, Rauste et al. 1994, Saatchi et al. 2011b, Sandberg et al. 2011, Ryan et al. 2012), the backscatter signal does not provide a direct measurement of forest volume or AGB (Woodhouse et al. 2012). This is because radar backscatter is sensitive to different properties of forest canopy

(structural, architecture) and moisture content in a forest ecosystem (Ulaby et al. 1990, Woodhouse 2006b, Lucas et al. 2010, Saatchi et al. 2007).

Model prediction and validation of forest AGB over large area using SAR backscatter would often requires large and independent field estimated biomass information. Moreover, identification of the saturation level to forest AGB at a particular wavelength is often difficult requiring repeated and numerous studies across different forest types. In fact, future research should focus on investigating the factors responsible for forest structure and backscatter to AGB relationship (Woodhouse et al. 2012, Broily and Woodhouse 2013, Broily et al. 2012). This includes the number stand density, level of branching in the canopy layer etc.

Relative to the reported positive results for SAR backscatter and AGB relationships, little work appears to have been done on investigating the S-band backscatter properties of forest. A particular study conducted in the mature oil palm and rubber plantation using JERS-1, ERS-1 and Almaz-1 data have reported good relationship of palm and rubber biomass to L- and C-band backscatter while insignificant relationship against S-band backscatter (Rosenqvist 1996). The study site is selected over Kedah and Penang states of West Malaysia where continuous planting, growth and clear felling of both rubber and oil palm at 20 -25 year cycle is practised with different ages and clear-cuts. The author has used S-band data acquired at standard high incidence angle ($\sim 50^\circ$) and reported that high incidence is likely to be the main factor responsible for poor relationships with palm/ rubber AGB.

Recently, few studies have analysed the S-band SAR data acquired during 2010 Campaign in Britain focusing on classification of agricultural crops, forested areas and habitat mapping in Wales (Guida et al. 2012, van Beijma et al. 2014, Natale et al. 2012) but, none of the studies have investigated the sensitivity of S-band backscatter to forest biophysical characteristics. This research have taken the opportunity to test the sensitivity of S-band backscatter to average tree DBH, canopy H and forest AGB at pixel to stand levels in the temperate mixed deciduous forest of the UK region.

2.8. Current knowledge gaps and research needs

The following research gaps have been identified:

1. The current knowledge of S-band SAR backscatter interactions with forest canopy structure is largely lacking in comparison to X-, C-, L- and P-band.
2. Knowledge of S-band scattering from soil characteristics (moisture content and surface roughness) and forest canopy components based on modelling approach has not been fully investigated and reported.
3. There is a lack of knowledge about the temporal S-band backscatter responses to varying levels of forest degradation.
4. There is no consistent information about the S-band backscatter sensitivity to forest biophysical characteristics (tree DBH, canopy H and forest AGB) and point of saturation to the varying AGB levels.

Through this thesis, an attempt has been made to address these knowledge gaps about S-band SAR backscatter sensitivity in forest ecosystem through data and modelling approach. This includes investigating the radiative nature of S-band backscatter to soil and forest canopy and its potential application to forest/ non-forest cover and change mapping and relating to biophysical characteristics over the mixed deciduous temperate forest of the UK region.

2.9. Research Questions

The research questions addressed for this study were:

1. What is the relationship between soil moisture content and surface roughness and forest canopy (deciduous, conifers) with S-band backscatter across polarisations and incidence angles and in comparison to other SAR frequencies?
2. What is the radiative behaviour of S-band backscatter in varying levels of forest degradation?
3. How accurately can forest/ non-forest cover be classified using S-band backscatter at different spatial scales?

4. Can multi-temporal S-band backscatter be useful for detecting forest cover change?
5. What is the relationship of S-band backscatter with forest biophysical characteristics in particular forest AGB and level of accuracy at varying scales?

2.10. Research Objectives

The objectives of this study were:

1. To examine the contributions of different scattering mechanisms from soil moisture and surface roughness and forest canopies for different frequencies, polarisations and incidence angles based on MIMICS-I model.
2. To investigate the S-band backscatter sensitivity to forest degradation using MIMICS-I simulations.
3. To classify S-band backscatter data to produce forest/non-forest cover and change maps using MLC algorithm and test the accuracy of forest cover maps at varying spatial resolution.
4. To derive average tree diameter, canopy height and forest AGB based on S-band data from 2010 and 2014 acquisitions using field data at pixel and stand levels and cross-validation between observed against predicted levels of AGB at pixel level.

2.11. Summary

There is clear evidence that the atmospheric CO₂ concentration is increasing due to human induced fossil fuel burning, cement production, land-use change particularly deforestation. However, the current and future responses of terrestrial ecosystem to changing atmospheric C and climate at different scales are a matter of current debate across disciplines. Generally, forest ecosystem acts both as a sink and source of CO₂ particularly at regional scales due to changing climate and land-use systems. From a regional to global perspective, satellite remote sensing provides a near real-time and consistent technique to monitor large-scale forest cover and changes due to high

spatial, temporal and spectral/ backscatter sensitivity to forest biophysical characteristics.

Since the last decades, numerous studies have highlighted the potential of SAR data to forest ecosystem due to its insensitivity to cloud cover and low illumination. Furthermore, backscatter at varying wavelengths is showing more sensitivity to forest biophysical characteristics due to more scattering with forest canopy components than spectral reflectance as a result of similar dimension (size and length) of the components (Rosenqvist et al. 2007).

However, the SAR backscatter sensitivity varies across wavelengths, polarisations and incidence angles in different forest types ranging from single to multi-species and in low to high biomass density. Of the different SAR wavelengths, knowledge related to S-band backscatter sensitivity to forest cover and biophysical retrieval has been largely lacking. In order to explore the potential of S-band backscatter to forestry applications, understanding the basic scattering mechanism to forest canopy component is critically important and essential to relate the biophysical characteristics. The use of microwave canopy scattering model serves as a useful and robust tool to interpret this basic scattering at varying SAR wavelengths and canopy structure. This information can thus be used to interpret with imaging SAR backscatter to forest biophysical characteristics.

Chapter 3: Materials and methods

3.1. Test sites

The study sites of Savernake Forest and Wytham Woods were chosen based on the diverse land cover in the regions, being covered by the recent AirSAR Campaign with S-band SAR sensor and supported by ground data in particular forest inventory. Savernake forest was selected because of the mixed deciduous forest and non-forest cover types. The different species of deciduous, conifers and mixed with varying age and growing stock volume existed in forest. The non-forest comprised three classes, i.e., grassland, clear-felled and bare-ground.

During the study period between 2010 and 2014, the forested area is managed with thinning operations while some of the sub-compartments have been completely removed through stand cutting. This stand removal took between December 2012 and July 2013 in few sub-compartments and planted with norway spruce and oak seedlings. Presently, the area is composed of left-over dry leaves, branches and grasses with few dead stumps refer to as 'Clear-felled' class. The second test site of Wytham Woods was selected because of mixture of ancient semi-natural woodland and existence of timber removal with plantation resulting to changing in the species composition.

3.1.1. Savernake forest

Savernake forest (51°23'13"N, 1°43'19"W) is located near Marlborough in southern England (Figure 3.1). The forest is one of the typical ancient woodlands in the country over 1000 years old. It is widely studied temperate forest in the country. The site is overall a flat topography having an average elevation of 107 m and 1 % slope with South-East aspect (Crutchley et al. 2009).

The climatic parameters of the site have been recorded to be approximately 750 mm (annual precipitation) and 11.3 °C (average annual temperature). Geologically, the parent soil material is characterized by Jurassic Clay (Oxford) with Eutric vertisol type of soil, 4.7-6.2 soil pH. Although Savernake forest covers a total area of 19 km² but this research focuses an area of 7.49km² (~749 hectares) covered by the SAR

data. Main deciduous species comprise ancient beech (*Fagus sylvatica*), birch (*Betula pendula*) and oak (*Quercus spp.*) with mixed species of yew, ash, common lime, crab apple, elm, field maple, hazel, horse chestnut, rowan, willow, sweet chestnut and wild cherry. Dominant coniferous species consisted of scots pine (*Pinus sylvestris*), corsican pine (*Pinus nigra*), norway spruce (*Picea abies*) and western hemlock (*Tsuga heterophylla*). Presently, the forest reflects mixed stands of temperate deciduous and coniferous species with varying densities, height, growing stocks, and age classes. The forest is managed by the UK Forestry Commission (FC) for 999 years on leased with sub-compartment of 4 ha average size.

Within the Savernake forest, areas with forest and grassland represent the major land cover. The main grass species found in Savernake are *Lonicera periclymenum*, *Deschampsia cespitosa*, *Poa trivialis* and *Holcus mollis* with different percentage of spatial coverage. A series of management operations have been undertaken in Savernake forest between December 2012 and July 2013. For example, two sub-compartments of varying sizes ~ 3.45 ha and 5.2 ha have been completely clear-felled followed by plantation with nearly 24000 douglas fir and 6000 oak seedlings. Otherwise, most of the sub-compartments were subject to thinning operations to ensure enhanced timber production and regeneration purpose.

3.1.2. Wytham Woods

Wytham Woods (51°47'N, 1°20'W) is situated in the west Oxfordshire in England. The site represents a mixture of ancient semi-natural woodland, UK National Vegetation Classification community W8 *Fraxinus excelsior- Acer campestre-Mercurialis perennis* woodland (Hall et al. 2004) covering approximately 340 ha. The airborne data covers around 248 ha (approximately 2.5 km²) (Figure 3.1). The site has been continuously covered by trees (Peterken and Game 1984) while recently managed by timber removal and plantation (e.g. beech, sycamore) where the species composition (ash and sycamore species) has been or likely to change over time (Morecroft et al. 2008). Since the last decades, it has become one of the most studied temperate deciduous woodland in the country related to ash die-back disease (Kirby et al. 2014), long-term monitoring plots for soil respiration (Fenn et

al. 2010b), aboveground productivity, respiration and leaf production (Butt et al. 2009, Fenn et al. 2010a).

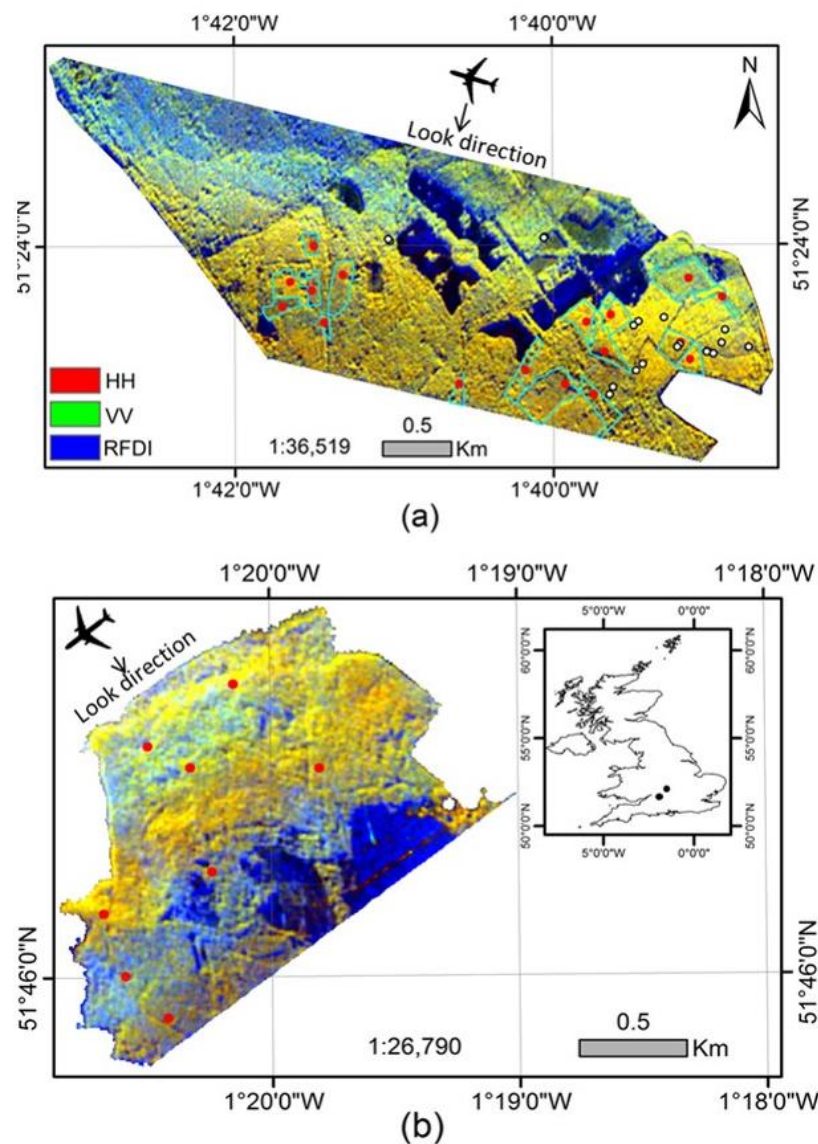


Figure 3.1. 6 m pixel spacing S-band data acquired over Savernake (top) and Wytham (bottom) in 2014 (False colour composite: red: HH, green: VV, blue: RFDI) with sampled compartments (cyan polygon), training plots (red dot in both Savernake and Wytham) and validation plots (white with black dot) (Savernake). Image reproduced with copyright permission from the Airbus Defence and Space, UK.

However, no major silvicultural operation has been carried out in the site over the last decades. The stands are of different ages and biomass levels with ash, birch, sycamore and oak as dominant deciduous species while the ground vegetation is

predominantly dogs' mercury, nettle, bluebells and pendulous sedge. The aboveground forest canopy components particularly leaves and wood production has been observed to be the greatest contributor approximately 60% to productivity in Wytham site resulting to positive net carbon sink in comparison to respiration (Fenn et al. 2010a).

The site is located on topography at an average altitude of 60-179 m. The soil is mostly a stagni-vertic cambisol, derived from clay, with areas of arenihaplic luvisols and calcareic cambisols. Since 1992, metrological data have been recorded on site as part of the UK Environmental Change Network (ECN) monitoring programme (Morecroft et al. 1998). For the period 1993-2012 mean annual temperature was 10°C and mean annual precipitation was 726 mm (Butt et al. 2009, Environmental 2014).

3.2. SAR Data

3.2.1. Airborne SAR Campaigns

In Europe, there exist large national forest inventories which provide an opportunity to investigate the capabilities of different SAR sensors to forest canopy characteristics. A number of SAR airborne campaigns have been undertaken in Europe. This includes the MAESTRO-I campaign during August 1989 utilising AIRSAR sensor in four European test sites: Les Landes (France), Freiburg (Germany), Flevoland (The Netherlands) and Thetford (U.K.) focusing on SAR bands at P-, L- and C- band frequencies (Baker et al. 1994, Basili et al. 1994, Beaudoin et al. 1994, De Grandt et al. 1994, Dobson et al. 1992, Foody et al. 1994, Israelsson et al. 1994, Le Toan et al. 1992, Lemoine et al. 1994, Rauste et al. 1994).

This also includes the European Multi-sensor Airborne Campaign (EMISAR) in 1994/1995 (Attema and Wooding 1994); SAR and Hyperspectral Airborne Campaign (SHAC) in Thetford forest in 2000 (Balzter et al. 2001); BioSAR 2007, 2008 and 2010 Campaigns in Sweden (Hajnsek et al. 2008, Hajnsek et al. 2009, Ulander et al. 2011). All the above mentioned airborne SAR campaigns have mostly utilised the SAR bands at P-, L-, C- and X- frequencies. However, airborne SAR campaign that focuses on S-band has not been conducted so far.

3.2.2. The UK AirSAR Campaign

For the first time, extensive S-band SAR campaign have been conducted over the temperate region of UK known as the ‘AirSAR Campaign’ in 2010 and 2014. The Airborne SAR Demonstrator Facility ‘AirSAR’ is a collaborative project operated by Airbus Defence and Space (UK) with the Natural Environment Research Council (NERC) and the Satellite Applications Catapult (Airbus 2013a). Specifically, Airbus Defence and Space supported the established airborne SAR demonstrator installed on NERC research survey aircraft (Airbus 2013b). The provision of these SAR data to research and development is being supported by the Satellite Applications Catapult.

The frequency bands are S-band (3.1-3.3 GHz) and X-band (9.5-9.7 GHz) with a swath width of 1.92 km and narrow to wide incidence angles between 16° to 43.3°. The Single-Look Complex (SLC) imagery is provided in 0.75 m pixel spacing with 4.48 azimuth and 1 range looks (Airbus 2013a). SAR data as summarized in Table 3.1 were collected in separate occasions where soil conditions were neither too dry nor wet due to clear weather condition. For forestry applications, AirSAR acquired S-band SAR data over the mixed forests of Savernake forest and Wytham Woods are used in this research. This campaign provides an opportunity to investigate the potential of S-band signal to forest environment (Airbus 2013b).

Table 3.1. Summary of S-band AirSAR images used in this research.

Sites	Acquisition date	Incidence angles (°)	Polarisation	Pixel size (m)
Savernake	16 June 2010	22 – 39.9	Quad	0.75
Wytham	23 June 2014	16 – 43.3	Quad	0.75
Savernake	24 June 2014	16 – 42.5	Quad	0.75

3.2.3. SAR data processing

3.2.3.1. Single Look Complex data

The level 1.1, Single Look Complex (SLC) S-band products of Savernake forest and Wytham Woods for 2010 and 2014 were procured and pre-processed. The digital number (DN) is the intensity of the complex pixel value.

$$DN = \sqrt{Q^2 + I^2} \quad (3.1)$$

where Q and I are the respective real and imaginary parts of the complex pixel value. Each pixel in the SLC imagery contained the amplitude and phase of the electromagnetic wave measured in the four polarimetric channels. Using the amplitude image, the radar intensity information has been calculated as the square of the amplitude for both real and imaginary parts. For the antenna pattern correction, different orders of polynomial fitting were performed where the 5th order polynomial algorithm provided the best fit.

In SAR imagery, slant range is the actual measured range derived from the time delay of an echo. But, the transformation of this slant range information to discriminate features on the real world relates to the ground range as near-range and far-range (Woodhouse 2006a). This transformation was done by using information obtained from the imagery. For both 2010 and 2014 data, this corresponds to flight altitude (3.06 km from ground), slant-range (3.2 km from ground) and 0.75 m pixel spacing.

3.2.3.2. Multi-looking

In all types of coherence data including SAR imagery there is random interference (constructive and destructive) of the wavelets scattered by the target within one resolution pixel creating salt-and-pepper-like granulation called speckle (Woodhouse 2006a). The presence of speckle in SAR data reduces the visibility of the imagery hence decreasing the discrimination of the target. Thus, reducing the speckle would improve the discrimination of different classes more efficiently. This can be done with independent measurements during the measurement process itself, by splitting up the azimuth beam into many sub-beams. This technique is known to be “multi-look technique” by incoherently averaging the neighbouring pixels in the

imagery thereby reducing the speckle effect and improving the image interpretability (Woodhouse 2006a). However, the number of looks required to effectively tackle the problem of speckle in an imagery is not accurately define though a minimum of 9 looks are reported for considerable clearer separability of distributed targets such as forest canopies and agriculture areas (Woodhouse et al. 2011).

Conversion of SLC imagery into multi-look complex both in the azimuth and range directions at the cost of spatial resolution was performed using 5 number of range looks and 5 number of azimuth looks kernel window corresponding to 3.75 m pixel spacing on the ground. This was performed by using SAR Tools of the Next ESA SAR Toolbox (NEST DAT 4C-1.1) with independent looks criteria at 5 number of looks in both range and azimuth direction.

3.2.3.3. Speckle filtering

Various adaptive filters have been widely used preserving the radiometric and textual information without the loss of information. These include Frost, Lee, Kuan, GammaMap, Mean, Median, Enhanced Frost, Enhanced Lee and Local Sigma filters. Both Frost and Lee filters are based on the multiplicative speckle model and local statistics to preserve edges and sharpness (Frost et al. 1982, Lee 1980). Kuan filter uses the multiplicative speckle model and local statistics similar to the Lee filter with a different weighting function for preserving edges (Zhenghou and Fung 1994).

The GammaMap filter works with the maximum *a posteriori* (MAP) similar to the Kuan filter which assumes a gamma distribution of speckle (Lopes et al. 1990). Both Mean and Median filters are the simplest despeckle filters where the central pixel of a window size is replaced by either average or median of the neighbouring pixels (Qiu et al. 2004). Both Enhanced Frost and Enhanced Lee filter uses local statistics which preserves edges and texture information based on the adaptation of the Frost and Lee filters respectively (Lopes et al. 1990). The local Sigma filter uses the local standard deviation to reduce speckle and preserve finer details including low contrast areas (Eliason and McEwen 1990).

The multi-look imagery was de-speckled using nine different filters as mentioned above at three different window sizes of 3 x 3, 5 x 5 and 7 x 7 kernels using ENVI 4.4. To test the ideal speckle filter for this dataset, the mean and standard deviation (SD) of backscattered returns for all the polarisations are analysed. It was found that the Enhanced Frost filter performed best in terms of effectively reducing the speckle effect while maintaining the minimum variation of adjacent pixels in each homogenous class in all the moving windows (HH polarisation in Savernake site shown in Figure 3.2). Therefore, for further analysis, a 5 x 5 kernel for this dataset was used.

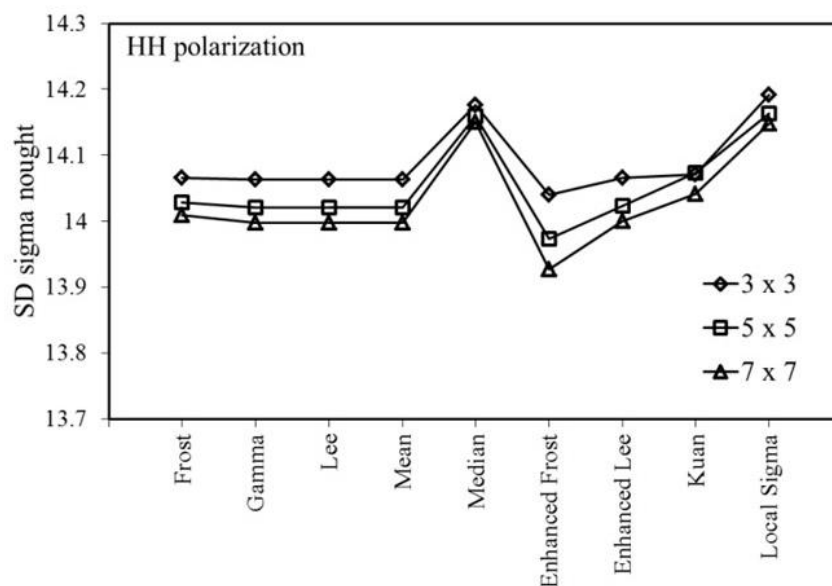


Figure 3.2. Comparison of different adaptive filters at different kernels (2014 acquired HH-polarisation in Savernake forest).

3.2.3.4. Geometric correction

The geometric correction refers to the projection of the SAR imagery to ground range with the aid of a reference surface. The ground reference data is assumed to be having information related to true x, y and z coordinate system where every pixel can be ideally projected (Woodhouse 2006a). As the study area is having less topographic slope effect, geo-coding of the SAR imagery is done using an Ordnance Survey map as reference with 30 and 42 widely distributed Ground Control Points (GCP) for Savernake and Wytham Woods respectively with second- order

polynomial and nearest neighbour re-sampling technique at 3.75 m pixel spacing achieving RMSE of half a pixel.

3.2.3.5. Backscatter sigma-nought (σ_0) derivation

SAR systems provide an advantage if they can provide well-calibrated measurements of backscattering that is radiometrically calibrated. Comparatively, it is easier to calibrate SAR imagery based on external target with known RCS characteristics. For example, a set of distributed targets or point target have been commonly used for calibration where corner reflectors are commonly employed for point target calibration (Dobson et al. 1986).

For the absolute radiometric calibration of airborne demonstrator data, trihedral corner reflectors were placed in the near, centre and far locations of the swath with corresponding incidence angles at 22.11° , 30.38° and 39.96° at Baginton (Coventry airport) in 2010 and Staverton airfield in 2014 (Figure 3.3). Finally, the radar backscatter coefficient with sigma-nought (σ_0) was calculated using the Equation (3.2) according to the Airbus Defence and Space technical report (Airbus 2013b):

$$[\sigma_0 = 10 \log_{10}(DN^2) - K_{cal}] \quad (3.2)$$

where: σ_0 = radar backscatter (dB), DN = pixel amplitude and K_{cal} = calibration constant. The calibration constants for Savernake forest are 71.5 dB for HH and VH, and 71.47 dB for VV and HV polarisations for the image acquired on 16 June 2010, and 71.8 dB for HH, VH and 72.62 dB for VV and HV polarisations for the image acquired on 24 June 2014. The calibration constants for Wytham Woods are 81.46 dB for HH and VH and 81.9 dB for VV and HV polarisations for the image acquired on 23 June 2014.

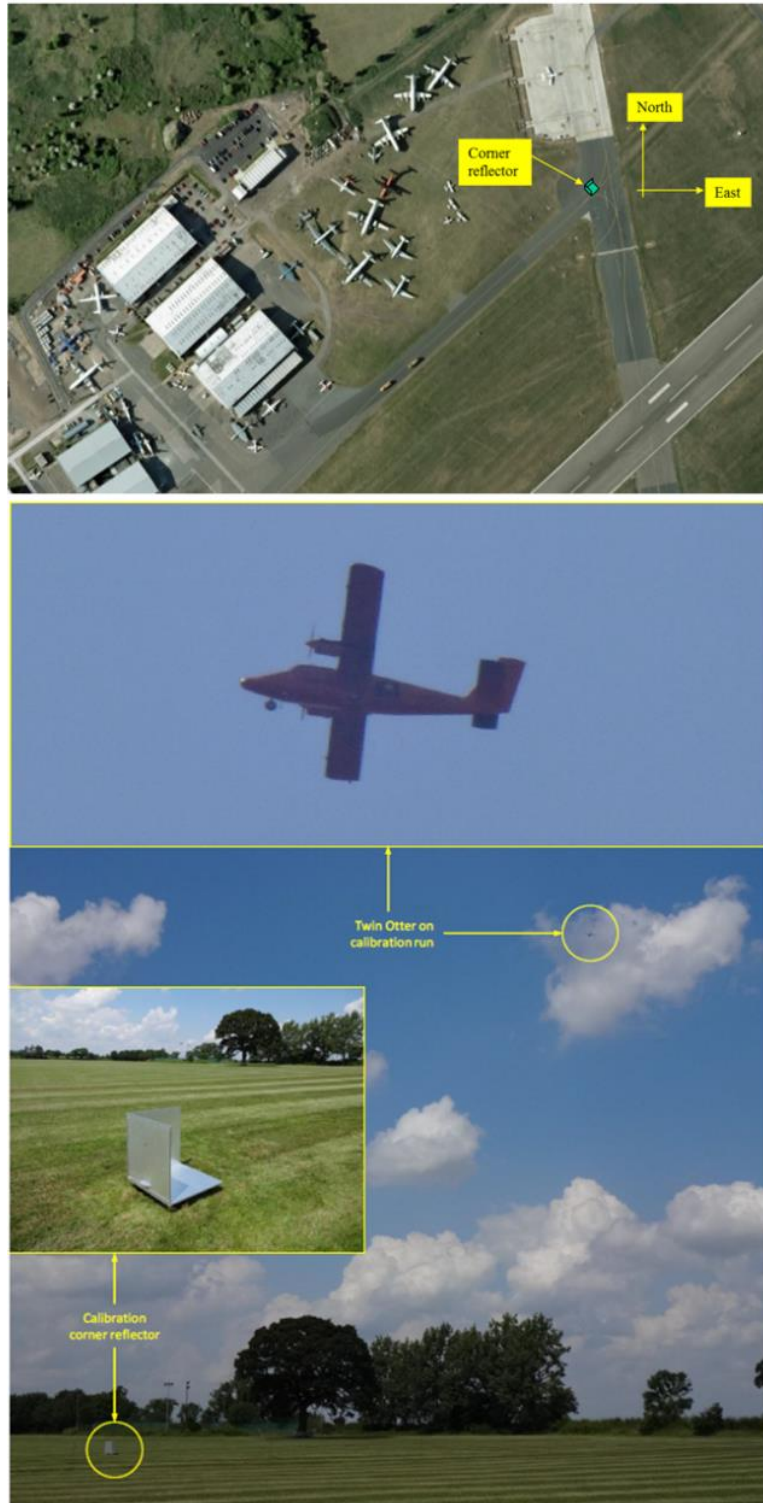


Figure 3.3. Calibration target location and orientation at Baginton (Coventry airport) in 2010 (top) and Twin Otter overflying calibration corner reflector near Staverton airfield in 2014 (below) (Source: Airbus (2013b)). Image reproduced with copyright permission from the Airbus Defence and Space, UK.

3.3. Field data

3.3.1. Forestry Commission GIS

For Savernake forest, the Forestry Commission Geographical Information System (FC GIS) database is a spatially comprehensive vector database of forest type, species, planting year, planting density and yield class for each forest stand. This database contains 215 sub-compartments for Savernake forest. The digital sub-compartment data were projected to the United Kingdom projection of the SAR image data with OSGB 1936. Information on forest type and tree species are used to train the Maximum Likelihood Classification (MLC) algorithm. Additionally, the ancient tree database contains approximately 2640 point locations within the image area. Each point contains detailed attribute information including diameter at breast height (DBH), canopy height (H) and tree species having a maximum tree DBH of 350 cm and canopy height of 35 m. This dataset is used to validate the accuracy of the produced F/NF classified maps (Figure 3.4).

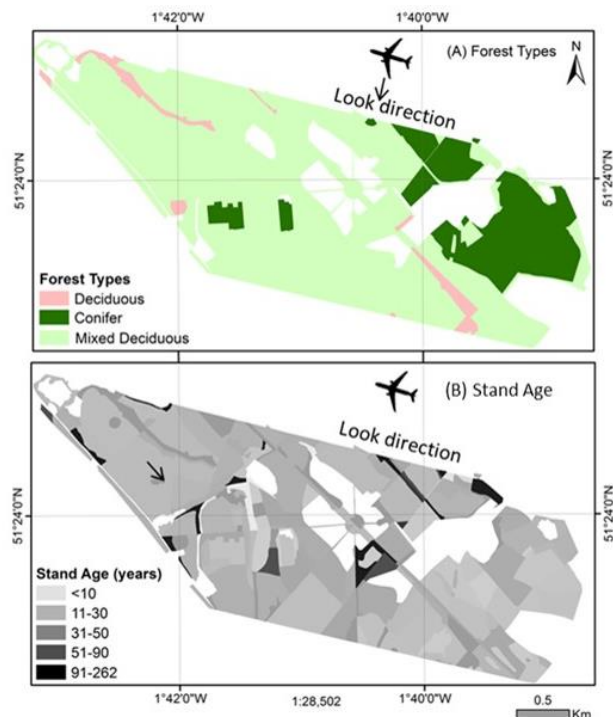


Figure 3.4. Forest types (A) and stand age (B) in Savernake forest (Source: Forestry Commission sub-compartment GIS database supported by Thomas Blythe). Image reproduced with copyright permission from the Forestry Commission, Bristol and Savernake.

3.3.2. Sample plot data for Savernake Forest and Wytham Woods

Depending on the nature of the study, different plot designs of varying sizes and shapes are adopted for different forest types. For example, plots are generally either square, rectangle, circular or triangular and dimensionless (point sampling). In areas where the undergrowth is less dense, sample plots with circular in shape could be easily employed as having the smallest periphery in relation to area and consequently the lowest number of borderline trees however, it is sometimes difficult to decide which are the trees that are inside or outside the plot as the boundary is curved (Köhl et al. 2006).



Figure 3.5. Example of a circular plot (top) with plot selection- at least 100 m distance from pathway (middle) and tree measurements (bottom) in Savernake Forest during March 2015. Image obtained by the author in March 2015.

In August 2012, a total of 38 sample plots each having a circular sample area of 20 m diameter was surveyed covering both deciduous and coniferous forest types. Two plots were collected based on random sampling between young and mature stands giving a total of 19 sub-compartments.

In each plot, individual tree data were collected that include: (i) trunk diameter for all trees with diameter at breast height ≥ 10 cm, (ii) canopy height measurements for subset of tallest trees and (iii) species identification of all trees for estimation of their wood density. These plots were sampled by Pedro Rodriguez- Veiga and Bernard Spies as part of their PhD research at the University of Leicester.

Following the same field protocol, second field campaign was carried out during March 2015 after the second SAR campaign in June 2014. This relates to 32 sample plots with 16 sub-compartments covering the remaining compartments, being surveyed by 10 researchers: Heiko Balzter, Pedro Rodriguez- Veiga, James Wheeler, Valentin Louis, Marc Padilla-Parellada, Thomas Potter, Chloe Barnes and Ramesh Ningthoujam with Alexander Edwards-Smith and Jaime Polo Bermejo from Cranfield University (figure 3.5).

For Wytham Woods, the Environmental Change Network database is a spatially comprehensive database of tree species, tree diameter at breast height and canopy height on the basis of Sykes and Lane (1996) protocol covering over 10 m² sample plots (Environmental 2014). The sample plots were collected during 2012 by the Centre for Ecology and Hydrology research team.

3.4. Methodology

Broadly, three methods have been used in this research. These methods are: First, MIMICS-I model (version 1.5) simulation for identifying radiative behaviour from soil components and forest canopy in X-, C-, S-, L- and P-band frequency with an additional simulation for forest degradation. This simulation was performed using Fortran Compiler on ALICE High Performance Computing Facility at the University of Leicester (details given in section 3.4.1). Secondly, pre-processing and classification of S-band SAR data (forest/ non-forest cover and change mapping) at different spatial resolutions were conducted using Environment for Visualizing Images (ENVI 4.4), Next ESA SAR Toolbox (NEST DAT 4C-1.1) and

Environmental Systems Research Institute (ESRI)'s Arc GIS 10.1 tools (details given in sections 3.2.3 and 3.4.2). Thirdly, retrieval of forest biophysical characteristics particularly forest AGB using S-band backscatter at stand level and cross-validation of predicted AGB against field measured AGB in line to NovaSAR-S configurations were performed (details given in section 3.4.3).

3.4.1. MIMICS-I simulation

The availability of the FC GIS database and field data (2012 and 2015), Savernake forest has been selected as a potential test site for investigating the radiative nature of S-band radar backscatter to soil and forest canopy components by modelling and the method is given in Figure 3.6.

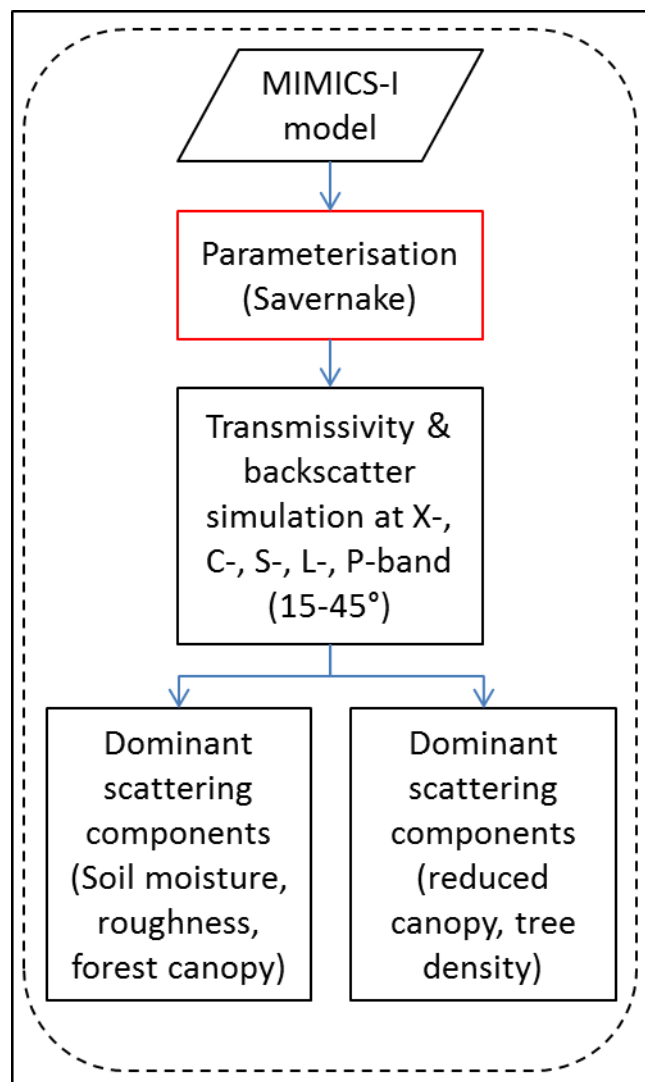


Figure 3.6. Methodology flowchart for MIMICS-I modelling.

This modelling study uses the radiative transfer model MIMICS- I (Ulaby et al. 1990) as a tool for investigating SAR backscatter predictions and dominant scattering from forest canopies. MIMICS-I model consider details of vegetation layer with several types of scatterers in the canopy. The input parameters for MIMICS-I can be divided into two major classes related to: 1) microwave characteristics (frequency, polarisation and incidence angle) and 2) physical descriptions of canopy (layers of leaves, needles, branches and trunk) as well as soil properties (soil moisture content and surface roughness). Specifically, the input parameters are defined in order related to configuration (general overall params for the simulation), sensor (operating frequencies and incidence angles), environmental conditions (temperature) and ground surface parameters (dielectric constant). This is followed by the structural characteristics of the canopy at two levels: (1) canopy level: tree height, crown depth, trunk height, canopy densities and (2) tree level: geometric distributions of the canopy components- type, size, density and orientation and moisture content of branch, leaf and needle (given in Appendix I).

Forest biophysical parameters were assumed to have remained unchanged between the 2010 and 2014. Therefore, tree density, diameter at breast height, canopy height and branch size were assumed constant. A small number of model parameters need to be adjusted for the different imaging conditions of the two sets of radar observations in 2010 and 2014, namely soil moisture content and structure of the stands. The soil moisture information was derived from Wytham Woods test site, being collected by the Centre for Ecology and Hydrology in 23 June 2014.

Different percentage of soil components for sand, silt and clay were derived from 1 km soil data set of Batjes (2015). Ground measurements such as density of leaves, needles and branches including their spatial orientation are extremely difficult to obtain and were not available for this site. Therefore, an estimate or a reasonable value from the literature is assumed for such structural canopy parameters. All the estimated values are derived from the MIMICS-I model technical report (Ulaby et al. 1988b). A list of input parameters of MIMICS is given in Table 3.2. In this study, radar backscatter data are simulated for deciduous and conifer stands as function of radar frequency, polarisation and incidence angles. For inter-comparison, the radar frequency range at 0.42 GHz (36 cm), 1.25 GHz (24 cm); 3.10 GHz (15 cm), 4.75 GHz (5.6 cm) and 10.00 GHz (2 cm) corresponding to P-,

L-, S-, C-, and X-band respectively with incidence angles between 15° - 45° is used.

Table 3.2. Numerical values of input parameters for MIMICS-I model: bold = estimated; normal = measured.

Parameter	Deciduous (Birch)	Coniferous (Norway spruce)
<i>Trunk layer</i>		
Height (m)	8	8, 16
Diameter (cm)	24	20.8
Canopy density (m ⁻²)	0.11	0.2 , 0.1 , 0.05
Moisture (gravimetric)	0.5	0.6
<i>Crown layer</i>		
Crown thickness (m)	1, 2, 3,10	11
Leaf/ needle density (m ⁻³)	100, ..., 2000	5000,...,100000
Leaf/ needle moisture (gravimetric)	0.8	0.8
Leaf Area Index (single-sided)	5	11.9
Branch density (Primary, Secondary, 3 rd , 4 th) (m ⁻³)	4.1, 0.04, 0.45, 0.37	3.4
Branch length (Primary, Secondary, 3 rd , 4 th) (m)	0.75, 1.15, 0.52, 0.33	2.0
Branch diameter (Primary, Secondary, 3 rd , 4 th) (cm)	0.7, 1.6, 0.9, 0.57	2.0
Branch Moisture	0.4	0.6
Soil root mean square height (cm)	0.45, 1, 2, 3, 4, 5	0.45
Soil Correlation length (cm)	18.75	18.75
Soil moisture (volumetric)	0.15 – 0.5	0.15 – 0.5
Soil Sand (%)	53	53
Soil Silt (%)	28	28
Soil Clay (%)	19	19
Leaf/ needle/ branch orientation	uniform	uniform
dielectric constant (trunk, branch)	0.4	0.6
Dielectric constant (Leaf)	0.8	0.8

Two radar parameters related to canopy transmissivity and backscatter are investigated. Radar canopy transmissivity is related to the power transmission coefficient for propagation from the forest component at a specified incidence angle while backscatter is the overall scattering returns (attenuation) from forest canopy in a pixel cell. The predicted sensitivity of backscatter to forest canopy is investigated in terms of both canopy transmissivity and backscatter (in decibel) for all frequencies while only S-band backscatter for soil properties. The predicted backscatter was regressed using the logarithmic model against soil moisture, surface roughness and backscatter across look angle and derived error (RMSE). In this, six different experiments based on MIMICS-I have been investigated.

Model experiment 1:

In this experiment, all the canopy parameters i.e., trunk, branches, leaf/ needle are either excluded or switch off during the simulation (given in Appendix II). It can be considered as radar backscatter interactions with bare-ground with varying degree of moisture content. The environment is considered to be have temperature of soil and standing water with 20°C as these parameters seemed to have negligible effect over the returned backscatter (earlier result run with 11.5°C). Ground system composed of different parameters related to underlying soil types such as sandy, silty and clay soil type with different proportion and salinity of standing water with 2.5 ppt (parts per thousand) having soil volumetric moisture content of 0.1 to 0.5 m³ water/m³ soil.

Model experiment 2:

For the experiment related to surface roughness of soil, all the parameters are similar to bare-ground system of soil moisture consisting of different proportions of soil types with sandy, silty and clay soil type with soil volumetric moisture content of 0.1 to 0.5 m³ water/m³ soil. The standard deviation of surface (*rms*) height of soil is set between 1 to 5 cm surface roughness having a Gaussian auto-correlated length of 15.00 cm (given in Appendix III).

Model experiment 3:

The parameters for environment and ground variables are set similarly to the soil in this experiment. This case resembles to deciduous forest e.g. birch stand with crown layer consisting of both leaves and branches with standing trunk.

Based on the tree architectural characteristics, majority of the deciduous trees have lateral branches as longest growth than the main terminal shoot with repetitive branch forking into a large spreading crown resulting to disappearance of the central stem (Figure 3.7). Additionally, diameter and length of the branches decreases with branching generation (e.g. young branches) resulting to more numerous (density) with increasing height (Zimmermann and Brown 1971).

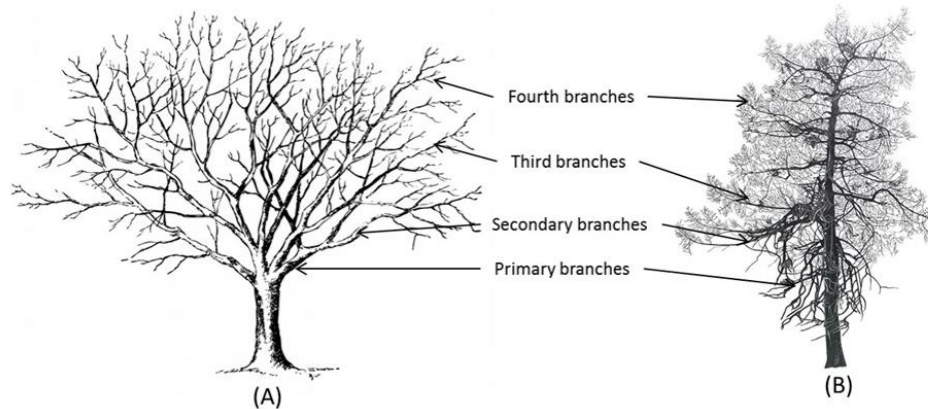


Figure 3.7. Tree architectural characteristics of deciduous (without leaves) (A) (Source: <http://www.publicdomainpictures.net/view-image.php?image=95625&picture=tree&large=1>) and coniferous species (with needles) (B) (Source: <http://www.cattogallery.co.uk/assets/galleries/274/annie-ovenden-larch-tree.jpg>). Image obtained by the author from webpages with source.

Five sets of approaches have been simulated: one related to entirely leaf-dominated where the leaves are randomly oriented or distributed having 6.76 cm diameter and 0.1 cm thickness. For a 2 meter crown thickness with 830 leaves per cubic meter and 8 meter trunk height is simulated in the model using physical optics. The second approach resembles the branch-dominated birch stand during senescence season having primary branch of 0.75 meter long with 0.7 cm diameter spreading a uniform orientation and specific probability density function (given in appendices IV, V and VI). Furthermore, an effect of different levels of branches (up to fourth) having

different diameter, length and number density was also simulated for L-, S-, C- and X-band.

The radiative behaviour of different canopy components in varying moisture content was simulated in third approach while combination of both leaves and branches was simulated in fourth approach. The relationship between varying stand height (2 -18 m) and backscatter responses was simulated in fifth approach. In this, the effects of leaves-branches at individual and combined and moisture effect as a function of wavelengths, polarisations and incidence angles to transmissivity and backscatter have been investigated.

Model experiment 4:

This experiment resembles analysis performed on a coniferous forest e.g. Norway spruce stand. Coniferous trees have the main terminal shoot outgrows the lateral branches giving a cone-shaped crowns with clearly defined bole (Figure 3.7). The branch characteristics follow a similar trend like deciduous species with low density, reduced length and diameter branches to height (Zimmermann and Brown 1971).

In this simulation, both the needles and branches are included in the crown layer (given in Appendix VII). The needles were assumed to be randomly distributed or oriented with at least 2 cm long and 0.1 cm in diameter. For an 11 meter crown layer with 16 meter trunk height and 85,000 needles per cubic meter corresponding to leaf area index (LAI of 11.9) and identical branches with deciduous species is simulated in the model based on physical optics. Moreover, 11 meter crown thickness with 8 m trunk height was also simulated. The parameters for environment and ground variables are similar to previous simulations. In this, the effects of needles-branches as a function of wavelengths, polarisations and incidence angles to transmissivity and backscatter have been investigated. Additionally, varying needle densities ranging from 5000 to 100,000 needles per cubic meter area have been simulated.

Additionally, an effect of different levels of branches (up to fourth) having different diameter, length and number density was also simulated for L-, S-, C- and X-band. Finally, simulated S-band backscatter from soil and forest canopies (deciduous and

conifer) are combined to investigate the different behaviour of backscatter across different land cover (forest and non-forest).

Model experiment 5:

Taking the case of a typical birch stand, from the radar perspective, the backscatter return is a function of radar wavelength, polarisation and incidence angles.

Backscatter is also dependent on the structure and nature of the stand (young to mature, different management practices, varying stock volume and density etc). In general, at shorter wavelength X- and C- band, backscatter behaves volume scattering from upper canopy layer of leaves, twigs and small branches as maximum attenuation before reaching the ground surface. On the contrary, L- and P- band backscatter exhibited volume with strong double-bounce scattering from the canopy layer and ground/trunk interaction due to more penetrating level in the canopy.

After the fire is occurred, the radar backscatter with either double-bounce or surface scattering or combined becomes important contributor because of more interaction with ground and lesser canopy components in almost all wavelengths (Kalogirou et al. 2014). However, this depends on the severity of fire and condition of forest properties under investigated. The dominating strong double-bounce scattering only persists provided piles of branches and stumps (remaining snags) lying on the ground still exist. Otherwise, the surface scattering becomes the major contributor to the return backscatter due to clear-up areas resembling scattering from bare-ground or forest floor without vegetation.

The experiment related to reduce canopy components due to fire as a proxy of degradation involves seven different simulation. This resembles to birch stand having 2000 trees per hectare with crown layer comprising of leaves, branches and standing trunk (given in Appendix VIII). Firstly, forest canopy with 2 meter crown thickness having leaf density of 5000 leaves, 5.1 branches per cubic meter and 8 meter trunk is simulated as 'high density canopy'. Fire impacts were qualitatively assessed based on the degree of canopy damage. This canopy damage was assumed based on the field observation according to Kalogirou et al. (2014) and classified into three categories according to opening of canopy gaps.

The second simulation relates to ‘Low canopy damage’ with canopy layer having 830 leaves, 4.1 branches and 8 meter trunk similar to Model experiment 3. Third and fourth simulation refers to leaf-dominated and branch-dominated when leaves and branches were consumed in repeated fire events as ‘moderate canopy damage’ resulting to large canopy gaps. The ‘severe canopy damage’ is quite similar to the standing trunk on the ground when all leaves and branches were consumed completely by fire. Finally, two scenarios focusing on bare ground having dry (low moisture) with smooth bare ground (low soil *rms*) and wet (50% moisture content) with rough surface ground (5cm *rms*) are simulated.

Model experiment 6:

A different approach is applied, instead of changing the forest canopy components (i.e., crown density and canopy gaps), MIMICS-I have been simulated as a function of number of trees in an area (stand density). Forest stand density is mainly governed by a combination of natural processes (natural thinning, competition) and external drivers such as logging of commercial value species. Selective logging creates homogenous canopy structure (Okuda et al. 2003) with large canopy gaps and increased light intensities (Osazuwa-Peters et al. 2015) and reduction in stem density and forest AGB (Blanc et al. 2009). They also create forest fragmentation (Asner et al. 2006) and are highly susceptible to fire (Cochrane 2003).

The experiment related to stand density of birch involves varying tree density: 5000 (very dense canopy), 2500 (dense canopy), 1250 (low density canopy), 625 (open canopy) and 300 (savannah type) having varying levels of stock volume/ biomass, that is reduced level of biomass from high density to low density trees.

3.4.2. Airborne S-band derived forest/non-forest and change detection maps

To investigate the potential of airborne S-band data for mapping forest and non-forest cover and change detection, the mixed deciduous forest and different non-forest classes (that is grassland, clear-felled and grassland) of Savernake provides an ideal set of environment. This also includes the recent stand removal in few sub-compartments during the study period and the availability of FC GIS and ancient database supported by field data. The method related to investigating the capability

of S-band backscatter for mapping forest cover and change has been given in Figure 3.8.

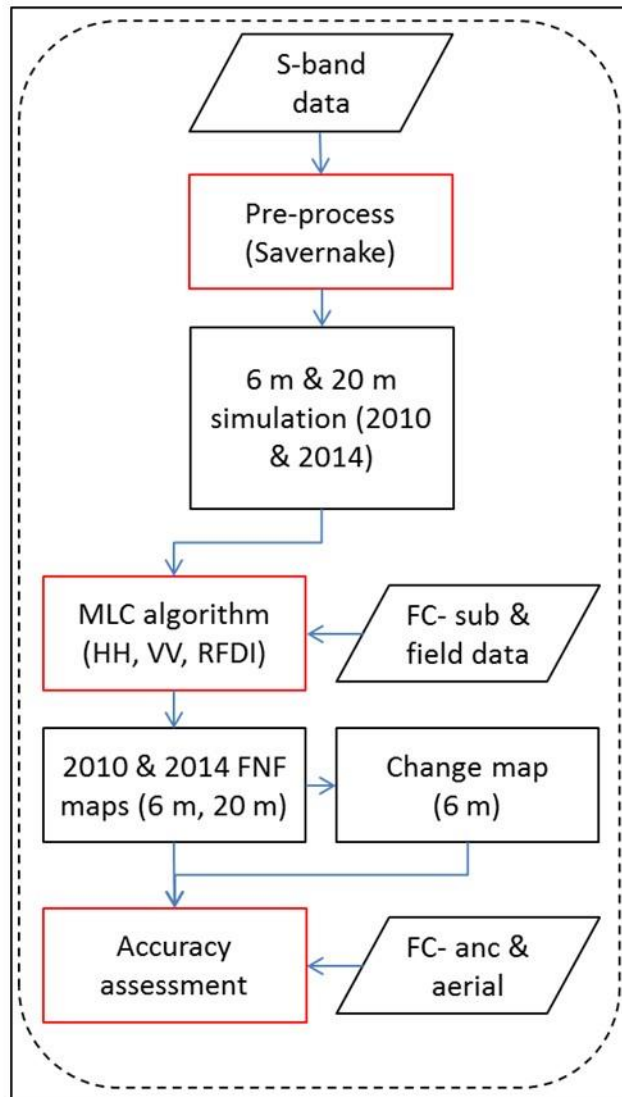


Figure 3.8. Methodology flowchart for mapping forest/ non-forest and change detection. *MLC: maximum likelihood classification, RFDI: Radar Forest Degradation Index, FC- sub/ - anc: Forestry Commission sub-compartment/ ancient database.

3.4.2.1. SAR data interpretation, land cover legend and classification

Over Savernake forest, two S-band images were acquired on 16 June 2010 and 24 June 2014 and have been utilized to map F/NF and monitor the forest change during these two periods. These two datasets were acquired with similar pixel spacing of

0.75 m having varying incidence angles: narrow look angle in 2010 against wider observation in 2014 data (refer to Table 3.1). The two imageries were also geo-registered by manually selecting ground control points (GCPs) over manmade targets such as road intersection, sub-compartment junction and houses etc. and wrapping one image to the other in ENVI 4.4.

To perform forest cover change detection analysis, these datasets are radiometrically re-calibrated. S-band DN values acquired on 16 June 2010 was re-calibrated based on 2014 data using the basic statistics (minimum, maximum, mean DN values) of all polarisations from all land cover. The maximum DN values were 3398, 6601 and 1530 in 16 June 2010 while 24356, 32658 and 5040 in 24 June 2014 for HH, VV and HV polarisations. Therefore, a correction factor of 7.16, 4.94 and 3.29 for HH, VV and HV polarisations were applied to 16 June 2010 to match the intensity of 24 June 2014 data assumed to have made some corrections in the 2010 data. This is being verified by linear regression models based on 2640 known tree targets from the ancient tree database based on corrected 2010 and original 2014 data (Figure 3.9).

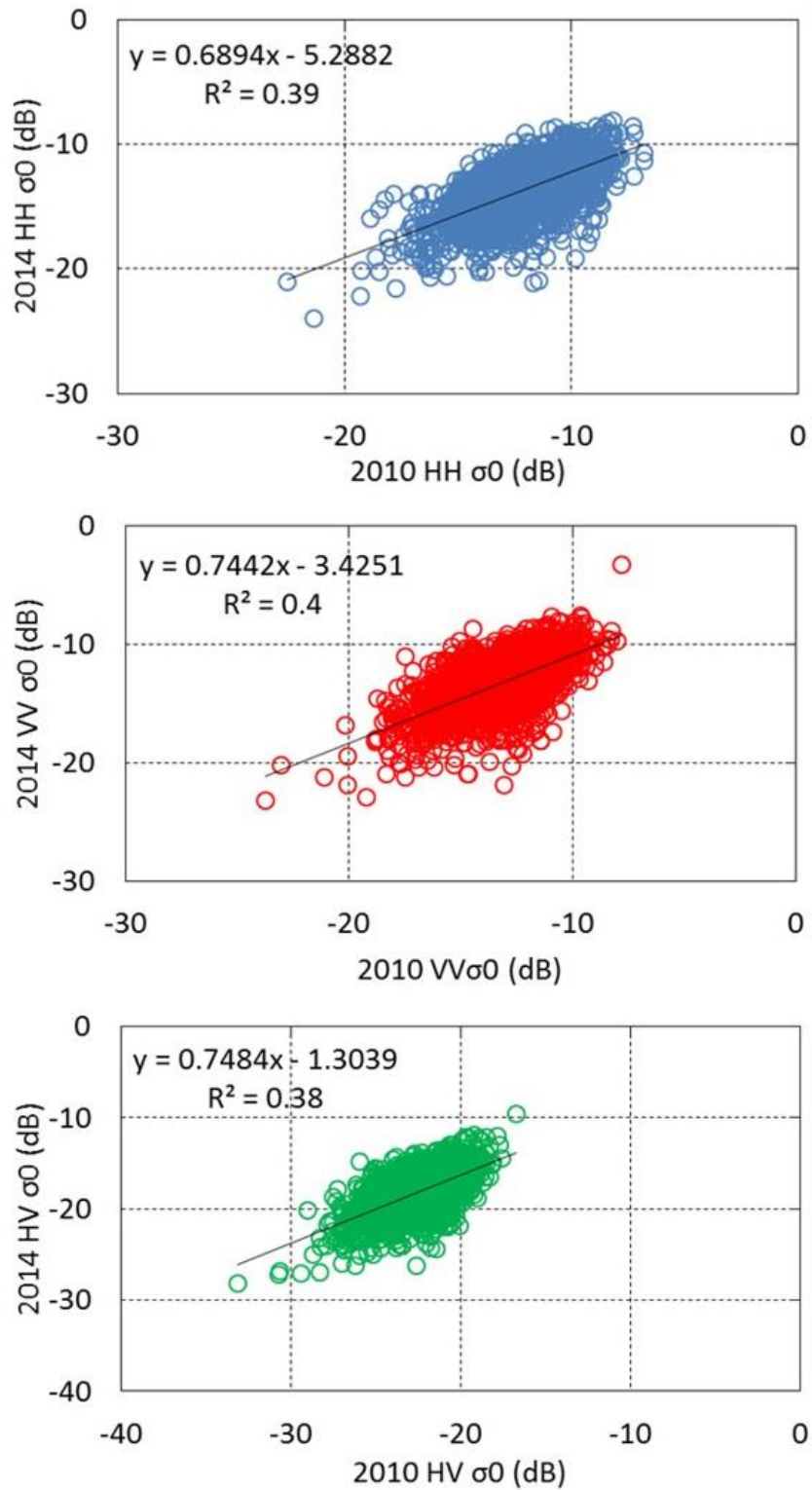


Figure 3.9. S-band backscatter comparison for forest (2640 ancient tree points) class between re-scaled 2010 and 2014 SAR imageries.



Figure 3.10. Field photos for deciduous forest (A) and non-forest (B-clear-felled, C-bare-ground and D-grassland) in Savernake site. Image obtained by the author in March 2015.

Two broad land cover classes based on ground truth and S-band backscatter behavior of different polarisations have been identified: Forest and Non-Forest (Figure 3.10 A, B, C and D). The non-forest comprised three classes, i.e., grassland, clear-felled and bare-ground. The definitions and interpretation guidelines used in this methodology are given in Table 3.3.

Table 3.3. Definition of Forest and Non-forest classes.

Class	Definition
Forest	Land dominated by deciduous, conifer and mixed trees with canopy height ≥ 3 m, >20 years old and at least 50 tonnes/ha of aboveground biomass.
Grassland	Land dominated by non-woody annual vegetation less than 1 m in height.
Clear-felled	Open area previously occupied by forest due to stand-replacement disturbance. The area is composed of left-over dry leaves, branches and grasses with few dead stumps. This took place between December 2012 and July 2013 in few sub-compartments and planted with norway spruce and oak seedlings.
Bare-ground	Land surface without any vegetation. This class includes natural and artificial bare surfaces e.g. bare soil, roads and pathways between sub-compartments in the forest.

In the first classification approach, only forest and non-forest are defined as the main land cover classes (Figure 3.10). The ratio between the HH- and HV-backscatter was calculated and utilised for classification. It is also known as the ‘Radar Forest Degradation Index’ (RFDI) because HH backscatter is sensitive to both volume and double-bounce scattering while HV backscatter is mostly sensitive to volume scattering from forest canopies (Mitchard et al. 2012).

In the second approach of classification, non-forest class has been classified further into three classes (grassland, clear -felled areas and bare -ground). The definitions and interpretation guidelines used in this methodology are given in Table 3.3. These

classes of non-forest and forest are defined based on the field sample plots and FC GIS data points and are used for training the classification algorithm.

Different algorithms have been developed for land cover classification particularly related to forest cover types. Amongst the different algorithms, studies have shown that Maximum Likelihood Classification (MLC) algorithm have been considered superior to other classifier approaches (Mather et al. 1998). MLC algorithm works with class probability density functions assuming a multivariate normal distribution and often achieves better accurate results with SAR data than other classifiers (Alberga 2007, Kuplich et al. 2000, Morel et al. 2011).

3.4.2.2. Spatial resolution simulation and change detection

The changing information content of S-band radar backscatter was examined for different spatial resolutions by re-sampling from the original 0.75 m to different spatial resolutions and repeating the classification. The spatial aggregation is performed for each polarisation bands using nearest neighbour resampling with the aid of Ordnance Survey master map. The spatial scales of the forthcoming NovaSAR-S imaging modes of 6 m and 20 m are studied. For the assessment of classification accuracy, independent 20 non-forest and 21 forest points based on ancient tree database and aerial photo were incorporated along with the training plots resulting to 126 forest and 130 non-forest points to provide cross-validation. These sample points were collected at the boundaries of classes (forest to clear - felled, forest to bare -ground, forest to grassland) where mixed pixels with different land cover exists and are often associated with high error (Foody 2002). Therefore, an attempt has been made to highlight the accuracies of forest cover and its change maps focusing on the mixed pixels in addition to the homogenous classes. A confusion matrix was computed and the Overall accuracy, User's and Producer's accuracies and Kappa coefficient (κ) were calculated. A cross-comparison with the ALOS PALSAR-based global forest cover map by the Japan Aerospace Exploration Agency (JAXA) at 25 m scales was also carried out (JapanAerospaceExplorationAgency 2014) .

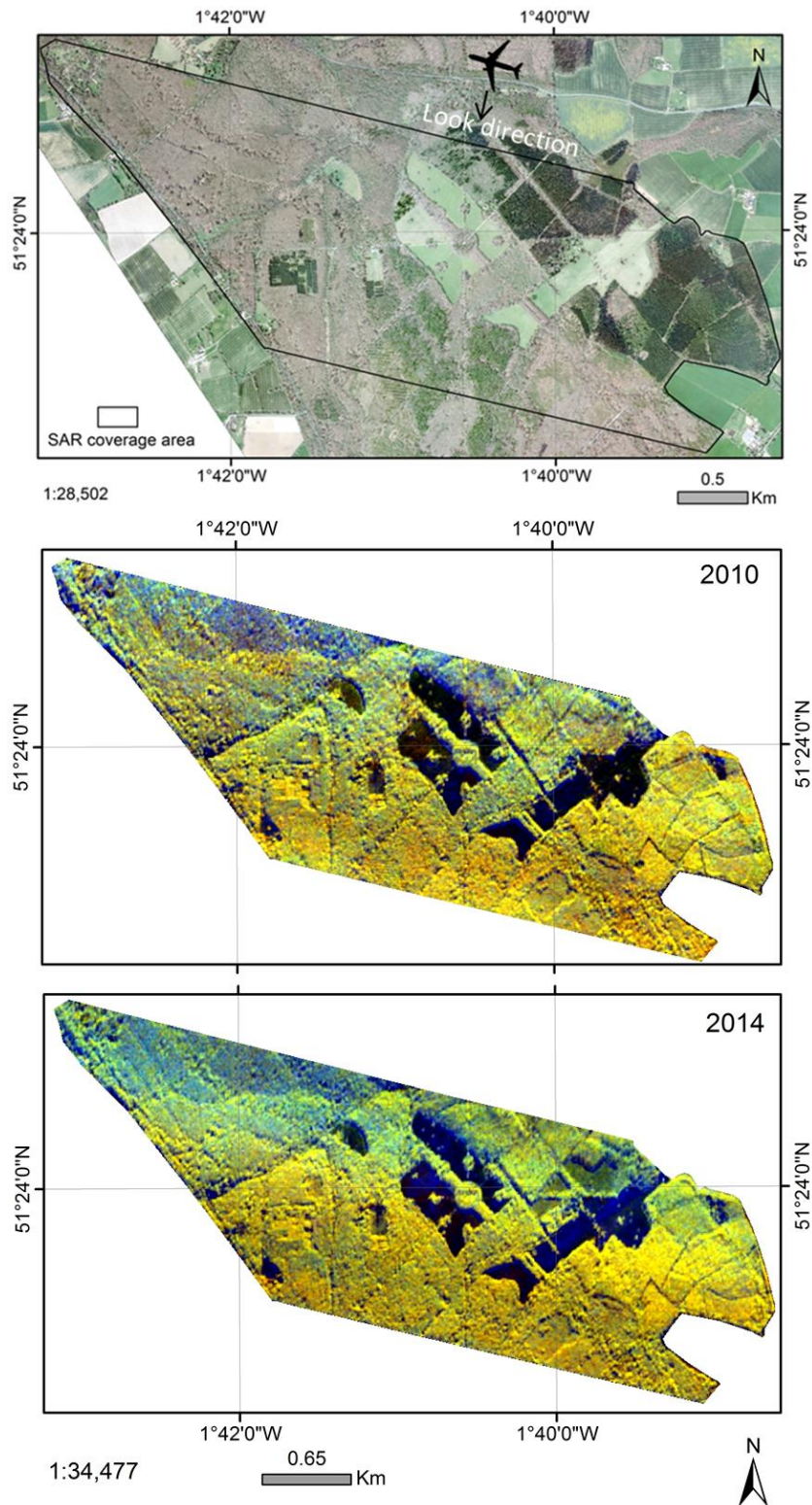


Figure 3.11. Aerial photo (top) and 6 m S-band SAR data acquired in 2010 (middle) and 2014 (bottom) over Savernake forest as HH-, VV- backscatter and RFDI data in red, green and blue channel (Source: Airbus 2013a). Image reproduced with copyright permission from the Airbus Defence and Space, UK.

For forest cover change detection analysis, the classified F/NF maps derived from the 2010 and 2014 S-band acquisitions (Figure 3.11) were assessed for changes due to management operations (i.e., clear-felling and thinning) based on a post-classification technique. The Global Forest Watch (2000- 2014) product at 30 m based on multi-temporal Landsat data from the global forest change project (Hansen et al. 2014) was also utilized for cross-comparison (figure 8 d). Both PALSAR and Landsat-based products are intended to support the interpretation of the S-band derived maps as these products are generated at global and medium resolutions scale.

3.4.3. S-band derived forest biophysical retrieval

For relating forest structure and AGB to S-band backscatter, the mixed temperate forest of Savernake Forest and Wytham Woods were chosen for this objective. The occurrence of mixed species with varying levels of ages (10-262 years old), tree diameter at breast height, canopy height, maximum canopy cover and AGB ranges and the acquisition of SAR data during peak growing season offers an opportunity to explore the relationship between forest biophysical characteristics and S-band backscatter at different scales. The method related to the retrieval of forest biophysical parameters using S-band backscatter is given in Figure 3.12. For example, maximum wood structure production particularly in trunk and branches was found during closed canopy (June-September) in Wytham which coincides with the airborne SAR data on 23 June 2014. The statistical relationship of average tree diameter (DBH) and canopy height (H) against S-backscatter are performed at stand level resolutions utilising SAR data acquired on 23 and 24 June 2014 over Wytham Woods and Savernake Forest.

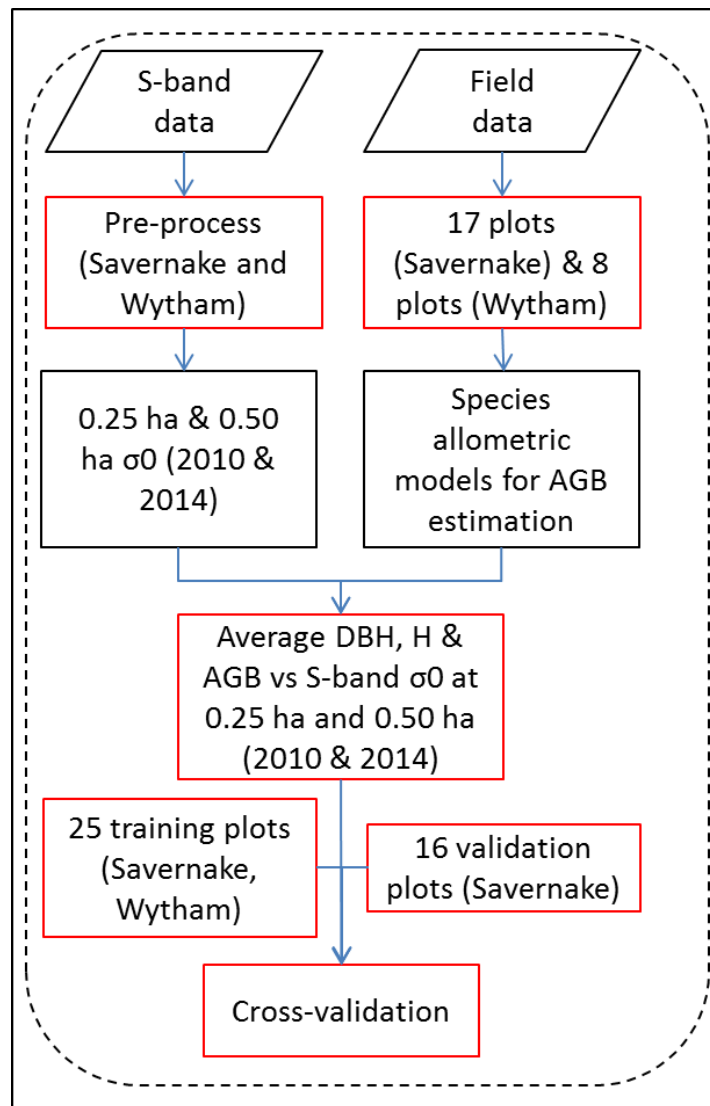


Figure 3.12. Methodology flowchart for forest biophysical retrieval * DBH: tree diameter at breast height, H: canopy height and σ_0 : backscatter sigma-nought.

At the individual tree-level, the AGB was estimated using the allometric equations of Zianis et al. (2005) and Bunce (1968) which were specific to British tree species (including European genera) and tree size measurements as inputs for Savernake and Wytham respectively. The allometric equations for different species used in this analysis are given in Table 3.4. From the tree-level estimates of AGB, plot level of estimates of biomass was obtained by the summation of single tree AGB in each plot. Finally, the estimated AGB is measured in units of 1 metric tonnes per hectare (t/ha) for statistical comparison with S-band backscatter.

Table 3.4. Allometric equations used to estimate tree above-ground biomass.

Species	Equations	Unit	Source
(Scientific name)			
Scots pine (<i>P.sylvestris</i>)	$e^{(0.981+(2.289 \cdot (\ln 3.14 \cdot D)))}$	g	(Zianis et al. 2005)
Corsican pine (<i>P. nigra</i>)	$e^{(-1.457+(1.8647 \cdot (\ln D)))}$	kg	
Norway spruce (<i>P. abies</i>)	$(-43.13+2.25 \cdot D)+(0.452 \cdot D^2)$	kg	
Western hemlock (<i>T. heterophylla</i>)	$e^{(-1.457+(1.8647 \cdot (\ln D)))}$	kg	
Beech (<i>F. sylvatica</i>)	$(0.1143) \cdot D^{(2.503)}$	kg	
Birch (<i>B. pendula</i>)	$(-2.4166+2.4227) \cdot e^{(D)}$	kg	
Oak (<i>Quercus spp.</i>)	$e^{(-5.284602 + (2.4682 \cdot (\ln D)))}$	kg	(Bunce 1968)
Sycamore (<i>A.pseudoplatanus</i>)	$e^{(-5.644074 + (2.5189 \cdot (\ln D)))}$	kg	
Ash (<i>F. excelsior</i>)	$e^{(-5.308133 + (2.4882 \cdot (\ln D)))}$	kg	

Of the total 19 sub-compartments in Savernake, 2 sub-compartments were discarded in the analysis. First, 1 sub-compartment was located at the very edge of the SAR imagery (near to 15° incidence angle range) having erroneous values caused by the re-sampling method. The second sub-compartment was discarded due to large diameter trees ≥ 70 cm resulting to an AGB much larger than 700 t/ha.

The backscatter response from forest stand is a combination of different sources, e.g. forest parameters, layover of tree canopy, speckle, geolocation errors and border effects including moisture content. Although, the impacts of these factors are difficult to quantify, studies have shown the role of spatial resolution as an important factor in understanding the spatial variability of forest structure and AGB (Saatchi et al. 2011b, Sandberg et al. 2011). In order to analyse statistical regression for biomass to SAR backscatter relationship, the very high-resolution S-band data were simulated (re-sampled) to stand size at 0.25 ha and 0.5 ha.

The fully polarimetric S-band backscatter were then regressed against plot-measured AGB at pixel and stand (0.25 ha and 0.5 ha) levels. This was done utilising SAR data acquired on 16 June 2010, 23 and 24 June 2014 in Wytham and Savernake sites. The forest stands with 17 (9 deciduous, 8 conifer) and 8 (deciduous) plots from Savernake and Wytham Woods were used to develop a regression model describing the relationship between AGB and S-band backscatter, referred to as training plots. Quantification of the S-band signal saturation level to field calculated AGB was also performed. Furthermore, using the best logarithmic model, prediction of AGB at 0.25 ha was performed. The second data set consisted of field measurements made during April 2015 in Savernake. These 16 forest stands (10 deciduous, 6 conifers) were used to validate the developed biomass regression models, referred to as validation plots. This includes biomass error estimation based on RMSE calculated by comparing model prediction to field measured AGB using model training (25) and validation (16) plots.

3.5. Summary

In this chapter, the characteristics of the two test sites related to this research were addressed. A full description of the different data sets comprising of SAR data and field data surveyed in 2012 and 2015 is given. This also includes the different SAR-processing techniques and methods for different objectives. Finally, data for MIMICS-I model and forest structure and biomass estimation were also covered.

Chapter 4: Soil and forest backscattering with S-band SAR using MIMICS-I simulation

4.1. Introduction

Several studies have reported capability of SAR data in mapping forest cover and biophysical parameters retrieval. However, the basic knowledge of scattering at microwave domain from canopy can only be realised using microwave canopy models to support and understand the embedded information in a SAR signal (i.e., backscatter). Therefore, this chapter explains the qualitative knowledge of the scattering mechanisms for S-band signal from forest canopy and soil in different experimental settings that is soil moisture, surface roughness and canopy components with varying moisture, leaves/ branch / tree densities and stand height.

Many studies have shown the potential of SAR data in particular longer wavelengths for relating to forest biophysical characteristics across different forest types (Beaudoin et al. 1994, Dobson et al. 1992, Imhoff 1995, Rauste et al. 1994, Soja et al. 2013). Moreover, accurate identification of forest degradation/ clear-cut has been reported utilising longer SAR wavelength (Pantze et al. 2014, Ryan et al. 2012). Because SAR backscatter contains information related to forest canopy structure and AGB and hence influencing the backscatter from the forest degradation e.g. fire (Ferrazzoli et al. 1997). This includes the dynamic backscatter changes due to fire-affected forested areas utilising multi-temporal SAR data particularly at C-band frequency (Siegert and Ruecker 2000, French et al. 1996). In all of these studies, the impacts of fire in forest appears to be mainly governed by the reduction in the canopy components and changes in soil moisture and exposure of surface using empirical and modelling (Kalogirou et al. 2014, Tanase et al. 2010).

In Brazilian Amazon, MIMICS model simulations predicted that at L-band frequency, discrimination of primary forest against regeneration and soil (wet and dry) is possible by their stronger backscatter returns due to double bounce scattering from ground/trunk interaction from the canopy while opposite for C-band due to quick saturation level at low biomass and single bounce scattering from leaves and branches (Grover et al. 1999). Utilizing multi-temporal JERS-1 data has shown a

dynamic range of reduced -4 to -6 dB corresponding to either early stage of plantation while opposite for post fire or degradation in the southern Sumatra Island of Indonesia (Takeuchi et al. 2000).

Studies have shown that longer wavelengths are sensitive to variations in the moisture and surface roughness of soil (Shi et al. 1997) and vary as a function of incidence angle (Rahman et al. 2008). For example, SAR backscatter increases with increasing soil moisture ranging between 0 and 40% (Baghdadi et al. 2007) following a logarithmic function (Ulaby et al. 1986). With S-band, sensitivity of soil moisture to backscatter was found positive between observed and soil moisture retrieval at VV-polarisation channel for HJ-1C simulation (Du et al. 2010). At S-band, it has been reported that the main scattering comes from the needles and branches of young fir conifer due to random scattering (Lopez-Sanchez et al. 2000).

To account for studies related to forest cover, biomass, identify degradation or clear felled using S-band data, knowledge of the radiative nature of S-band scattering with forest canopy is essential. Microwave canopy backscatter model assists to understand the complex interaction of microwave backscatter with different components of the canopy as a function of wavelength, incidence angle and polarisations (Ulaby et al. 1990). The main objective of this chapter is to examine the contributions of different scattering mechanisms from soil moisture and surface roughness and forest canopies for different frequencies, polarisations and incidence angles based on MIMICS-I model. This also includes investigating the S-band backscatter sensitivity to forest degradation using MIMICS-I simulation.

4.2. Methods

This modelling study uses the radiative transfer model MIMICS- I (Ulaby et al. 1990) as a tool for investigating SAR backscatter predictions and dominant scattering from forest ecosystem. The available FC GIS database and field data collected in 2012 and 2015 provides Savernake forest to be prospective test site for investigating the radiative nature of SAR backscatter data particularly at S-band to soil and forest canopy components utilising the MIMICS-I model. Details are given in section 3.4.1.

4.3. Results and discussion

4.3.1. Ground scattering as a function of soil moisture and surface roughness

The simulation results for bare-ground as a function of moisture and surface roughness as described in section 3.4.1 with Model experiments 1 and 2 is described below:

What is the relationship between soil moisture and S-band backscatter across polarisations and incidence angle range?

This experiment was simulated on the basis of backscatter sensitivity to moisture content and surface roughness of soil. For S-band signal relationship to soil moisture, the simulated radar backscatter from bare-ground ranges between -20 to -60 dB for HH and VV polarisations across the incidence angle range. At medium incidence angle range, relationship of S-band backscattering with soil volumetric moisture content between 0.1 and 1 m³ water/m³ soil is 6.43 dB and a smaller change with 6.03 dB is estimated for an increase in *rms* height of only 0.1 cm in both co-polarisations. It can be observed that the backscatter increases with soil moisture at constant soil surface roughness along the incidence angle range (Figure 4.1).

At average incidence angle ~30°, S-band backscatter shows a strong significant relationship with soil moisture content up to 40% moisture content (logarithmic model: $r^2 = 0.98$, $P < 0.0001$) for both HH- (RMSE 0.31) and VV- (RMSE 0.39) polarisations. This result supports the observation made by Baghdadi et al. (2007) where the backscatter sensitivity becomes constant beyond 40% soil moisture and then decreases with increasing soil moisture. The highest sensitivity of S-band backscatter to soil moisture was found at medium incidence angles (30-37°) like the C-band data (Rahman et al. 2008). Based on these results, there is a scope of estimating the soil moisture change based on multi-temporal S-band backscatter (Du et al. 2010).

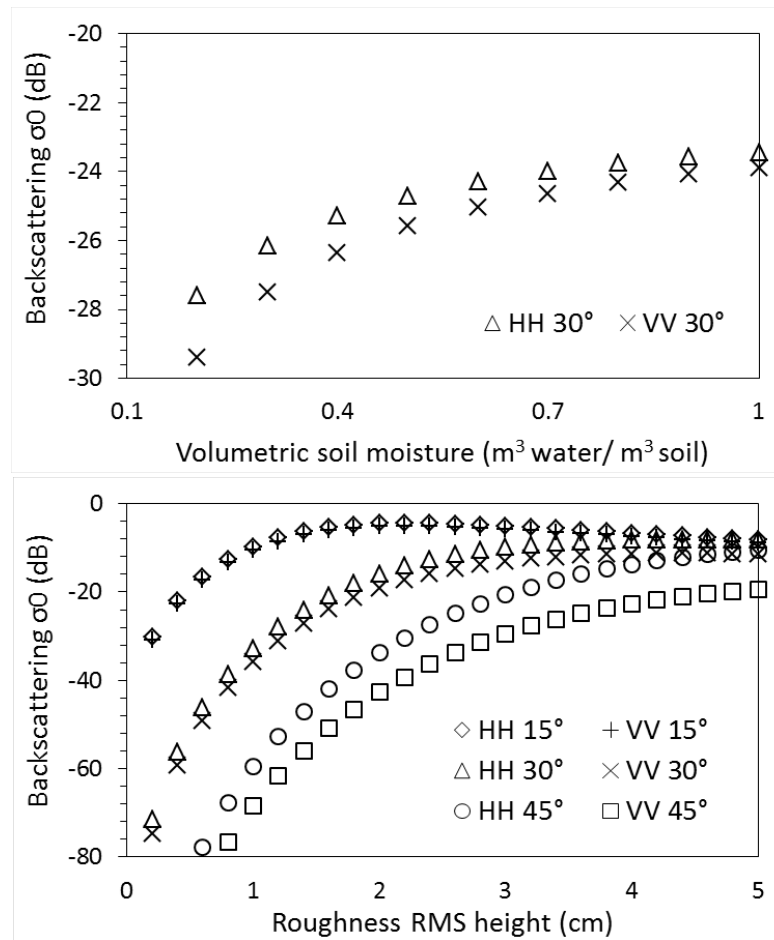


Figure 4.1. S-band ground backscatter vs. soil volumetric moisture ($\text{m}^3 \text{ water} / \text{m}^3 \text{ soil}$) (top) and soil RMS height (cm) (bottom) for co-polarisation at 15°, 30° and 45° radar incidence range.

What is the relationship between soil surface roughness and S-band backscatter across polarisations and incidence angle range?

For soil roughness simulation, sensitivity of S-band backscatter ranges slightly higher between -10 to -60 dB across the incidence angle range. When the soil surface roughness (*rms* height) was increased from 1 to 5 cm as a function of different incidence angle range, a higher backscatter in all co-polarisations was observed. At near incidence angle range, the backscatter increases gradually up to 2 cm and then decreases, however the sensitivity of S-backscatter to soil roughness for medium incidence angle range persists up to 3 cm and then saturates thereafter. In the far incidence angle range, the sensitivity of backscatter increases little bit further than medium incidence angle range (Figure 4. 1).

At medium incidence angle range $\sim 30^\circ$, S-band backscatter shows more significant relationship with soil surface roughness (logarithmic model: $r^2 = 0.95$, $P < 0.0001$) for both HH- (RMSE 3.55) and VV-(RMSE 3.56) polarisations. Similar strong relationship also exists between surface roughness and backscatter at high incidence angles. This result shows that S-band backscatter is sensitive to soil surface roughness at medium to high incidence angles similar to X-band (Aubert et al. 2011).

4.3.2. Deciduous crown layer with leaves and branches

The simulation results for deciduous forest canopy layer with leaves and branches as described in section 3.4.1 with Model experiment 3 is described below:

What is the relationship between leaves and branch densities, leaf-dominated, branch-dominated, varying levels of moisture content and stand height in deciduous canopy layer across frequencies, polarisations and incidence angle range?

Canopy Transmissivity

Figure 4.2 shows the simulated canopy transmissivity for deciduous canopy related to leaf-dominated, branch dominated and combined effect of leaf density across the frequencies at 830 leaves and 3.4 branch density. The simulated canopy transmissivity for crown layer with leaves and branches deciduous canopy shows high transmissivity value in L-band than shorter (X- and C-band) and medium (S-band) wavelengths. At shorter wavelength X-band, very low crown transmissivity of 0.05 has been observed in leaf-dominated canopy. On the contrary, a fully foliated crown appears to be transparent at the L-band measurements reaching up to 0.7. The S- and C-band shows greater crown transmissivity values than X-band but lesser than L-band sensitivity (Figure 4.2 a, b). Thus, simulated crown transmissivity decreases with increasing incidence angles in all the frequencies and polarisations at 830 leaves density with corresponding single-sided leaf area index of 5.0.

In the case of branch canopy without leaves, the simulated canopy transmissivity for co-polarisations for all frequencies are very close to 1 except for X-band (0.6) due to the lower volume density of branches (Figure 4.2 a, b). The canopy transmissivity also decreases along the incidence angle range and in increasing frequency for both

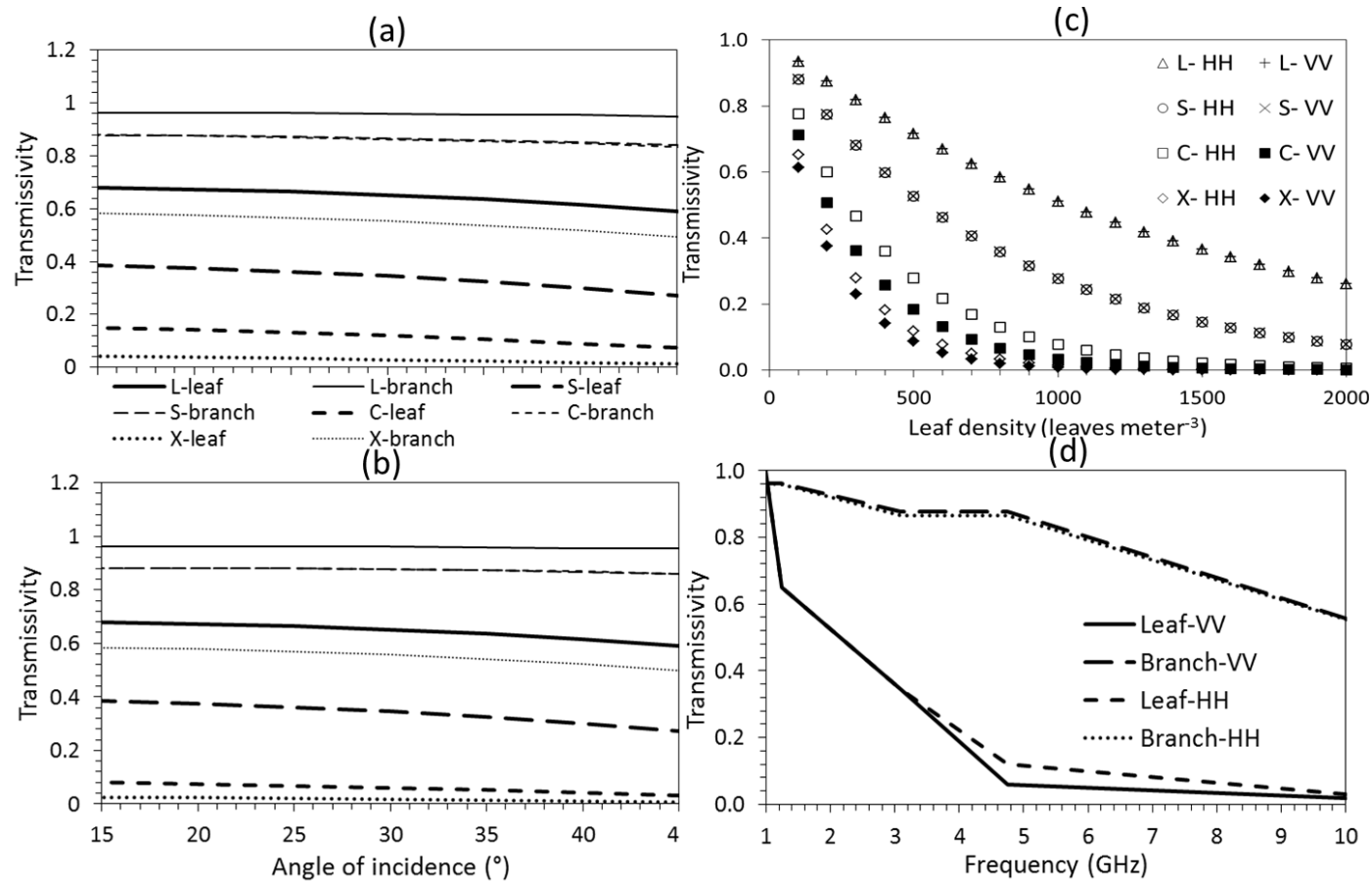


Figure 4.2. HH (a) and VV (b) polarisations crown transmissivity vs. scattering angle from 830 leaves per cubic meter and 4.1 branches per cubic meter, crown transmissivity vs. density of leaves at 30° scattering angle (c) and crown transmissivity vs. frequency for Birch for L-, S-, C- and X-bands (d).

co-polarisation with maximum value at L-band. This appears that backscatter returns in winter will exhibit strong scattering from forest canopy particularly in L- and S-band with co-polarisations across the incidence angle range. However, the strong return would be from both direct ground and ground/trunk interactions due to leaf-off and easy penetration of radar pulse reaching the ground surface.

The model suggests a decreasing trend in overall canopy transmissivity for all the frequencies and polarisations against the leaf density. This was expected, as the density of leaf increases, the radar pulse will be less efficient in penetrating through the closed crown canopy (Figure 4.2 c). Greater sensitivity of leaf density to crown transmissivity is particularly observed in shorter wavelengths (X- and C-band) with a rapid decline up to 700 leaves/ m density while a slow and further decline up to 1200 leaves/m (S-band) and 2000 leaves/m (L-band) was observed. In general, Figure 4.2 d shows the crown transmissivity as a function of frequency, confirming that the simulated crown transmissivity decreases with increasing leaves and branch densities across incidence angle range and frequency in both co-polarisations from 1 to nearly 0 in the case of leaf-dominated and 1 to 0.6 (branch-dominated) simulations. In L- and S-band, the transmissivity decreases to 0.3 at 2000 and 1200 leaf density respectively, while similar values of transmissivity was achieved by C- and X-band at very low density ~700 leaves.

Total Backscatter

The simulated total canopy backscatter as a function of incidence angle range for all the frequencies (L-, S-, C- and X-band) have been highlighted in Figure 4.3. The characteristics of the HH and VV polarisations of crown layer with leaf and branches signify quite differently where scattering exists between -3 to -15 dB for HH polarisation while a weaker backscatter between -10 and -20 dB for VV polarisation across incidence angle range (45 to 15°). In leaf dominated simulation, strongest backscatter occur at S-band between -5 to -8 dB (HH polarisation) and -10 to -15 dB (VV polarisation), while the minimum scattering arises from X-band between -8 to -13 dB (HH polarisation) and -15 to -18 dB (VV polarisation) with average scattering shared by both shorter wavelengths in the HH and VV polarisations respectively. In the case of cross-polarisations, the scattering is

relatively weaker and ranges between -25 to -35 across the incidence angle range. In fact, they are similar to strong attenuation shared by longer L- band followed by S- band in comparison to shorter wavelengths.

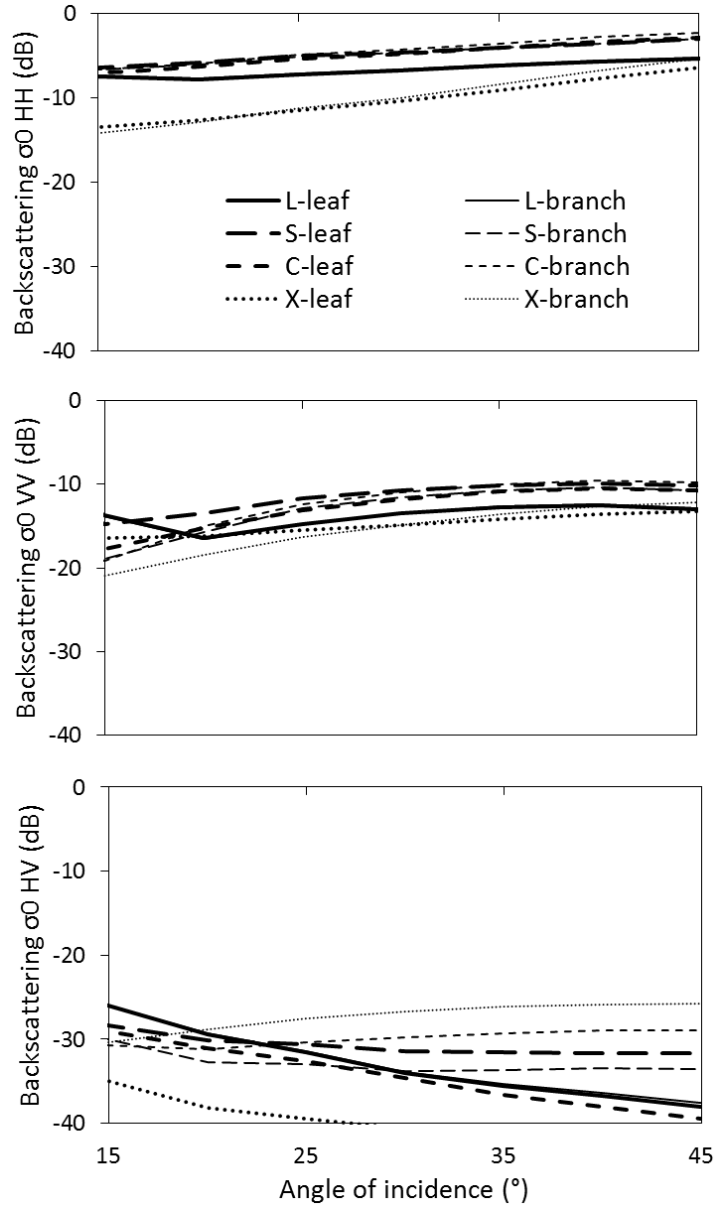


Figure 4.3. Total co- and cross-polarisations canopy backscatter vs. scattering angle from 830 leaves and 4.1 branch density Birch for L-, S-, C- and X-band.

In relation to branch canopy without leaves in winter season, simulated total canopy backscatter for both co- and cross-polarisations are different but the character of each does not change with the frequency. In the case of HH polarisation, total canopy backscatter for L-band is quite higher than both S- and C-band along the

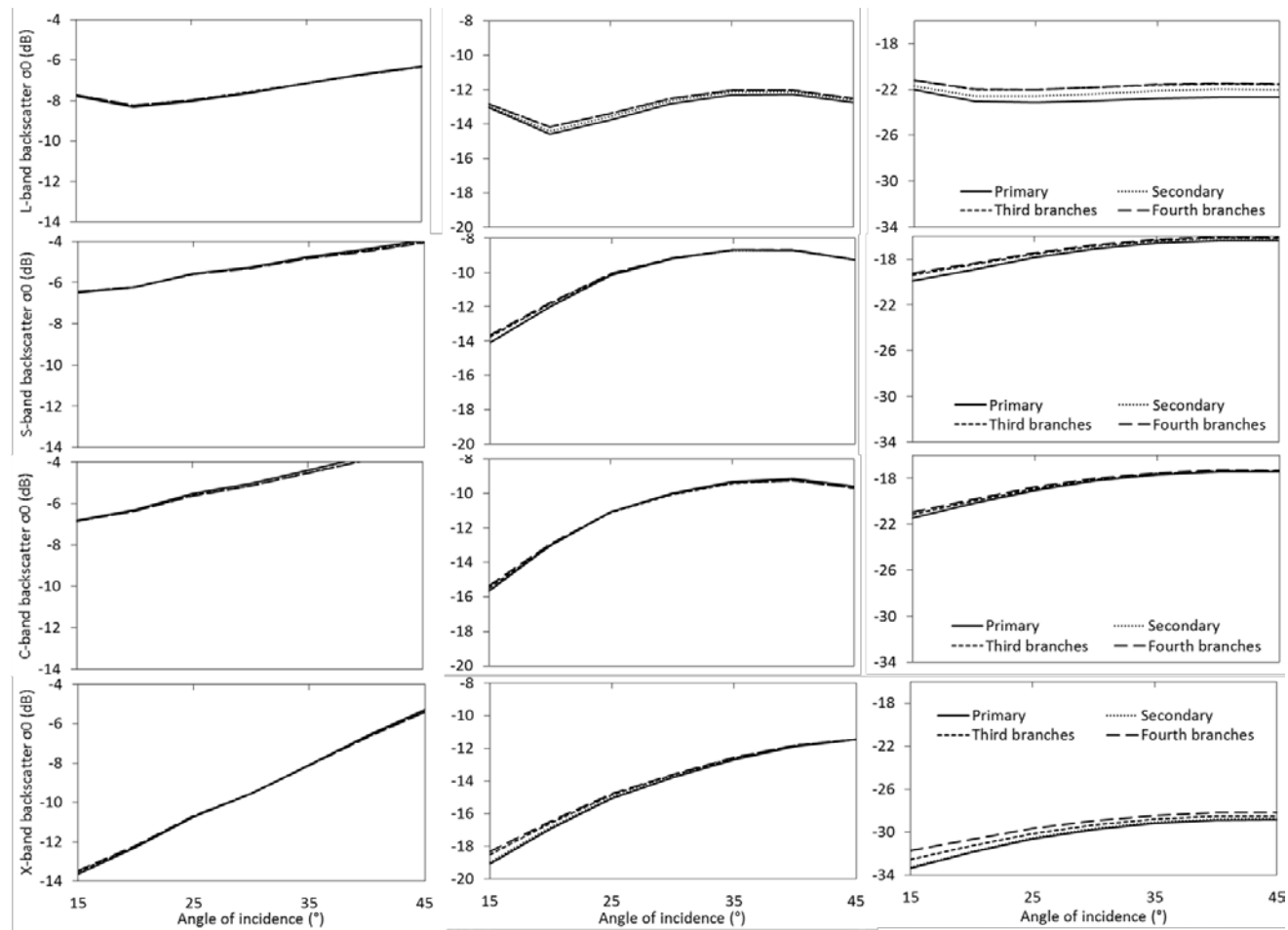


Figure 4.4. Total co- and cross-polarisations canopy backscatter vs. scattering angle from 4.1 branch density Birch at different branch levels for L-, S-, C- and X-band.

incidence angle range. However, both S- and C-band also exhibited a relatively higher total canopy backscatter in the far range direction. A higher total canopy backscatter is observed for both S- and C-band over L-band along the angle of incidence for VV polarisation. In relation to cross-polarisations, C- and X-band shows higher total canopy backscatter than longer L-band along the incidence angle range.

With different branch levels, strongest backscatter is evident for all polarisations for all bands with maximum at longer wavelength L-band and S-band for fourth level of branches in comparison to either primary and combined with secondary branches (Figure 4.4). Both the density of branches and higher branch levels showed a significant backscatter from forest canopies.

In general, the strong backscatter attenuation perceived by shorter to medium wavelength may be due to the multiple volume scattering from branches and twigs while ground/trunk interaction at longer L-band. Backscatter attenuation from branches shows a substantial effect on both co-and cross-polarisations characteristics but following similar pattern with the leaf-dominated canopy layer. Hence, SAR backscatter at L-band including S-band acquired during winter season will display a strong backscatter from primary branches, direct ground and ground/trunk interaction, possibly useful for forest structure retrieval. For example, better L-band backscatter prediction during winter season has been observed by Bosisio and Dechambre (2004), who investigated the radar backscatter sensitivity to seasonal variations in a 20 year old oak stand in Paris (France) using MIMICS.

The simulated backscatter returns from the forest canopy (*i.e.*, leaves, branches and trunk) is a function of dielectric constants of different canopy parts in terms of moisture content and physical temperature. At S-band, simulated backscatter signals from leaves decreases across the radar incidence range as a function of moisture content (dielectric) with lower sensitivity (logarithmic model: $r^2 = 0.7, 0.69$ and $0.57, P < 0.0001$) for HH- (RMSE 0.46), VV- (RMSE 0.47) and HV- (RMSE 0.92) polarisations at 0.5 volumetric moisture content (Figure 4.4). Whereas backscattering from trunk/branch increases across the radar incidence range. Similar pattern is also observed with total backscatter returns from the canopy.

With varying moisture content between 0.1 and 0.7 m³ water/m³ in different canopy parts, S-band backscatter shows a significant relationship with branch and trunk components (logarithmic model: r² = 0.95, 0.98 and 0.78, P <0.0001) for HH- (RMSE 0.29), VV- (RMSE 0.49) and HV- (RMSE 3.25) polarisations at average incidence angle range of 30° (Figure 4.5).

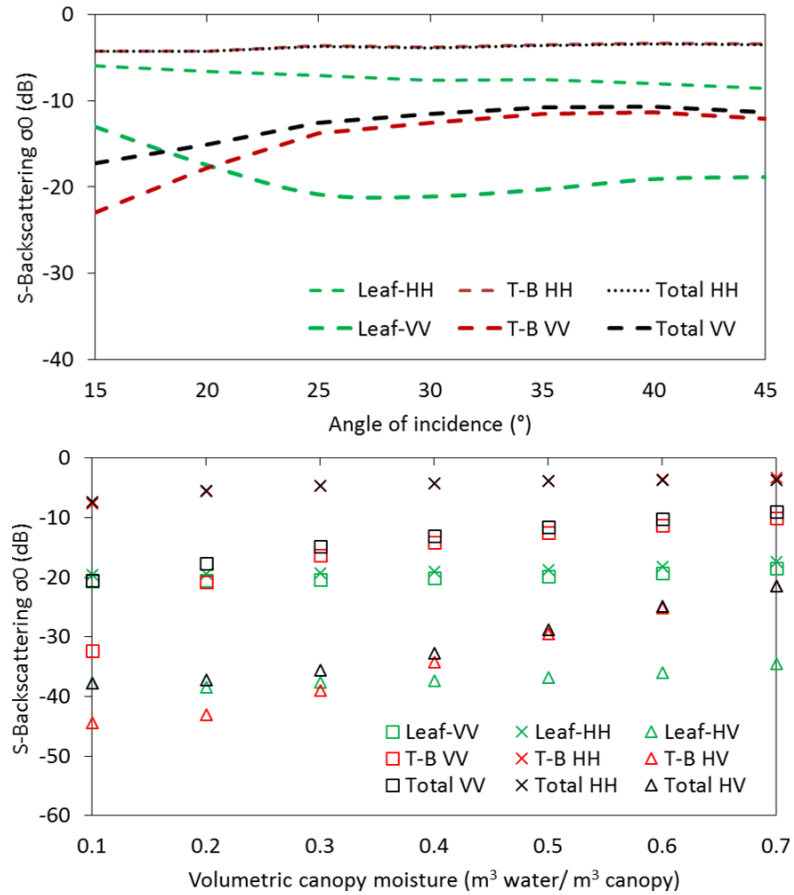


Figure 4.5. S-band backscatter vs. canopy parts at 0.5 volumetric moisture (m³ water/m³ canopy) across incidence angles (top) and at varying volumetric moisture (m³ water/m³ canopy) at 30° radar range (bottom) where T- and B- represents trunk and branches respectively.

The contribution of the individual interactions to the simulated total canopy backscatter across radar incidence angle range across different frequencies are investigated and shown in Figure 4.6. The simulated total backscatter for leaf-branch canopy layer as a function of frequency for all polarisations behaved differently with some resemblance that of leaf- and branch- dominated in the case of co-polarisation while branch-dominated behaviour in the case of cross-polarisation.

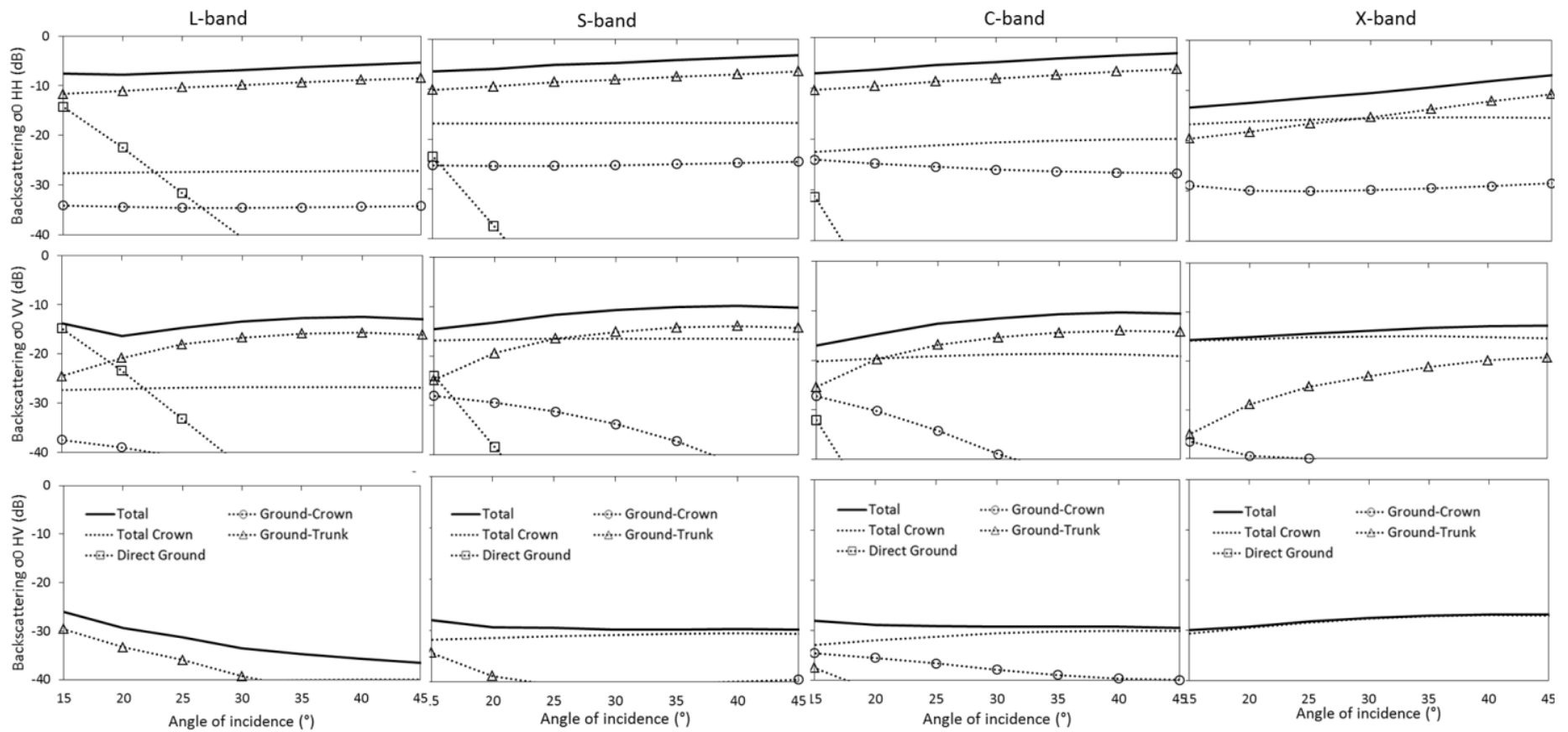


Figure 4.6. Total co- and cross-polarisations canopy backscatter components vs. scattering angle from 830 leaves and 4.1 branch density Birch at primary branch level for L-, S-, C- and X-band.

For L-band, simulated total canopy backscatter originates from ground/trunk interactions in HH and VV polarisations with some contribution from total crown (Figure 4.6 A). These interactions are closely related to leaf-dominated simulation. In the case of branch-dominated canopy layer, the longer L- band also predicted total backscatter for co-polarisations from ground/trunk interaction due to absence of leaves and more penetration reaching the ground layer. In the cross-polarisations, the dominant scattering also arises from ground/trunk interaction with some volume scattering in the far incidence angle range. The reason for ground/trunk interaction as the dominant scattering mechanism to the total backscatter is due to longer wavelength in comparison to the size of the leaf. This demonstrates the ability of L-band with 23 cm radar pulse for easy penetration in comparison to relative sizes of the leaves (Ulaby et al. 1990, Beaudoin et al. 1994, Liang et al. 2005).

For S-band, simulated total backscatter for leaf-branch canopy originates from ground/trunk interaction in HH polarisation while a combination of both ground/trunk and volume scattering at VV polarisation. On the contrary, direct crown has fully taken over as the main dominating factor to the total backscatter for cross-polarisation (Figure 4.6 B). This could be due to the reduced transmittance as a function of increasing leaf and branch density with HV polarisation signal (Figure 4.2 c). The transition of double-bounce scattering from ground/trunk to volume scattering from the direct crown is more significant in the higher frequencies (C- and X-band) due to shorter wavelength in size and incapable to pass through the leaf and branch components. In all the polarisations, backscatter from direct ground (a function of soil moisture and roughness) is lower across the incidence angle range than forest canopy backscatter.

Additionally, the depth of crown and density of leaves/ branches played a significant role in the strength of the backscatter signal. This result shows that S-band backscatter can interact with different canopy components particularly with large branch, trunk and ground layer depending on the canopy structure. This modelling result supports the studies reported by Fransson et al. (1999) and Yatabe and Leckie (1995) who could differentiate clear-cut stands against forest using Almaz S-band data. Furthermore, the predicted S-band backscatter could also provide some information related to forest structure including biophysical parameters due to

ground/trunk interaction as dominant scattering but lesser than longer L-band and seeks further investigation.

For the shorter wavelengths at C- and X-band, the simulated total backscatter arises from a combination of both ground/trunk and direct crown scatterings for co-polarisations (Figure 4.6 C, D). This direct or total crown scattering primarily originates from the small branches and foliage leaves. As a result scattering from ground/trunk were attenuated largely by the top of the canopy. For X-band, the dominant scattering to the simulated backscatter level is first directly from crown particularly in near range followed by double bounce interactions via ground/trunk scattering beyond 35° incidence angle for HH polarisation. In contrast, VV polarisation showed volume scattering from direct crown canopy mechanism with little ground/trunk sensitivity due to shorter wavelength in relation to canopy components. The cross-polarisation displayed a strong total crown scattering in C- and X-band due to the combination of direct crown and crown-ground interactions.

Generally, the direct crown interaction mechanism is more of a significant contributor to total backscatter at C- and X-band unlike the L- and S-band in all the polarisations across the radar incidence range. However, the ground/trunk interaction seems to be little contributor to overall backscatter particularly in case of co-polarisations while, negligible in the case of cross-polarisations for higher frequencies. Overall, it gives an impression that C- and X-band backscatter could only pick up the interaction from the crown canopy rather than other interactions possibly due to lower penetration level than L- and S-band.

Figure 4.7 shows the simulated backscatter for all polarisations from longer wavelength at P-band through S-band to shorter wavelengths at X-band in different branch levels. With the fourth level of branches, strong backscatter is evident for all polarisations in comparison to primary branch level for all SAR frequencies (Figure 4.6). At P- band, dominant scattering occurred through interaction between the trunks and large branches and the ground surface in all polarisations. With other SAR frequencies, major scattering is found through direct crown interaction for most polarisations in high density and fourth level of branches.

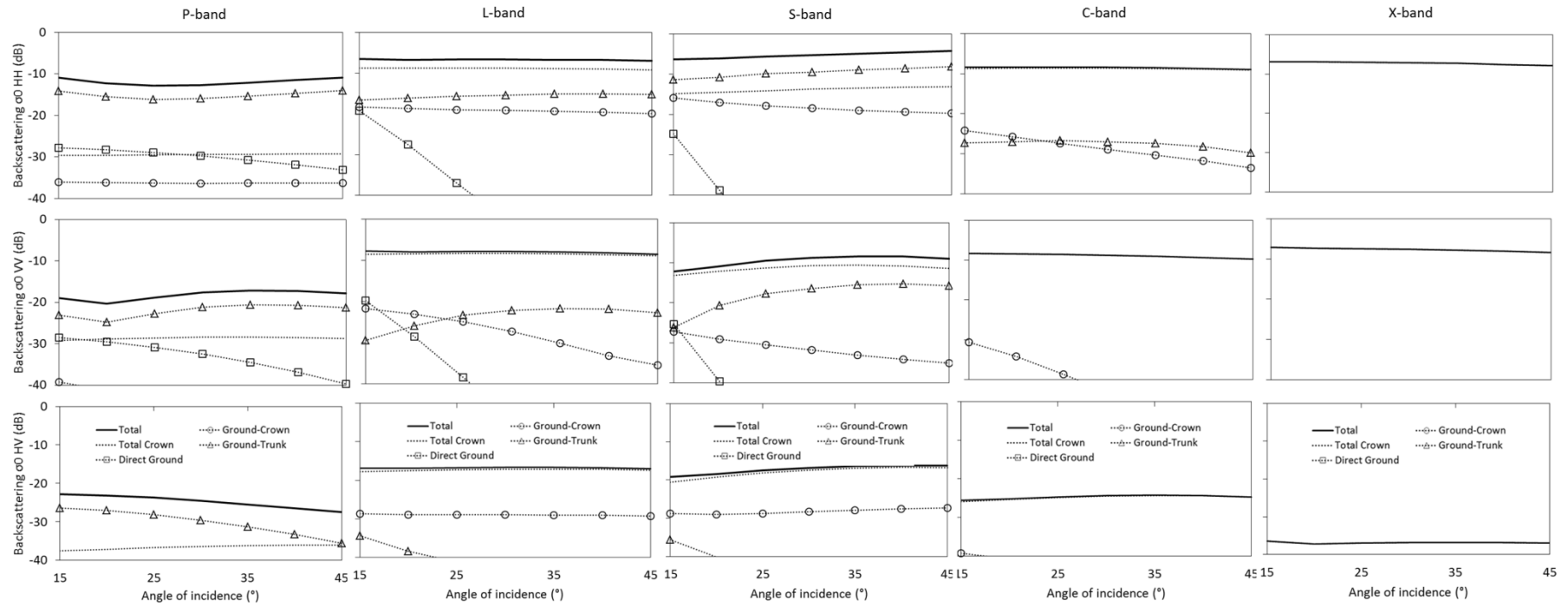


Figure 4.7. Total co- and cross-polarisations canopy backscatter components vs. scattering angle from 830 leaves and 4.1 branch density Birch at fourth branch levels for P-, L-, S-, C and X-band.

In relation to simulated total canopy backscatter as a function of frequency at 30° incidence angle range, co-polarisations showed an increasing trend from longer wavelength at P-/L-band to S-band and decreases to C-/X-band for small branch diameter (1 -3 cm) (Figure 4.8 A). Similar trend of total canopy backscatter with cross-polarisations is also evident across frequencies (Figure 4.8 C). However, in both co- and cross polarisations strong total canopy backscatter is evident at P-/L-band and then decreases along the radar frequencies with larger size branch at 5 cm (Figure 4.8 A, C). Thus, longer wavelength at P-/ L-band radar backscatter shows strongest with thick branches in comparison to other wavelengths but weaker than S-band radar backscatter with smaller branches.

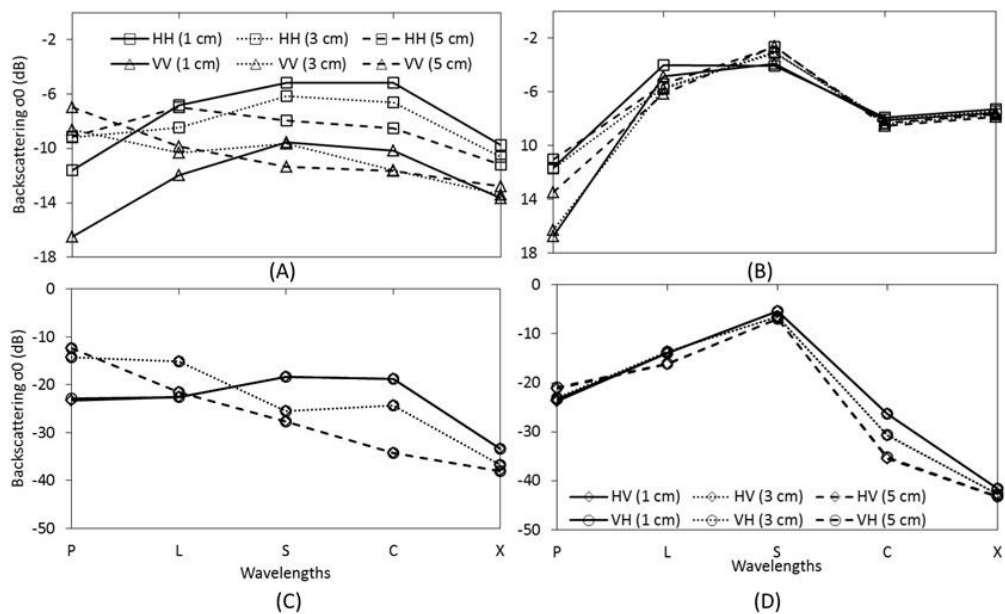


Figure 4.8. Total canopy backscatter vs. SAR wavelengths from 4.1 branches per cubic meter, primary branch diameter (1 cm, 3 cm, 5 cm) (A, C) with 830 leaves per cubic meter (B, D) Birch stand at 30° scattering angle for co- and cross-polarisations.

When the leaves were added to different branch density of varying sizes, co-polarisations shows similar backscatter sensitivity at L-and S-band higher than longer wavelength at P-band and shorter wavelengths with small branch size. With thick branches size up to 5 cm, S-band shows strongest total canopy backscatter in comparison to both longer wavelength at P-/ L-band and shorter wavelengths at C-

and X-band (Figure 4.8 B). This trend is more evident with cross-polarisation between S-band and other wavelengths (figure 4.8 D). The main reason for a higher backscatter return at S-band than longer wavelength at P-/ L-band could be due to the sensitivity of the S-band signal within a range of diameter thickness of branches and differences in the moisture condition in branches and leaves when the model was simulated. This clearly shows the sensitivity of dielectric constant (i.e., moisture content) of canopy components in predicting the radar backscatter signal.

Additionally, the structure of forest stand could be a potential attribute to the S-band backscatter behaviour. For example, study in a 20 year old oak stand in Paris (France) utilising both MIMICS and Karam models have reported low backscatter with longer wavelength at L-band and shorter wavelength at C-band due to the lack of forest heterogeneity cover (Bosisio and Dechambre 2004). However, the sensitivity of S-band total canopy backscatter to the diameter of branch as outlined above need further investigation since the transition from Rayleigh to optical scattering depends on the physical size and shape of the scattering target, for instance diameter of the branch (Woodhouse 2006b).

Figure 4.9 shows the total backscatter at 30° incidence angle range for stand canopy height across frequencies and polarisations. At L-band, dominant scattering originates from branches and stems. With the increasing canopy height, the backscatter comes more from ground/trunk interactions and less from direct layer scattering particularly at HH polarisation. However, this backscatter trend changes at VV polarisation from intermediate canopy height with scattering from the crown layer at cross-polarisation. At S-band, dominant backscatter comes from the ground/trunk interaction up to 5 m stand height (HH-polarisation) and high scattering comes from the crown layer with increasing stand height in all polarisations. This trend is clearly observed in higher frequencies at C- and X-band.

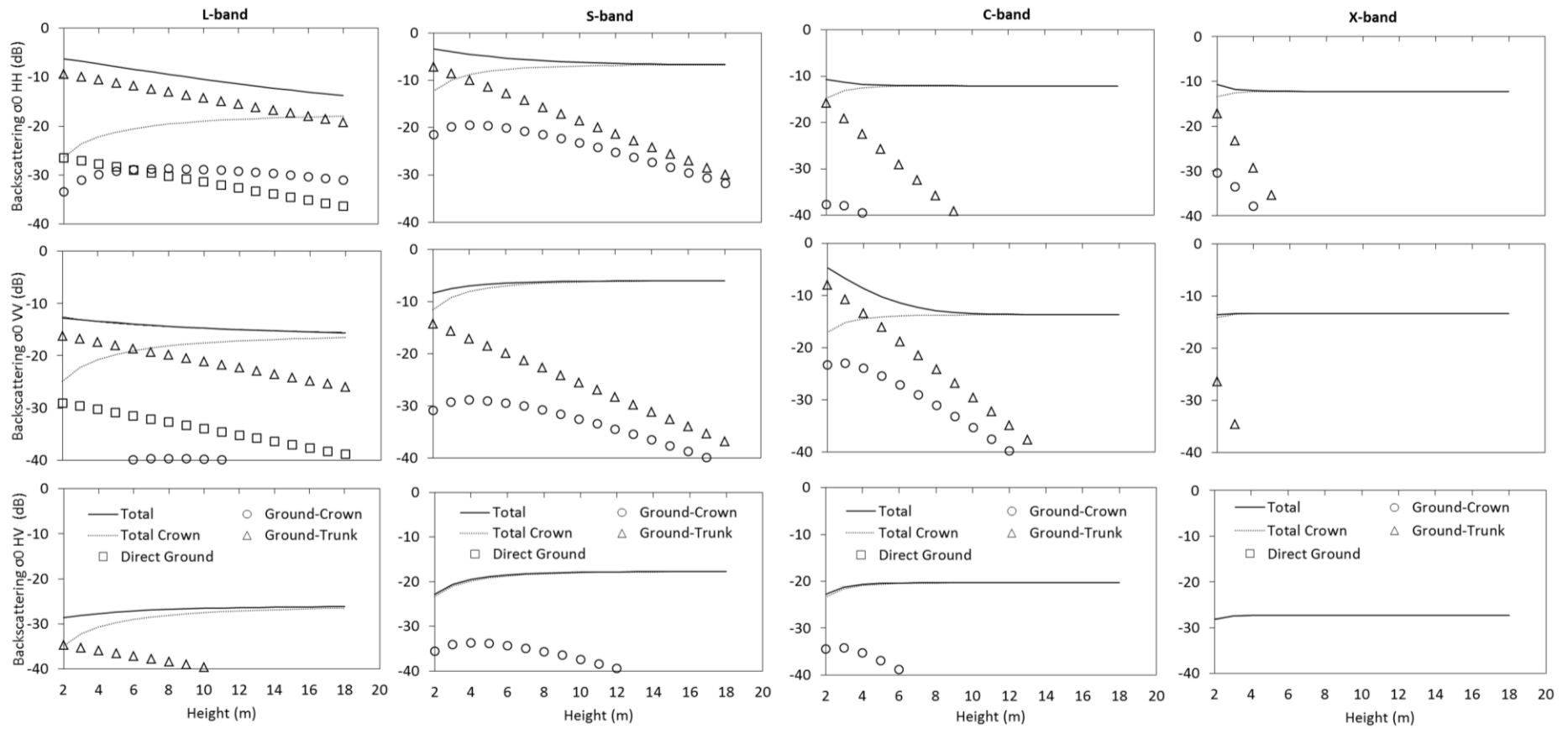


Figure 4.9. Total co- and cross-polarisations canopy backscatter components vs. canopy stand height (m) from 830 leaves and 4.1 branch density Birch for L-, S-, C- and X-band at 30° incidence angle.

4.3.3. Coniferous crown layer with needles and branches

The simulation results for coniferous forest canopy layer with needles and branches as described in section 3.4.1 with Model experiment 4 is described below:

What is the relationship between needle density and needle-branch canopy layer across frequencies, polarisations and incidence angle range?

Canopy Transmissivity

The simulated canopy transmissivity for crown layer with needles and branches for Norway spruce is showing very small values in comparison to Birch stand. For example, longer wavelength L-band is showing more transmissivity value than shorter to medium wavelengths (Figure 4.10 a, b). Thus, crown transmissivity decreases with increasing incidence angle range in all the frequencies for both HH- and VV- polarisations at 85,000 needle and 3.4 branch densities. Small values of crown transmissivity are due to the high density of needles and branches used to model the canopy with 11 meter crown layer thickness.

In relation to the effect of needle density, the simulated crown transmissivity drastically decreases with increasing needle density (5000 to 100,000) irrespective of frequency and polarisations (Figure 4.10 c). In general, the crown transmissivity as a function of frequency decreases in both HH and VV polarisations due to dense needles and tree architecture with multiple branches. Moreover, the radiometric length of the radar pulse across the frequencies makes it unsuitable for penetration within the forest canopy (Figure 4.10 d).

Total backscatter

The simulated total canopy backscatter across radar incidence range for all the frequencies (L-, S-, C- and X-band) have been highlighted in Figure 4.11 for co- and cross- polarisations. The characteristics of the co-polarisations for L-, C- and X-band are showing strong backscatter attenuation in comparison to S- band signal.

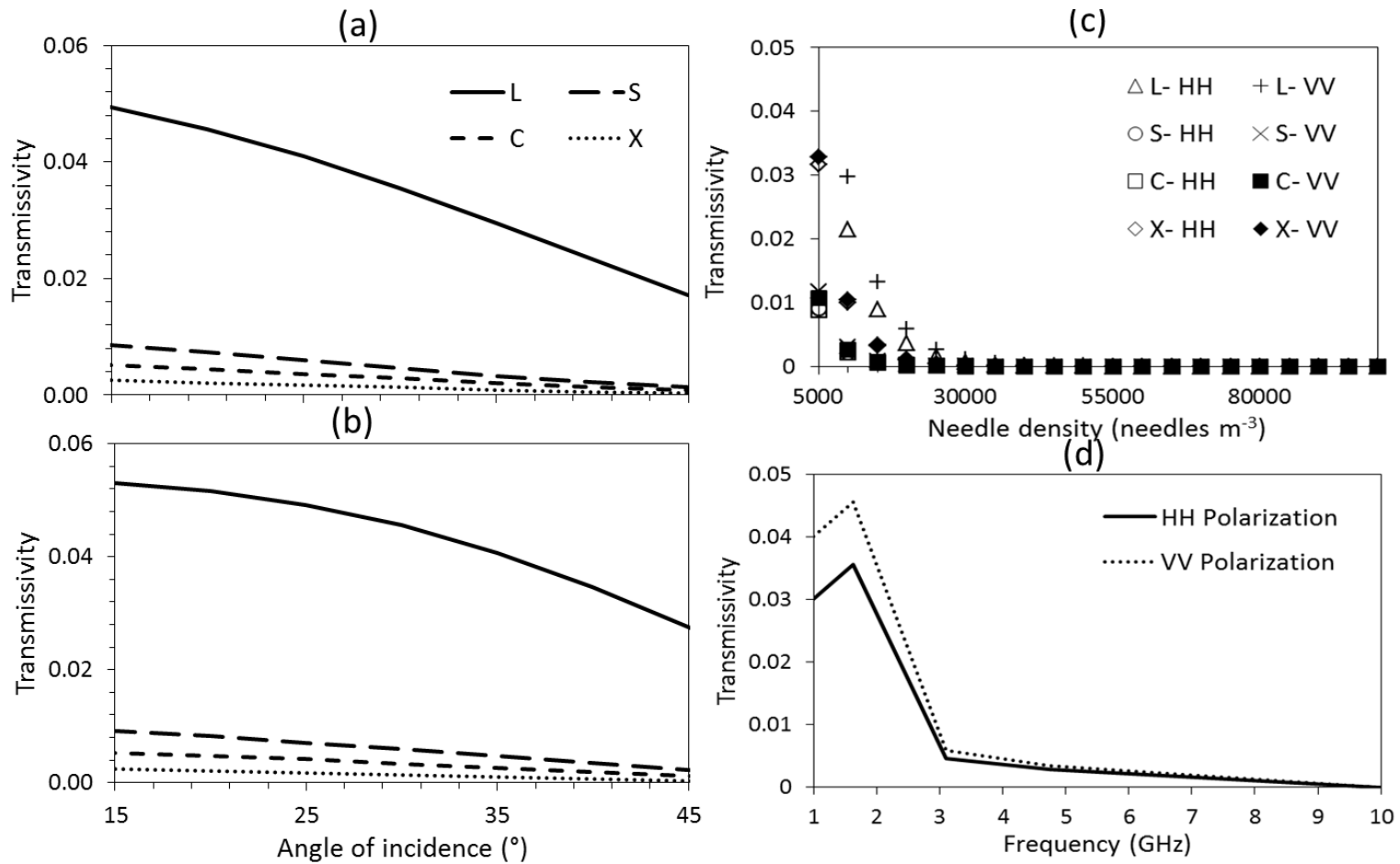


Figure 4.10. Horizontal (a) and Vertical (b) polarisation crown transmissivity vs. scattering angle from 85,000 needles and 3.4 branches per cubic meter Norway spruce, needle density at 30° scattering angle (c) and versus frequency at 30° scattering angle for L-, S-, C- and X-band.

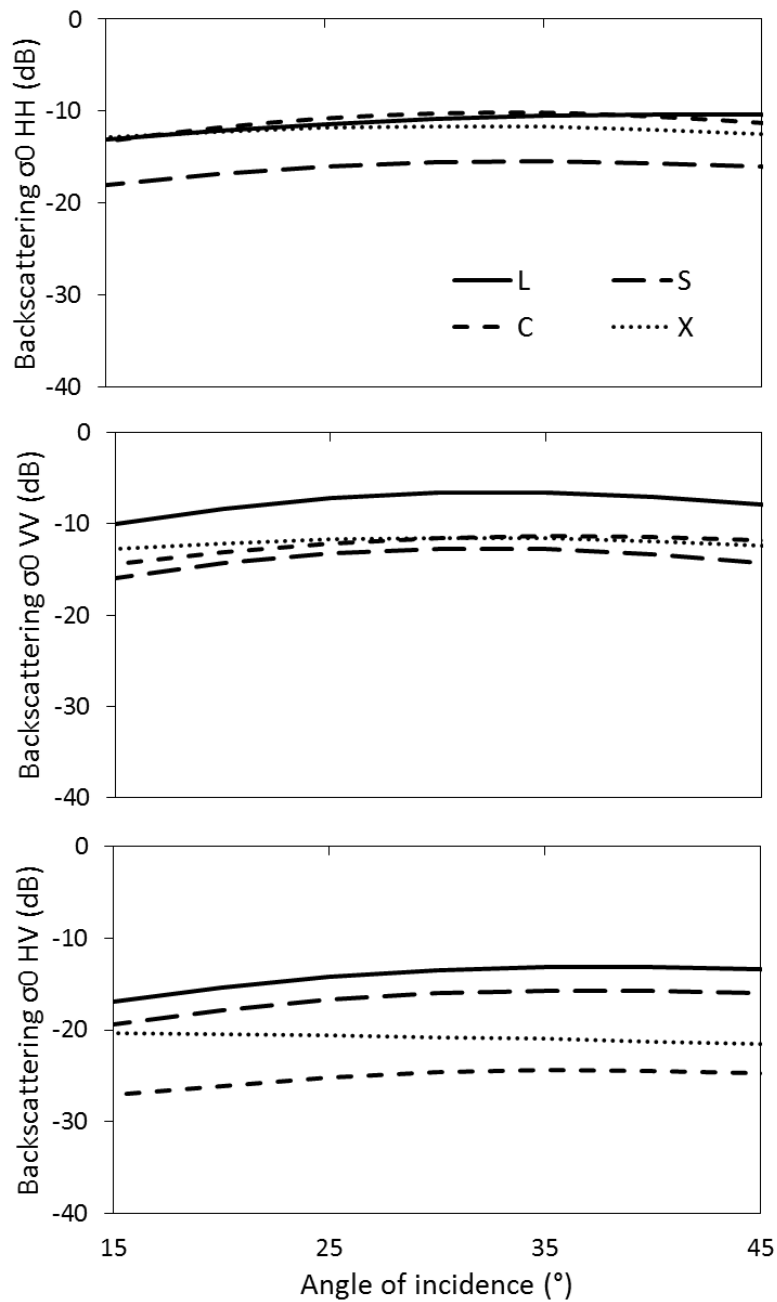


Figure 4.11. Total co-polarisation (top, middle) and cross-polarisation (bottom) canopy backscatter vs. scattering angle from 85,000 needles and 3.4 branch density Norway spruce for L-, S-, C- and X-band.

On the contrary, the HV polarisation shows strong scattering with L- and S-band followed by X- and C-band along the radar incidence angle range. Overall, it seems that both needle and branch densities have a substantial effect on both co-and cross-polarisations.

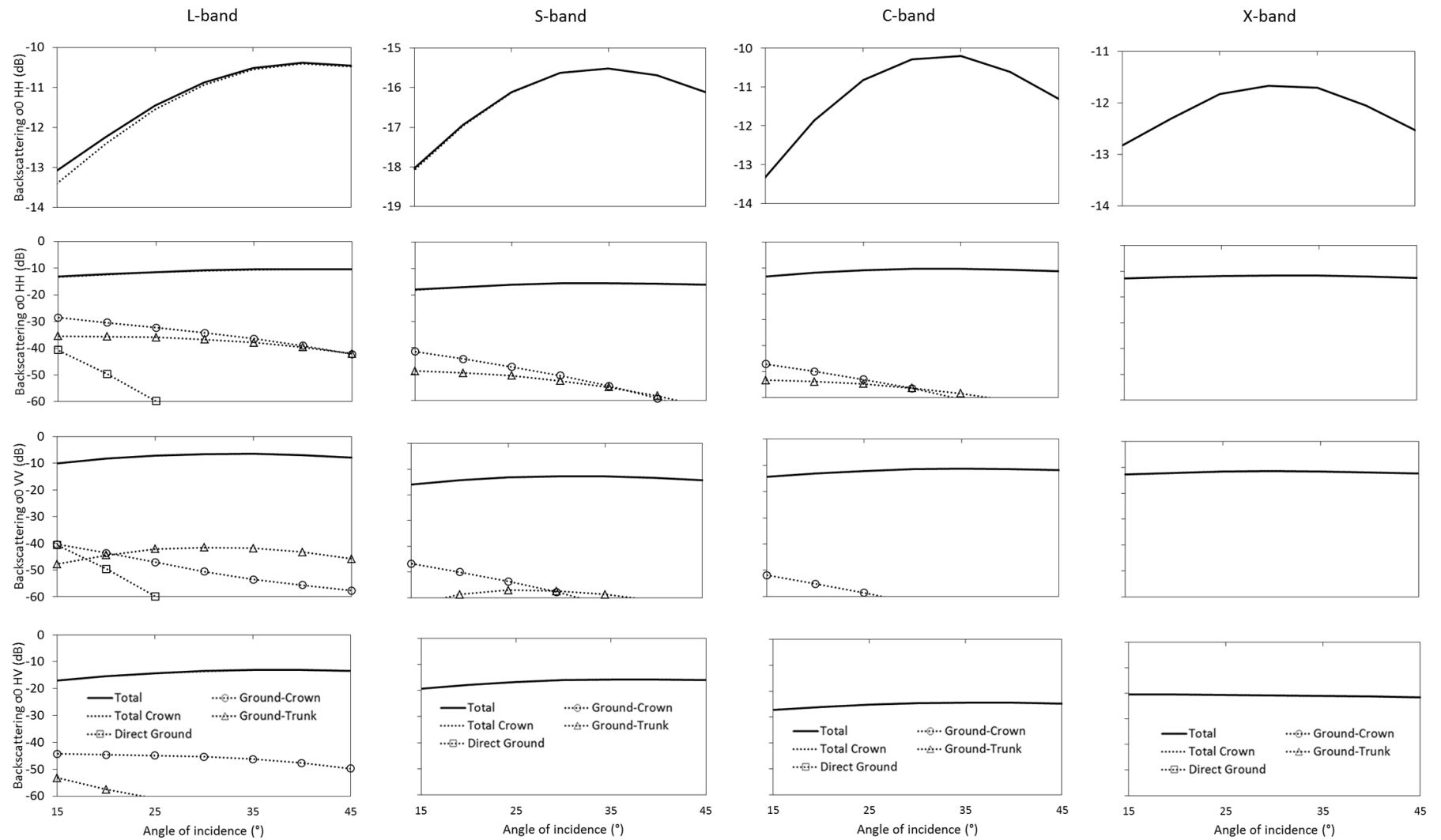


Figure 4.12. Total co-and cross-polarisations canopy backscatter components vs. scattering angle from needle-branch canopy layer 85,000 needles and 3.4 branch density Norway spruce for L-, S-, C- and X-band.

The contribution of the individual interactions to the total canopy backscatter as a function of radar incidence range and frequencies are shown in Figure 4.12. At L-band, the simulated total backscatter for all polarisations is dominated by the direct crown backscatter component with some minor ground-crown and ground/trunk interaction across the incidence angle range. This is due to the low crown transmissivity as a direct relationship with a high needle and branches densities and 11 meter crown thickness layer. In general, conifers are cone-shaped having steep vertical layer from top to bottom with increased needles and branch density at the bottom layer. The needle number density seems to be the main factor responsible for weak scattering from the sub-canopy layers and as a result of which the woody components (that is branches and trunk) are insignificant contributor to the total backscatter (Bosisio and Dechambre 2004).

At S-band, the simulated total canopy backscatter for both co- and cross-polarisations is dominated by the direct crown backscatter component across the incidence angle range. This is due to the lower volume scattering as the main scattering arises from the needles and branches of conifer canopy (Lopez-Sanchez et al. 2000). In this frequency unlike longer wavelength at L-band, all the polarisations resembles to leaf-branch deciduous species particularly in HH polarisation with some ground and crown in cross-polarisation.

In comparison to longer wavelengths, both shorter wavelengths at C- and X-band also displayed the direct crown component to be the major contributor to the simulated total backscatter for both co- and cross-polarisations across the incidence angle range. In these frequencies, all the polarisations does not show any other components to be a contributing factor for the total backscatter signal due to shorter wavelength and a high needle density canopy layer (Beaudoin et al. 1994, Le Toan et al. 1992, Liang et al. 2005, Ulaby et al. 1990). Additionally, the weak relationship between SAR backscatter and conifer species canopies could also be due to homogeneity in forest structure (e.g. stand height) in comparison to complex deciduous stand (Bosisio and Dechambre 2004).

Figure 4.13 shows the simulated total canopy backscatter decreases as a function of frequency irrespective of the polarisations for coniferous stands. The co-

polarisations showed strongest total canopy backscatter from longer wavelength at L-band and then decrease along the frequencies for thinner to thick branches and needle density (Figure 4.13. A). Similar trend is also evident with cross-polarisations as a function of varying branch thickness (Figure 4.13. B). For both the polarisations, simulated S-band total canopy backscatter shows strongest than longer wavelength at L-band and shorter wavelengths for medium size branch thickness of 3 cm. This shows that the diameter of the branch cylinder in coniferous canopy reflects varying sensitivity at radar wavelengths and polarisations. The above results with strong total canopy backscatter sensitivity from both forest types at S-band frequency need further investigation as a function of physical size, density of branch, needles and their moisture conditions.

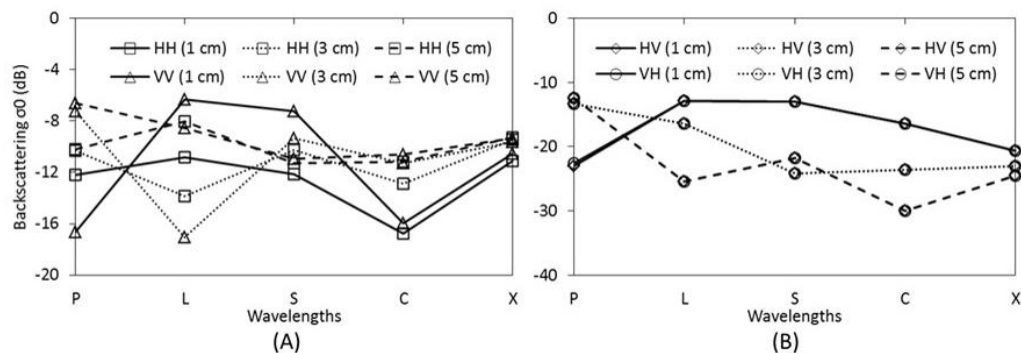


Figure 4.13. Total canopy backscatter vs. frequency from 85,000 needles and 3.4 branch density per cubic meter at varying branch sizes (1 cm, 3 cm, 5 cm) for co- (A) and cross-polarisations (B) Norway spruce at 30° scattering angle.

4.3.4. S-band backscatter responses from soil against forest canopy

What is the relationship of soil and forest canopy (deciduous and conifers) to the S-band backscatter signal?

In this experiment, forest canopies simulations with MIMICS-I suggest strong S-band radar total backscatter returns particularly in deciduous stands and slightly weaker scattering from coniferous canopies (Figure 4.14). Total backscatter at HH polarisation is high due to ground/trunk interactions from the deciduous canopy, higher than for a coniferous canopy. This trend is also evident for VV polarisation. In all the polarisations, backscatter from bare-ground (a function of soil moisture

and surface roughness) is lower across the incidence angle range than forest canopy backscatter. The simulation suggests that S-band backscatter can differentiate forest and non-forest due to the loss of the double-bounce scattering scattering from ground/trunk interaction when the canopy is removed. In comparison to the model predictions, the observed S-band radar backscatter coefficients from the airborne data reveals similar trends but with lower sensitivity for both forest types and soil properties. The radiative scattering mechanisms at S-band simulated by MIMICS-I show a similar behaviour like the longer wavelength at L-band for forested areas (Grover et al. 1999).

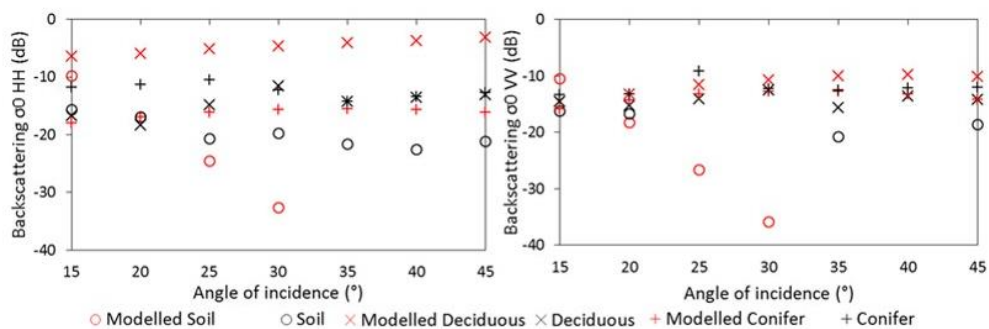


Figure 4.14. Simulated forest canopy (deciduous, conifers) and soil total backscatter relationship as a function of radar incidence range at S-band (modelled against SAR data).

4.3.5. Reduced canopy components

The simulation results for deciduous forest canopy degradation as a function of reduced canopy components as described in section 3.4.1 with Model experiment 5 is described below:

What is the radiative behaviour of S-band backscatter to reduced canopy component?

The simulation results related to forest degradation at L- and S-band backscatter as reported in this study represent the radiative behaviour of L- and S-band as a function of canopy structure and stand density based on the field data and existing literature on forest fire and logging to radar backscatter. However, the disturbance related to forest fire does not exist in the study sites.

Microwave scattering for birch stands with changing canopy characteristics are simulated taking forest fire as the external driver. The simulation resembles birch deciduous stand at low 0.012 tree density, 16.18 m canopy height, 38 cm DBH and 342.43 t/ha AGB with leaf-branch and trunk component prior to fire outbreak. In the post fire scenario, different scenarios related to secondary branches-leaf with trunk, primary branches-leaf with trunk and only trunk were simulated as a function of repeated fire occurrence in the same stand. Basically, the upper canopy of the tree contains foliage component primarily leaves, twigs and small branches. The high density of leaves and their relative high moisture content in comparison to other woody parts may therefore allow lower level of radar signal penetration in shorter SAR wavelength. Thus, removal of canopy components such as leaves and branches by fire could affect the backscatter from the canopy as a function of radar wavelength and polarisations (Ferrazzoli et al. 1997).

In Figure 4.15 (A) simulated backscatter signal from VV polarisation in the longer wavelength at L-band displayed a strong scattering in all the cases and particularly in open canopy due to repeated fire outbreak in the leaf- and branch-dominated. This is due to more penetration level of L-band allowing stronger scattering mechanism similar to large branches, stem or forest floor (Le Toan et al. 1992). On the contrary, a weaker and reduced scattering has been observed in the cross-polarisation from high density canopy through leaf- and branch-dominated cases.

A reduced backscatter returns have also been observed from the trunk only due to open canopy and more single scattering from direct ground and ground/trunk interaction. Further weaker but greater backscatter variability has been observed from forest floor in both polarisations. This is commonly observed in burn forest sites due to increased soil exposure through burning of canopy components, making soil drier and comparatively smoother (Kalogirou et al. 2014). On the other hand, strong backscatter return was evident from the rough soil with wet condition particularly in co-polarisation due to sensitivity to both high moisture content and surface roughness. Similar trend has been related to the temporal backscatter variability with JERS-1 data acquired in post fire (Takeuchi et al. 2000).

In the S-band frequency, co-polarisation (i.e., VV) also displayed a strong backscatter signal in the high canopy with fourth branches density and decreases in

varying levels of reduced canopy structure due to repeated fire occurrence (Figure 4.15 B). In the case of cross-polarisation, greater variability of backscatter dynamic range can be more prominently evident in comparison to co-polarisation with around 10 dB difference. For example, maximum backscatter variability could be evident from the standing trunk only without canopy foliage due to ground/trunk interaction similar to leaf-off winter condition. Therefore, removal of canopy components such as leaves and branches over time affects the backscatter from the canopy in a decreasing order particularly in S-band frequency.

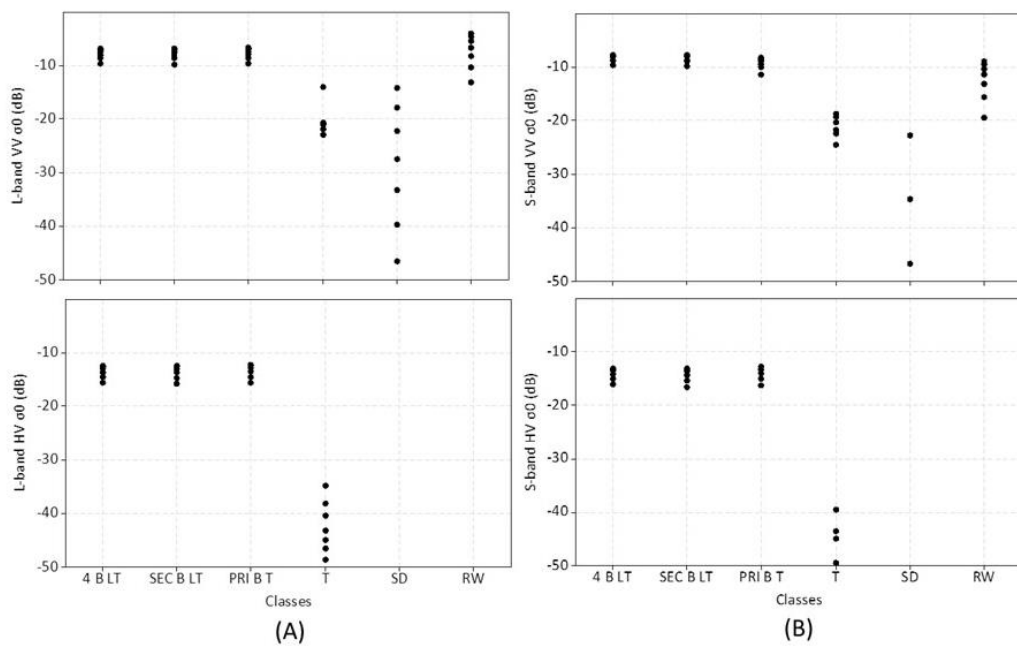


Figure 4.15. Simulated backscatter for forest degradation as a function of canopy structure for deciduous stand at 0.012 tree density, 16.18 m canopy height, 38 cm DBH and 342.43 t/ha AGB for L- (A) and S-band (B) for VV- and HV- polarisations (15° - 45° incidence angles) where 4 B: fourth branches, SEC B: secondary branches, PRI B: primary branch, L: leaf, T: trunk, SD: smooth dry soil and RW: rough surface wet soil.

A weaker and reduced backscatter was also observed in the S-band frequency from the soil layer particularly in smooth and dry moisture condition while strong backscatter arises from the rough surface with high moisture condition in the co-polarisation. This result seems to be consistent with backscatter using C-band data in Mediterranean region where higher soil moisture content increases backscatter

(Tanase et al. 2010). Finally, sensitivity of the overall total canopy backscatter from reduced canopy components caused by fires would depend on the condition of the canopy component (leaves, branches) including moisture content and underlying soil conditions (Tanase et al. 2010, Ferrazzoli et al. 1997, Kalogirou et al. 2014) due to the transition of radar backscatter from volume (canopy) to single (bare soil) scattering.

4.3.6. Reduced tree density

The simulation results for deciduous forest canopy layer with leaves and branches as described in section 3.4.1 with Model experiment 6 is described below:

What is the radiative nature of S-band backscatter to varying tree number density?

Degraded forest can also be related to a reduction in number of tree density in an area due to selective logging for a particular species of high commercial value. The simulation resembles degradation of mixed deciduous stands with selective logging as an external driver. This can be related to more opening of canopy gap due to canopy damage and fragmentation (Asner et al. 2006) due to long-term impacts of logging and are more prone to fire (Cochrane 2003). For instance, a closed canopy stand displayed strong backscatter at L- and S-band due to large number of trees. This strong backscatter can be due to the relative scattering mechanisms from ground/trunk interactions from the forest canopy. In this scenario, reductions in the strength and dynamic range of the backscatter have been observed across the radar incidence range in low tree density. This means, a weaker radar return has been observed from either bare-ground with low-vegetated or low tree density (e.g. savannah ecosystem) or combination of both due to forest canopy gaps.

With the decreasing number of tree density, a reduced simulated total canopy backscatter has been observed in L-band in almost all the polarisations particularly at medium incidence angle (Figure 4.16. A). Co-polarisations show a reduced backscatter from high number of tree density to low tree density but this reduction in backscatter is not prominent on average. This may be due to less attenuation from the upper canopy layer, providing more energy penetration and expectation of more scattering returns from available large tree trunks in low density. Possibly a strong ground scattering through low density canopy could be the basic reason for such a

scattering nature. A weaker backscatter has been observed in the cross-polarisations particularly in HV with some level of backscatter dynamic range of 5 -6dB. The cross-polarisation showed maximum backscatter range relative to co-polarisations. That is, the dynamic backscatter ranges between 6 dB, 3 dB and 2 dB for HV, VV and HH polarisations respectively.

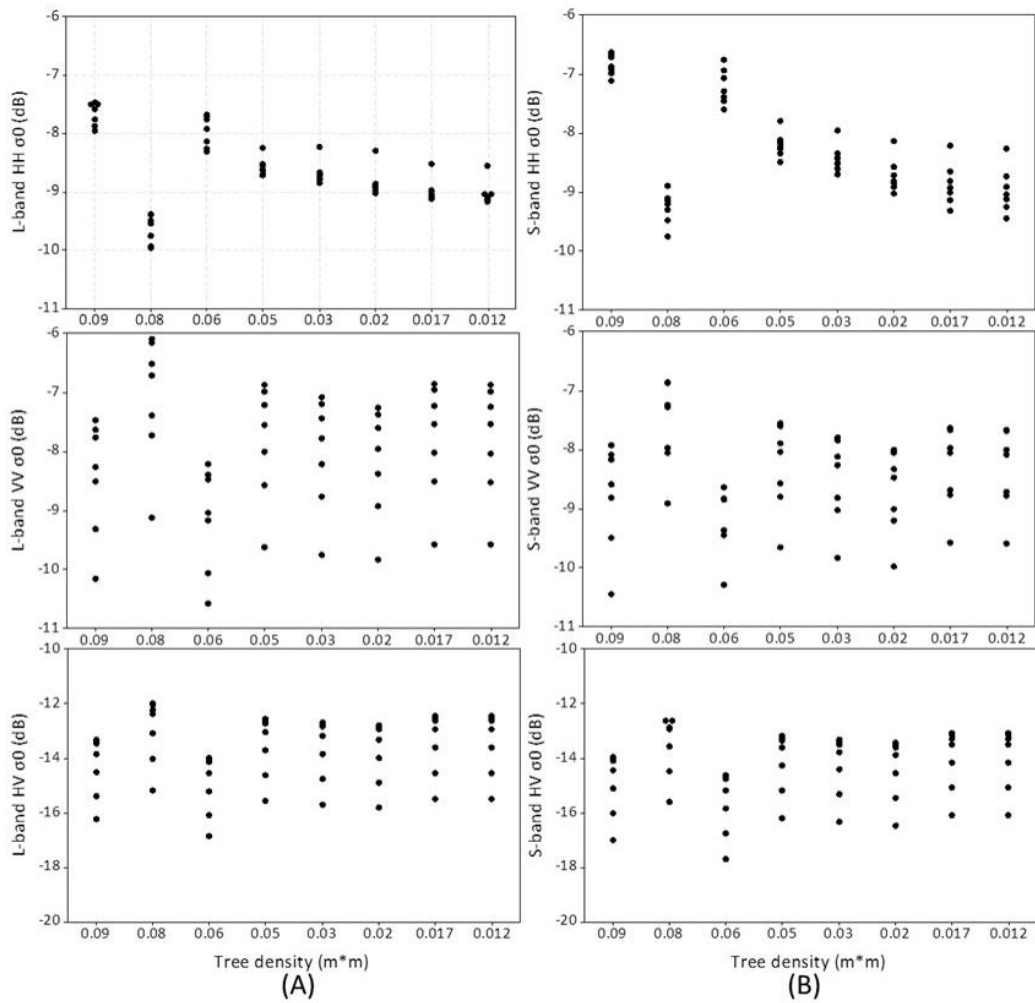


Figure 4.16. Simulated backscatter for forest degradation as a function of tree density with varying canopy height, DBH and AGB for L- (A) and S-band (B) (15° -45° incidence angles).

At S-band frequency, the overall strength of the simulated total canopy backscatter signal decreases due to low tree canopy cover in terms of area (Figure 4.16. B). In particular, a gradual decrease in S-band signal from high number of tree density (0.06 m²) up to open canopy 0.012 has been evident due to ground/trunk interaction.

Beyond a number density of 0.05 m^2 , a drastic reduction in the total canopy backscatter from S-band signal has been observed possibly due to more single scattering from soil and lesser volume scattering from fewer trees in the stand.

As a function of tree number density, relatively low variability in backscatter is found for S-band in comparison to longer wavelength at L-band in all polarisations. Similarly, a dynamic backscatter range between 6 dB, 4 dB and 3 dB for HV, VV and HH polarisations for S-band frequency has been observed.

Reduced backscatter variability is also observed in low tree density due to loss of volume scattering with more open area and less scattering from existing tree stands. If the soil components as highlighted in the reduced canopy characteristics were incorporated, there is a possibility that a strong backscatter from both soil conditions (smooth-dry and rough-wet) will inevitably overcome the backscatter return from the forest canopy. This shows that the high tree density increases the backscatter return due to more volume scattering (multiple) with canopy components and ground/trunk interactions while a mixture of weak and single scattering from soil properties and lesser volume scattering from lower number of tree density across frequencies and polarisation. This can also be related to the saturation of radar backscatter to the stand number density rather than the canopy opacity. Hence, the relationship of forest biophysical variable and radar backscatter depends on the trends in the stand –level structure where number density is a significant parameter for allometric models and provides useful information in the radiative behaviour of radar backscatter (Woodhouse 2006b).

4.4. Summary

The radiative transfer MIMICS-I has been applied to the modelling of backscatter signal from both deciduous and coniferous canopies including bare-ground for all the SAR frequencies.

The modelling experiments revealed six main results:

1. Simulated S-band backscatter shows a significant sensitivity to both soil moisture content (up to 40%) and soil surface roughness particularly at medium incidence range.

2. Simulated S-band backscatter was found to be more sensitive to forest canopy cover than shorter wavelengths at C- and X-band due to ground/trunk interactions being dominant in deciduous species.
3. There was sensitivity of S-band backscatter to the crown layer component. For both forest types studied, the presence of leaves and needles provided strong backscatter particularly in co-polarisations with radar incidence range. For deciduous type, simulated backscatter from branches also show a substantial effect when simulated in winter condition. The sensitivity of the simulated S-band backscatter to branch and trunk components with varying moisture content, polarisations and incidence range.
4. The MIMICS-I model also confirmed that longer wavelength at P-/ L- and S-band shows higher backscatter returns from forest canopies than shorter wavelengths at C- and X-band as stated by Ulaby et al. (1990).
5. At S-band, dominant scattering comes from the ground/trunk interaction up to 5 m stand height (HH polarisation) followed by the crown layer with increasing stand height.
6. A low S-band backscatter return has been predicted as a function of temporal backscatter changes due to reduced canopy characteristics (structure) and low tree number density.

At this stage from the modelling perspective, the simulated S-band canopy backscatter is sensitive to forest structure particularly in co-polarisations and this simulation result needs further investigation using field data. Though, study conducted by Woodhouse (2006b) using the radiative transfer cylinder model incorporated with a macroecological model reported the backscatter-biomass relationship possibly due to single-scattering layer between Rayleigh to Optical scattering. In all the simulations particularly related to deciduous species, there is some scope to relate with forest structure due to the ground/trunk interaction as the dominant scattering. In conclusion, S-band SAR data have been found to be sensitive to soil properties (that is soil moisture and surface roughness) and forest canopy structure. This reported radiative nature of S-band backscatter sensitivity to soil and forest canopy will be useful in studies related to mapping forest cover and retrieval of forest structure including aboveground biomass.

Chapter 5: Forest/non-forest and change mapping using airborne S-band SAR backscatter

5.1. Introduction

The radiative transfer MIMICS-I model simulations presented in chapter 4 provides a thorough understanding of the basic scattering mechanisms associated in forest canopy as a function of microwave radiative transfer and underlying forest characteristics. The dominant double-bounce scattering at S-band from forest canopy particularly with deciduous species reveals potential for mapping forest/non-forest cover. Therefore, in this chapter, an effort was made to examine the suitability of S-band backscatter in classification of forest against non-forest and derive forest cover changes utilizing Maximum Likelihood algorithm at different spatial resolutions simulated to NovaSAR-S configurations.

Globally, forest play a pivotal role in biophysical interactions and biogeochemical exchanges (Foley et al. 1994) and constitute one of the dynamic component of the global carbon cycle (Ciais et al. 1997) in the form of forest AGB (Groombridge and Jenkins 2002). Hence, timely and accurate forest cover monitoring algorithm and data products are essential for monitoring and management of forest (Hansen et al. 2008). SAR sensors with different band-widths (X-, C- and L-bands) have emerged as a complementary tool for accurate mapping of forest/ non-forest (F/NF) and forest cover change due to their cloud penetration, weather independent and sensitivity to forest structure (Schlund et al. 2014, Thiel et al. 2006, Shimada et al. 2014). In particular, Shimada et al. (2014) have generated global F/NF cover maps (2007 -2010) at 25 m scale based on HV backscatter PALSAR data reporting around 85% overall accuracy. They used region-specific threshold values of HV backscatter as forest and non-forest and found a stable temporal backscatter during this period in both HH and HV polarisations at global scale.

Few studies have investigated S-band backscatter responses to soil, agricultural crops and forest species. For example, sensitivity of soil moisture to S-band backscatter was found positive between observed and soil moisture retrieval at VV-polarisation channel for HJ-1C simulation (Du et al. 2010). Moreover, volume

scattering in maize plant was observed with S-band backscatter due to uniform distribution over the whole plant (Lopez-Sanchez et al. 2006). Using MIMICS simulation, S-band backscatter shows sensitivity to the temporal dynamics of the structure of wheat crop (Sun et al. 2012). In the young fir, S-band backscatter arises from the needles and branches due to random scattering (Lopez-Sanchez et al. 2000). The capability of S-band backscatter to map agricultural crop canopy (Guida et al. 2012) and forested areas (Natale et al. 2012) using integration of H/α and Pauli's decomposition techniques and salt marsh habitat mapping using Random Forest algorithm (van Beijma et al. 2014) have also been explored.

Studies led by Yatabe and Leckie (1995) and Fransson et al. (1999) have demonstrated the mapping of correctly classified clear-felled and forested areas using S-band Almaz-1 in boreal forest of Canada and Sweden respectively. However, there have been no consistent studies on the S-band SAR backscatter in mapping F/NF and forest cover changes in the temperate forested areas including the UK region. Therefore, the main objective of this chapter is to classify S-band backscatter data to produce forest/non-forest cover and change maps using MLC algorithm at varying spatial resolution and test the accuracy utilising PALSAR-based (25 m spatial) and Landsat-based (30 m spatial) products respectively.

5.2. Methods

To investigate the potential of airborne S-band data for mapping forest and non-forest cover and change detection, the mixed deciduous forest and different non-forest classes (that is grassland, clear-felled and grassland) of Savernake is selected (Figure 5.1). During the study period, management operations involving stand removal in few sub-compartments have also been carried out in Savernake. The availability of FC GIS, ancient database and field visits in 2012 and 2015 supports this study. The pre-processing of S-band SAR data and methodology are given in sections 3.2.3 and 3.4.2 respectively.

Prior to classification, the different scattering behaviour from forest and non-forest stands at S-band backscatter was examined for all channels. From the backscatter histogram of forest and non-forest classes, bimodal shape distribution has been observed in all the polarisations. It further shows that the distribution with backscatter at HH and VV polarisations always exceeding than at HV

polarisation. This observation was confirmed by analysing the scattering behaviour of S-band for all polarisations between F and NF classes based on training sample points of FC sub-compartment (figure 5.1).

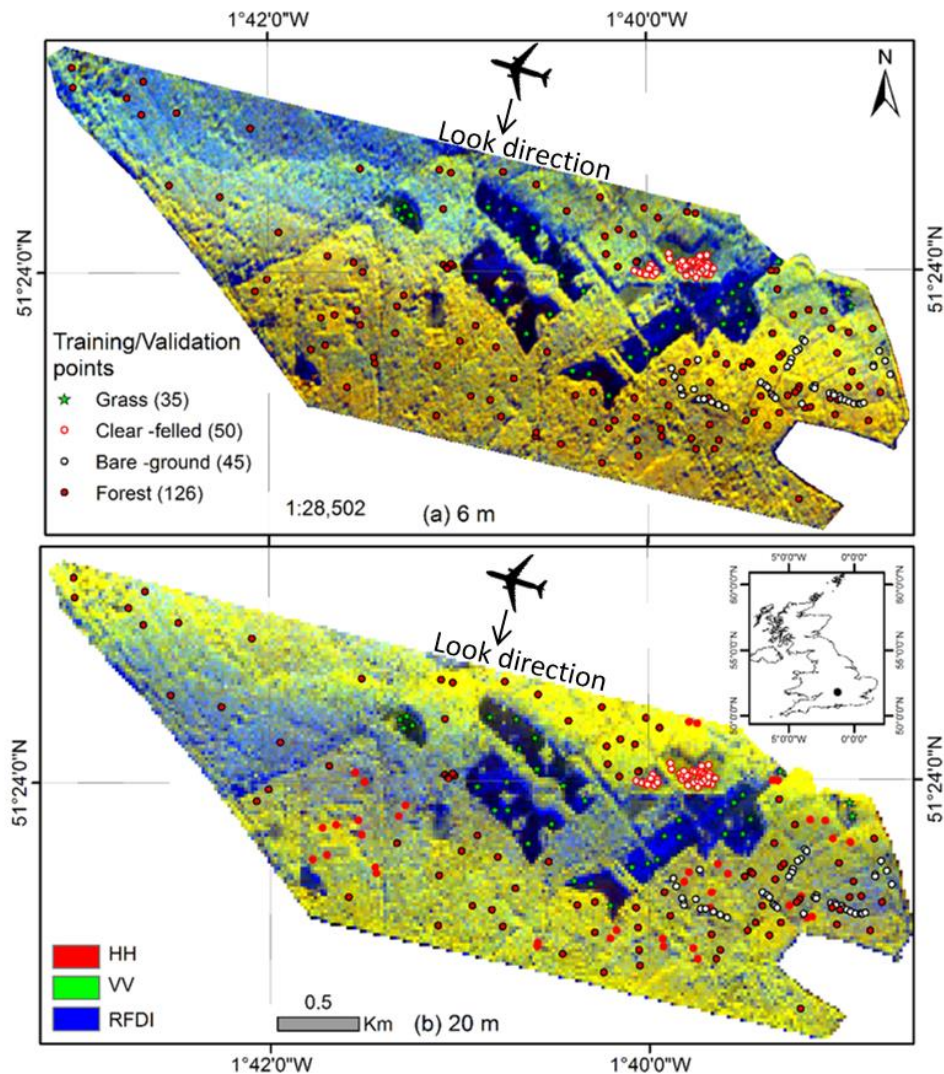


Figure 5.1. Field, FC GIS, ancient tree plot locations for 126 forest and 130 non-forest (training and validation plots) overlaid on 2014 acquired S-band FCC at 6 m (a) and 20 m (b) pixel resolutions for Savernake forest. Image reproduced with copyright permission from the Airbus Defence and Space, UK and Forestry Commission.

Figure 5.2 shows box-plots illustrating the scattering returns of fully-polarisation at S-band in 105 forest and 105 non-forest plots including different non-forest classes with the training plot locations depicted in figure 5.1.

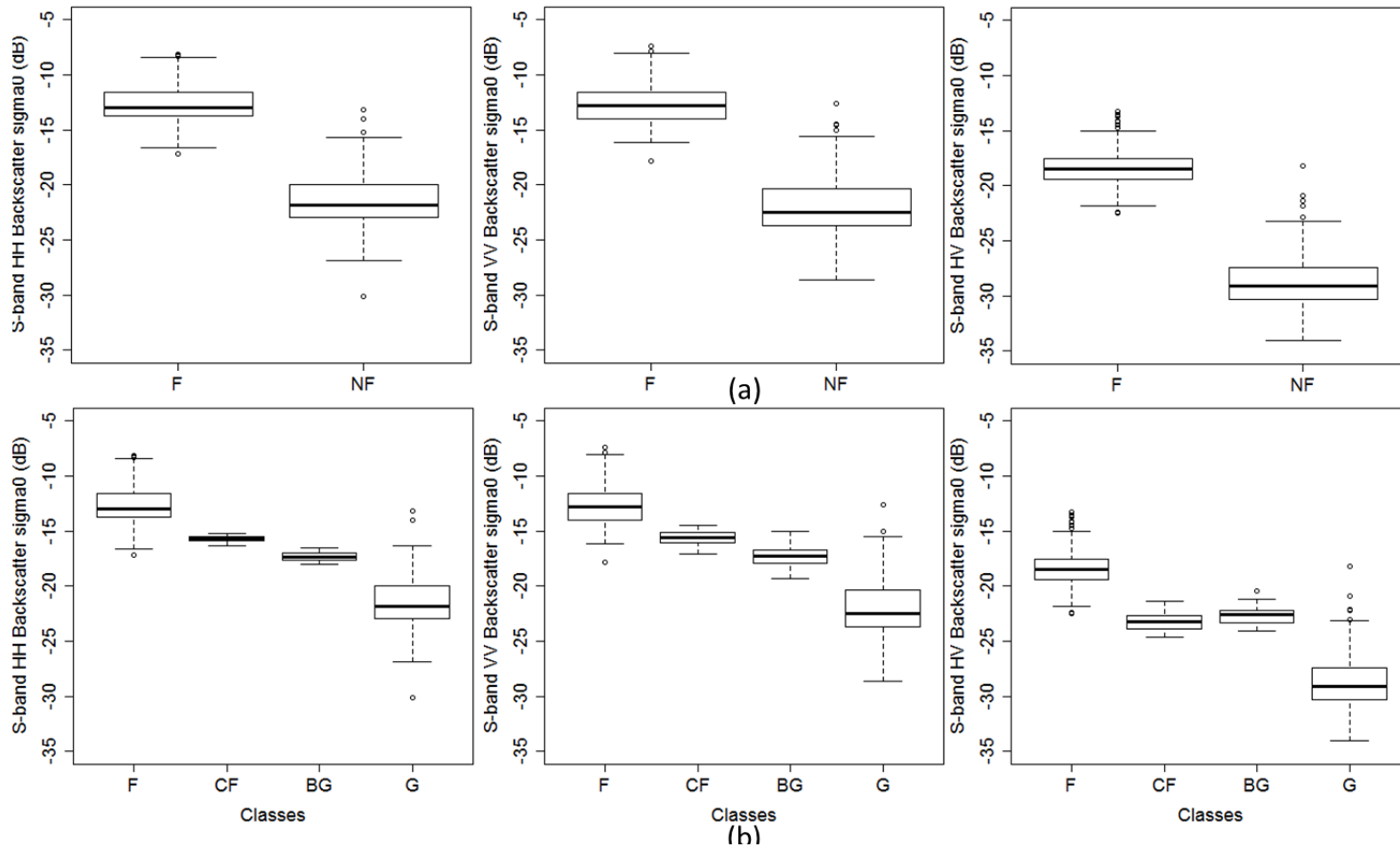


Figure 5.2. Box-plots of scattering returns of S-band SAR backscatter in 105 (F- Forest) and 105 (NF- Non-forest) sample plots (a) and different non-forest types with 50 (CF- Cleared-felled), 45 (BG- Bare-ground) and 10 (G- Grassland) sample plots (b). The central box in each box plot shows the inter-quartile range and median; whiskers indicate the 10th and 90th percentiles.

Stronger backscatter returns arise from forested areas in comparison to non-forest class. Both HH- and HV-polarisation provides the ideal channel for delineating the F and NF. It is due to these differences in returns from forest canopies against grassland and bare-ground, enabling for mapping forest cover where a mixture of different classes exists. Thus, the VV- returns recorded the highest backscatter in both forest and non-forest classes than other polarisations.

5.3. Results and Discussion

5.3.1. Mapping F/NF

Using the S-band backscatter information from HH- and VV- polarisations and the RFDI in the MLC algorithm, mapping of F/NF classes over Savernake forest was performed at the NovaSAR-S 6 m and 20 m resolutions (Figure 5.3).

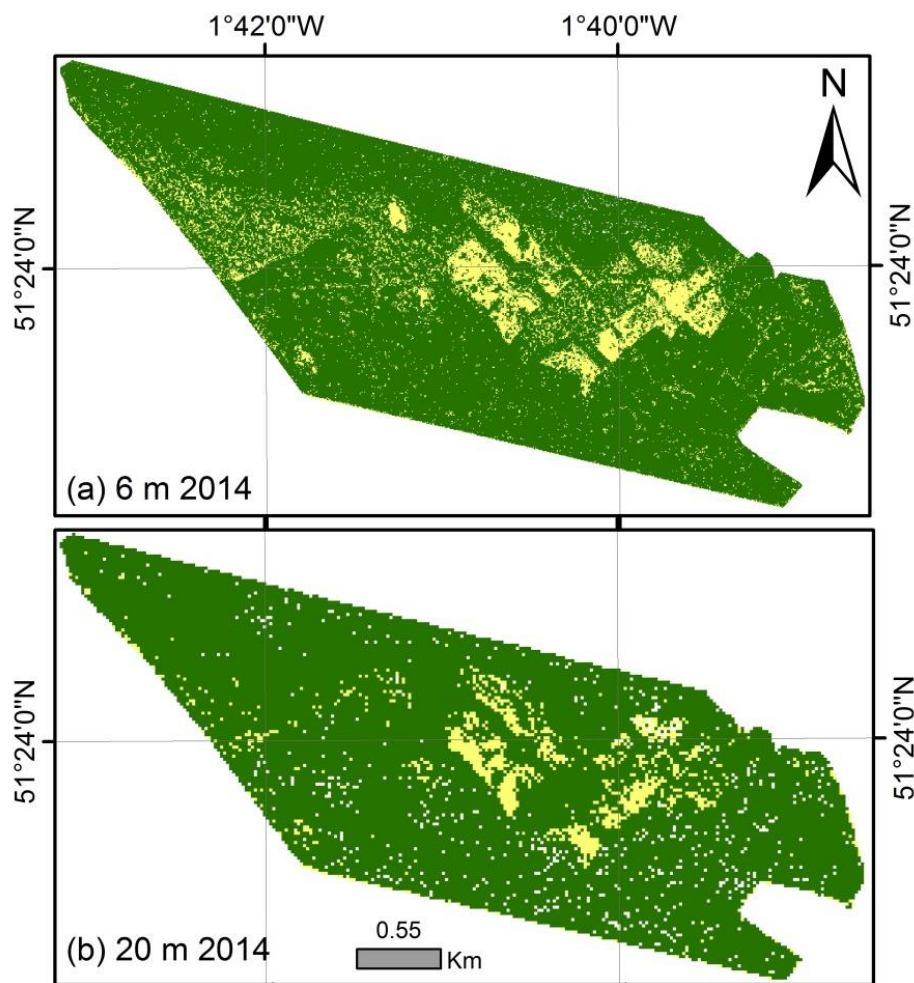


Figure 5.3. F/NF cover map of Savernake using S-band polarimetry and maximum likelihood algorithm at 6 m (a) and 20 m (b) resolutions.

For 6 m resolution, forest class is the dominant category in the Savernake with an area covering 648 ha. This dominant category corresponds to 86% in comparison to 88.26% based on the FC sub-compartment database. At the spatial resolution of the 20 m resolution, an over-estimation of forest class was observed, resulting in an estimated 696 ha of forest (Table 5.1).

Table 5.1. Area distribution of F/NF cover for Savernake forest.

Class	6 m area (ha)	20 m area (ha)
Forest	648.1	696.5
Non-forest	94.05	48.0
Total (ha)	742.15	744.5

The ability to delineate forest against non-forest class at S-band frequency is due to strong double-bounce scattering as a function of ground/trunk interaction dominantly from forest canopy than the surrounding areas without woody vegetation. Similar good result with S-band sensitivity to forested areas have been found in the Baginton site of Southern England using entropy H / mean angle α and Pauli's polarimetric decompositions (Natale et al. 2012). This strong scattering arises dominantly from deciduous forest species primarily due to the complex structural behavior in comparison to the conifers species. For coniferous species, a lower volume scattering (possibly random scattering) has been observed at S-band frequency due to high needles and branch densities (Lopez-Sanchez et al. 2000) (refer to Chapter 4 result predicted by MIMICS-I modelling). In the classified map at 20 m resolution, the non-forested areas has been misclassified to forest class possibly due to the inability to capture the finer details of varying surface roughness of the different non-forested classes at coarser spatial scale.

5.3.2. Detailed land cover classification

The different backscatter responses in the various non-forest land cover types in the study site provides an opportunity to investigate the sensitivity of S-band backscatter to different non-forested surface types (Figure 5.4 and Table 5.2). At 6 m resolution, grassland occupied around 50 ha area. In general, grass leaves have

erect inclination without woody stem but showing minimal leaf clumping with intermediate soil brightness. The lower backscatter returns from grasses at S-band could be due to weaker radar backscatter returns as a result of the specular phenomenon (smooth surface) of the grasses in comparison to roughness of the complex forest structure (Guida et al. 2012, Sun et al. 2012).

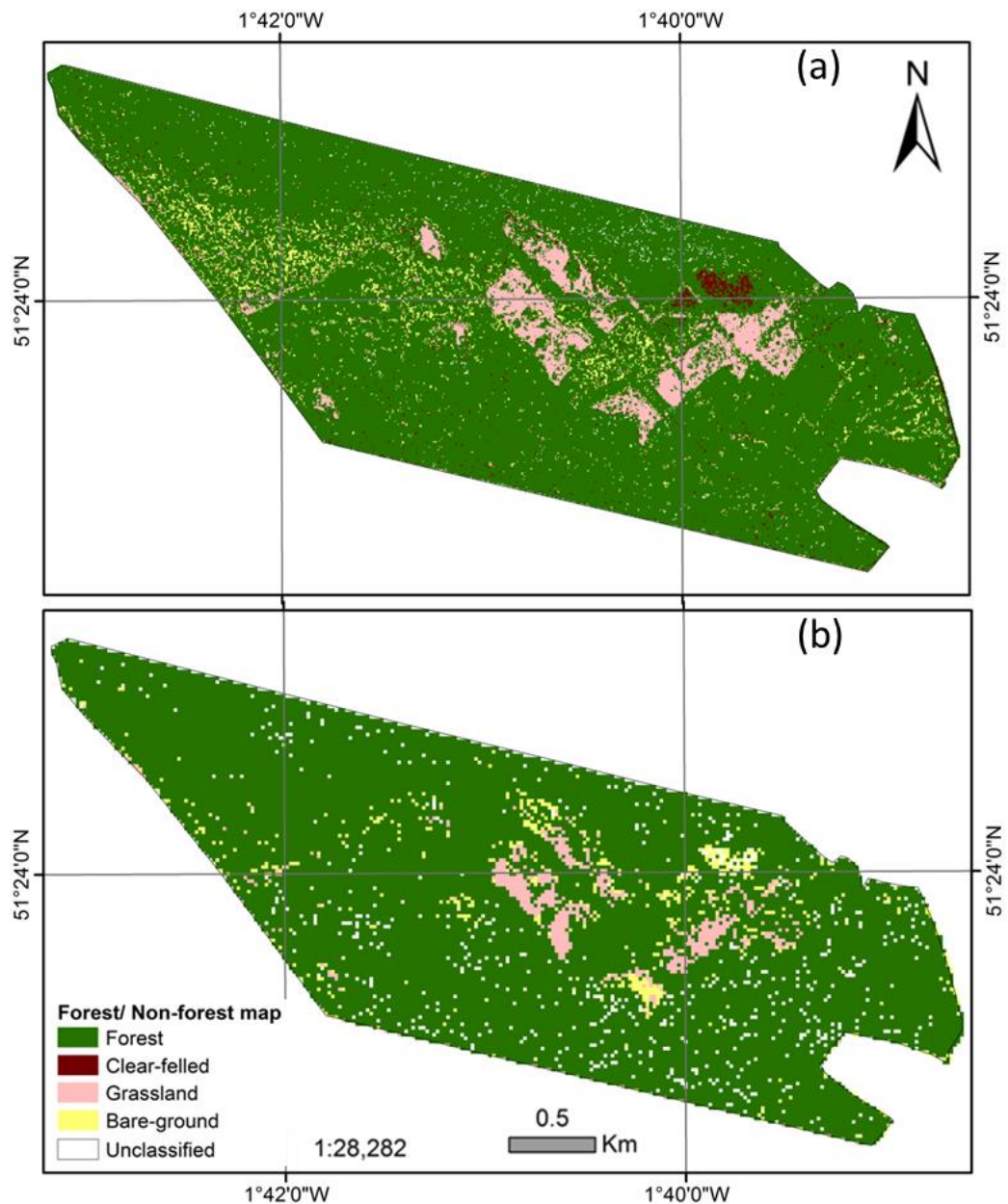


Figure 5.4. Forest and different non-forest cover map of Savernake using S-band polarimetry and maximum likelihood algorithm at 6 m (a) and 20 m (b) resolutions.

Bare-ground and clear-felled areas occupy 29 ha and 13 ha of the classified map at 6 m resolution. The distinctive backscatter signatures of bare-ground and clear-felled areas at 6 m resolution is likely due to the sensitivity of S-band backscatter to

surface roughness within these areas. On the basis of the observation data, both bare-ground and clear-felled areas show similar scattering mechanism (Figure 5.2). Clear-felled areas are often covered with dead leaves and grasses, giving the area a very rough surface after logged operations. The areas in the study site were planted with norway spruce and oak seedlings, further increasing the surface roughness. In contrast, bare-ground has no vegetation cover and appears as a relatively smooth surface to the radar.

Similarly, the 20 m resolution classification also reported little grassland (23 ha) and bare-ground (20 ha). In this classification map, the clear-felled area have been misclassified as bare-ground, possibly due to the different classes shared as mixed pixels at 20 m resolution which the algorithm could not reasonably mapped. This is a possible reason for the misclassification of non-forested areas as forest whereas the finer details related to bare-ground and clear-felled were captured by 6 m resolution. Another reason could be due to the different moisture content of grasses, clear-felled and forest classes where S-band backscatter is also sensitive to moisture content of the soil layer and forest canopies (Du et al. 2010). Closer observation of the classified maps reveals that S-band SAR differentiates forested areas with high backscatter very accurately.

Table 5.2. Area distribution of different non-forest classes for Savernake forest.

Class	6 m area (ha)	20 m area (ha)
Forest	648.1	696.5
Clear-felled	13.37	20.36
Grassland	50.33	23.04
Bare-ground	29.88	0
Unclassified	0.47	2.25
Total (ha)	742.15	

5.3.3. Accuracy assessment

The overall accuracy of the F/NF at 6 m resolution classified map turned out to be 70% and Kappa coefficient (κ) 0.4 when compared with forest plot locations, ancient tree database and aerial photo. Users' accuracies exceeded 70% for non-forest but was lower for forest (65%) while the producers' accuracy for forest and non-forest achieved higher accuracy around 71% and 68% respectively (Table 5.3).

In relation to 20 m resolution, 20 m resolution derived F/NF classified maps produces a lower 63.67% overall accuracy and Kappa coefficient (κ) 0.27 (Table 5.4). A reduced accuracy in both Users' and Producers' has been observed in comparison to 6 m results.

The overall accuracy of the forest against different non-forest classes at both spatial resolutions revealed lower overall accuracy level than F/NF classified maps. For example, an overall accuracy of 52.34% and Kappa coefficient (κ) 0.31 for 6 m while 36.72% overall accuracy and Kappa coefficient (κ) 0.07 for 20 m (Tables 5.5 and 5.6). However, relatively higher individual class accuracy level has been observed for all the non-forest classes at 6 m resolution particularly for clear-felled and grassland (producer's accuracy level for clear-felled around 71%).

Closer observation between the F/NF maps classified at 6 m and 20 m for Savernake site revealed that the individual class accuracy for both the classes achieved lower accuracy level in 20 m than 6 m accuracy. This result can also be extended to the classified maps produced with different non-forest classes at 6 m resolution. As a result, the overall accuracy for 20 m in classified map shows lower accuracy level than 6 m derived maps. This confirms that spatial resolution has some influence on S-band backscatter particularly in non-forested areas with lower accuracy level in produced maps. The maximum likelihood algorithm could classify F/NF and different non-forest classes achieving around 70% and 52.34% overall accuracy respectively with S-band backscatter at finer resolution 6 m.

Table 5.3. Confusion matrix for forest/ non-forest cover classified map at 6 m resolution for Savernake forest against forest plot locations and ancient tree database. Overall accuracy = 69.9%, Kappa coefficient (κ) = 0.4.

Actual class	Predicted class		Total	User's Accuracy (%)
	F	NF		
F	82	44	126	65.08
NF	33	97	130	74.62
Total	115	141	256	
Producer's Accuracy (%)	71.30	68.79		

*F- Forest, NF- Non-forest

Table 5.4. Confusion matrix for forest/ non-forest cover classified map at 20 m resolution for Savernake forest against forest plot locations and ancient tree database. Overall accuracy = 63.67%, Kappa coefficient (κ) = 0.27.

Actual class	Predicted class		Total	User's Accuracy (%)
	F	NF		
F	73	53	126	57.94
NF	40	90	130	69.23
Total	113	143	256	
Producer's Accuracy (%)	64.60	62.94		

*F- Forest, NF- Non-forest

Table 5.5. Confusion matrix for forest/ clear-felled/grassland/bare-ground cover classified map at 6 m resolution for Savernake forest against forest plot locations and ancient tree database. Overall accuracy = 52.34%, Kappa coefficient (κ) = 0.31.

Actual class	Predicted class				Total	User's Accuracy (%)
	F	CF	G	BG		
F	82	7	33	4	126	65.08
CF	16	28	6	0	50	56.00
G	9	1	22	3	35	62.86
BG	8	3	32	2	45	4.44
Total	115	39	93	9	256	
Producer's Accuracy (%)	71.30	71.79	23.66	22.22		

*F- Forest, CF- Clear-felled, G- Grassland, BG-Bare-ground

Table 5.6. Confusion matrix for forest/ clear-felled/grassland/bare-ground cover classified map at 20 m resolution for Savernake forest against forest plot locations and ancient tree database. Overall accuracy = 36.72%, Kappa coefficient (κ) = 0.07.

Actual class	Predicted class				Total	User's Accuracy (%)
	F	CF	G	BG		
F	73	47	0	6	126	57.94
CF	6	13	25	6	50	26.00
G	5	12	5	13	35	14.29
BG	29	12	1	3	45	6.67
Total	113	84	31	28	256	
Producer's Accuracy (%)	64.60	15.48	16.13	10.71		

*F- Forest, CF- Clear-felled, G- Grassland, BG-Bare-ground

At the pixel level, S-band backscatter can reproduce forest cover maps in line with other SAR frequencies focusing on F/NF classification (Schlund et al. 2014, Shimada et al. 2014). This is validated using the global forest cover product of PALSAR at 25 m, though S-band derived maps are having lower accuracy level. There is a fair agreement between S-band derived F/NF maps and PALSAR product (Figure 5.5).

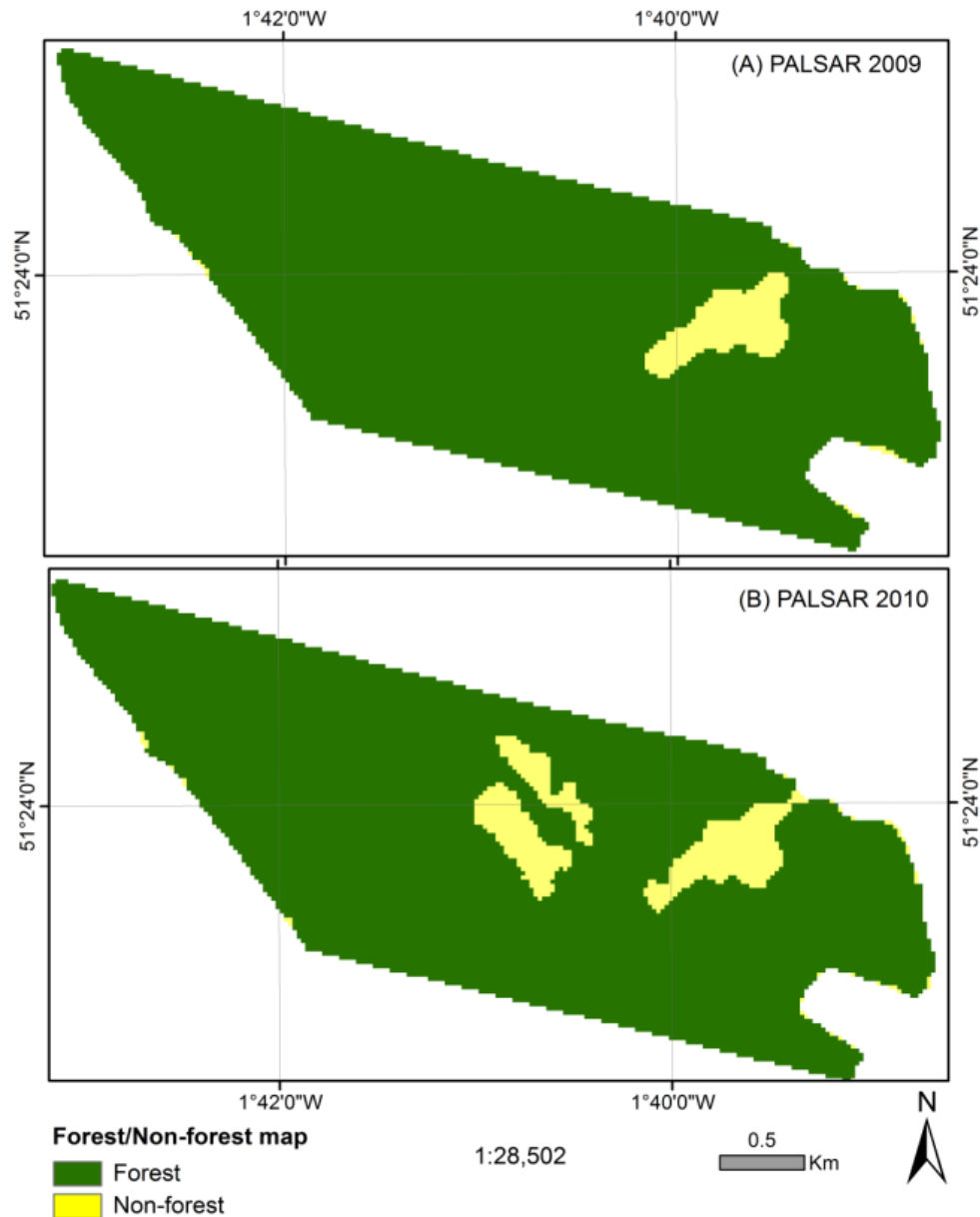


Figure 5.5. F/NF cover map of Savernake produced by L-band PALSAR for 2009 (A) and 2010 (B) at 25 m pixel resolution (Source: (JapanAerospaceExplorationAgency 2014)). Image reproduced with copyright permission from the Japan Aerospace Exploration Agency.

However, PALSAR forest cover map of 2009 has missed out a portion of non-forest (i.e., grassland) while the majority of the forested area is correctly mapped. This may be due to the coarse resolution size of 25 m PALSAR data which has missed out in comparison to the airborne datasets. Comparatively, the PALSAR based 2010 data reproduced a combination of both forest and grassland (non-forest) almost similar with S-band derived 20 m map. This shows that S-band data, similar to L-band data, has a robust capacity to map forest and different non-forest classes as shown above, which may be due to the radiative nature of the S-band backscatter and higher spatial resolution of airborne data.

The present findings also support previous results of Guida et al. (2012); Natale et al. (2012) and van Beijma et al. (2014). However, S-band backscatter could not differentiate the different forest types most likely due to the overall complex combination of weak to strong volume scattering from canopy components shared by different forest types in contrary to the observations of van Beijma et al. (2014). Moreover, the standard MCL algorithm could not differentiate the existing different forest types and need further investigation using advanced classification algorithm such as Random forest.

5.3.4. Forest cover change analysis

The F/NF cover map derived using S-band backscatter acquired during 2014 reveals that area with forest stands have been correctly classified by MLC algorithm with 70% accuracy level at higher resolution. This is due to strong S-band backscatter returns from forest canopy primarily originated from ground/trunk interactions and relatively homogenous areas. Although temporal forest cover changes between 2010 and 2014 have been observed based on S-band backscatter derived forest cover maps. The greater confident of this major change within Savernake forest have been observed particularly with the clear-felled areas in two sub-compartments (3.45 ha and 5.2 ha) where the forest stand have been completely removed. This has been confirmed using field observation in 2015 and the FC database. Thus, the clear-felled areas are correctly classified as changed in F/NF map of the year 2014 which was

previously classified as forest in the year 2010. Figure 5.6 (C) depicts change map showing areas undergoing changes from forest to non-forest (red colour) between 2010 and 2014 at 6 m resolution.

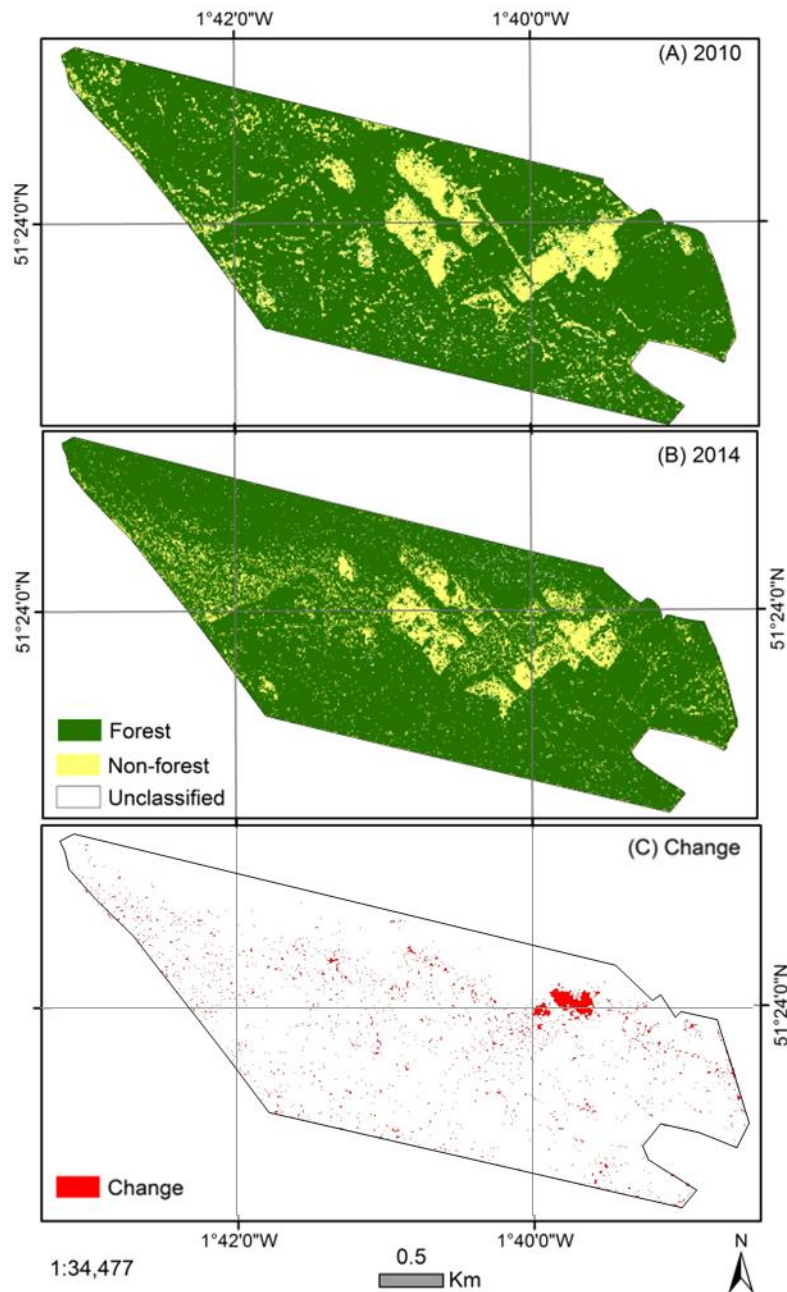


Figure 5.6. Change detection map showing areas undergoing changes from forest to non-forest (red) from 2010 to 2014 at 6 m resolution.

The second evidence comes from the percent tree cover (2000 to 2013) and forest loss (2013-2014) data using multi-temporal Landsat data at 30 m spatial resolution (see

figure 5.7), confirming the forest change between 2010 and 2014. According to Landsat-derived forest loss data, the areas of the two clear-cut sub-compartments are around 2.3 ha and 4.9 ha. Hence, multi-temporal S-band backscatter has identified changes in forest cover ideally at sub-hectare area and at finer resolution. However, due to imperfect calibration between imageries, varying incidence angles and sensitivity of S-band backscatter to different forest canopy structures (e.g. thinning) in different acquisition dates, the areas that have changed from forest to non-forest classes are somewhat different particularly along the class boundaries, where the pixels have mixed land cover types (Table 5.7).

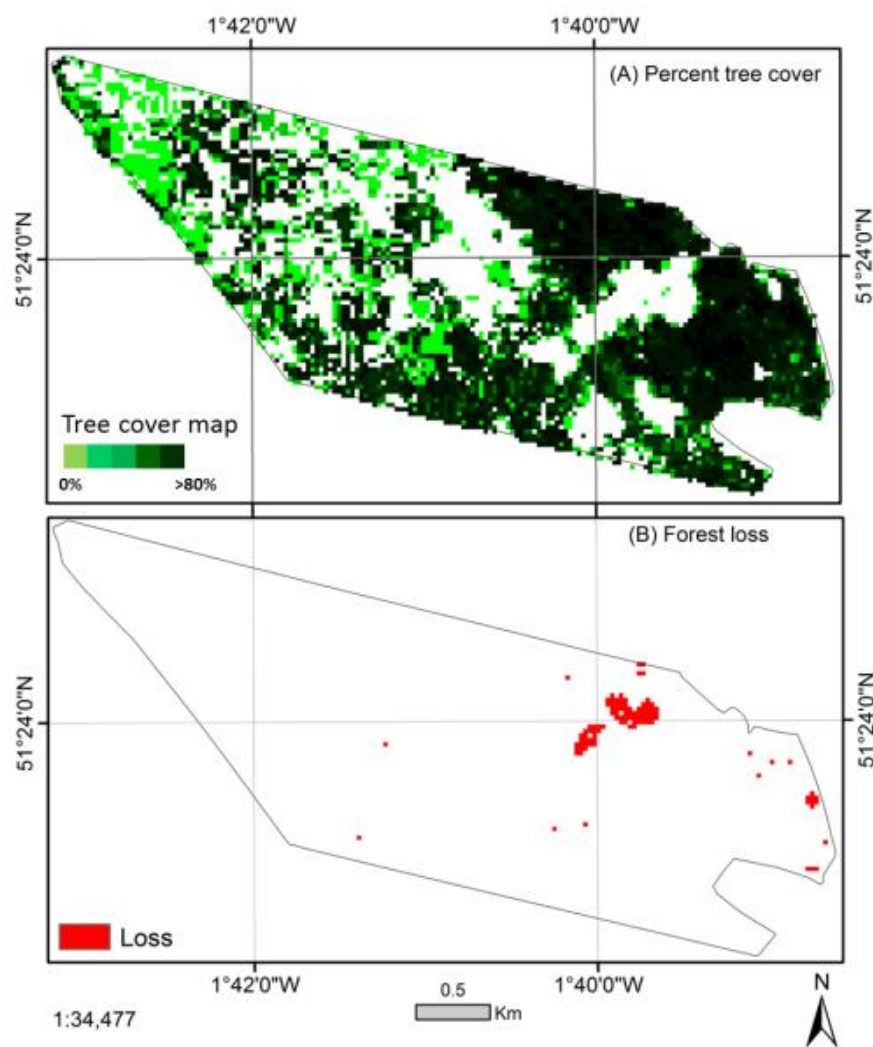


Figure 5.7. Percent tree cover (2000) (A) and forest loss (2013-2014) (B) at 30 m Landsat data from Hansen et al. (2014). Image reproduced with copyright permission from the Global Forest Change, University of Maryland.

Table 5.7. Area distribution of F/NF cover for Savernake forest between 2010 and 2014 at 6 m resolution.

Class	6 m area 2010 (%)	6 m area 2014 (%)
Forest	88	80
Non-forest	12	20
Total (ha)	100	

A small portion of non-forest in 2010 (Figure 5.6 B) shows a transition to forest in 2014. This could be a false detection or a plantation that has grown sufficiently to change the radiometric signature at S-band. Previous studies conducted by Yatabe and Leckie (1995) and Fransson et al. (1999) have highlighted the good capability of S-band in mapping of clear-felled and forested areas in boreal forest of Canada and Sweden. Based on the result from the temperate forest site at Savernake forest presented here, the S-band SAR backscatter at all polarisations has proved suitable for monitoring forest cover change at an accuracy level of 70% similar to that achievable from L-band SAR data between 85 and 90% (Thiel et al. 2006). This study suggests that the S-band sensor to be carried in NovaSAR-S and NISAR satellites could be useful for operational forest cover change detection, e.g. clear-felled as a function of time and in regions with persistent cloud cover such as the tropics (Lynch et al. 2013, Natale et al. 2012) and in boreal winter with low sun angles (Yatabe and Leckie 1995, Fransson et al. 1999).

5.4. Summary

High resolution S-band radar data in the context of the AirSAR campaign in Britain was utilised for assessing the mapping of forest/non-forest, different non-forest types and forest cover changes. This study was conducted in a temperate mixed forest of Savernake forest in England where different species of deciduous and coniferous grow. The mapping was conducted in two scenarios: one related to forest/non-forest and second with different non-forest types (grassland, cleared-felled and bare-ground) that are found in the study area. Using the Maximum likelihood classification algorithm with HH- and VV- polarisation and the Radar Forest Degradation Index

(RFDI) forest/non-forest and different non-forest types are mapped at 6 m and 20 m resolutions corresponding to StripMap and ScanSAR resolution modes of NovaSAR-S.

This part of the evaluation has underpinned four main conclusions related to forest cover and change mapping from S-band SAR data. These conclusions are:

1. S-band backscatter data could differentiate forest and non-forest classes using HH-, VV- backscatter and RFDI data in MLC algorithm.
2. The most accurate F/NF cover map with 70% overall accuracy (Kappa coefficient of $\kappa = 0.41$) was derived using 6 m spatial resolution with MLC algorithm.
3. S-band backscatter could also mapped different non-forest classes (52 % overall accuracy and Kappa coefficient, $\kappa = 0.31$) particularly recently clear-felled areas at sub-hectare level (71 % producer's accuracy) due to strong against weak scattering from forest canopy and soil respectively.
4. Multi-temporal S-band backscatter could detect changes in forest cover particularly clear-felled ideally at sub-hectare area (3 -5 ha) and reliable accuracy due to the loss of the double-bounce scattering from ground/trunk interaction when the canopy is removed.

Chapter 6: Airborne S-band SAR backscatter relationships to forest biophysical characteristics

6.1. Introduction

As the previous chapters have shown the potential of simulated S-band backscatter with more penetrating level than shorter wavelength SAR band (Chapter 4) and resulting to mapping F/NF classification with 70% overall accuracy level and Kappa coefficient of $\kappa = 0.41$ (Chapter 5). This chapter deals with the regression tests between S-band backscatter and forest biophysical parameters particularly aboveground biomass (AGB) and level of saturation point based on regression model at stand level from the future NovaSAR-S and NISAR perspectives.

A major global carbon sink has been found in forest ecosystems particularly in old-growth forests as AGB (Luyssaert et al. 2008). Forest AGB is estimated with sample plot measurements from forest inventories e.g. in the tropics (Chave et al. 2015, Chave et al. 2005) and in Europe (Nabuurs et al. 1997, Liski et al. 2006). This approach of biomass measurement has been regarded as highly accurate; however, it involves some uncertainty primarily due to the use of allometric models to derive the forest AGB rather than direct measurements. Additionally, tree level AGB estimates involve errors when upscaled to plot or landscape scale (Chen et al. 2015). In the absence of large-scale inventory plots, most efforts for quantifying the distribution of biomass have focused on interpolation techniques at landscape or continental scale (Malhi et al. 2006). Due to the nature of the sampling with low temporal repeat frequency and a small number of inventory plots, the use of Earth Observation (EO) data acquired by satellite sensors are often being combined with field measurements (Liu et al. 2015, Saatchi et al. 2011a, Baccini et al. 2012).

For example, EO-based estimations have been shown to be similar to predictions derived from field estimates when averaging at large scales e.g. stand, landscape or even continental scale (Saatchi et al. 2015). However, differences between biomass estimates are being reported particularly in regions with few sampling sites (Mitchard

et al. 2014). Ground measured forest AGB can be related to SAR backscatter (Woodhouse et al. 2012) for biomass prediction at plot to stand levels which also involves uncertainty due to complex forest structure and indirect biomass measurements (Clark and Kellner 2012). Recently, allometric models derived using diameter and height information usually yields less biased estimates of forest AGB (Chave et al. 2015).

Longer SAR wavelengths at L- and P-band are sensitive to forest AGB due to deeper penetration and more scattering from canopy components, e.g. in boreal (Sandberg et al. 2011), temperate (Beaudoin et al. 1994, Le Toan et al. 1992) and in tropical forest (Saatchi et al. 2011b). However, the range of SAR sensitivity to forest biomass also depends on the radar incidence angle and forest canopy structure (homogeneity to complex density) that control the radar signal penetration into the canopy. Amongst the different radar wavelengths, studies focusing on S-band data for structure and biomass characterisation are scarcely investigated due to lack of long-term data. Almaz-1 S-band backscatter has been reported as having a very narrow dynamic range and similar average backscatter values in all the vegetation types (Rosenqvist 1996) including palm and rubber plantations. Furthermore, Rosenqvist (1996) questioned the effect of high incidence angle ($\sim 50^\circ$) to be the main factor responsible for this insignificant result in the Malaysian test site against the studies by Olsson et al. (1991) and Brown et al. (1992).

The sensitivity of S-band backscatter to forest structure and biophysical parameters in the temperate forest environment has not been investigated. For the first time, this chapter have made an attempt to assess the sensitivity of S-band backscatter with forest biophysical parameters in the mixed temperate forest of Savernake forest and Wytham Woods. Therefore, the main objective of this chapter is to derive average tree diameter (DBH), canopy height (H) and AGB based on S-band data from 2010 and 2014 acquisitions using field data at stand level and cross-validation between observed against predicted levels of AGB.

6.2. Methods

To investigate the relationship between S-band backscatter and forest structure and biophysical parameters, the mixed deciduous forest of Savernake and Wytham Woods were chosen (refer Figures 3.1 and 6.1) based on mixed species with varying levels of stand ages, tree average DBH, canopy height and AGB ranges. Details of S-band SAR data processing, field data, AGB estimation and methodology are given in sections 3.2.3, 3.3 and 3.4.3.

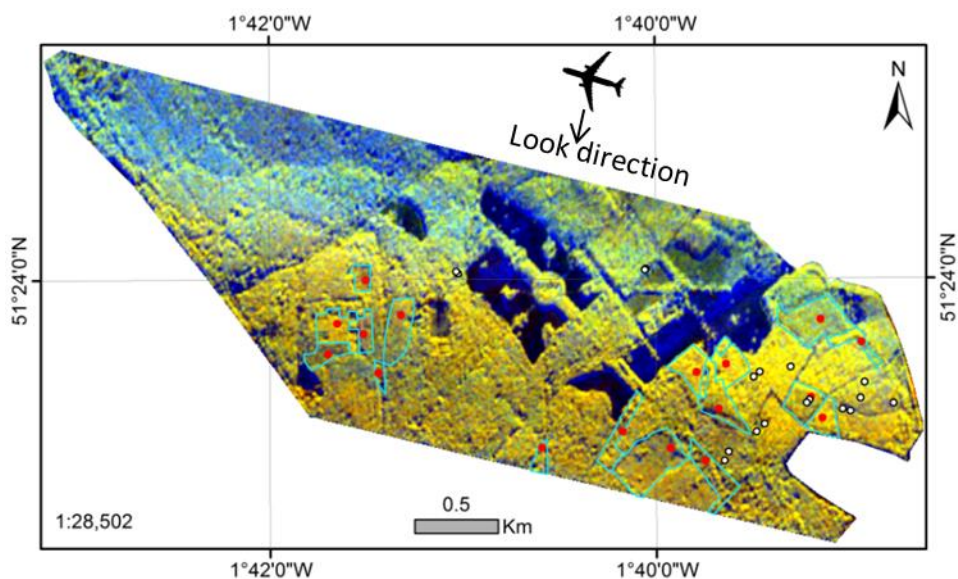


Figure 6.1. 6 m resolution S-band data over Savernake in 2014 (FCC: red: HH, green: VV, blue: RFDI) with sampled compartments (cyan polygon) and 17 training plots (red dot) in 2012 and 16 validation plots (white with black dot) in 2015. Image reproduced with copyright permission from the Airbus Defence and Space, UK and Forestry Commission.

6.3. Results and Discussion

6.3.1. Field data

According to the field plot information surveyed in Savernake forest in 2012, the smallest and largest sub-compartment corresponds to ~ 0.36 ha and ~ 10.31 ha respectively with an average size of ~ 3.5 ha. In comparison to the sub-compartment, the field plots are relatively small size at ~ 0.01 ha and ~ 0.03 ha for Wytham and Savernake sites respectively. The average tree DBH and canopy height related to field

measured plots for Savernake are 20.35 cm and 17.0 m respectively. Wytham Woods yielded average tree DBH and canopy H around 24.47 cm and 15.0 m respectively. Based on a total of 17 plots obtained in 2012, Savernake forest yielded a minimum, average and maximum AGB of ~31.4 t/ha, 223.8 t/ha and 410 t/ha respectively. On the other hand, a minimum, average and maximum AGB of ~52.1 t/ha, 208.59 t/ha and 520.1 t/ha were recorded based on 8 sample plots from Wytham site. When the biomass information for both sites was combined, an average AGB value of 218.9 t/ha was observed. The second data set for Savernake forest related to 16 sub-compartments, yielded a minimum, average and maximum AGB of ~32.9 t/ha, 228.7 t/ha and 469.3 t/ha respectively.

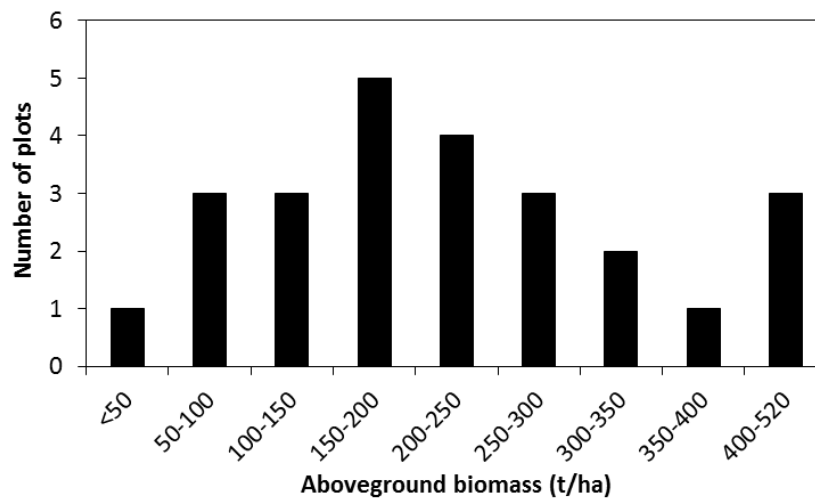


Figure 6.2. Histogram distribution of the training plots measured AGB below 600 t/ha used to estimate (25 plots) the backscatter-AGB relationship.

Figure 6.2 shows total number of plots ($n = 25$) with varying levels of biomass (31.4-520.1 t/ha) used to relate plot measured AGB against S-band backscatter for both the sites. The SAR data acquired in both June 2010 and 2014 for Savernake and 2014 for Wytham sites at stand levels were analysed. Table 6.1 shows the plot derived average tree DBH, canopy height and forest AGB values and their corresponding backscatter retrieved from 2014 S-band data across polarisations and spatial resolutions at 0.25 ha stand level.

Table 6.1. Summary of field measured forest variables and S-band backscatter for 2010 and 2014 at 0.25 ha scale.

Biomass	Average height	Average DBH	Stem	Basal area	2010			2014		
					HH σ_0 dB	VV σ_0 dB	HV σ_0 dB	HH σ_0 dB	VV σ_0 dB	HV σ_0 dB
<i>T ha⁻¹</i>	<i>m</i>	<i>cm</i>	<i>stems 0.25 ha⁻¹</i>	<i>m² 0.25 ha⁻¹</i>						
31.41	9.20	17.73	7	1.53	-12.79	-13.87	-23.86	-13.41	-14.07	-18.34
52.12	5.91	12.58	6	1.92	-18.06	-20.52	-27.32	-16.52	-19.25	-25.57
81.85	10.89	12.68	20	3.23	-10.83	-13.29	-21.83	-13.55	-14.00	-19.16
85.09	6.17	7.19	89	3.24	-13.14	-13.83	-22.70	-15.18	-15.26	-20.39
104.20	13.00	16.08	5	3.26	-17.59	-19.64	-27.99	-15.53	-18.64	-25.15
113.96	15.30	18.34	5	3.65	-12.18	-15.43	-21.31	-12.53	-15.90	-16.52
122.92	14.95	26.85	8	4.38	-11.20	-13.55	-21.85	-14.11	-14.83	-19.26
152.40	16.92	18.78	6	4.80	-13.32	-15.31	-20.40	-11.94	-14.12	-19.90
157.04	13.33	19.06	19	6.49	-12.68	-11.94	-17.15	-11.90	-10.34	-15.82
168.87	13.89	15.95	9	5.42	-12.70	-16.27	-22.39	-12.52	-16.50	-21.86
169.97	19.24	28.55	18	9.56	-10.96	-11.99	-22.00	-13.67	-12.66	-17.19
200.77	10.01	8.33	15	0.07	-12.49	-14.78	-22.97	-13.40	-14.00	-17.96
204.77	21.90	36.10	7	5.85	-12.97	-13.38	-22.19	-11.58	-12.17	-16.39
210.51	15.32	26.98	13	6.56	-11.54	-13.51	-22.97	-14.33	-14.74	-19.97
239.17	20.22	29.35	17	12.16	-11.18	-12.50	-22.04	-11.09	-12.11	-16.10
242.09	15.34	18.67	47	13.02	-9.03	-9.66	-20.32	-11.44	-10.50	-15.64
255.43	13.11	18.46	9	7.70	-11.20	-15.68	-20.11	-9.58	-14.51	-18.88
264.24	23.52	33.51	10	7.44	-10.09	-12.11	-20.76	-10.27	-11.14	-15.36
284.44	23.65	32.70	12	8.20	-9.42	-11.36	-21.33	-10.57	-11.05	-15.16
301.64	22.38	22.96	8	9.12	-9.89	-14.71	-19.25	-9.89	-14.60	-19.21
342.43	16.18	38.01	5	8.83	-12.35	-14.68	-23.81	-13.26	-13.94	-18.83
356.36	27.04	42.71	12	14.14	-11.39	-12.64	-21.74	-11.26	-12.09	-16.36
401.67	10.47	12.32	22	2.19	-10.14	-12.85	-21.48	-11.68	-12.56	-16.95
410.07	14.88	23.05	14	5.25	-9.86	-11.47	-21.35	-10.15	-11.42	-16.26
520.13	21.88	23.95	8	13.55	-10.43	-12.67	-19.43	-10.63	-12.92	-19.35

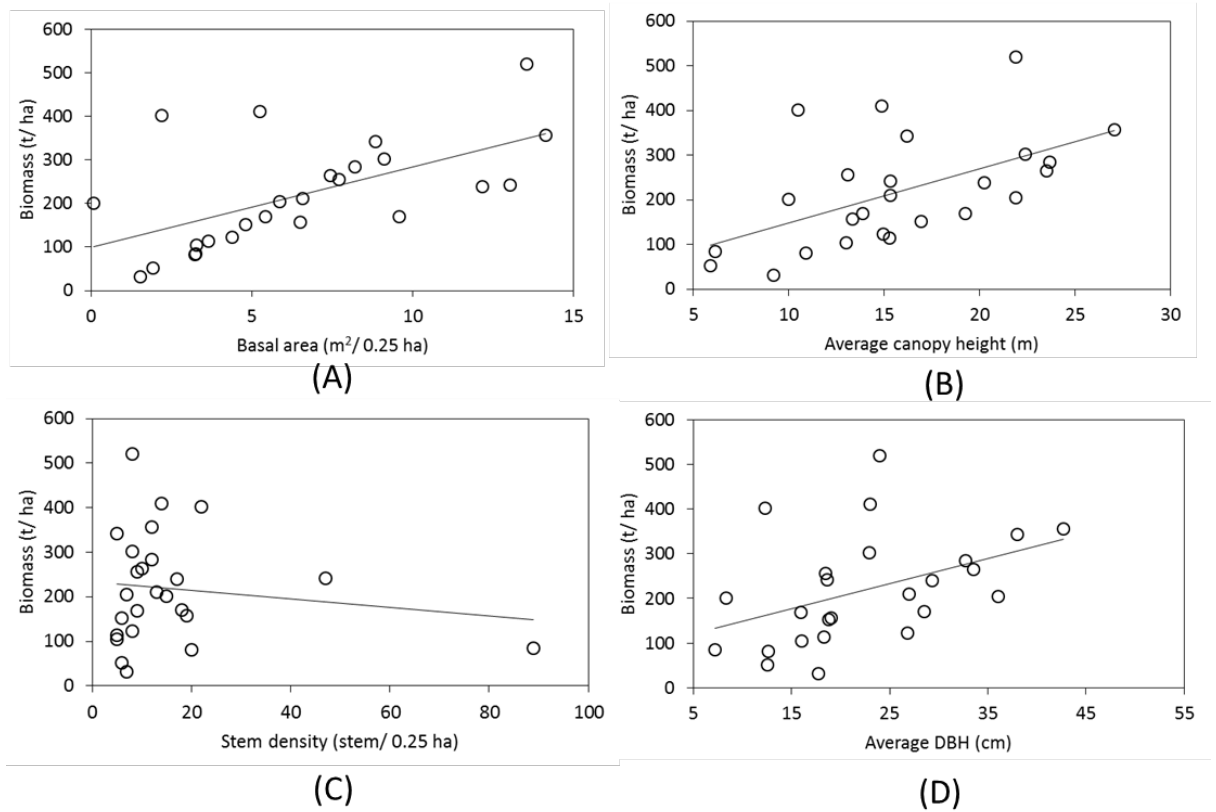


Figure 6.3. Biomass values for the field plots against basal area (A), average canopy height (B), Stem number density (C) and average tree diameter (D).

Table 6.2. Statistical relationships between field calculated aboveground biomass to basal area, average canopy height, stem number density and average tree diameter.

Biomass (t/ ha)	Basal area	Average canopy height	Stem density	Average DBH
R ²	0.34	0.3	0.01	0.18
RMSE	100.82	103.94	123.38	112.64
P value	**	**	ns	*
n	25			

P-value significance level: **<0.005, *<0.05, ns- no significant.

The calculated aboveground biomass values were significantly related to basal area and average canopy height in comparison to stem number density and average DBH of the plots (figure 6.3 and Table 6.2). The relationships of biomass to basal area and average canopy height was giving an $r^2 = 0.34$ and $r^2 = 0.3$ ($p < 0.005$) (linear model). However, a weaker correlation between biomass and the average DBH for each plot

when a linear model was fitted ($r^2 = 0.18$, $p < 0.05$). The poor distribution of stem densities also compromises the poor correlation with forest biomass.

6.3.2. S-band backscatter sensitivity to forest structure

Different logarithmic relationships were found between S-band backscatter and basal area, average canopy height, stand density and average diameter at breast height (Figure 6.4, 6.5, 6.6 and 6.7). For basal area, weaker logarithmic relationship was found with S-band σ_0 backscatter at 0.25 ha for both years with highest with HH polarisation (Table 6.3). There was a significant response to average canopy height in HH polarisation for both years ($R^2 = 0.28$ for 2010, $p < 0.05$ and $R^2 = 0.45$ for 2014, $p < 0.0005$) (Table 6.4). This sensitivity appeared to occur quite early in both years up to about 9 -10 meter height as the saturation level. A weaker relationship was found with stem density in all the polarisations except VV polarisation for 2010 data (VV: $R^2 = 0.3$ for 2010, $p < 0.1$) (Table 6.5). Similarly, a weaker and insignificant relationship was found between average DBH for the plot and all polarisations (Table 6.6).

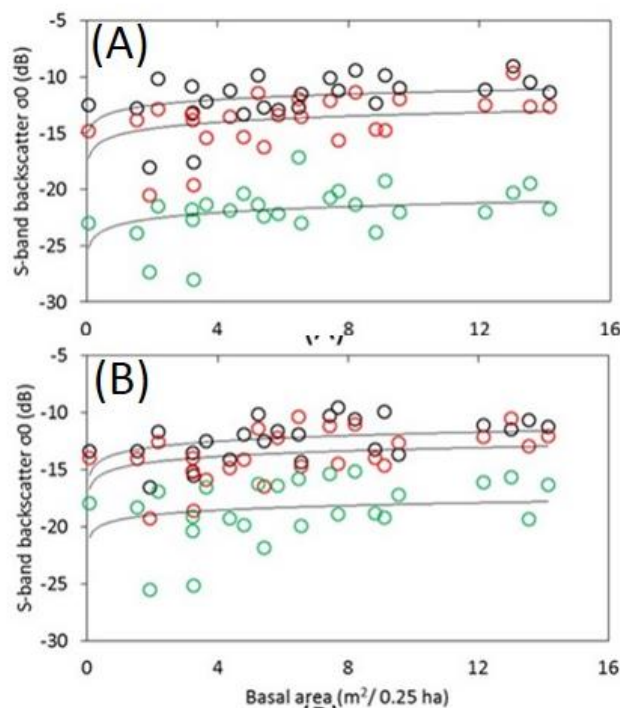


Figure 6.4. Basal area relationship with S-band backscatter (σ_0) at 0.25 ha for 2010 (A) and 2014 (B).

Table 6.3. Statistical relationships between S-band backscattering (σ_0) to basal area.

	2010			2014		
	HH	VV	HV	HH	VV	HV
R ²	0.12	0.12	0.13	0.17	0.11	0.05
RMSE	2.07	2.3	2.15	1.71	2.20	2.72
P value	ns	ns	ns	*	ns	ns
n	25					

P-value significance level: * <0.05 , ns- no significant.

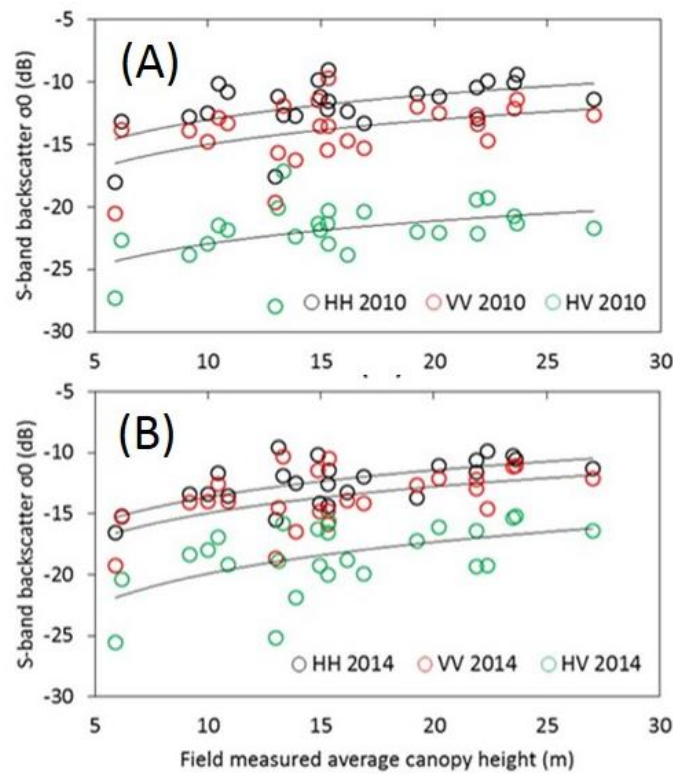


Figure 6.5. Average canopy height relationship with S-band backscatter (σ_0) at 0.25 ha for 2010 (A) and 2014 (B).

Table 6.4. Statistical relationships between S-band backscatter (σ_0) to average canopy height.

	2010			2014		
	HH	VV	HV	HH	VV	HV
R ²	0.28	0.21	0.21	0.45	0.29	0.28
RMSE	1.87	2.18	2.05	1.40	1.96	2.36
P value	*	*	*	***	**	**
n	25					

P-value significance level: *** <0.0005 , ** <0.005 , * <0.05 , ns- no significant.

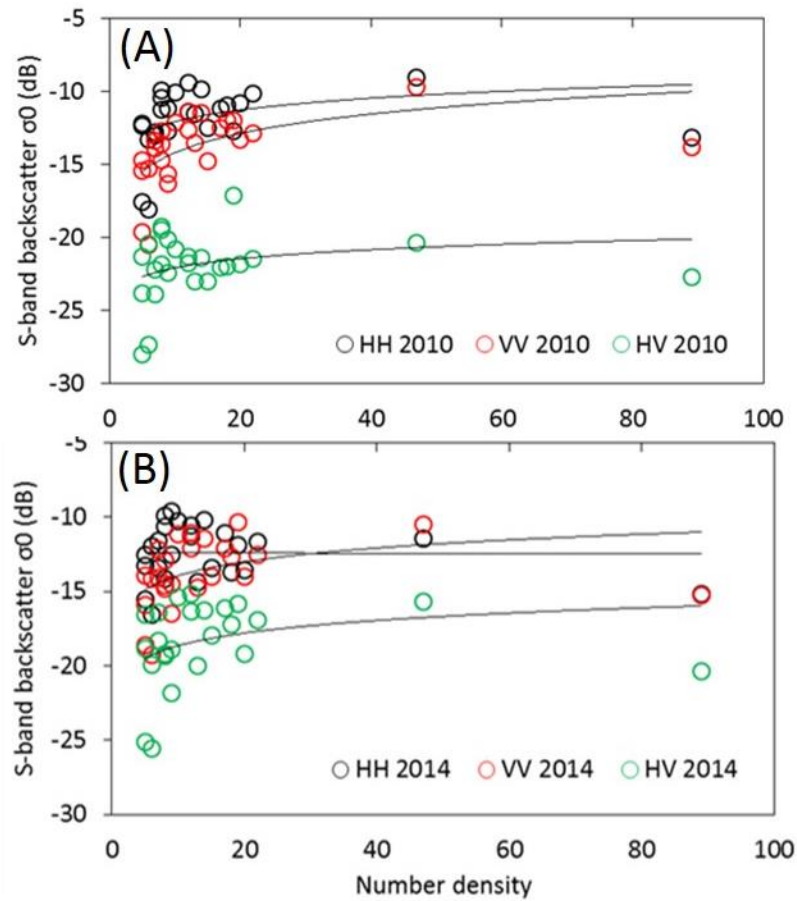


Figure 6.6. Stand number density relationship with S-band backscatter (σ_0) at 0.25 ha for 2010 (A) and 2014 (B).

Table 6.5. Statistical relationships between S-band backscattering (σ_0) to stand number density.

	2010			2014		
	HH	VV	HV	HH	VV	HV
R^2	0.13	0.3	0.07	0.03	0.16	0.09
RMSE	2.19	2.34	2.3	1.86	2.3	2.78
P value	ns	*	ns	ns	ns	ns
n	25					

P -value significance level: * <0.1 , ns- no significant.

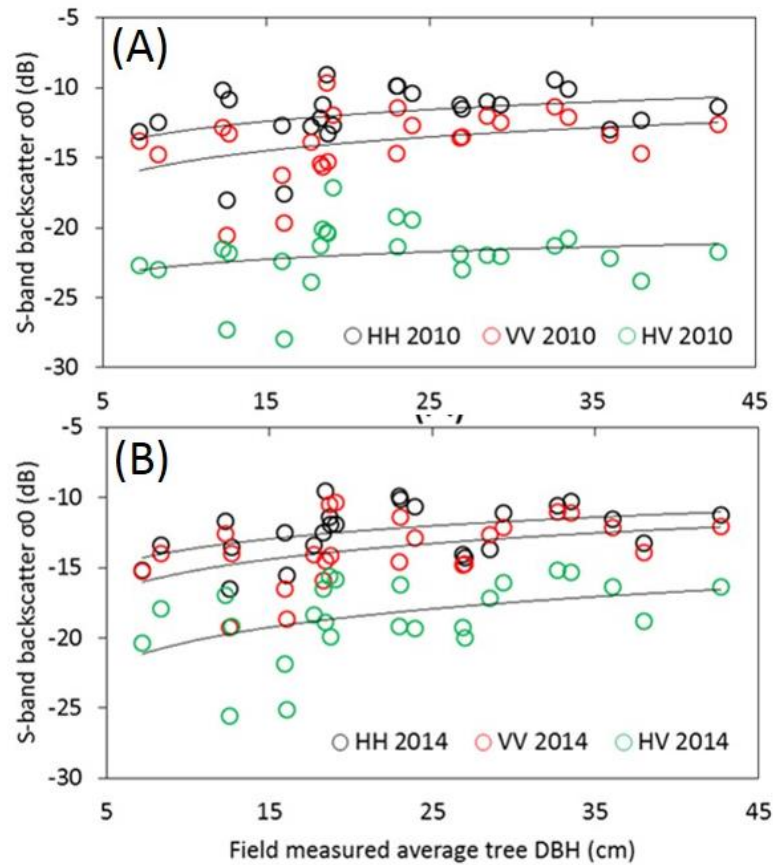


Figure 6.7. Average tree diameter relationship with S-band backscatter (σ_0) at 0.25 ha for 2010 (A) and 2014 (B).

Table 6.6. Statistical relationships between S-band backscattering (σ_0) to average tree diameter.

	2010			2014		
	HH	VV	HV	HH	VV	HV
R^2	0.11	0.13	0.04	0.2	0.2	0.19
RMSE	2.07	2.29	2.26	1.7	2.09	2.53
<i>P</i> value	ns	ns	ns	*	*	*
n	25					

P-value significance level: * <0.05 , ns- no significant.

At this stage, the sensitivity of radar S-band backscatter to average tree DBH and canopy height revealed varying weak to strong relationships in different polarisations and the reasons in this study are unclear, and further studies are needed to fully

understand the behaviour for S-band backscatter responses to diameter and height. One possibility could be through the phase information using interferometric mode of S-band frequency. At this level of analysis it seems that derivation of forest AGB focusing on those allometric equations related to both tree DBH and canopy height H will show some positive relationship with S-backscatter. Generally, biomass is estimated using DBH as the main variable in allometric models. Recently, Chave et al. (2015) have reported the importance of stand height information in the allometric models deriving yields with less biased estimates of forest AGB. Finally, the positive relationship between average canopy height H and stand density against S-band backscatter may be due to reduction in speckle noise at the plot level, confirming the influence of scale of field estimated DBH and H at plot level to backscatter relationship.

6.3.3. S-band backscatter sensitivity to forest aboveground biomass

The relationship of S-band polarimetry from 16 June 2010; 23 and 24 June 2014 are plotted against plot AGB (Figure 6.8). Both co- and cross- polarised backscatter is highly dependent on AGB and show better sensitivity to forest biomass at stand level for both years in both sites. For both forest sites, lower dynamic range of backscatter (around 8 dB) was observed in both 2014, whereas a slightly higher dynamic backscatter range (around 10 dB) for all polarisations was observed for 2010 data. S-band backscatter increases with biomass up to some levels around 100 t/ha in all polarisations, after which no further sensitivity is observed. This trend is easily evident in 2014 data in comparison to 2010 data. For instance, HH polarised backscatter acquired in 2014 produces the highest sensitivity to AGB with $R^2 = 0.5$ (1.34 RMSE, p-value <0.0001) while $R^2 = 0.37$ (1.75 RMSE, p-value <0.005) in 2010 for both forest sites (Table 6.7).

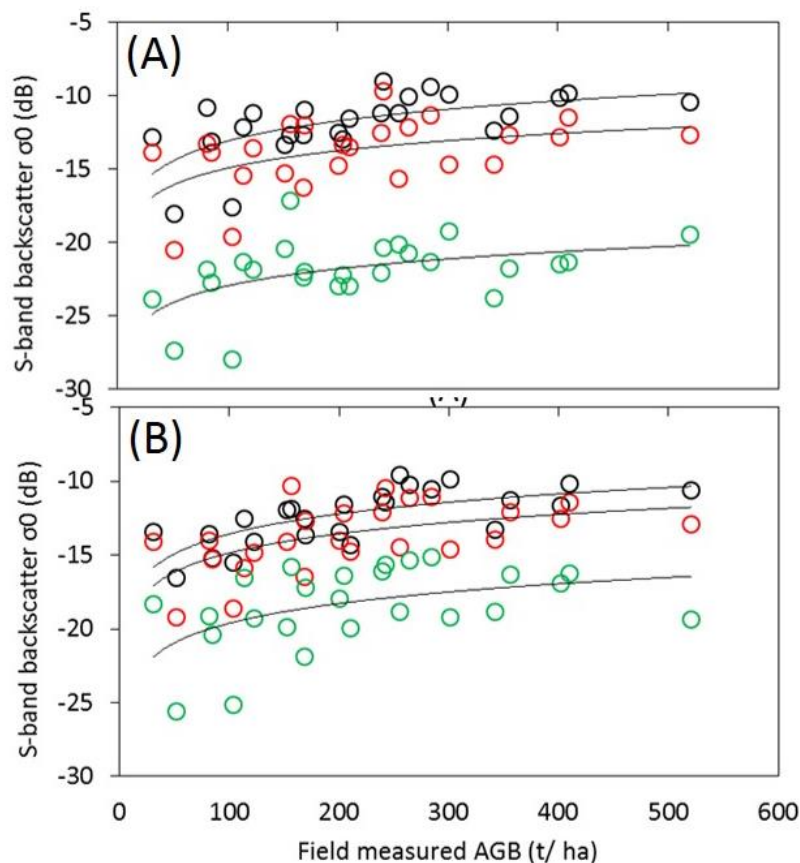


Figure 6.8. Above-ground biomass relationship with S-band backscatter (σ_0) for 2010 (A) and 2014 (B).

Table 6.7. Results from the regression models relating S-band backscatter (σ_0) acquired in 2010- 2014 to plot biomass from combined sites.

	Slope	R ²	RMSE	Relative Error	Slope Confidence Interval Lower 95%	Upper95%
16 June 2010, 23 June 2014						
HH	1.97	0.37	1.75 (0.0012) **	2.8	-28.0	-16.41
VV	1.70	0.22	2.17 (0.0172) *	3.47	-29.96	-15.58
HV	1.67	0.24	2.01 (0.012) *	3.23	-37.31	-23.97
23 and 24 June 2014						
HH	1.95	0.5	1.34 (0.0001) ***	2.15	-27.03	-18.12
VV	1.87	0.3	1.94 (0.0044) **	3.11	-29.97	-17.06
HV	1.92	0.22	2.46 (0.0175) *	3.95	-36.67	-20.32

P-value significance level: ***<0.0001, **<0.005, *<0.05, ns- no significant.

VV polarised backscatter acquired in 2014 show medium sensitivity to AGB with R² = 0.3 (1.94 RMSE, *p*-value <0.005) while R² = 0.22 (2.17 RMSE, *p*-value <0.05) in

2010 data for the study sites. Finally, the 2014 acquired HV polarised backscatter produces the lowest sensitivity to AGB with $R^2 = 0.22$ (2.46 RMSE, p-value <0.05) while $R^2 = 0.24$ (2.01 RMSE, p-value <0.05) in 2010 data.

In comparison to the forest properties e.g. average tree DBH, canopy height, the S-band radar backscatter provides a consistent sensitivity over forest AGB at 0.25 ha resolution. Hence, at the stand level analysis with 25 m resolution, S-band backscatter data with forest AGB proved to be a positive relationship particularly in co-polarised backscatter. This relationship between S-band backscatter and biomass could be due to averaging a larger number of pixels with reduced speckle noise. Studies in tropical rainforest of La Selva (Costa Rica) have observed plot sizes at least with 0.25 ha to be sufficient to achieve normal distribution of basal area and biomass over forest landscape (Clark and Clark 2000, Saatchi et al. 2011b). However, for this study the accuracy of the spatial averages of backscatter to biomass relationship is reduced if the area size is beyond 0.25 ha. This reduced relationship when up scaled up to 0.5 ha stand plot size maybe due to lack of field data greater than 0.25 ha or no longer sufficient enough to derive the underlying forest biophysical information against the average backscatter returns.

6.3.4. Estimation of forest aboveground biomass using S-band backscatter

The logarithmic model was used for relating plot AGB to S-band backscatter coefficient as

$$\sigma^{\circ} \text{ (dB)} = \text{Constant} + \text{Slope} * \ln(\text{AGB}) \text{ (t/ha)} \quad (6.1)$$

For further analysis, the AGB was predicted based S-band radar backscatter acquired on 16 June 2010 and 23 and 24 June 2014 at 0.25 ha resolution for both sites as input. For both forest sites, the predicted AGB based on 2010 data ranges from 18.75 to 978.67 t/ha, 4.34 to 1038.98 t/ha and 23.34 to 796.71 t/ha for HH, VV and HV polarisations respectively. Additionally, AGB was predicted ranging between 22.19 to 772.88 t/ha, 10 to 761.48 t/ha and 5.67 to 914.7 t/ha for HH, VV and HV polarisations respectively for the 2014 data (Figure 6.9). For Savernake forest, the S-band has identified aboveground biomass with the majority of biomass up to 300 t/ha (Figure 6.9 for HH-backscatter). This is more evident in 2010- derived than 2014 -derived based biomass predictions.

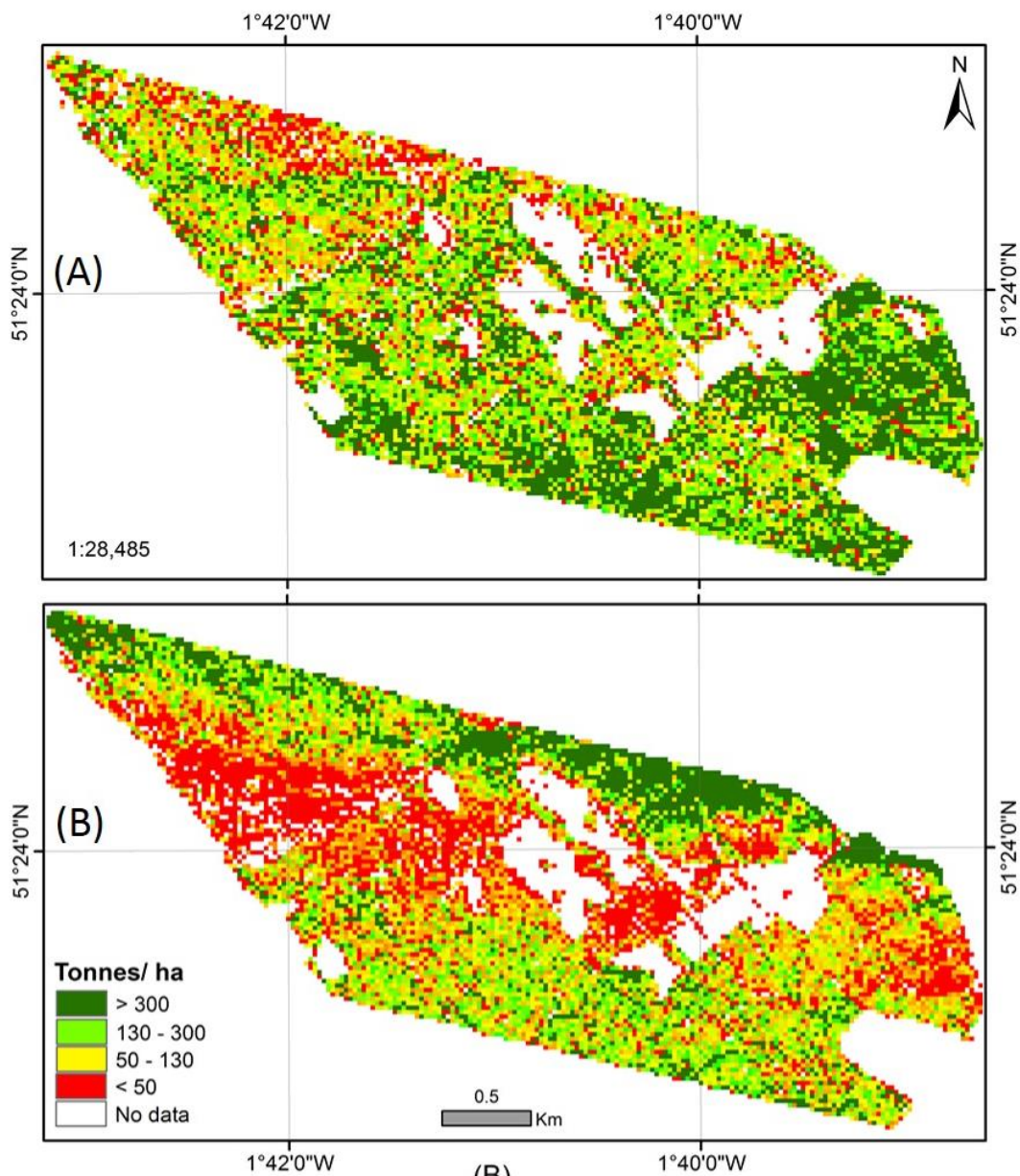


Figure 6.9. Predicted AGB maps using S-band HH backscatter at 0.25 ha scale for Savernake forest in 2010 (A) and 2014 (B) using field biomass estimates.

Biomass prediction for 2014 data are having biomass >300 t/ha and reaching up to 550 t/ha particularly in conifer stands. This may be possible as the conifers in these sub-compartments are having age between 20 and 75 years old stands with high biomass content. However, there are distinct differences in some areas between the maps and field estimates. Areas with grassland have been identified as forest biomass below 100 t/ha particularly in 2010 map maybe due to the mixed backscatter in this

areas. Comparing both the biomass maps and field data, it seems that predicted biomass for 2010 data is under-estimated for high biomass stands particularly conifer compartments while over-estimated for low biomass stands in the case of 2014 data. Both these errors (over- and under-estimations) are primarily confined in those areas where field data is largely lacking and therefore, the actual biomass has not been properly captured by the S-band radar derived model.

Both the maps revealed a general agreement for the sites with biomass ≤ 150 t/ha which S-band backscatter seems to be sensitive while large differences in AGB predictions between 2010 and 2014 may be due to imperfect radiometric calibration, varying incidence angles between the SAR imageries and field data acquired in 2012 and 2015 resulting to differing biomass allometric models for both SAR data. This needs to be investigated further for assessing the temporal biomass change in the study site during four year timescale.

6.3.5. Accuracy of S-band backscatter-biomass regression

The relationship between AGB recorded by field observations and those predicted by the linear regression model is shown in Figures 6.10, 6.11 and 6.12 for 0.25 ha resolution in different polarisations for both years over Savernake site. It can be observed that the relationships are good for low biomass level stands, but most of the stands having high biomass are either under- (HH-polarised) or over-estimated (VV- and HV-polarised).

For the model training plots, forest AGB predicted at 25 m resolution for 2014 was better than 2010 predictions. For instance, HH-polarisation produced RMSE of 90.63 t/ha while HV-polarisation produced a larger error of 114 t/ha. On the other hand, forest AGB predictions for 2010 produces relatively larger RMSE variations between 99.39 to 119.03 t/ha in all polarisations (Table 6.8). The stands with biomass above 200 t/ha are consistently under-estimated.

For the validation plots in Savernake forest, the errors were larger. Forest AGB predictions were found better for all polarisations with 2014 data than 2010 data. For instance, VV-polarisation displayed RMSE of 97.91 and 107.8 t/ha with highest

correlation $R^2 = 0.47$ and 0.35 , respectively. HH-polarisation produced RMSE of 108.4 and 114.23 t/ha with correlation $R^2 = 0.35$ and 0.27 respectively. Similarly, larger error ranges varied between 97.91 to 129.91 t/ha was predicted by the model for all polarisations with varying weak to good relationships (Table 6.8). Comparing all polarisations, it is seen that S-band co-polarised backscatter is better suited for biomass estimation than the cross-polarisation backscatter. For Savernake site, summary of observed and predicted values of AGB (t/ha) based on independent validation stands (16 stands) from 2010 and 2014 at 0.25 ha are given in appendices IX and X.

Table 6.8. Results of biomass regression models using S-band backscatter (σ_0) in Savernake and Wytham at 0.25 ha resolution. R^2 is the coefficient of correlation and $RMSE_c$ is the root mean square error calculated using cross-validation of the training plots (25 stands) for 2010 and 2014. $RMSE_v$ is the error when applying the regression model to the validation plots (16 stands).

	R^2	$RMSE_c(t/ha)$	R^2	$RMSE_v(t/ha)$
16 June 2010 and 23 June 2014				
HH	0.31	99.39 ns	0.27	114.23*
VV	0.06	115.63 ns	0.47	97.91**
HV	0.01	119.03*	0.28	113.67*
23 June and 24 June 2014				
HH	0.42	90.63**	0.35	108.4*
VV	0.1	113.28 ns	0.35	107.8**
HV	0.08	114.46 ns	0.06	129.91ns

P-value significance level: **<0.001, *<0.05, ns- no significant.

6.3.6. Uncertainty analysis

There are two major sources of uncertainty in this study: uncertainties in field data including allometric equations and biomass estimation using S-band radar signal. The uncertainty in field data measurement and AGB estimation from tree diameter measurements are considered very accurate in comparison to height measurements. Measurements of tree height using hypsometer in 2012 and digital laser rangefinder in 2015 suggested that our methods could also introduce some error. Since the species

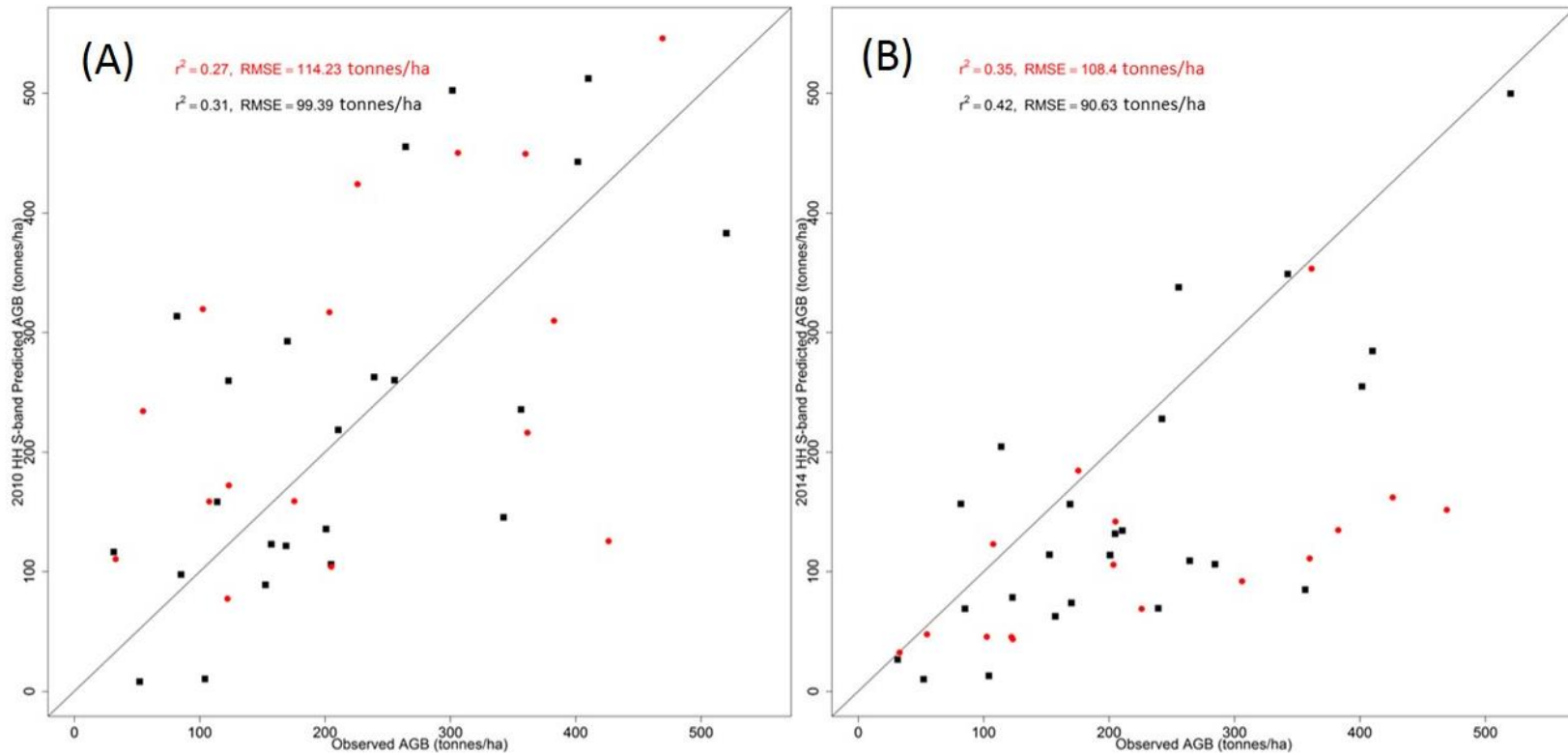


Figure 6.10. Results of biomass estimation using S-band backscatter (σ_0) based on training stands (25 stands-black square) and validation stands (16 stands- red circle) for HH-polarisation at 0.25 ha for 2010 (A) and 2014 (B). Locations of training and validation stands for Savernake are shown in Figure 6.1.

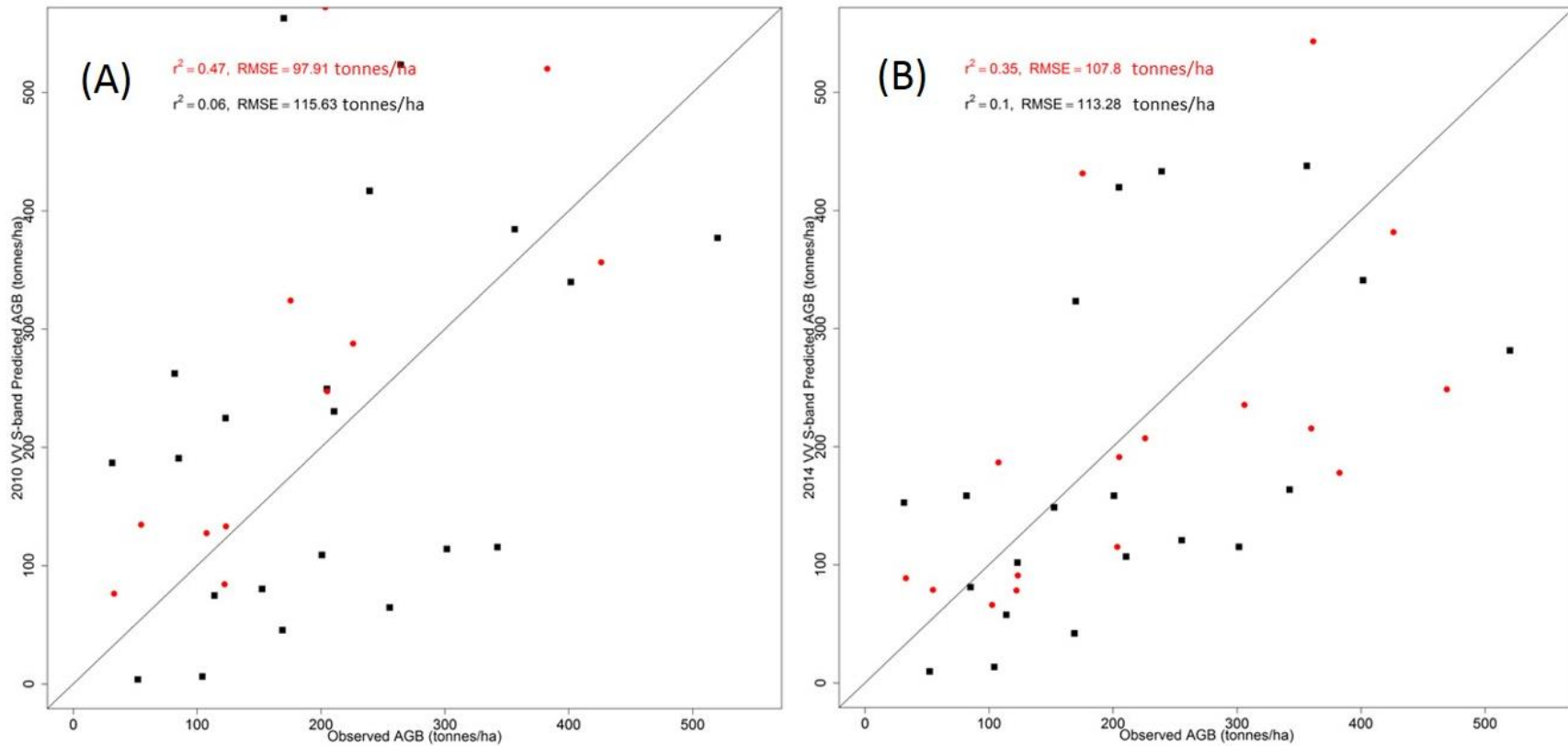


Figure 6.11. Results of biomass estimation using S-band backscatter (σ_0) based on training stands (25 stands-black square) and validation stands (16 stands- red circle) for VV-polarisation at 0.25 ha for 2010 (A) and 2014 (B). Locations of training and validation stands for Savernake are shown in Figure 6.1.

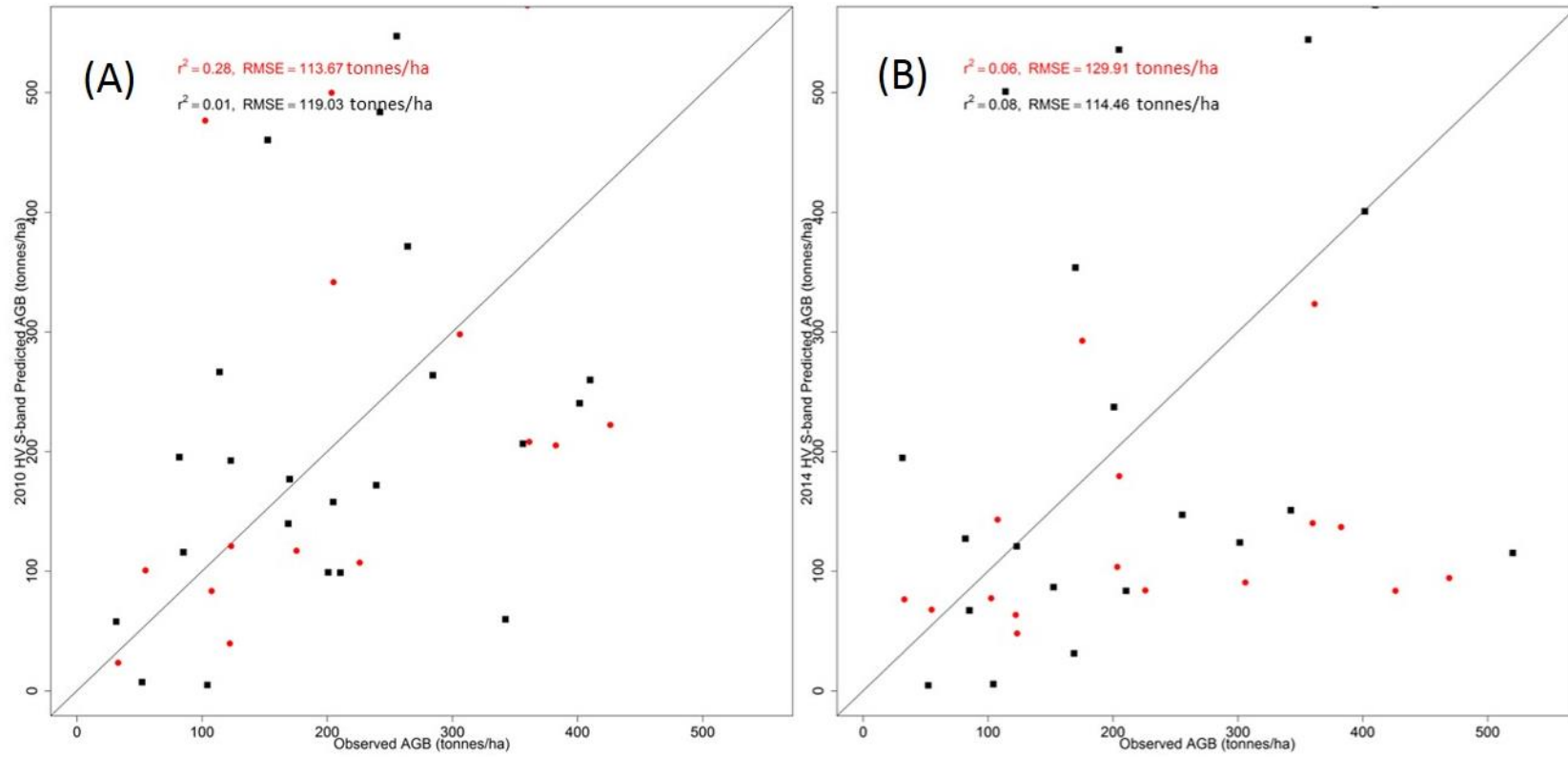


Figure 6.12. Results of biomass estimation using S-band backscatter (σ_0) based on training stands (25 stands-black square) and validation stands (16 stands- red circle) for HV-polarisation at 0.25 ha for 2010 (A) and 2014 (B). Locations of training and validation stands for Savernake are shown in Figure 6.1.

diversity in both study sites revealed few number, mis-identifications are likely to be relatively few, and given the similarities of wood density within a genus, unlikely to have a major effect on the biomass estimation (Chave et al. 2009, Chave et al. 2015). Generally, biomass is estimated using DBH as the main variable in allometric models (Chave et al. 2005). Recently, Chave et al. (2015) have reported the importance of stand height information in the allometric models deriving yields with less biased estimates of forest AGB. Other sources of errors in estimating the forest stand biomass could be related to spatial variability in forest structure and lack of sampling of small trees with DBH<10 cm. This can potentially introduce bias hence influencing the accurate field biomass estimates. However, this study has used the allometric equations of Bunce (1968) and Zianis et al. (2005) which were specific to British tree species rather than direct field estimation through tree harvesting and can potentially introduce errors (Chen et al. 2015, Clark and Kellner 2012). Lastly, biomass retrieval using S-band radar backscatter can also incur uncertainty due to the limited number of field sampled plots particularly in low stand density and tree with DBH<10 cm.

A wide consensus related to increasing backscatter for low biomass values and subsequently insensitivity at higher biomass values has been reported for different radar wavelengths particularly at low-frequencies (Woodhouse et al. 2012). For instance, in the hemi-boreal coniferous forest of Remningstorp region in southern Sweden, airborne P-band acquired at 28-50° incidence angle have achieved an accuracy of 18-27% error for HH- or HV-polarisation channel at 0.5 ha stand level (Sandberg et al. 2011). Similarly, Le Toan et al. (1992) and Beaudoin et al. (1994) have reported the best sensitivity of AGB with the P-band HV-polarisation having an estimated biomass error of around 20% than L- and C-band at 45° incidence angle in temperate pine plantation stand of Landes forest (France). In the tropical forest of Costa Rica, P- and L-band with incidence angles ranging from 20 to 60° in HV-polarisation backscatter showed strong sensitivity with accuracy level of 22.6 t/ha and 23.8 t/ha for AGB <300 t/ha and AGB <150t/ha respectively (Saatchi et al. 2011b). Using AIRSAR data, the sensitivity of forest biomass at C-, L- and P-band were around 20 t/ha, 40 t/ha and 100 t/ha respectively in coniferous forest of Landes and Duke and broadleaved evergreen of Hawaii (Imhoff 1995).

Positive relationships between S-band backscatter particularly HH- and HV- polarisation with average canopy height and stand density have been observed, which need further investigation. At stand level, S-band backscatter signal tends to increase with increasing biomass in both co- and cross-polarisations. For this study, S-band backscatter saturation point could be identified quite below less than 100 t/ha.

This study also utilizes SAR data acquired at 16-44° look angle which falls within the range of 38-44° reported by Brown et al. (1992) particularly at the near to mid-range direction and highlighted some relationship with biomass. However, the discouraging results with S-band backscatter to biomass reported by Olsson et al. (1991) and Rosenqvist (1996) used data acquired at very high incidence angles of around 53° and 50° respectively. Hence, the potential sensitivity of S-band backscatter to forest biophysical characteristics can be confirmed as positive result similar to Brown et al. (1992) to an extent where sensor look angle could play a significant role in detecting stand characteristics acquired at low to medium incidence angles.

6.4. Summary

For this study, four results related to S-band backscatter with forest biophysical characteristics are identified:

1. S-band backscatter shows weaker sensitivity to basal area, average tree diameter and stand density while good relationships with average canopy height ($R^2 = 0.28$ for 2010, $p < 0.05$ and $R^2 = 0.45$ for 2014, $p < 0.0005$) with co-polarisation at 25 m resolution.
2. Forest AGB shows sensitivity with S-band backscatter up to 100 t/ha particularly at HH (R^2 between 0.37 and 0.5) and VV- (R^2 between 0.22 and 0.3) polarisation at 25 m resolution.
3. The relationship of S-band backscatter with forest stands up to 300 t/ha biomass has shown least error between 90.63 and 99.39 t/ha.
4. S-band backscatter could possibly retrieve AGB in low biomass forests with least error in temperate forest having mixed deciduous species particularly at low to medium incidence angles.

Chapter 7: Synthesis and Conclusions

7.1. Introduction

Globally, terrestrial vegetation particularly forests are of interest to a wide section of the scientific community, environmentalist and policy makers due to their importance for socio-economic development and their pivotal role in biophysical interactions and biochemical exchanges in the global carbon cycle (Bojinski et al. 2014, Foley et al. 2005). Therefore, information related to forest cover extent, degradation, re-growth and carbon stocks is warranted on the operational basis (UNFCCC 2008). Towards this goal, satellite remote sensing has been a prime tool to obtain a robust and consistent data in a timely manner because of their large spatial coverage and frequent revisits (Townshend et al. 1991). Additionally, a system with independent weather capability is highly preferable due to persistent cloud cover and cost constraints over the large-scale forest (Cihlar 2000, DeFries et al. 2007). In this respect, SAR system serves to be a useful and complementary data (Lefsky and Cohen 2003, Simard et al. 2000). This thesis examines the overall potential of radar data with S-band frequency in forestry applications over the mixed deciduous temperate forest of the UK.

For the first time, an approach for mapping forest cover and relating to forest biophysical parameters with S-band backscatter in the temperate forest of the UK based on SAR data and model predictions has been systematically investigated. This includes the application of MIMICS-I model to understand the radiative nature of S-band signal through setting up different experiments from soil and forest canopy of different types (deciduous and conifers) and inter-comparison among different SAR wavebands.

Utilising the theoretical knowledge of S-band backscatter from physical modelling, mapping of forest/ non-forest cover and change detection using Maximum Likelihood Classification algorithm from airborne high-resolution S-band data was examined. This research found that S-band backscatter could be used for classifying forest and non-forest in varying accuracies up to 70% overall accuracy as the best possible map. The S-band backscatter was also found to be useful in detecting the clear-felled areas inside the forest being studied, which could be useful for

monitoring forest cover change in tropics with persistent cloud cover and higher latitudes having low-solar illumination. Finally, this study has demonstrated that S-band backscatter is also sensitive to forest AGB within a limited range, in particular forest stand with AGB below 100 t/ha possibly at low to medium incidence angles. This result is applicable for mixed broadleaf species of the temperate forest and need further cross-validation across temperate forest with similar forest types. The results and findings related to the four main objectives of this research work are summarized in this chapter.

7.2. To examine the contributions of different scattering mechanisms from soil moisture and surface roughness and forest canopies for S-band frequency across polarisations and incidence angles based on MIMICS-I model.

SAR backscatter interaction from forest has shown some relationships with forest biophysical characteristics such as species, crown cover, density, diameter, height and AGB to an extent. Several studies have used the SAR frequencies from X- to P-band with few exceptions at S-band. However, these relationships involve large uncertainty. Knowledge of S-band radar backscatter to forest and agricultural crop canopies (Guida et al. 2012, Natale et al. 2012) and AGB retrieval (Rosenqvist 1996) is very limited. For conifer species, the main scattering at S-band radar frequency comes from the needles and longer and thinner branches (Lopez-Sanchez et al. 2000) due to the homogenous structure of the canopy and random scattering. Moreover, sensitivity of soil moisture to S-band backscatter was found positive between observed and soil moisture retrieval at VV-polarisation for HJ-1C simulation (Du et al. 2010).

To account for forest biophysical retrieval and identify degradation or clear felled using S-band radar backscatter, knowledge of basic scattering associated with forest canopy is essential. From modelling approach, MIMICS-I model experiments in this research work suggest that the simulated S-band backscatter is very sensitive to forest structure and canopy components. In this study, different experiments have investigated S-band radar signal sensitivities to moisture content and surface roughness of soil and from deciduous and conifer canopy structure (Chapter 4).

Using MIMICS-I model, simulated S-band backscatter shows a significant sensitivity to both moisture content (up to 40%) and surface roughness (up to 3 cm) of bare-ground (soil) particularly in mid-to high- incidence angles. Additionally, simulated S-band backscatter was found to be more sensitive than shorter wavelengths at X- and C-band to forest canopies particularly deciduous species due to ground/trunk interaction as dominant mechanism at HH-polarisation. There was sensitivity of simulated S-band backscatter to the crown component, densities of leaf, needles and branches resulting to lower canopy transmissivity across radar incidence range.

Simulated S-band backscatter in leaf-off season has shown strong backscatter returns due to a mixture of volume scattering from ground/trunk interaction and single scattering from soil characteristics. Additionally, modelled S-band backscatter seems to have limited utility for stand height relationship due to the volume scattering from canopy components (leaves, branches) rather than the length of the stem/ canopy height. The model also confirmed that longer wavelength at L-band including S-band shows higher backscatter returns from forest canopy in comparison to shorter wavelengths (C- and X-band) as stated by Ulaby et al. (1990). This result clearly demonstrates that microwave canopy model is a robust tool and has broadened the knowledge on identifying the dominant scattering mechanism in a particular frequency and effects of slant-range direction from the forest canopy.

7.3. To investigate the S-band backscatter sensitivity to forest degradation (reduced canopy component and tree density) using MIMICS-I simulation.

Since SAR backscatter contains information related to forest canopy structure and hence influencing the backscatter from the forest degradation e.g. fire (Ferrazzoli et al. 1997). Identification of forest degradation or clear-cut has been reported utilising SAR data at L-band wavelength (Pantze et al. 2014, Ryan et al. 2012). Multi-temporal JERS-1 data has shown a dynamic range of reduced -4 to -6 dB in early plantation stage while opposite for post fire or degradation in the southern Sumatra Island of Indonesia (Takeuchi et al. 2000). Additionally, MIMICS model simulations predicted that at L-band frequency, discrimination of primary forest against regeneration and soil is possible due to strong double-bounce scattering from

ground/trunk interaction than shorter wavelengths C-band dominated by single scattering from leaves and branches (Grover et al. 1999).

Forest degradation caused by fire impacts have also reported the dynamic backscatter changes due to fire-affected forested areas utilising multi-temporal SAR data, for example C-band data (Siegert and Ruecker 2000, French et al. 1996). Impacts of fire in forest appears to be mainly governed by the reduction in the canopy components and changes in soil moisture and exposure of surface using empirical and modelling (Kalogirou et al. 2014, Tanase et al. 2010).

The potential use of remote sensing in forest disturbances specifically related to degradation of forest is quite challenging due to its inability to record small gaps and complex process of degradation. Therefore, an effort was made to undertake model experiments of fire-impacted reduced canopy components and selectively logged induced reduced stand density as a proxy to forest degradation from the existing literature knowledge.

MIMICS-I simulation suggest that at S-band, VV-polarisation channel displayed a strong backscatter returns in the high canopy density and reduced backscatter returns in varying levels of reduced canopy structure due to repeated fire occurrence. On the contrary, greater variability of backscatter dynamic range can be more prominently evident with cross-polarisation channel around 10 dB difference. This is evident from the standing trunk only without canopy components due to ground/trunk interaction similar to leaf-off winter season. Therefore, removal of canopy components that is leaves and branches over time affects the backscatter from the canopy in a decreasing order particularly in S-band wavelength. Similar weak and reduced backscatter trend is also observed in the S-band from the soil component particularly in smooth and dry moisture condition while strong backscatter arises from the rough surface with high moisture condition in the co-polarisation channel. The effect of soil moisture content to stronger backscatter is also seen with C-band data in the Mediterranean region (Tanase et al. 2010).

Reduced tree density due to selective logging has shown a weaker backscatter returns at S-band due to low canopy density in terms of area particularly in HV-

polarisation channel. The minimum backscatter variability is also observed in low density canopy due to more open area and less scattering from existing tree stands. If the soil components as discussed above were incorporated, there is a possibility that a strong backscatter from both soil conditions (smooth-dry and rough-wet) will inevitably overcome the backscatter return from the forest canopy. Finally, sensitivity of the overall backscatter returns from reduced canopy components due to fire and low density would result to the state of the canopy condition (moisture content) and underlying soil moisture and roughness (Tanase et al. 2010, Ferrazzoli et al. 1997, Kalogirou et al. 2014).

7.4. To classify S-band backscatter data to produce forest/non-forest cover and change maps using MLC algorithm and test the accuracy of forest cover maps at varying spatial resolution.

Several studies utilising different SAR bands highlighted the capability of mapping F/NF cover types (De Grandt et al. 1994). For instance, longer wavelength has been addressed for F/NF classification more accurately due to their strong sensitivity to structural and volumetric scattering from canopy in comparison to non-forested areas (Schlund et al. 2014, Thiel et al. 2006, Shimada et al. 2014).

Few studies have investigated the sensitivity of S-band radar data to agriculture crop canopies and forested areas. Airborne S-band backscatter data has shown sensitivity to crop and forested canopies based on the H/α and Pauli's decomposition techniques due to strong volume scattering from canopy components than non-vegetated areas (Guida et al. 2012, Natale et al. 2012). Studies have revealed the capability of mapping clear-felled and forested areas using multi-temporal S-band radar data from space-borne Almaz-1 in boreal forest of Canada and Sweden (Yatabe and Leckie 1995, Fransson et al. 1999). However, weak scattering at S-band radar frequency is observed for conifer species due to the longer and thinner branches with needles having homogenous stand structure (Lopez-Sanchez et al. 2000).

The present study provides an effort in investigating the S-band radar data in mapping F/NF cover over the temperate mixed forest of Savernake forest. First, S-

band backscatter could discriminate forest against non-forest class achieving around 70% overall accuracy (Kappa coefficient, $\kappa = 0.4$) at 6 m while reduced 63% overall accuracy (Kappa coefficient, $\kappa = 0.27$) at 20.25 m spatial spacing using HH-, VV-backscatter and RFDI data with MLC algorithm. This result supports the capability of mapping forest cover using S-band radar data due to strong scattering from forest canopy like other SAR wavelengths (Schlund et al. 2014, Thiel et al. 2006, Shimada et al. 2014) but at low accuracy level.

Secondly, S-band radar data could also differentiate different non-forest classes (that is grassland, clear-felled and bare-ground) with 52% overall accuracy (Kappa coefficient, $\kappa = 0.31$) particularly recently clear-felled areas at sub-hectare level (71 % producer's accuracy) due to the loss of volume scattering when the forest canopies are removed. This result support the studies conducted by Guida et al. (2012) and Natale et al. (2012) based on polarimetric decomposition on agriculture crop and forest canopies. However, this study also demonstrate that S-band radar data could not appropriately differentiate the different forest types due to mixed scattering (random scattering and volume scattering) from coniferous to deciduous stands.

Thirdly, multi-temporal S-band radar backscatter could also detect changes in forest cover particularly clear-felled areas ideally at sub-hectare level with reliable accuracy (71 % producer's accuracy) due to varying sensitivity to forest canopy and soil properties and further supports the result presented by Fransson et al. (1999) and Yatabe and Leckie (1995) from the boreal forest sites. In conclusion, high spatial and temporal resolution S-band SAR data comprise useful information suitable for operational forest cover and change detection e.g. clear-felled (Lynch et al. 2013, Fransson et al. 1999, Natale et al. 2012) particularly in the tropics and in higher northern latitudes where persistent cloud cover and low illumination are major problems.

7.5. To derive average tree diameter, canopy height and forest AGB based on S-band data from 2010 and 2014 acquisitions using field data at pixel and stand levels and cross-validation between observed against predicted levels of AGB at pixel level.

Longer SAR wavelengths at L- and P-band are sensitive to forest AGB due to deeper penetration and more scattering from canopy components, e.g. in boreal (Sandberg et al. 2011), temperate (Beaudoin et al. 1994, Le Toan et al. 1992) and tropical forest (Saatchi et al. 2011b). However, the range of sensitivity also depends on the radar incidence angle and forest canopy structure (young to mature, mono-species to complex density) that control the radar signal penetration into the canopy. Studies focusing on S-band backscatter to biophysical characteristics are scarcely investigated due to lack of historical data.

Earlier investigations focusing on S-band backscatter reported discouraging results with Almaz-1 to palm and rubber tree biomass due to very narrow dynamic ranges and similar average backscatter values for all the vegetation classes in the Kedah and Penang states of Malaysia (Rosenqvist 1996). It also seems that the varying sensor look angle as the most likely reason for weak sensitivity of S-band backscatter to forest biophysical characteristics (Brown et al. 1992, Olsson et al. 1991, Rosenqvist 1996).

The present study primarily focusing on the mixed deciduous temperate forest of Savernake forest and Wytham Woods revealed strong relationships between S-band backscatter against average canopy height in HH polarisation ($R^2 = 0.28$ for 2010, $p < 0.05$ and $R^2 = 0.45$ for 2014, $p < 0.0005$) at 25 m pixel spacing. A weaker logarithmic relationship was found with S-band backscatter at 0.25 ha for both years against basal area and stem density. Average DBH has a weaker and insignificant relationship with S-band backscatter for all polarisations.

In comparison to the forest properties e.g. average tree DBH, canopy height, the S-band radar backscatter provides a consistent sensitivity over forest AGB at 0.25 ha resolution. S-band backscatter increases with biomass up to some levels around 100 t/ha in all polarisations, after which no further sensitivity is observed. For instance, HH polarised backscatter acquired in 2014 produces the highest sensitivity to AGB

with $R^2 = 0.5$ (1.34 RMSE, p-value <0.0001) while $R^2 = 0.37$ (1.75 RMSE, p-value <0.005) in 2010 for both forest sites. VV polarised backscatter acquired in 2014 shows medium sensitivity to AGB with $R^2 = 0.3$ (1.94 RMSE, p-value <0.005) while $R^2 = 0.22$ (2.17 RMSE, p-value <0.05) in 2010 data for the study sites. Finally, the 2014 acquired HV polarised backscatter produces the lowest sensitivity to AGB with $R^2 = 0.22$ (2.46 RMSE, p-value <0.05) while $R^2 = 0.24$ (2.01 RMSE, p-value <0.05) in 2010 data. Hence, at the stand level analysis with 25 m pixel spacing, S-band backscatter data with forest AGB proved to be a positive relationship particularly in co-polarised backscatter.

In contrary to insignificant result with HH-polarisation S-band backscatter to palm and rubber tree biomass in Malaysia (Rosenqvist 1996), S-band backscatter could retrieve forest AGB in temperate forest dominated by mixed deciduous species acquired at low to medium incidence angles and further support the result presented by Brown et al. (1992) from boreal forest site. In conclusion, S-band backscatter could possibly retrieve AGB in low biomass forests with least error in temperate mixed deciduous forest particularly at low to medium incidence angles.

The main objectives of this thesis were to investigate the potential capability of least-studied S-band backscatter in relation to forest cover and forest biophysical retrieval in support to NovaSAR-S mission from the UK. The major findings of this research are as follows:

1. Total canopy scattering dominate the radar backscatter at S-band frequency with ground/trunk interactions as primary in co-polarisation channel with deciduous forest type. S-band backscatter is also sensitive to moisture content and surface roughness of the soil. The simulations suggest that delineation of forest cover and changes using S-band backscatter is possible due to sensitivity in forest canopies.
2. S-band SAR data could also discriminate the forest cover changes related to degradation. A low S-band backscatter has been predicted for degradation of forest due to reduced canopy structure and stand density. Using S-band derived forest change maps in combination with locally estimated allometric biomass could significantly improve the estimates of carbon emissions and fluxes particularly in priority areas such as degraded and regenerating forests.

3. Over large-scale mapping of forest cover, S-band SAR would provide a consistent result achieving around 70% overall accuracy level preferably at finer spatial resolution and detailed non-forest classes than L-band data. There is also an indication that multi-temporal S-band backscatter could detect changes in forest cover particularly clear-felled at sub-hectare level. This can be applicable for regional to global scale mapping of non-forest classes (grassland, clear-felled, plantation, bare-ground) and change particularly in tropics and temperate region where cloud cover and low-illumination respectively are major problems.
4. This research confirmed that S-band backscatter is sensitive to forest biophysical parameters particularly canopy height and forest AGB in varying sensitivities. A consistent and increasing sensitivity is observed for forest AGB up to 100 t/ha biomass forest stands with least error between 90.63 and 99.39 t/ha. The sensitivity of S-band backscatter to forest biophysical parameters shows that the regression model can be used to represent the relation between field measured forest AGB and S-band backscatter as indicated by statistical tests. However, this result is only applicable for temperate forest dominated by mixed deciduous species and need further investigation in similar forests across UK and in temperate forest.

7.6. Airborne demonstrator to space-borne NovaSAR perspectives

NovaSAR-S satellite is a complex payload with multi-mode having fully-polarimetry capabilities which can acquire data in both sun-synchronous and near equatorial orbits, the unique state-of-the-art covering pan-tropics and higher latitudes. This will carry S-band SAR sensor having phase array antenna consisting of 18 phase centres across track to collect data over 580 km using four operational modes under varying incidence angles, polarisations, spatial and temporal resolutions. Based on the results obtained from analysing Airborne demonstrator S-band data, four SAR characteristics (that is incidence angle, polarisation, spatial and temporal resolutions) for NovaSAR in forest studies have been addressed:

Incidence angle

Airborne experiments have been conducted utilising S-band SAR data acquired at incidence angles from 16 to 50°, and most indicate that the preferred incidence angle is in the average range of 30° (Guida et al. 2012, Natale et al. 2012). The minimum incidence angle is found to be 16°. However, the effect of incidence angles to S-band backscatter in forest and soil is not thoroughly studied and addressed. Study based on radiative transfer first order MIMICS-model have highlighted significant sensitivity to both soil moisture (up to 40%) and surface roughness of bare-ground (soil) particularly in mid-to high- incidence angles at S-band frequency (e.g. (Ulaby et al. 1990)). Additionally, S-band backscatter was found to be more sensitive to forest canopy particularly deciduous species at HH-polarisation across 15 -45° incidence range while in the intermediate range at VV-polarisation channel.

Utilising the space-borne Almaz-1, Brown et al. (1992) have utilised S-band data acquired in the range of 38-44° and reported some relationship with forest biomass. On the contrary, S-band backscatter data acquired at very high incidence angles of around 53° and 50° have shown limited utility to biomass retrieval Olsson et al. (1991) and Rosenqvist (1996). Hence, the utility of S-band backscatter to forest biophysical characteristics could be possible by acquiring NovaSAR data at low to medium incidence angles. This relates to the planned incidence angles ranging between 16-32° as prescribed by the NovaSAR at finer StripMap to ScanSAR Wide and can be useful for mapping forest cover and biophysical retrieval in these incidence range.

Polarisation

Study utilising the high-resolution airborne data have found strong sensitivity in all polarisation from forest canopy in comparison to non-forest classes. This is particularly associated with VV-polarisation channel. The Chinese HJ-1C radar sensor having VV-polarisation channel have also demonstrated similar sensitivity to both soil and forest characteristics. Using the HH-, VV- backscatter and RFDI data have produced forest/non-forest classification achieving accuracy level of 70% overall accuracy and Kappa coefficient (κ) of 0.4 at 6 m pixel spacing while a lower

63% overall accuracy (Kappa coefficient, $\kappa = 0.27$) at 20 m pixel spacing with MLC algorithm.

The present study primarily focusing on the mixed deciduous temperate forest of Savernake Forest and Wytham Woods revealed some sensitivity with S-band backscatter to forest AGB particularly at HH- (R^2 between 0.37 and 0.5) and VV- (R^2 between 0.22 and 0.3) polarisation at 25 m pixel spacing. When the predicted biomass was cross-validated against reference biomass up to 500 t/ha, least error between 90.63 and 99.39 t/ha has been achieved with HH-polarisation. In conclusion, the multiple polarisations from NovaSAR could produce forest cover maps at reasonable accuracy level and possibly could relate to forest biomass below 100 t/ha with least error.

Spatial resolution

The varying spatial resolutions, for example StripMap mode with 6 m pixel spacing have produced forest/non-forest cover map achieving 70% overall accuracy and Kappa coefficient ($\kappa = 0.4$) while lower 63% overall accuracy (Kappa coefficient, $\kappa = 0.27$) at the ScanSAR mode of 20 m pixel spacing using HH-, VV- backscatter and RFDI data with MLC algorithm. Due to the radiative nature of S-band backscatter, forest cover mapping reproduced reasonable accuracy level in line with PALSAR-based forest/non-forest map at pixel level.

Finer-spatial resolution StripMap data with 6 m pixel spacing could also be useful for detecting logged areas (e.g. clear-felled) at sub-hectare level due to canopy gaps and sensitivity of S-band backscatter to forest canopies and underlying soil properties. S-band backscatter in the mixed deciduous temperate forest of Savernake Forest and Wytham Woods revealed some relationship with forest AGB particularly with HH-polarisation at 25 m pixel spacing.

Temporal re-visits

Multi-temporal S-band backscatter could also detect changes in forest cover particularly clear-felled areas ideally at sub-hectare level and reliable accuracy due to its sensitivity to forest canopy components. Similar result with Almaz-1 data in detecting clear-felled from forest has also been found in the boreal forest of Sweden

(Fransson et al. 1999). This means that the high-temporal resolution of 1 (equatorial) to 4 days (sun-synchronous) at 6 m pixel spacing of StripMap mode in constellation could provide the necessary data for monitoring forest change in regions where deforestation and selective logging are active.

For instance, large-scale palm plantations in Borneo by clearing primary forest and selective logging operations in the Brazilian rainforest are some of the potential area of research with S-band data. To monitor dynamic changes associated with forest ecosystem, successful implementation programme requires updated information on land use changes across space and time. In other words, a continuous monitoring system is urgently required where NovaSAR could potentially be a prime candidate due to its sensitivity to forest/ vegetation canopy structure and ability to provide the continuous data throughout the year due to cloud penetration.

In conclusion, high spatial and temporal resolutions of NovaSAR sensor could provide valuable data suitable for operational forest monitoring e.g. clear-felled (Lynch et al. 2013, Fransson et al. 1999, Natale et al. 2012), forest degradation and large-scale deforestation in northern latitudes and tropics where low illumination and persistent cloud cover are major problems (Bird et al. 2013).

7.7. Limitations

Some of the assumptions in this study were:

1. MIMICS-I model only deals with monostatic (backscatter) radar systems and is not applicable to bistatic radar cross-section of forest canopies. Moreover, this model work with a single even-aged or mono-species and not appropriate to forest stands of mixed species composition and structure with multiple layers of canopies.
2. S-band backscatter acquired during dry season has highlighted suitability in forest cover mapping and backscatter-biomass relationships. The potential sensitivity of S-band backscatter to forest AGB in varying environmental conditions (such as soil moisture, changes in understory vegetation) during leaf-off season is largely lacking.

3. Due to varying incidence range and imperfect radiometric calibration of airborne S-band data, mapping of forest cover and forest change detection utilising MLC algorithm seems to be inadequate resulting to lower accuracy level.
4. Forest AGB estimation using stem diameter-biomass allometry is potentially associated with significant uncertainties even using site-specific model. Main sources of errors in estimating the forest stand biomass could be related to spatial variability in forest structure and lack of sampling of small trees with DBH<10 cm. This can potentially introduce bias hence influencing the accurate field biomass estimates. However, this study has used the allometric equations of Bunce (1968) and Zianis et al. (2005) which were specific to British tree species and European genera rather than direct field estimation through tree harvesting.
5. The lack of information related to horizontal variability of forest structure is clearly evident in the models.
6. The varying field plot sizes between 20 x 20 m² and 10 x 10 m² in Savernake forest and Wytham Woods respectively and existence of big trees within the plots (large aboveground biomass level) is also a limiting factor in this research.

7.8. Future work and recommendations

Some of the future work and recommendations include:

1. An important work is validating S-band backscatter derived from MIMICS-I model against SAR data from forest canopy. Due to the limited utility of MIMICS-I model with single even-aged or mono-species, the ‘Multi-MIMICS’ is recommended in future to test its advantages in Savernake forest. This includes simulation of different dimensions of trunk and branch and number tree density at S-band frequency using multi-MIMICS model.
2. Future investigations can also focus on improving the regression models utilising S-band radar backscatter for AGB estimation across large heterogeneous forest types and multiple spatial scales using S-band from the Chinese HJ-1C satellite and forthcoming NovaSAR-S and NISAR missions. This also includes the performance of mapping forest AGB from S-band SAR

data at the cost of spatial variability to identify the best suitable resolution with optimum accuracy level.

3. Information on S-band radar signal point of saturation and canopy components contribution to total backscatter can be carried out utilising Multi-MIMICS model parameterised with detailed field data particularly canopy components and moisture condition during the SAR data acquisition whether airborne or space-borne.
4. Lidar data could also be used to retrieve forest parameters such as tree height, crown diameter, stem diameter, basal area and tree density over Savernake forest and Wytham Woods. This could also include estimating forest structure and aboveground biomass by using field data in combination with stem volume and biomass expansion factor.

Appendices

Appendix I:

```
C*****
C234567890123456789012345678901234567890123456789012345678901234567890
12
C*****
C***** MIMICS Version 1.5a MODEL *****
C*****
C***** Master Program *****
C*****
C
C PROGRAM MIMICS_version_1_5asave
C
C*****
C----- Development begun 10-5-88 -----
C----- revised 10-5-88 -----

C*****
C DECLARE THE PARAMETERS IN THE 'PARAMETERS.INCLUDE' FILE.
C-----
C%include 'parameters.include'
include 'parameters.include'
C-----
C*****
C-----
C----- VARIABLE DECLARATIONS -----
C-----
C*****
C
C LOGICAL COMPUTE, WRITE_HEADER
C
C COMPLEX EPSILONR(N_EPS),EPSILONRC(N_EPS)
C
C COMMON /C_DIELECTRIC/ EPSILONR,EPSILONRC
C
C REAL FREQ_HERTZ, WAVELENGTH, k0, THETA, CTHETA, STHETA
C
C COMMON /RADAR_FREQ/ FREQ_HERTZ, WAVELENGTH, k0
COMMON /RADAR_ANGLE/ THETA, CTHETA, STHETA
C
C*****
C DECLARATIONS FROM SUBROUTINE INITIALIZE
C*****
C
C INTEGER LOOP_NUM(N_VARIABLES), LOOP_COUNT(N_VARIABLES)
LOGICAL OPEN, STEP_VARIABLE(N_VARIABLES)
LOGICAL STEP_THIS_TIME(N_VARIABLES)
LOGICAL CALL_SUB(N_CALLS,N_SUB_CALLS)
```

```

C
  LOGICAL LOG_CROWN
C
  COMMON /I_COUNT/ LOOP_NUM, LOOP_COUNT
  COMMON /L_FLAGS/ STEP_VARIABLE, STEP_THIS_TIME, CALL_SUB,
OPEN
C
C*****
C DECLARATIONS FROM SUBROUTINE READ_INPUT
C*****
C
C----- DECLARATIONS FROM SUBROUTINE READ_CONFIGURE -----
-
C
  LOGICAL LOG_CONSTITUENT(N_CONSTITUENTS)
  LOGICAL LOG_EPS_TABLE(N_CONSTITUENTS)
  LOGICAL LOG_DRY_DENSITY(N_CONSTITUENTS)
  LOGICAL LOG_PDF_TYPE(N_CONSTITUENTS,N_CONST_VARY)
  LOGICAL LOG_HIST(N_CONSTITUENTS)
C
  COMMON /L_CONFIGURE/ LOG_CONSTITUENT, LOG_EPS_TABLE,
&          LOG_DRY_DENSITY, LOG_PDF_TYPE, LOG_HIST
C
C----- DECLARATIONS FROM SUBROUTINE READ_SENSOR -----
C
  INTEGER FREQ_NUMBER, THETA_NUMBER
  REAL FREQ_DELTA, FREQ_VECT(I_VECT_LEN), FREQ_GHZ
  REAL THETA_DELTA, THETA_VECT(I_VECT_LEN), THETA_DEGREES
  LOGICAL LOG_FREQ_TABLE, LOG_THETA_TABLE
C
  COMMON /R_SENSOR/ THETA_DEGREES, FREQ_GHZ
  COMMON /R_SENSOR_DELTA/ THETA_DELTA, FREQ_DELTA
  COMMON /I_SENSOR/ THETA_NUMBER, FREQ_NUMBER
  COMMON /R_SENSOR_VECT/ THETA_VECT, FREQ_VECT
  COMMON /L_SENSOR/ LOG_FREQ_TABLE, LOG_THETA_TABLE
C
C----- DECLARATIONS FROM SUBROUTINE READ_ENVIRONMENT -----
----
C
  INTEGER T_SOIL_NUMBER, T_WATER_NUMBER, T_VEG_NUMBER
  REAL T_SOIL_DELTA, T_SOIL_VECT(I_VECT_LEN), T_SOIL
  REAL T_WATER_DELTA, T_WATER_VECT(I_VECT_LEN), T_WATER
  REAL T_VEG_VECT(I_VECT_LEN)
  REAL T_VEG_DELTA, T_VEG
  LOGICAL LOG_ENVIRONMENT(N_ENVIRONMENT)
C
  COMMON /R_ENVIRON/ T_SOIL, T_WATER, T_VEG
  COMMON /R_ENVIRON_DELTA/
  T_SOIL_DELTA, T_WATER_DELTA, T_VEG_DELTA

```

```

COMMON /I_ENVIRON/ T_SOIL_NUMBER, T_WATER_NUMBER,
T_VEG_NUMBER
COMMON /R_ENVIRON_VECT/ T_SOIL_VECT, T_WATER_VECT,
T_VEG_VECT
COMMON /L_ENVIRON/ LOG_ENVIRONMENT
C
C----- DECLARATIONS FROM SUBROUTINE READ_GROUND -----
C
INTEGER MV_SOIL_NUMBER, RMS_SOIL_NUMBER, LS_SOIL_NUMBER
INTEGER SAND_NUMBER, CLAY_NUMBER, SALT_NUMBER
REAL MV_SOIL_DELTA, RMS_SOIL_DELTA, LS_SOIL_DELTA
REAL SAND_DELTA, CLAY_DELTA, SALT_DELTA
REAL MV_SOIL_VECT(I_VECT_LEN), RMS_SOIL_VECT(I_VECT_LEN)
REAL LS_SOIL_VECT (I_VECT_LEN)
REAL SAND_VECT(I_VECT_LEN), CLAY_VECT(I_VECT_LEN)
REAL SALT_VECT(I_VECT_LEN)
REAL MV_SOIL, SAND, CLAY, RMS_SOIL, LS_SOIL
REAL SALT
LOGICAL
SOIL_SURFACE, WATER_SURFACE, SNOW_SURFACE, ICE_SURFACE
LOGICAL
LOG_MV_SOIL, LOG_ROUGH_SOIL(2), LOG_SOIL_TEXT, LOG_SALT
C
COMMON /R_SURFACE/ RMS_SOIL, LS_SOIL
COMMON /R_SOIL/ MV_SOIL, SAND, CLAY
COMMON /R_WATER/ SALT
C
COMMON /R_SURFACE_DELTA/ RMS_SOIL_DELTA, LS_SOIL_DELTA
COMMON /R_SOIL_DELTA/ MV_SOIL_DELTA, SAND_DELTA, CLAY_DELTA
COMMON /R_WATER_DELTA/ SALT_DELTA
C
COMMON /I_SURFACE/ RMS_SOIL_NUMBER, LS_SOIL_NUMBER
COMMON /I_SOIL/ MV_SOIL_NUMBER, SAND_NUMBER,
CLAY_NUMBER
COMMON /I_WATER/ SALT_NUMBER
C
COMMON /R_SURFACE_VECT/ RMS_SOIL_VECT, LS_SOIL_VECT
COMMON /R_SOIL_VECT/ MV_SOIL_VECT, SAND_VECT, CLAY_VECT
COMMON /R_WATER_VECT/ SALT_VECT
C
COMMON /L_SURFACE/ LOG_ROUGH_SOIL
COMMON /L_SOIL/ LOG_MV_SOIL, LOG_SOIL_TEXT
COMMON /L_WATER/ LOG_SALT
C
COMMON /L_SURFACE_TYPE/ SOIL_SURFACE, WATER_SURFACE,
& SNOW_SURFACE, ICE_SURFACE
C----- DECLARATIONS FROM SUBROUTINE READ_TRUNK -----
C
INTEGER MG_TRUNK_NUM, RHO_TRUNK_NUM, DENSITY_NUM

```

```

    INTEGER CROWN_HGHT_NUM, TRUNK_DIAM_NUM,
    TRUNK_HGHT_NUM
    REAL MG_TRUNK_DELTA, RHO_TRUNK_DELTA, DENSITY_DELTA
    REAL CROWN_HGHT_DELTA, TRUNK_DIAM_DELTA,
    TRUNK_HGHT_DELTA
    REAL MG_TRUNK_VECT(I_VECT_LEN),
    RHO_TRUNK_VECT(I_VECT_LEN)
    REAL DENSITY_VECT(I_VECT_LEN)
    REAL CROWN_HGHT_VECT(I_VECT_LEN),
    TRUNK_DIAM_VECT(I_VECT_LEN)
    REAL TRUNK_HGHT_VECT(I_VECT_LEN)
    REAL MG_TRUNK, RHO_TRUNK, DENSITY, CROWN_HGHT
    REAL TRUNK_DIAM, TRUNK_HGHT
    LOGICAL LOG_MG_TRUNK, LOG_RHO_TRUNK, LOG_DENSITY
    LOGICAL LOG_CROWN_HGHT, LOG_TRUNK_DIAM,
    LOG_TRUNK_HGHT
C
    COMMON /R_TRUNK/ MG_TRUNK, RHO_TRUNK, TRUNK_DIAM
    COMMON /R_TRUNK_DELTA/ MG_TRUNK_DELTA, RHO_TRUNK_DELTA,
    &          TRUNK_DIAM_DELTA
    COMMON /I_TRUNK/ MG_TRUNK_NUM, RHO_TRUNK_NUM,
    TRUNK_DIAM_NUM
    COMMON /R_TRUNK_VECT/ MG_TRUNK_VECT, RHO_TRUNK_VECT,
    &          TRUNK_DIAM_VECT
    COMMON /L_TRUNK/
    LOG_MG_TRUNK, LOG_RHO_TRUNK, LOG_TRUNK_DIAM
C
    COMMON /R_CANOPY/ DENSITY, CROWN_HGHT, TRUNK_HGHT
    COMMON /R_CANOPY_DELTA/ DENSITY_DELTA,
    CROWN_HGHT_DELTA,
    &          TRUNK_HGHT_DELTA
    COMMON /I_CANOPY/ DENSITY_NUM, CROWN_HGHT_NUM,
    TRUNK_HGHT_NUM
    COMMON /R_CANOPY_VECT/ DENSITY_VECT, CROWN_HGHT_VECT,
    &          TRUNK_HGHT_VECT
    COMMON /L_CANOPY/ LOG_DENSITY, LOG_CROWN_HGHT,
    LOG_TRUNK_HGHT
C
C----- DECLARATIONS FROM SUBROUTINE READ_LEAF -----
C
    INTEGER MG_LEAF_NUM, RHO_LEAF_NUM, LEAF_DENS_NUM
    INTEGER LEAF_DIAM_NUM, LEAF_TAU_NUM
    REAL MG_LEAF_DELTA, RHO_LEAF_DELTA, LEAF_DENS_DELTA
    REAL LEAF_DIAM_DELTA, LEAF_TAU_DELTA
    REAL MG_LEAF_VECT(I_VECT_LEN), RHO_LEAF_VECT(I_VECT_LEN)
    REAL LEAF_DENS_VECT(I_VECT_LEN)
    REAL LEAF_DIAM_VECT(I_VECT_LEN), LEAF_TAU_VECT(I_VECT_LEN)
    REAL MG_LEAF, RHO_LEAF, LEAF_DENS, LEAF_DIAM, LEAF_TAU
    LOGICAL LOG_MG_LEAF, LOG_RHO_LEAF, LOG_LEAF_DENS
    LOGICAL LOG_LEAF_DIAM, LOG_LEAF_TAU

```

```

C
COMMON /R_LEAF/
MG_LEAF,RHO_LEAF,LEAF_DENS,LEAF_DIAM,LEAF_TAU
COMMON /R_LEAF_DELTA/ MG_LEAF_DELTA, RHO_LEAF_DELTA,
&LEAF_DENS_DELTA, LEAF_DIAM_DELTA, LEAF_TAU_DELTA
COMMON /I_LEAF/ MG_LEAF_NUM, RHO_LEAF_NUM, LEAF_DENS_NUM,
&
LEAF_DIAM_NUM, LEAF_TAU_NUM
COMMON /R_LEAF_VECT/ MG_LEAF_VECT, RHO_LEAF_VECT,
&
LEAF_DENS_VECT, LEAF_DIAM_VECT, LEAF_TAU_VECT
COMMON /L_LEAF/ LOG_MG_LEAF, LOG_RHO_LEAF,
&
LOG_LEAF_DENS, LOG_LEAF_DIAM, LOG_LEAF_TAU
C
C----- DECLARATIONS FROM SUBROUTINE READ_NEEDLE -----
C
INTEGER MG_NDL_NUM, RHO_NDL_NUM, NDL_DENS_NUM
INTEGER NDL_DIAM_NUM, NDL_LNG_NUM
REAL MG_NDL_DELTA, RHO_NDL_DELTA, NDL_DENS_DELTA
REAL NDL_DIAM_DELTA, NDL_LNG_DELTA
REAL MG_NDL_VECT(I_VECT_LEN), RHO_NDL_VECT(I_VECT_LEN)
REAL NDL_DENS_VECT(I_VECT_LEN)
REAL NDL_DIAM_VECT(I_VECT_LEN), NDL_LNG_VECT(I_VECT_LEN)
REAL MG_NDL, RHO_NDL, NDL_DENS, NDL_DIAM, NDL_LNG
LOGICAL LOG_MG_NDL, LOG_RHO_NDL, LOG_NDL_DENS
LOGICAL LOG_NDL_DIAM, LOG_NDL_LNG
C
COMMON /R_NDL/ MG_NDL, RHO_NDL, NDL_DENS, NDL_DIAM,
NDL_LNG
COMMON /R_NDL_DELTA/
MG_NDL_DELTA, RHO_NDL_DELTA, NDL_DENS_DELTA,
&NDL_DIAM_DELTA, NDL_LNG_DELTA
COMMON /I_NDL/ MG_NDL_NUM, RHO_NDL_NUM, NDL_DENS_NUM,
&
NDL_DIAM_NUM, NDL_LNG_NUM
COMMON /R_NDL_VECT/ MG_NDL_VECT,
RHO_NDL_VECT, NDL_DENS_VECT,
&
NDL_DIAM_VECT, NDL_LNG_VECT
COMMON /L_NDL/ LOG_MG_NDL, LOG_RHO_NDL, LOG_NDL_DENS,
&
LOG_NDL_DIAM, LOG_NDL_LNG
C
C----- DECLARATIONS FROM SUBROUTINE READ_PRIMARY_BRANCH ----
-----
C
INTEGER MG_BR1_NUM, RHO_BR1_NUM, BR1_DENS_NUM
INTEGER BR1_DIAM_NUM, BR1_LNG_NUM
REAL MG_BR1_DELTA, RHO_BR1_DELTA, BR1_DENS_DELTA
REAL BR1_DIAM_DELTA, BR1_LNG_DELTA
REAL MG_BR1_VECT(I_VECT_LEN), RHO_BR1_VECT(I_VECT_LEN)
REAL BR1_DENS_VECT(I_VECT_LEN)
REAL BR1_DIAM_VECT(I_VECT_LEN), BR1_LNG_VECT(I_VECT_LEN)
REAL MG_BR1, RHO_BR1, BR1_DENS, BR1_DIAM, BR1_LNG
LOGICAL LOG_MG_BR1, LOG_RHO_BR1, LOG_BR1_DENS

```

```

LOGICAL LOG_BR1_DIAM, LOG_BR1_LNG
C
COMMON /R_BR1/ MG_BR1, RHO_BR1, BR1_DENS, BR1_DIAM, BR1_LNG
COMMON /R_BR1_DELTA/
MG_BR1_DELTA, RHO_BR1_DELTA, BR1_DENS_DELTA,
& BR1_DIAM_DELTA, BR1_LNG_DELTA
COMMON /I_BR1/ MG_BR1_NUM, RHO_BR1_NUM, BR1_DENS_NUM,
& BR1_DIAM_NUM, BR1_LNG_NUM
COMMON /R_BR1_VECT/ MG_BR1_VECT, RHO_BR1_VECT,
BR1_DENS_VECT,
& BR1_DIAM_VECT, BR1_LNG_VECT
COMMON /L_BR1/ LOG_MG_BR1, LOG_RHO_BR1, LOG_BR1_DENS,
& LOG_BR1_DIAM, LOG_BR1_LNG
C
C----- DECLARATIONS FROM SUBROUTINE READ_NESTING -----
C
INTEGER PARAM_NUM(N_VARIABLES), INEST(N_VARIABLES)
COMMON /I_NEST/ PARAM_NUM, INEST
C
REAL GRND_REFLECT_MAT(4,4), GRND_BACK_MAT(4,4)
COMMON /R_GROUND_MATS/ GRND_REFLECT_MAT,
GRND_BACK_MAT
C
C----- DECLARATIONS FROM SUBROUTINE TRUNK_LAYER -----
C
REAL EXP_KAPPA_T_p(4,4), EXP_KAPPA_T_m(4,4)
COMMON /TRUNK_EXT/ EXP_KAPPA_T_p, EXP_KAPPA_T_m

REAL TRUNK_PHASE_MAT_p(4,4,2), TRUNK_PHASE_MAT_m(4,4,2)
COMMON /TRUNK_PHASE/ TRUNK_PHASE_MAT_p,
TRUNK_PHASE_MAT_m

C-----
C DECLARE THE CONSTANTS IN THE 'CONSTANTS.INCLUDE' FILE.
C-----
c%include 'constants.include'
include 'constants.include'
C-----
C
C*****
C*****
C***** MAIN DRIVER ROUTINE *****
C*****
C
C-- Read input data, initialize fixed constants, set output files flag --
C
CC print *, 'calling read_input'
CALL READ_INPUT
CC print *, 'calling init'

```

```

        CALL INITIALIZE(COMPUTE)
i = 0
c
        DO WHILE(COMPUTE)
i=i+1
c
c----- set constants based on input parameters -----
c         these constants vary as a function of input parameters
c         i.e. wavelength and theta(radians)
C----- also check for looping which varies input parameters -----
c
CC        print *, 'calling start_loop'
        CALL START_LOOP(WRITE_HEADER, COMPUTE, LOG_CROWN)

CC        DO i=1, N_CALLS
CC          DO j=1, N_SUB_CALLS
CC            print *, 'call_sub(' , i , ', ' , j , ') = ' , call_sub(i, j)
CC          ENDDO
CC        ENDDO

c
c----- compute dielectric constants -----
c
IF(CALL_SUB(1,1)) THEN
CC        print *, 'calling dielectric'
        CALL DIELECTRIC(EPSILONR, EPSILONRC)
ENDIF

C
c----- compute ground specular reflectivity matrix and -----
backscattering phase matrix -----
c
IF(CALL_SUB(2,1)) THEN
CC        print *, 'calling ground layer'
        CALL GROUND_LAYER
ENDIF

C
C The numbers below are sigvv and sighh.
C
        PRINT*, ''
        PRINT*, 'I = ', I

c
c----- compute trunk layer phase and extinction matrices -----
c
IF(CALL_SUB(3,1)) THEN
CC        print *, 'calling trunk layer'
        CALL TRUNK_LAYER(LOG_CONSTITUENT(1))
ENDIF

c
c----- compute crown layer phase and extinction matrices -----

```

```

c
IF(CALL_SUB(4,1)) THEN
print *,'calling crown_layer'
      CALL CROWN_LAYER(LOG_CROWN)
      ENDIF

c
c----- compute stokes matrix of the canopy -----
c
print *,'calling solve_canopy'
      CALL SOLVE_CANOPY(LOG_CONSTITUENT(1),LOG_CROWN)
C
C----- FORMAT DATA FOR DESIRED OUTPUT TYPE -----
C
CC      print *,'calling format_output'
      CALL FORMAT_OUTPUT

C
C-----      and output results      -----
C
CC      print *,'calling write_data'
      CALL WRITE_DATA(WRITE_HEADER)

c
      ENDDO

c
c----- clean up and close files -----
c
CC      print *,'calling finish'
      CALL FINISH

c
c-----
c
      STOP
      END

```

Appendix II: Sensitivity to soil moisture

**** Forest Canopy Backscatter Model Output File -- Like-polarisation Sigma0 Values

**** Forest Canopy Backscatter Model Output File -- Cross-polarisation Sigma0 Values

Trunks = F, Primary Branches = F, Secondary Branches = F, 3rd Branches = F, 4th Branches = F, 5th Branches = F, 6th Branches = F, Leaves = F, Needles = F

SOIL_SURFACE = T, WATER_SURFACE = F, SNOW_SURFACE = F, ICE_SURFACE = F

Dielectric Lookup Tables: Trunk = F, Primary Branch = F, Secondary Branch = F, 3rd Branch = F, 4th Branch = F, 5th Branch = F, 6th Branch = F, Leaf = F, Needle = F, Ground = F

CONSTITUENT ORIENTATION AND SIZE DISTRIBUTIONS:

Nesting Data:

Variable Number = 1 3

Nesting Order = 1 2

Number of Loops = 7 10

Family Number 1

RADAR Look Angle = 15.0 – 45.0 Degrees, Radar Frequency = 3.10GHz (15 cm).

Canopy Density = 0.0 Trees per square meter, Crown Height = 0.0 meters, Trunk Height = 0.0 meters, Vegetation Temperature = 20.0 degrees C.

Soil Volumetric Moisture = 0.1 – 1.0 (water weight/volume weight), Soil RMS Roughness = 1.0 cm, Soil Correlation Length = 15.0 cm, Soil % Sand = 10.0 cm, Soil % Clay = 60.0 cm, Soil Temperature = 20.0 degrees C, Model Type = Physical Optics.

Appendix III: Sensitivity to soil surface roughness

**** Forest Canopy Backscatter Model Output File -- Like-polarisation Sigma0 Values

**** Forest Canopy Backscatter Model Output File -- Cross-polarisation Sigma0 Values

Trunks = F, Primary Branches = F, Secondary Branches = F, 3rd Branches = F, 4th Branches = F, 5th Branches = F, 6th Branches = F, Leaves = F, Needles = F

SOIL_SURFACE = T, WATER_SURFACE = F, SNOW_SURFACE = F, ICE_SURFACE = F

Dielectric Lookup Tables: Trunk = F, Primary Branch = F, Secondary Branch = F, 3rd Branch = F, 4th Branch = F, 5th Branch = F, 6th Branch = F, Leaf = F, Needle = F, Ground = F

CONSTITUENT ORIENTATION AND SIZE DISTRIBUTIONS:

Nesting Data:

Variable Number = 1 3

Nesting Order = 1 2

Number of Loops = 7 10

Family Number 1

RADAR Look Angle = 15.0 – 45.0 Degrees, Radar Frequency = 3.10GHz (15 cm).

Canopy Density = 0.0 Trees per square meter, Crown Height = 0.0 meters, Trunk Height = 0.0 meters, Vegetation Temperature = 20.0 degrees C.

Soil Volumetric Moisture = 0.0(water weight/volume weight), Soil RMS Roughness = 0.1 – 5.0 cm, Soil Correlation Length = 15.0 cm, Soil % Sand = 10.0 cm, Soil % Clay = 60.0 cm, Soil Temperature = 20.0 degrees C, Model Type = Physical Optics.

Appendix IV: Leaf-dominated deciduous canopy

**** Forest Canopy Backscatter Model Output File -- Transmissivity Values ****

**** Forest Canopy Backscatter Model Output File -- Like-polarisation Sigma0 Values

**** Forest Canopy Backscatter Model Output File -- Cross-polarisation Sigma0 Values

Trunks = T, Primary Branches = F, Secondary Branches = F, 3rd Branches = F, 4th Branches = F, 5th Branches = F, 6th Branches = F, Leaves = T, Needles = F

SOIL_SURFACE = T, WATER_SURFACE = F, SNOW_SURFACE = F, ICE_SURFACE = F

Dielectric Lookup Tables: Trunk = T, Primary Branch = F, Secondary Branch = F, 3rd Branch = F, 4th Branch = F, 5th Branch = F, 6th Branch = F, Leaf = T, Needle = F, Ground = T

CONSTITUENT ORIENTATION AND SIZE DISTRIBUTIONS:

Trunk Orient PDF = 2, Form = $(1/0.85903)*\text{COS}(\text{THETA}_c)**8$ Size PDF = 1, Form = HISTOGRAM DATA

Leaf Orient PDF = 1, Form = $0.5*\text{SIN}(\text{Theta}_d)$ - Uniform Size PDF = 0, Form = DEFAULT VALUES

Prim Br Orient PDF = 14, Form = $(1.23)*\text{SIN}(\text{THETA}_c+30)**20$ Size PDF = 0, Form = DEFAULT VALUES

Nesting Data:

Variable Number = 1

Nesting Order = 1

Number of Loops = 7

Family Number 1

RADAR Look Angle = 15.0 – 45.0 Degrees, Radar Frequency = 1.25GHz (24 cm); 3.10GHz (15 cm), 4.75GHz (5.6 cm) and 10.00 GHz (2 cm).

Canopy Density = 0.11 Trees per square meter, Crown Height = 2.0 meters, Trunk Height = 8.0 meters, Vegetation Temperature = 20.0 degrees C.

Surface Dielectric = $5.680 - j 1.130$, Soil RMS Roughness = 0.4 cm, Soil Correlation Length = 18.75 cm, Model Type = Physical Optics

Trunk Gravimetric Moisture = 0.5, Trunk Dry Density = 0.408, Trunk Diameter = 24.0 cm

Leaf Gravimetric Moisture = 0.8, Leaf Dry Density = 0.005 cm, Leaf Density = 830leaves per cubic meter, Leaf Diameter = 6.18 cm, Leaf Thickness = 0.1cm.

Appendix V: Branch-dominated deciduous canopy

**** Forest Canopy Backscatter Model Output File -- Transmissivity Values ****

**** Forest Canopy Backscatter Model Output File -- Like-polarisation Sigma0 Values

**** Forest Canopy Backscatter Model Output File -- Cross-polarisation Sigma0 Values

Trunks = T, Primary Branches = T, Secondary Branches = F, 3rd Branches = F, 4th Branches = F, 5th Branches = F, 6th Branches = F, Leaves = F, Needles = F

SOIL_SURFACE = T, WATER_SURFACE = F, SNOW_SURFACE = F, ICE_SURFACE = F

Dielectric Lookup Tables: Trunk = T, Primary Branch = T, Secondary Branch = F, 3rd Branch = F, 4th Branch = F, 5th Branch = F, 6th Branch = F, Leaf = F, Needle = F, Ground = T

CONSTITUENT ORIENTATION AND SIZE DISTRIBUTIONS:

Trunk Orient PDF = 2, Form = $(1/0.85903)*\text{COS}(\text{THETA}_c)^{**8}$ Size PDF = 1, Form = HISTOGRAM DATA

Leaf Orient PDF = 1, Form = $0.5*\text{SIN}(\text{Theta}_d)$ –UniformSize PDF = 0, Form = DEFAULT VALUES

Prim Br Orient PDF = 14, Form = $(1.23)*\text{SIN}(\text{THETA}_c+30)^{**20}$ Size PDF = 0, Form = DEFAULT VALUES

Nesting Data:

Variable Number = 1

Nesting Order = 1

Number of Loops = 7

Family Number 1

RADAR Look Angle = 15.0 – 45.0 Degrees, Radar Frequency = 1.25GHz (24 cm); 3.10GHz (15 cm), 4.75GHz (5.6 cm) and 10.00 GHz (2 cm).

Canopy Density = 0.11 Trees per square meter, Crown Height = 2.0 meters, Trunk Height = 8.0 meters, Vegetation Temperature = 20.0 degrees C.

Surface Dielectric = $5.680 - j 1.130$, Soil RMS Roughness = 0.4 cm, Soil Correlation Length = 18.75 cm, Model Type = Physical Optics

Trunk Gravimetric Moisture = 0.5, Trunk Dry Density = 0.408 cm, Trunk Diameter = 24.0 cm

Branch Gravimetric Moisture = 0.4, Branch Dry Density = 0.1, Branch Density = 4.1
branches per cubic meter, Branch Diameter = 0.7 cm, Branch Length = 0.75 meters.

Appendix VI: Leaf-branch deciduous canopy

**** Forest Canopy Backscatter Model Output File -- Transmissivity Values ****

**** Forest Canopy Backscatter Model Output File -- Like-polarisation Sigma0 Values

**** Forest Canopy Backscatter Model Output File -- Cross-polarisation Sigma0 Values

Trunks = T, Primary Branches = T, Secondary Branches = F, 3rd Branches = F, 4th Branches = F, 5th Branches = F, 6th Branches = F, Leaves = T, Needles = F

SOIL_SURFACE = T, WATER_SURFACE = F, SNOW_SURFACE = F, ICE_SURFACE = F

Dielectric Lookup Tables: Trunk = T, Primary Branch = T, Secondary Branch = F, 3rd Branch = F, 4th Branch = F, 5th Branch = F, 6th Branch = F, Leaf = T, Needle = F, Ground = T

CONSTITUENT ORIENTATION AND SIZE DISTRIBUTIONS:

Trunk Orient PDF = 2, Form = $(1/0.85903)*\text{COS}(\text{THETA}_c)^{**8}$ Size PDF = 1, Form = HISTOGRAM DATA

Leaf Orient PDF = 1, Form = $0.5*\text{SIN}(\text{Theta}_d)$ - Uniform Size PDF = 0, Form = DEFAULT VALUES

Prim Br Orient PDF = 14, Form = $(1.23)*\text{SIN}(\text{THETA}_c+30)^{**20}$ Size PDF = 0, Form = DEFAULT VALUES

Nesting Data:

Variable Number = 1

Nesting Order = 1

Number of Loops = 7

Family Number 1

RADAR Look Angle = 15.0 – 45.0 Degrees, Radar Frequency = 1.25GHz (24 cm); 3.10GHz (15 cm), 4.75GHz (5.6 cm) and 10.00 GHz (2 cm).

Canopy Density = 0.11 Trees per square meter, Crown Height = 2.0 meters, Trunk Height = 8.0 meters, Vegetation Temperature = 20.0 degrees C.

Surface Dielectric = $5.680 - j 1.130$, Soil RMS Roughness = 0.4 cm, Soil Correlation Length = 18.75 cm, Model Type = Physical Optics

Trunk Gravimetric Moisture = 0.5, Trunk Dry Density = 0.408 cm, Trunk Diameter = 24.0 cm

Leaf Gravimetric Moisture = 0.8, Leaf Dry Density = 0.005, Leaf Density = 830leaves per cubic meter, Leaf Diameter = 6.18 cm, Leaf Thickness = 0.1 cm

Branch Gravimetric Moisture = 0.4, Branch Dry Density = 0.1, Branch Density =4.1 branches per cubic meter, Branch Diameter = 0.7 cm, Branch Length = 0.75 meters.

Appendix VII: Needle-branch coniferous canopy

**** Forest Canopy Backscatter Model Output File -- Transmissivity Values ****

**** Forest Canopy Backscatter Model Output File -- Like-polarisation Sigma0 Values

**** Forest Canopy Backscatter Model Output File -- Cross-polarisation Sigma0 Values

Trunks = T, Primary Branches = T, Secondary Branches = F, 3rd Branches = F, 4th Branches = F, 5th Branches = F, 6th Branches = F, Leaves = F, Needles = T

SOIL_SURFACE = T, WATER_SURFACE = F, SNOW_SURFACE = F, ICE_SURFACE = F

Dielectric Lookup Tables: Trunk = F, Primary Branch = F, Secondary Branch = F, 3rd Branch = F, 4th Branch = F, 5th Branch = F, 6th Branch = F, Leaf = F, Needle = T, Ground = F

CONSTITUENT ORIENTATION AND SIZE DISTRIBUTIONS:

Trunk Orient PDF = 2, Form = $(1/0.85903)*\text{COS}(\text{THETA}_c)**8$ Size PDF = 1, Form = HISTOGRAM DATA

Needle Orient PDF = 1, Form = $0.5*\text{SIN}(\text{Theta}_n)$ - Uniform Size PDF = 0, Form = DEFAULT VALUES

Prim Br Orient PDF = 14, Form = $(1.23)*\text{SIN}(\text{THETA}_c+30)**20$ Size PDF = 0, Form = DEFAULT VALUES

Nesting Data:

Variable Number = 1

Nesting Order = 1

Number of Loops = 7

Family Number 1

RADAR Look Angle = 15.0 – 45.0 Degrees, Radar Frequency = 1.25GHz (24 cm); 3.10GHz (15 cm), 4.75GHz (5.6 cm) and 10.00 GHz (2 cm).

Canopy Density = 0.1 Trees per square meter, Crown Height = 11.0 meters, Trunk Height = 8.0 meters, Vegetation Temperature = 20.0 degrees C.

Soil Volumetric Moisture = 0.1, Soil RMS Roughness = 0.45 cm, Soil Correlation Length = 15.0 cm, Soil % Sand = 20.0 cm, Soil % Clay = 10.0 cm, Soil Temperature = 20.0 degrees C., Model Type = Physical Optics

Trunk Gravimetric Moisture = 0.6, Trunk Dry Density = 0.408 cm, Trunk Diameter = 20.8 cm

Needle Gravimetric Moisture = 0.8, Needle Dry Density = 0.377, Needle Density = 0.8500E+05 needles per cubic meter, Needle Diameter = 0.1 cm, Needle Length = 2.0 cm

Branch Gravimetric Moisture = 0.6, Branch Dry Density = 0.1, Branch Density = 3.4 branches per cubic meter, Branch Diameter = 2.0 cm, Branch Length = 2.0 meters.

Appendix VIII: Reduced canopy components

**** Forest Canopy Backscatter Model Output File -- Like-polarisation Sigma0 Values

Trunks = T, Primary Branches = T, Secondary Branches = F, 3rd Branches = F, 4th

Branches = F, 5th Branches = F, 6th Branches = F, Leaves = T, Needles = F

SOIL_SURFACE = T, WATER_SURFACE = F, SNOW_SURFACE = F,

ICE_SURFACE = F

Dielectric Lookup Tables: Trunk = F, Primary Branch = F, Secondary Branch = F, 3rd

Branch = F, 4th Branch = F, 5th Branch = F, 6th Branch = F, Leaf = F, Needle = F,

Ground = F

CONSTITUENT ORIENTATION AND SIZE DISTRIBUTIONS:

Trunk Orient PDF = 2, Form = $(1/0.85903)*\text{COS}(\text{THETA}_c)**8$ Size PDF = 1,

Form = HISTOGRAM DATA

Leaf Orient PDF = 1, Form = $0.5*\text{SIN}(\text{Theta}_d)$ - Uniform Size PDF = 0, Form =

DEFAULT VALUES

Prim Br Orient PDF = 14, Form = $(1.23)*\text{SIN}(\text{THETA}_c+30)**20$ Size PDF = 0,

Form = DEFAULT VALUES

Nesting Data:

Variable Number = 1

Nesting Order = 1

Number of Loops = 7

Family Number 1

RADAR Look Angle = 15.0 – 45.0 Degrees, Radar Frequency = 1.25GHz (24 cm);

3.10GHz (15 cm), 4.75GHz (5.6 cm) and 10.00 GHz (2 cm).

Canopy Density = 0.2 Trees per square meter, Crown Height = 2.0 meters, Trunk

Height = 8.0 meters, Vegetation Temperature = 20.0 degrees C.

Soil Volumetric Moisture = 0.15, Soil RMS Roughness = 0.45 cm, Soil Correlation

Length = 15.0 cm, Soil % Sand = 10.0 cm, Soil % Clay = 60.0 cm, Soil Temperature =

20.0 degrees C., Model Type = Physical Optics

Trunk Gravimetric Moisture = 0.5, Trunk Dry Density = 0.408 cm, Trunk Diameter =

24.0 cm

Leaf Gravimetric Moisture = 0.8, Leaf Dry Density = 0.005 cm, Leaf Density = 5000

leaves per cubic meter, Leaf Diameter = 6.18 cm, Leaf Thickness = 0.1 cm

Branch Gravimetric Moisture = 0.4, Branch Dry Density = 0.1 cm, Branch Density =

5.1 branches per cubic meter, Branch Diameter = 0.7 cm, Branch Length = 0.75 meters.

Canopy Density = 0.11 Trees per square meter, Crown Height = 2.0 meters, Trunk

Height = 8.0 meters, Vegetation Temperature = 20.0 degrees C.

Soil Volumetric Moisture = 0.15, Soil RMS Roughness = 0.45 cm, Soil Correlation

Length = 15.0 cm, Soil % Sand = 10.0 cm, Soil % Clay = 60.0 cm, Soil Temperature =

20.0 degrees C., Model Type = Physical Optics

Trunk Gravimetric Moisture = 0.5, Trunk Dry Density = 0.408 cm, Trunk Diameter =

24.0 cm

Leaf Gravimetric Moisture = 0.8, Leaf Dry Density = 0.005 cm, Leaf Density =

830leaves per cubic meter, Leaf Diameter = 6.18 cm, Leaf Thickness = 0.1 cm

Branch Gravimetric Moisture = 0.4, Branch Dry Density = 0.1 cm, Branch Density = 4.1

branches per cubic meter, Branch Diameter = 0.7 cm, Branch Length = 0.75 meters

Appendix IX. Summary of observed and predicted values of AGB (t/ha) for combined sites based on training stands (25 stands) and validation stands (16 stands) from 2010 0.25 ha stand level.

Observed AGB <i>T ha⁻¹</i>	Training Predicted AGB			Observed AGB <i>T ha⁻¹</i>	Validation Predicted AGB		
	HH	VV	HV		HH	VV	HV
	<i>T ha⁻¹</i>	<i>T ha⁻¹</i>	<i>T ha⁻¹</i>		<i>T ha⁻¹</i>	<i>T ha⁻¹</i>	<i>T ha⁻¹</i>
31.41	102.96	258.72	192.56	32.99	110.50	76.20	23.34
52.12	8.43	2.85	1.37	54.88	234.16	134.52	100.47
81.85	159.20	315.84	253.31	102.59	319.38	585.98	476.54
85.09	79.52	233.36	184.61	107.69	158.52	127.33	83.28
104.20	18.75	4.34	1.84	122.23	77.23	84.13	39.49
113.96	211.17	28.63	796.71	123.29	171.99	132.97	120.80
122.92	163.11	318.02	306.25	175.45	158.93	323.97	116.99
152.40	339.98	97.42	74.02	203.60	316.83	572.06	499.77
157.04	256.31	687.13	774.62	205.05	104.11	247.27	341.39
168.87	212.88	18.95	18.66	225.95	423.93	287.62	107.09
169.97	148.05	470.69	414.35	306.15	450.18	954.30	297.78
200.77	100.50	301.0	285.46	360.04	449.30	1038.98	572.80
204.77	150.46	451.66	466.94	361.61	216.07	705.29	207.91
210.51	114.35	311.53	249.77	382.74	309.67	520.00	205.11
239.17	196.38	518.28	480.26	426.33	125.45	356.32	222.09
242.09	236.44	868.18	682.54	469.39	545.95	721.68	620.91
255.43	2283.93	74.49	151.62				
264.24	187.09	477.21	466.94				
284.44	207.79	570.67	529.93				
301.64	1778.37	70.02	120.23				
342.43	115.28	253.44	185.91				
356.36	151.68	433.40	402.86				
401.67	296.39	628.36	572.54				
410.07	275.62	650.34	614.24				
520.13	978.67	222.39	108.96				

Appendix X. Summary of observed and predicted values of AGB (t/ha) for combined sites based on training stands (25 stands) and validation stands (16 stands) from 2014 0.25 ha stand level.

Observed AGB	Training Predicted AGB			Observed AGB	Validation Predicted AGB		
	HH	VV	HV		HH	VV	HV
<i>T ha⁻¹</i>							
31.41	108.93	152.61	194.71	32.99	55.79	123.69	183.22
52.12	22.19	9.68	4.56	54.88	79.90	110.40	166.28
81.85	101.40	158.41	127.20	102.59	76.74	93.47	185.28
85.09	44.04	81.01	67.17	107.69	192.07	250.77	304.00
104.20	36.82	13.40	5.67	122.23	76.35	109.79	157.62
113.96	170.87	57.62	500.88	123.29	73.75	126.58	125.92
122.92	76.14	101.84	120.77	175.45	124.08	406.88	286.91
152.40	231.08	148.61	86.62	203.60	167.13	158.49	234.16
157.04	235.86	1111.14	720.39	205.05	219.23	256.51	365.24
168.87	171.75	41.87	31.31	225.95	112.54	276.82	197.73
169.97	95.36	323.23	353.73	306.15	146.94	312.55	210.05
200.77	109.49	158.41	237.17	360.04	174.76	287.31	298.93
204.77	277.81	419.54	535.86	361.61	92.38	348.11	209.27
210.51	68.03	106.84	83.53	382.74	209.08	239.55	293.39
239.17	356.96	433.15	622.92	426.33	247.83	494.39	196.84
242.09	298.44	1020.44	790.95	469.39	233.12	329.14	217.08
255.43	772.88	120.75	147.10				
264.24	543.01	725.86	914.70				
284.44	465.75	761.48	1014.79				
301.64	659.53	115.1	123.94				
342.43	117.62	163.55	150.97				
356.36	327.22	437.79	544.27				
401.67	263.95	340.90	400.67				
410.07	577.39	625.36	573.27				
520.13	451.67	281.46	115.25				

Bibliography

- Airbus (2013a) *Airborne SAR Demonstrator Facility (AIRSAR) Flight Plan*, Issue: 1.2, Airbus Defence and Space.
- Airbus (2013b) *Airborne SAR Demonstrator Facility (AirSAR) D2: User Guide*, Issue 1, Airbus Defence and Space.
- Alberga, V. (2007) 'A study of land cover classification using polarimetric SAR parameters', *International Journal of Remote Sensing*, 28(17), 3851-3870.
- Arino, O., Bicheron, P., Achard, F., Latham, J., Witt, R. and Weber, J. E. (2008) *GLOBCOVER the most detailed portrait of earth* 136
- Asner, G. P., Broadbent, E. N., Oliveira, P. J., Keller, M., Knapp, D. E. and Silva, J. N. (2006) 'Condition and fate of logged forests in the Brazilian Amazon', *Proc Natl Acad Sci U S A*, 103(34), 12947-50.
- Asner, G. P., Rudel, T. K., Aide, T. M., Defries, R. and Emerson, R. (2009) 'A Contemporary Assessment of Change in Humid Tropical Forests', *Conservation Biology*, 23(6), 1386-1395.
- Attema, E. and Wooding, M. (1994) *EMAC Experimenters Handbook. Programme for 1995*.
- Attema, E. P. W. and Ulaby, F. T. (1978) 'Vegetation modeled as a water cloud', *Radio Science*, 13(2), 357-364.
- Aubert, M., Baghdadi, N., Zribi, M., Douaoui, A., Loumagne, C., Baup, F., El Hajj, M. and Garrigues, S. (2011) 'Analysis of TerraSAR-X data sensitivity to bare soil moisture, roughness, composition and soil crust', *Remote Sensing of Environment*, 115(8), 1801-1810.
- Avissar, R. and Werth, D. (2005) 'Global Hydroclimatological Teleconnections Resulting from Tropical Deforestation', *Journal of Hydrometeorology*, 6(2), 134-145.
- Baccini, A., Goetz, S. J., Walker, W. S., Laporte, N. T., Sun, M., Sulla-Menashe, D., Hackler, J., Beck, P. S. A., Dubayah, R., Friedl, M. A., Samanta, S. and Houghton, R. A. (2012) 'Estimated carbon dioxide emissions from tropical deforestation improved by carbon-density maps', *Nature Clim. Change*, 2(3), 182-185.

- Baghdadi, N., Aubert, M., Cerdan, O., Franchistéguy, L., Viel, C., Eric, M., Zribi, M. and Desprats, J. (2007) 'Operational Mapping of Soil Moisture Using Synthetic Aperture Radar Data: Application to the Touch Basin (France)', *Sensors*, 7(10), 2458.
- Baker, J. R., Mitchell, P. L., Cordey, R. A., Groom, G. B., Settle, J. J. and Stileman, M. R. (1994) 'Relationships between physical characteristics and polarimetric radar backscatter for Corsican pine stands in Thetford Forest, U.K', *International Journal of Remote Sensing*, 15(14), 2827-2849.
- Ballantyne, A. P., Alden, C. B., Miller, J. B., Tans, P. P. and White, J. W. C. (2012) 'Increase in observed net carbon dioxide uptake by land and oceans during the past 50 years', *Nature*, 488, 70–72.
- Balzter, H. (2001) 'Forest mapping and monitoring with interferometric synthetic aperture radar (InSAR)', *Progress in Physical Geography*, 25(2), 159-177.
- Balzter, H., Luckman, A., Skinner, L., Rowland, C. and Dawson, T. (2007a) 'Observations of forest stand top height and mean height from interferometric SAR and LiDAR over a conifer plantation at Thetford Forest, UK', *International Journal of Remote Sensing*, 28(6), 1173-1197.
- Balzter, H., Rowland, C. and Saich, P. (2007b) 'Forest canopy height and carbon estimation at Monks Wood National Nature Reserve, UK, using dual-wavelength SAR interferometry', *Remote Sensing of Environment*, 108(3), 224-239.
- Balzter, H., Saich, P., Luckman, A., Skinner, J. and Grant, L. (2001) 'Forest stand structure from airborne polarimetric InSAR', in *Proceedings of 3rd international symposium on retrieval of bio- and geophysical parameters from SAR data for land applications*, Sheffield, UK, 11 -14th September 2001, ESA SP-475, 321-326.
- Ban, Y., Hu, H. and Rangel, I. M. (2010) 'Fusion of Quickbird MS and RADARSAT SAR data for urban land-cover mapping: object-based and knowledge-based approach', *International Journal of Remote Sensing*, 31(6), 1391-1410.
- Bartholomé, E. and Belward, A. S. (2005) 'A new approach to global land cover mapping from earth observation data ', *International Journal of Remote Sensing*, 26, 1959-1977.
- Basili, P., Quarto, P., Ciotti, P., D'Auria, G., Marzano, F. S. and Pierdicca, N. (1994) 'Assessment of polarimetric features to discriminate land cover from the

MAESTRO 1 campaign', *International Journal of Remote Sensing*, 15(14), 2887-2899.

Batjes, N. H. (2015) *World soil property estimates for broad-scale modelling (WISE30sec)*, Report 2015/01, ISRIC - World Soil Information, Wageningen.

Beaudoin, A., Le Toan, T., Goze, S., Nezry, E., Lopes, A., Mougin, E., Hsu, C. C., Han, H. C., Kong, J. A. and Shin, R. T. (1994) 'Retrieval of forest biomass from SAR data', *International Journal of Remote Sensing*, 15(14), 2777-2796.

Billington, C., Kapos, V., Edwards, M., Blyth, S. and Iremonger, S. (1996) 'Estimated original forest cover map-a first attempt. World Conservation Monitoring Centre (<http://www.unep-wcmc.org/forest/original.htm>)', [online], available: [accessed

Bird, R., Whittaker, P., Stern, B., Angli, N., Cohen, M. and Guida, R. (2013) 'NovaSAR-S A low cost approach to SAR applications, Synthetic Aperture Radar', in *IEEE on Asia-Pacific Conference*, 84-87.

Blanc, L., Echard, M., Herault, B., Bonal, D., Marcon, E., Chave, J. and Baraloto, C. (2009) 'Dynamics of aboveground carbon stocks in a selectively logged tropical forest', *Ecological Applications*, 19(6), 1397-1404.

Bojinski, S., Verstraete, M., Peterson, T. C., Richter, C., Simmons, A. and Zemp, M. (2014) 'The Concept of Essential Climate Variables in Support of Climate Research, Applications, and Policy', *Bulletin of the American Meteorological Society*, 95(9), 1431-1443.

Bonan, G. B. (2008) 'Forests and climate change: forcings, feedbacks, and the climate benefits of forests', *Science*, 320(5882), 1444-9.

Bonnell, T. R., Reyna-Hurtado, R. and Chapman, C. A. (2011) 'Post-logging recovery time is longer than expected in an East African tropical forest', *Forest Ecology and Management*, 261(4), 855-864.

Bosisio, A. V. and Dechambre, M. (2004) 'Predictions of microwave attenuation through vegetation: a comparison with measurements', *International Journal of Remote Sensing*, 25(19), 3973-3997.

Breidenbach, J., Ortiz, S. M. and Reich, M. (2009) 'Forest monitoring with TerraSAR-X: first results', *European Journal of Forest Research*, 129(5), 813-823.

- Brolly, M. and Woodhouse, I. H. (2013) 'Vertical backscatter profile of forests predicted by a macroecological plant model', *International Journal of Remote Sensing*, 34(4), 1026-1040.
- Brolly, M., Woodhouse, I. H., Niklas, K. J. and Hammond, S. T. (2012) 'A Macroecological Analysis of SERA Derived Forest Heights and Implications for Forest Volume Remote Sensing', *PLoS ONE*, 7(3), e33927.
- Brown, R. J., Brisco, B., Ahern, F., Yatabe, S. M. and Drieman, J. (1992) 'Preliminary ERS-1 assessment for Canadian agriculture and forestry applications', in *Proceedings of the First ERS-1 Symposium*, Cannes, France, 4-6 November 1992, 611-616.
- Brown, S. (1997) *Estimating Biomass and Biomass Change of Tropical Forests: A Primer*, Food and Agriculture Organization, Rome.
- Bunce, R. G. H. (1968) 'Biomass and production of trees in a mixed deciduous woodland: I. Girth and height as parameters for the estimation of tree dry weight', *Journal of Ecology*, 5, 759-775.
- Bunker, D. E., DeClerck, F., Bradford, J. C., Colwell, R. K., Perfecto, I., Phillips, O. L., Sankaran, M. and Naeem, S. (2005) 'Species Loss and Aboveground Carbon Storage in a Tropical Forest', *Science*, 310(5750), 1029-1031.
- Butchart, S. H. M., Walpole, M., Collen, B., van Strien, A., Scharlemann, J. P. W., Almond, R. E. A., Baillie, J. E. M., Bomhard, B., Brown, C., Bruno, J., Carpenter, K. E., Carr, G. M., Chanson, J., Chenery, A. M., Csirke, J., Davidson, N. C., Dentener, F., Foster, M., Galli, A., Galloway, J. N., Genovesi, P., Gregory, R. D., Hockings, M., Kapos, V., Lamarque, J.-F., Leverington, F., Loh, J., McGeoch, M. A., McRae, L., Minasyan, A., Morcillo, M. H., Oldfield, T. E. E., Pauly, D., Quader, S., Revenga, C., Sauer, J. R., Skolnik, B., Spear, D., Stanwell-Smith, D., Stuart, S. N., Symes, A., Tierney, M., Tyrrell, T. D., Vié, J.-C. and Watson, R. (2010) 'Global Biodiversity: Indicators of Recent Declines', *Science*, 328(5982), 1164-1168.
- Butt, N., Campbell, G., Malhi, Y., Morecroft, M., Fenn, K. and Thomas, M. (2009) *Initial results from establishment of a long-term Broadleaf monitoring plot at Wytham Woods, Oxford, UK* Oxford.
- Cartus, O., Santoro, M. and Kelldorfer, J. M. (2012) 'Mapping forest aboveground biomass in the Northeastern United States with ALOS PALSAR dual-polarization L-band', *Remote Sensing of Environment*, 124, 466-478.

- Castro, K. L., Sanchez-Azofeifa, G. A. and Rivard, B. (2003) 'Monitoring secondary tropical forests using space-borne data: Implications for Central America', *International Journal of Remote Sensing*, 24(9), 1853-1894.
- Chave, J., Andalo, C., Brown, S., Cairns, M. A., Chambers, J. Q., Eamus, D., Fölster, H., Fromard, F., Higuchi, N., Kira, T., Lescure, J.-P., Nelson, B. W., Ogawa, H., Puig, H., Riéra, B. and Yamakura, T. (2005) 'Tree allometry and improved estimation of carbon stocks and balance in tropical forests', *Oecologia*, 145(1), 87-99.
- Chave, J., Coomes, D. A., Jansen, S., Lewis, S. L., Swenson, N. G. and Zanne, A. E. (2009) 'Towards a worldwide wood economics spectrum', *Ecology Letters*, 12(4), 351-366.
- Chave, J., Rejou-Mechain, M., Burquez, A., Chidumayo, E., Colgan, M. S., Delitti, W. B., Duque, A., Eid, T., Fearnside, P. M., Goodman, R. C., Henry, M., Martinez-Yrizar, A., Mugasha, W. A., Muller-Landau, H. C., Mencuccini, M., Nelson, B. W., Ngomanda, A., Nogueira, E. M., Ortiz-Malavassi, E., Pelissier, R., Ploton, P., Ryan, C. M., Saldarriaga, J. G. and Vieilledent, G. (2015) 'Improved allometric models to estimate the aboveground biomass of tropical trees', *Glob Chang Biol*, 20(10), 3177-90.
- Chen, Q., Laurin, G. V. and Valentini, R. (2015) 'Uncertainty of remotely sensed aboveground biomass over an African tropical forest: Propagating errors from trees to plots to pixels', *Remote Sensing of Environment*, 160, 134-143.
- Churkina, G. and Running, S. W. (1998) 'Contrasting Climatic Controls on the Estimated Productivity of Global Terrestrial Biomes', *Ecosystems*, 1(2), 206-215.
- Churkina, G., Running, S. W., Schloss, A. L., Intercomparison, Participants, T., OF, ThE., Potsdam and NpP, M. (1999) 'Comparing global models of terrestrial net primary productivity (NPP): the importance of water availability', *Glob Chang Biol*, 5(S1), 46-55.
- Ciais, P., Denning, A. S., Tans, P. P., Berry, J. A., Randall, D. A., Collatz, G. J., Sellers, P. J., White, J. W. C., Trolier, M., Meijer, H. A. J., Francey, R. J., Monfray, P. and Heimann, M. (1997) 'A three-dimensional synthesis study of $\delta^{18}\text{O}$ in atmospheric CO₂: 1. Surface fluxes', *Journal of Geophysical Research*, 102(D5), 5857.
- Ciais, P., Sabine, C., Bala, G., Bopp, L., Brovkin, V., Canadell, J., Chhabra, A., DeFries, R., Galloway, J., Heimann, M., Jones, C., Le Quéré, C., Myneni, R. B., Piao, S. and Thornton, P. (2013) *Carbon and Other Biogeochemical Cycles*,

Cambridge University Press, Cambridge, United Kingdom and New York, NY, USA.

- Cihlar, J. (2000) 'Land cover mapping of large areas from satellites: Status and research priorities', *International Journal of Remote Sensing*, 21(6-7), 1093-1114.
- Clark, D. B. and Clark, D. A. (2000) 'Landscape-scale variation in forest structure and biomass in a tropical rain forest', *Forest Ecology and Management*, 137(1-3), 185-198.
- Clark, D. B. and Kellner, J. R. (2012) 'Tropical forest biomass estimation and the fallacy of misplaced concreteness', *Journal of Vegetation Science*, 23, 1191-1196.
- Cochrane, M. A. (2003) 'Fire science for rainforests', *Nature*, 421(6926), 913-919.
- Cox, P. M., Betts, R. A., Jones, C. D., Spall, S. A. and Totterdell, I. J. (2000) 'Acceleration of global warming due to carbon-cycle feedbacks in a coupled climate model', *Nature*, 408, 184-187.
- Crutchley, S. P., Small, F. and Bowden, M. (2009) *Savernake Forest: A report for the National Mapping Programme*.
- De Grandt, G. F., Lemoine, G. G., De Groof, H., Lavallo, C. and Sieber, A. J. (1994) 'Fully polarimetric classification of the Black Forest MAESTRO 1 AIRSAR data', *International Journal of Remote Sensing*, 15(14), 2755-2775.
- DeFries, R., Achard, F., Brown, S., Herold, M., Murdiyarso, D., Schlamadinger, B. and de Souza, C. (2007) 'Earth observations for estimating greenhouse gas emissions from deforestation in developing countries', *Environmental Science & Policy*, 10(4), 385-394.
- DeFries, R. S., Hansen, M., Townshend, J. R. G. and Sohlberg, R. (1998) 'Global land cover classifications at 8 km spatial resolution: The use of training data derived from Landsat imagery in decision tree classifiers', *International Journal of Remote Sensing*, 19(16), 3141-3168.
- Defries, R. S. and Townshend, J. R. G. (1994) 'NDVI-derived land cover classifications at a global scale', *International Journal of Remote Sensing*, 15(17), 3567-3586.

- Dixon, R. K., Solomon, A. M., Brown, S., Houghton, R. A., Trexler, M. C. and Wisniewski, J. (1994) 'Carbon Pools and Flux of Global Forest Ecosystems', *Science*, 263(5144), 185-190.
- Dlugokencky, E. and Tans, P. (2014) 'Trends in atmospheric carbon dioxide, National Oceanic & Atmospheric Administration, Earth System Research Laboratory (NOAA/ESRL)', [online], available: <http://www.esrl.noaa.gov/gmd/ccgg/trends> [accessed 01 February 2016].
- Dobson, M., Ulaby, F., Brunfeldt, D. and Held, D. (1986) 'External calibration of SIR-B imagery with area-extended and point targets', *I.E.E.E. Transactions on Geoscience and Remote Sensing*, 24(4), 453-461.
- Dobson, M. C., Ulaby, F. T., Le Toan, T., Beaudoin, A. and Kasischke, E. S. (1992) 'Dependence of radar backscatter on conifer forest biomass', *I.E.E.E. Transactions on Geoscience and Remote Sensing*, 30, 412-415.
- Dong, J., Kaufmann, R. K., Myneni, R. B., Tucker, C. J., Kauppi, P. E., Liski, J., Buermann, W., Alexeyev, V. and Hughes, M. K. (2003) 'Remote sensing estimates of boreal and temperate forest woody biomass: carbon pools, sources, and sinks', *Remote Sensing of Environment*, 84(3), 393-410.
- Dong, J., Xiao, X., Sheldon, S., Biradar, C. M., Duong, N. D. and Hazarika, M. (2012) 'A comparison of forest cover maps in Mainland Southeast Asia from multiple sources: PALSAR, MERIS, MODIS and FRA', *Remote Sensing of Environment*, 127, 60-73.
- Drezet, P. M. L. and Quegan, S. (2007) 'Satellite-based radar mapping of British forest age and Net Ecosystem Exchange using ERS tandem coherence', *Forest Ecology and Management*, 238(1-3), 65-80.
- Du, J., Shi, J. and Sun, R. (2010) 'The development of HJ SAR soil moisture retrieval algorithm', *International Journal of Remote Sensing*, 31(14), 3691-3705.
- Durden, S. L., Zyl, J. J. V. and Zebker, H. A. (1989) 'Modeling and observation of the radar polarization signature of forested areas', *I.E.E.E. Transactions on Geoscience and Remote Sensing*, 27, 290-301.
- Eliason, E. M. and McEwen, A. S. (1990) 'Adaptive box filters for removal of random noise from digital images', *Photogrammetric Engineering and Remote Sensing*, 56, 453-458.

- Elizavetin, I. V. and Paillou, P. (1997) 'Study of surface scattering properties in S-band using radar image simulation', *Radar*, 811-815.
- Englhart, S., Keuck, V. and Siegert, F. (2011) 'Aboveground biomass retrieval in tropical forests — The potential of combined X- and L-band SAR data use', *Remote Sensing of Environment*, 115(5), 1260-1271.
- Environmental, C. N. (2014) 'data citation code: ECN:RN12/14', *Dataset accessed 2014-12-15 at <http://data.ecn.ac.uk>*
- FAO (2012a) *Global forest land-use change 1990-2005*. Rome: Food and Agriculture Organization of the United Nations.
- FAO (2012b) *Forest Resource Assessment (FRA) 2010*. Rome: Food and Agricultural Organization of the United Nations.
- Federici, S., Tubiello, F. N., Salvatore, M., Jacobs, H. and Schmidhuber, J. (2015) 'New estimates of CO₂ forest emissions and removals: 1990–2015', *Forest Ecology and Management*, 352, 89-98.
- Fenn, K. M., Malhi, Y., Morecroft, M., Lloyd, C. and Thomas, M. (2010a) 'Comprehensive description of the carbon cycle of an ancient temperate broadleaved woodland', *Biogeosciences Discuss.*, 7(3), 3735-3763.
- Fenn, K. M., Malhi, Y. and Morecroft, M. D. (2010b) 'Soil CO₂ efflux in a temperate deciduous forest: Environmental drivers and component contributions', *Soil Biology and Biochemistry*, 42(10), 1685-1693.
- Ferrazzoli, P., Paloscia, S., Pampaloni, P., Schiavon, G., Sigismondi, S. and Solimini, D. (1997) 'The potential of multifrequency polarimetric SAR in assessing agricultural and arboreous biomass', *I.E.E.E. Transactions on Geoscience and Remote Sensing*, 35(1), 5-17.
- Foley, J. A., DeFries, R., Asner, G. P., Barford, C., Bonan, G. B., Carpenter, S. R., Chapin, F. S., Coe, M. T., Daily, G. C., Gibbs, H. K., Helkowski, J. H., Holloway, T., Howard, E. A., Kucharik, C. J., Monfreda, C., Patz, J. A., Prentice, I. C., Ramankutty, N. and Snyder, P. K. (2005) 'Global Consequences of Land Use', *Science*, 309(5734), 570-574.
- Foley, J. A., Kutzbach, J. E., Coe, M. T. and Levis, S. (1994) 'Feedbacks between climate and boreal forests during the holocene epoch', *Nature*, 371, 52–54.

- Foody, G. M. (2002) 'Status of land cover classification accuracy assessment', *Remote Sensing of Environment*, 80(1), 185-201.
- Foody, G. M., McCulloch, M. B. and Yates, W. B. (1994) 'Crop classification from C-band polarimetric radar data', *International Journal of Remote Sensing*, 15(14), 2871-2885.
- Fransson, J. E. S., Walter, F. and Olsson, H. (1999) 'Identification of clear felled areas using SPOT P and Almaz-1 SAR data', *International Journal of Remote Sensing*, 20(18), 3583-3593.
- French, N. H. F., Kasischke, E. S., Bourgeau-Chavez, L. L. and Harrell, P. A. (1996) 'Sensitivity of ERS-1 SAR to variations in soil water in fire-disturbed boreal forest ecosystems', *International Journal of Remote Sensing*, 17(15), 3037-3053.
- Friedl, M. A., Sulla-Menashe, D., Tan, B., Schneider, A., Ramankutty, N., Sibley, A. and Huang, X. (2010) 'MODIS Collection 5 global land cover: Algorithm refinements and characterization of new datasets', *Remote Sensing of Environment*, 114(1), 168-182.
- Friedlingstein, P., Cox, P., Betts, R., Bopp, L., Von Bloh, W., Brovkin, V., Cadule, P., Doney, S., Eby, M., Fung, I., Bala, G., John, J., Jones, C., Joos, F., Kato, T., Kawamiya, M., Knorr, W., Lindsay, K., Matthews, H. D., Raddatz, T., Rayner, P., Reick, C., Roeckner, E., Schnitzler, K.-G., Schnur, R., Strassmann, K., Weaver, A. J., Yoshikawa, C. and Zeng, N. (2006) 'Climate–Carbon Cycle Feedback Analysis: Results from the C⁴MIP Model Intercomparison', *Journal of Climate*, 19, 3337–3353.
- Frost, V. S., Stiles, J. A., Shanmugan, K. S. and Holtzman, J. C. (1982) 'A model for radar images and its application to adaptive digital filtering of multiplicative noise', *IEEE Trans. Pattern Anal. Mach. Intell. PAMI-4*, 2, 157-166.
- Giri, C., Zhu, Z. and Reed, B. C. (2005) 'A comparative analysis of the Global Land Cover 2000 and MODIS land cover data sets', *Remote Sensing of Environment*, 94(1), 123-132.
- GOFC-GOLD (2010) 'SOURCEBOOK GOFC-GOLD Report Version COP16-1'.
- Groombridge, B. and Jenkins, M. D. (2002) *World Atlas of Biodiversity*, Berkeley: University of California Press, Berkeley.

- Grover, K., Quegan, S. and Freitas, C. D. (1999) 'Quantitative estimation of tropical forest cover by SAR', *I.E.E.E. Transactions on Geoscience and Remote Sensing*, 37, 479-490.
- Guida, R., Natale, A., Bird, R., Whittaker, P., Cohen, M. and Hall, D. (2012) 'Canopy classification with S-Band polarimetric SAR data', in *IEEE IGARSS*, 6535-6538.
- Hajnsek, I., Scheiber, R., Keller, M., Horn, R., Lee, S., Ulander, L. M. H., Gustavsson, A., Sandberg, G., Toan, T. L., Tebaldini, S., Guarnieri, A. M. and Rocca, F. (2009) *BioSAR 2008 technical assistance for the development of airborne SAR and geophysical measurements during the BioSAR 2008 Experiment: draft final report –BioSAR campaign*.
- Hajnsek, I., Scheiber, R., Ulander, L. M. H., Gustavsson, A., Sandberg, G., Tebaldini, S., Guarnieri, A. M., Rocca, F., Bombardini, F. and Pardini, M. (2008) *BioSAR 2007 technical assistance for the development of airborne SAR and geophysical measurements during the BioSAR 2007 experiment: final report without synthesis*.
- Hall, F. G., Bergen, K., Blair, J. B., Dubayah, R., Houghton, R. A., Hurtt, G. C., Kellndorfer, J. M., Lefsky, M., Ranson, J. K., Saatchi, S. S., Shugart, H. H. and Wickland, D. (2011) 'Characterizing 3D vegetation structure from space: Mission requirements', *Remote Sensing of Environment*, 115(11), 2753-2775.
- Hall, J. E., Kirby, K. J. and Whitbread, A. M. (2004) *National Vegetation Classification: Field guide to woodland*, Peterborough, UK: Joint Nature Conservation Committee.
- Hansen, M. C., Potapov, P. V., Moore, R., Hancher, M., Turubanova, S. A., Tyukavina, A., Thau, D., Stehman, S. V., Goetz, S. J., Loveland, T. R., Kommareddy, A., Egorov, A., Chini, L., Justice, C. O. and Townshend, J. R. G. (2013) 'High-resolution global maps of 21st-century forest cover change', *Science*, 342(6160), 850-3.
- Hansen, M. C., Potapov, P. V., Moore, R., Hancher, M., Turubanova, S. A., Tyukavina, A., Thau, D., Stehman, S. V., Goetz, S. J., Loveland, T. R., Kommareddy, A., Egorov, A., Chini, L., Justice, C. O. and Townshend, J. R. G. (2014) 'Global Forest Change 2000–2014', [online], available: http://earthenginepartners.appspot.com/science-2013-global-forest/download_v1.2.html [accessed 26 November 2015].
- Hansen, M. C., Stehman, S. V., Potapov, P. V., Loveland, T. R., Townshend, J. R. G., DeFries, R. S., Pittman, K. W., Arunarwati, B., Stolle, F., Steinger, M. K., Carroll, M. and DiMiceli, C. (2008) 'Humid tropical forest clearing from 2000 to

2005 quantified by using multitemporal and multiresolution remotely sensed data', *Proceedings of the National Academy of Sciences*, 105(27), 9439-9444.

- Harrell, P. A., Bourgeau-Chavez, L. L., Kasischke, E. S., French, N. H. F. and Christensen Jr, N. L. (1995) 'Sensitivity of ERS-1 and JERS-1 radar data to biomass and stand structure in Alaskan boreal forest', *Remote Sensing of Environment*, 54(3), 247-260.
- Harrell, P. A., Kasischke, E. S., Bourgeau-Chavez, L. L., Haney, E. M. and Christensen Jr, N. L. (1997) 'Evaluation of approaches to estimating aboveground biomass in Southern pine forests using SIR-C data', *Remote Sensing of Environment*, 59(2), 223-233.
- Herold, M., Mayaux, P., Woodcock, C. E., Baccini, A. and Schmullius, C. (2008) 'Some challenges in global land cover mapping: An assessment of agreement and accuracy in existing 1 km datasets', *Remote Sensing of Environment*, 112(5), 2538-2556.
- Herold, M., Woodcock, C. E., Antonio di, G., Mayaux, P., Belward, A. S., Latham, J. and Schmullius, C. C. (2006) 'A joint initiative for harmonization and validation of land cover datasets', *I.E.E.E. Transactions on Geoscience and Remote Sensing*, 44(7), 1719-1727.
- Hsu, C. C., Han, H. C., Shin, R. T., Kong, J. A., Beaudoin, A. and Le Toan, T. (1994) 'Radiative transfer theory for polarimetric remote sensing of pine forest at P band', *International Journal of Remote Sensing*, 15(14), 2943-2954.
- Hurt, G. C., Fisk, J., Thomas, R. Q., Dubayah, R., Moorcroft, P. R. and Shugart, H. H. (2010) 'Linking models and data on vegetation structure', *Journal of Geophysical Research: Biogeosciences*, 115(G2), n/a-n/a.
- Hyypä, J. and Hallikainen, M. (1993) 'A helicopter-borne eight-channel ranging scatterometer for remote sensing. II. Forest inventory', *IEEE Transactions on Geoscience and Remote Sensing*, 31(1), 170-179.
- Hyypä, J., Hyypä, H., Inkinen, M., Engdahl, M., Linko, S. and Zhu, Y. (2000) 'Accuracy comparison of various remote sensing data sources in the retrieval of forest stand attributes', *Forest Ecology and Management*, 128, 109-120.
- Hyypä, J., Pulliainen, J., Hallikainen, M. and Saatsi, A. (1997) 'Radar-derived standwise forest inventory', *IEEE Transactions on Geoscience and Remote Sensing*, 35(2), 392-404.

- Imhoff, M. L. (1995) 'Radar backscatter and biomass saturation: ramifications for global biomass inventory ', *I.E.E.E. Transactions on Geoscience and Remote Sensing*, 33, 511-518.
- Israelsson, H., Askne, J. and Sylvander, R. (1994) 'Potential of SAR for forest bole volume estimation', *International Journal of Remote Sensing*, 15(14), 2809-2826.
- Ivanov, A. Y. and Litovchenko, K. T. (1997) 'Oceanological results from the ALMAZ-1 mission an overview', *Proceedings of the IEEE International Geoscience and Remote Sensing*, 539-541.
- JapanAerospaceExplorationAgency (2014) 'New global 25m-resolution PALSAR-2/PALSAR mosaic and Global Forest / Non-forest Map ', [online], available: http://www.eorc.jaxa.jp/ALOS/en/palsar_fnf/fnf_index.htm [accessed 1 June 2015].
- Joos, F. and Spahni, R. (2008) 'Rates of change in natural and anthropogenic radiative forcing over the past 20,000 years', *Proceedings of the National Academy of Sciences*, 105(5), 1425-1430.
- Jung, M., Henkel, K., Herold, M. and Churkina, G. (2006) 'Exploiting synergies of global land cover products for carbon cycle modeling', *Remote Sensing of Environment*, 101(4), 534-553.
- Kalogirou, V., Ferrazzoli, P., Della Vecchia, A. and Fomelis, M. (2014) 'On the SAR Backscatter of Burned Forests: A Model-Based Study in C-Band, Over Burned Pine Canopies', *IEEE TRANSACTIONS ON GEOSCIENCE AND REMOTE SENSING*, 52(10), 6205-6215.
- Karam, M. A., Amar, F., Fung, A. K., Mougin, E., Lopes, A., Le Vine, D. M. and Beaudoin, A. (1995) 'A microwave polarimetric scattering model for forest canopies based on vector radiative transfer theory', *Remote Sensing of Environment*, 53, 16-30.
- Karam, M. A. and Fung, A. K. (1988) 'Electromagnetic scattering from a layer of finite length, randomly oriented, dielectric, circular cylinders over a rough interface with application to vegetation', *International Journal of Remote Sensing*, 9, 1109-1134.
- Karjalainen, M., Kankare, V., Vastaranta, M., Holopainen, M. and Hyypä, J. (2012) 'Prediction of plot-level forest variables using TerraSAR-X stereo SAR data', *Remote Sensing of Environment*, 117, 338-347.

- Kauppi, P. E., Mielikäinen, K. and Kuusela, K. (1992) 'Biomass and Carbon Budget of European Forests, 1971 to 1990', *Science*, 256(5053), 70-74.
- Kiage, L. M., Walker, N. D., Balasubramanian, S., Babin, A. and Barras, J. (2005) 'Applications of Radarsat-1 synthetic aperture radar imagery to assess hurricane-related flooding of coastal Louisiana', *International Journal of Remote Sensing*, 26(24), 5359-5380.
- Kim, D.-H., Sexton, J. O., Noojipady, P., Huang, C., Anand, A., Channan, S., Feng, M. and Townshend, J. R. G. (2014) 'Global, Landsat-based forest-cover change from 1990 to 2000', *Remote Sensing of Environment*, 155, 178-193.
- Kirby, K. J., Bazely, D. R., Goldberg, E. A., Hall, J. E., Isted, R., Perry, S. C. and Thomas, R. C. (2014) 'Changes in the tree and shrub layer of Wytham Woods (Southern England) 1974-2012: local and national trends compared', *Forestry*, 87(5), 663-673.
- Köhl, M., Magnussen, S. and Marchetti, M. (2006) *Sampling Methods, Remote Sensing and GIS Multiresource Forest Inventory*, Springer-Verlag Berlin Heidelberg New York ISBN-13 978-3-540-32571-0
- Kuplich, T. M., Freitas, C. C. and Soares, J. V. (2000) 'The study of ERS-1 SAR and Landsat TM synergism for land use classification', *International Journal of Remote Sensing*, 21(10), 2101-2111.
- Lang, M. W., Kasischke, E. S., Prince, S. D. and Pittman, K. W. (2008) 'Assessment of C-band synthetic aperture radar data for mapping and monitoring Coastal Plain forested wetlands in the Mid-Atlantic Region, U.S.A', *Remote Sensing of Environment*, 112(11), 4120-4130.
- Le Quéré, C., Peters, G. P., Andres, R. J., Andrew, R. M., Boden, T. A., Ciais, P., Friedlingstein, P., Houghton, R. A., Marland, G., Moriarty, R., Sitch, S., Tans, P., Arneeth, A., Arvanitis, A., Bakker, D. C. E., Bopp, L., Canadell, J. G., Chini, L. P., Doney, S. C., Harper, A., Harris, I., House, J. I., Jain, A. K., Jones, S. D., Kato, E., Keeling, R. F., Klein Goldewijk, K., Körtzinger, A., Koven, C., Lefèvre, N., Maignan, F., Omar, A., Ono, T., Park, G. H., Pfeil, B., Poulter, B., Raupach, M. R., Regnier, P., Rödenbeck, C., Saito, S., Schwinger, J., Segschneider, J., Stocker, B. D., Takahashi, T., Tilbrook, B., van Heuven, S., Viovy, N., Wanninkhof, R., Wiltshire, A. and Zaehle, S. (2014) 'Global carbon budget 2013', *Earth System Science Data*, 6(1), 235-263.

- Le Toan, T., Beaudoin, A., Riom, J. and Guyon, D. (1992) 'Relating Forest Biomass to SAR Data', *I.E.E.E. Transactions on Geoscience and Remote Sensing*, 30, 403-411.
- Le Toan, T., Quegan, S., Davidson, M. W. J., Balzter, H., Paillou, P., Papathanassiou, K., Plummer, S., Rocca, F., Saatchi, S., Shugart, H. and Ulander, L. (2011) 'The BIOMASS mission: Mapping global forest biomass to better understand the terrestrial carbon cycle', *Remote Sensing of Environment*, 115(11), 2850-2860.
- Lee, J. S. (1980) 'Digital image enhancement and noise filtering by use of local statistics', *IEEE Trans. Pattern Anal. Mach. Intell.*, vol. PAMI-2, 2, 165-168.
- Lefsky, M. A. and Cohen, W. B. (2003) 'Selection of remotely sensed data ' in Wulder, M. A., Franklin, S.E., ed. *Remote Sensing of Forest Environments: Concepts and Case Studies*, Boston: Kluwer Academic Publishers, 13–46.
- Lemoine, G. G., de Grandi, G. F. and Sieber, A. J. (1994) 'Polarimetric contrast classification of agricultural fields using MAESTRO 1 AIRSAR data', *International Journal of Remote Sensing*, 15(14), 2851-2869.
- Lewis, S. L., Lloyd, J., Sitch, S., Mitchard, E. T. A. and Laurance, W. F. (2009) 'Changing Ecology of Tropical Forests: Evidence and Drivers', *Annual Review of Ecology, Evolution, and Systematics*, 40(1), 529-549.
- Lewis, S. L., Malhi, Y. and Phillips, O. L. (2004) 'Fingerprinting the impacts of global change on tropical forests', *Philosophical Transactions of the Royal Society of London B: Biological Sciences*, 359(1443), 437-462.
- Liang, P., Moghaddam, M., Pierce, L. E. and Lucas, R. M. (2005) 'Radar Backscattering Model for Multilayer mixed-species forests', *I.E.E.E. Transactions on Geoscience and Remote Sensing*, 43, 2470-2383.
- Lin, H. C., J. Pei, Z. Zhang, S. Hu, X. (2009) 'Monitoring sugarcane growth using Envisat ASAR data', *I.E.E.E. Transactions on Geoscience and Remote Sensing*, 47, 2572-2580.
- Liski, J., Lehtonen, A., Palosuo, T., Peltoniemi, M., Eggers, T., Muukkonen, P. and Mäkipää, R. (2006) 'Carbon accumulation in Finland's forests 1922–2004 – an estimate obtained by combination of forest inventory data with modelling of biomass, litter and soil', *Ann. For. Sci.*, 63(7), 687-697.

- Liu, Y. Y., van Dijk, A. I. J. M., de Jeu, R. A. M., Canadell, J. G., McCabe, M. F., Evans, J. P. and Wang, G. (2015) 'Recent reversal in loss of global terrestrial biomass', *Nature Clim. Change*, 5(5), 470-474.
- Lopes, A., Touzi, R. and Nezry, E. (1990) 'Adaptive speckle filters and scene heterogeneity', *I.E.E.E. Transactions on Geoscience and Remote Sensing*, 28, 992-1000.
- Lopez-Sanchez, J. M., Ballester-Berman, J. D. and Fortuny-Guasch, J. (2006) 'Indoor Wide-Band Polarimetric Measurements on Maize Plants A Study of the Differential Extinction', *I.E.E.E. Transactions on Geoscience and Remote Sensing*, 44(4), 758-767.
- Lopez-Sanchez, J. M., Fortuny-Guasch, J., Cloude, S. R. and Sieber, A. J. (2000) 'Indoor Polarimetric Radar Measurements on Vegetation Samples at L, S, C and X band', *Journal of Electromagnetic Waves and Applications*, 14(2), 205-231.
- Loveland, T. R., Reed, B. C., Brown, J. F., Ohlen, D. O., Zhu, Z., Yang, L. and Merchant, J. W. (2000) 'Development of a global land cover characteristics database and IGBP DISCover from 1 km AVHRR data', *International Journal of Remote Sensing*, 21, 1303-1330.
- Lu, D. (2005) 'Aboveground biomass estimation using Landsat TM data in the Brazilian Amazon', *International Journal of Remote Sensing*, 26(12), 2509-2525.
- Lucas, R. M., Armston, J., Fairfax, R., Fensham, R., Accad, A., Carreiras, J., Kelley, J., Bunting, P., Clewley, D., Bray, S., Metcalfe, D., Dwyer, J., Bowen, M., Eyre, T., Laidlaw, M. and Shimada, M. (2010) 'An Evaluation of the ALOS PALSAR L-Band Backscatter -Above Ground Biomass Relationship Queensland, Australia: Impacts of Surface Moisture Condition and Vegetation Structure', *IEEE JOURNAL OF SELECTED TOPICS IN APPLIED EARTH OBSERVATIONS AND REMOTE SENSING*, 3(4), 576-593.
- Lucas, R. M., Clewley, D., Accad, A., Butler, D., Armston, J., Bowen, M., Bunting, P., Carreiras, J., Dwyer, J., Eyre, T., Kelly, A., McAlpine, C., Pollock, S. and Seabrook, L. (2014) 'Mapping forest growth and degradation stage in the Brigalow Belt Bioregion of Australia through integration of ALOS PALSAR and Landsat-derived foliage projective cover data', *Remote Sensing of Environment*, 155, 42-57.
- Lucas, R. M., Cronin, N., Moghaddam, M., Lee, A., Armston, J., Bunting, P. and Witte, C. (2006) 'Integration of radar and Landsat-derived foliage projected cover for woody regrowth mapping, Queensland, Australia', *Remote Sensing of Environment*, 100(3), 388-406.

- Lucht, W., Prentice, I. C., Myneni, R. B., Sitch, S., Friedlingstein, P., Cramer, W., Bousquet, P., Buermann, W. and Smith, B. (2002) 'Climatic Control of the High-Latitude Vegetation Greening Trend and Pinatubo Effect', *Science*, 296(5573), 1687-1689.
- Luyssaert, S., Schulze, E. D., Borner, A., Knohl, A., Hessenmoller, D., Law, B. E., Ciais, P. and Grace, J. (2008) 'Old-growth forests as global carbon sinks', *Nature*, 455(7210), 213-5.
- Lynch, J., Maslin, M., Balzter, H. and Sweeting, M. (2013) 'Choose satellites to monitor deforestation', *Nature*, 496, 293-294.
- Malhi, Y., Meir, P. and Brown, S. (2002) 'Forests carbon and climate change', *Philosophical Transactions of the Royal Society London A*, 360(360), 1567-1591.
- Malhi, Y. and Phillips, O. L. (2004) 'Tropical forests and global atmospheric change: a synthesis', *Philosophical Transactions of the Royal Society of London B: Biological Sciences*, 359(1443), 549-555.
- Malhi, Y., Wood, D., Baker, T. R., Wright, J., Phillips, O. L., Cochrane, T., Meir, P., Chave, J., Almeida, S., Arroyo, L., Higuchi, N., Killeen, T. J., Laurance, S. G., Laurance, W. F., Lewis, S. L., Monteagudo, A., Neill, D. A., Vargas, P. N., Pitman, N. C. A., Quesada, C. A., Salomão, R., Silva, J. N. M., Lezama, A. T., Terborgh, J., Martínez, R. V. and Vinceti, B. (2006) 'The regional variation of aboveground live biomass in old-growth Amazonian forests', *Glob Chang Biol*, 12(7), 1107-1138.
- Malingreau, J. P., de Grandi, G. F., Leysen, M., Mayaux, P. and Simard, M. (1997) *The ERS-1 Central Africa Mosaic: a new role for radar remote sensing in global studies of the tropical ecosystem*, translated by 1725-1727 vol.4.
- Margono, B. A., Turubanova, s., Zhuravleva, I., Potapov, P., Tyukavina, A., Baccini, A., Goetz, S. J. and Hansen, M. C. (2012) 'Mapping and monitoring deforestation and forest degradation in Sumatra (Indonesia) using Landsat time series data sets from 1990 to 2010', *Environmental Research Letters*, 7(3), 034010.
- Mather, P. M., Tso, B. and Koch, M. (1998) 'An evaluation of Landsat TM spectral data and SAR-derived textural information for lithological discrimination in the Red Sea Hills, Sudan', *International Journal of Remote Sensing*, 19(4), 587-604.

- Mayaux, P., Grandi, G. F. D., Rauste, Y., Simard, M. and Saatchi, S. (2002) 'Large-scale vegetation maps derived from the combined L-band GRFM and C-band CAMP wide area radar mosaics of Central Africa', *International Journal of Remote Sensing*, 23(7), 1261-1282.
- McDonald, K. C. and Ulaby, F. T. (1993) 'Radiative transfer modelling of discontinuous tree canopies at microwave frequencies', *International Journal of Remote Sensing*, 14, 2097-2128.
- MEA (2005) *Millennium Ecosystem Assessment, Ecosystems and Human Well-being: Synthesis*, Island Press, Washington, DC.
- Mermoz, S., Réjou-Méchain, M., Villard, L., Le Toan, T., Rossi, V. and Gourlet-Fleury, S. (2015) 'Decrease of L-band SAR backscatter with biomass of dense forests', *Remote Sensing of Environment*, 159, 307-317.
- Miles, L. and Kapos, V. (2008) 'Reducing Greenhouse Gas Emissions from Deforestation and Forest Degradation: Global Land-Use Implications', *Science*, 320(5882), 1454-1455.
- Mitchard, E. T. A., Feldpausch, T. R., Brienen, R. J. W., Lopez-Gonzalez, G., Monteagudo, A., Baker, T. R., Lewis, S. L., Lloyd, J., Quesada, C. A., Gloor, M., ter Steege, H., Meir, P., Alvarez, E., Araujo-Murakami, A., Aragão, L. E. O. C., Arroyo, L., Aymard, G., Banki, O., Bonal, D., Brown, S., Brown, F. I., Cerón, C. E., Chama Moscoso, V., Chave, J., Comiskey, J. A., Cornejo, F., Corrales Medina, M., Da Costa, L., Costa, F. R. C., Di Fiore, A., Domingues, T. F., Erwin, T. L., Frederickson, T., Higuchi, N., Honorio Coronado, E. N., Killeen, T. J., Laurance, W. F., Levis, C., Magnusson, W. E., Marimon, B. S., Marimon Junior, B. H., Mendoza Polo, I., Mishra, P., Nascimento, M. T., Neill, D., Núñez Vargas, M. P., Palacios, W. A., Parada, A., Pardo Molina, G., Peña-Claros, M., Pitman, N., Peres, C. A., Poorter, L., Prieto, A., Ramirez-Angulo, H., Restrepo Correa, Z., Roopsind, A., Roucoux, K. H., Rudas, A., Salomão, R. P., Schiatti, J., Silveira, M., de Souza, P. F., Steininger, M. K., Stropp, J., Terborgh, J., Thomas, R., Toledo, M., Torres-Lezama, A., van Andel, T. R., van der Heijden, G. M. F., Vieira, I. C. G., Vieira, S., Vilanova-Torre, E., Vos, V. A., Wang, O., Zartman, C. E., Malhi, Y. and Phillips, O. L. (2014) 'Markedly divergent estimates of Amazon forest carbon density from ground plots and satellites', *Global Ecology and Biogeography*, 23(8), 935-946.
- Mitchard, E. T. A., Saatchi, S. S., Baccini, A., Asner, G. P., Goetz, S. J., Harris, N. L. and Brown, S. (2013) 'Uncertainty in the spatial distribution of tropical forest biomass: a comparison of pan-tropical maps', *Carbon Balance Manag*, 8(1), 10.
- Mitchard, E. T. A., Saatchi, S. S., White, L. J. T., Abernethy, K. A., Jeffery, K. J., Lewis, S. L., Collins, M., Lefsky, M. A., Leal, M. E., Woodhouse, I. H. and

- Meir, P. (2012) 'Mapping tropical forest biomass with radar and spaceborne LiDAR in Lopé National Park, Gabon: overcoming problems of high biomass and persistent cloud', *Biogeosciences*, 9(1), 179-191.
- Mollicone, D., Freibauer, A., Schulze, E. D., Braatz, S., Grassi, G. and Federici, S. (2007) 'Elements for the expected mechanisms on 'reduced emissions from deforestation and degradation, REDD' under UNFCCC', *Environmental Research Letters*, 2(4), 045024.
- Morecroft, M. D., Stokes, V. J., Taylor, M. E. and Morison, J. I. L. (2008) 'Effects of climate and management history on the distribution and growth of sycamore (*Acer pseudoplatanus* L.) in a southern British woodland in comparison to native competitors', *Forestry*, 81(1), 59-74.
- Morecroft, M. D., Taylor, M. E. and Oliver, H. R. (1998) 'Air and soil microclimates of deciduous woodland compared to an open site', *Agricultural and Forest Meteorology*, 90(1-2), 141-156.
- Morel, A. C., Saatchi, S. S., Malhi, Y., Berry, N. J., Banin, L., Burslem, D., Nilus, R. and Ong, R. C. (2011) 'Estimating aboveground biomass in forest and oil palm plantation in Sabah, Malaysian Borneo using ALOS PALSAR data', *Forest Ecology and Management*, 262(9), 1786-1798.
- Myneni, R. B., Dong, J., Tucker, C. J., Kaufmann, R. K., Kauppi, P. E., Liski, J., Zhou, L., Alexeyev, V. and Hughes, M. K. (2001) 'A large carbon sink in the woody biomass of Northern forests', *Proceedings of the National Academy of Sciences*, 98(26), 14784-14789.
- Nabuurs, G. J., Päivinen, R., Sikkema, R. and Mohren, G. M. J. (1997) 'The role of European forests in the global carbon cycle—A review', *Biomass and Bioenergy*, 13(6), 345-358.
- Natale, A., Guida, R., Bird, R., Whittaker, P., Hall, D. and Cohen, M. (2012) 'Validation of S-band data performance for future space borne SAR missions', in *European Conference on Synthetic Aperture Radar, Nurnberg, Germany*, 75-78.
- Nemani, R. R., Keeling, C. D., Hashimoto, H., Jolly, W. M., Piper, S. C., Tucker, C. J., Myneni, R. B. and Running, S. W. (2003) 'Climate-Driven Increases in Global Terrestrial Net Primary Production from 1982 to 1999', *Science*, 300(5625), 1560-1563.
- Okuda, T., Suzuki, M., Adachi, N., Quah, E. S., Hussein, N. A. and Manokaran, N. (2003) 'Effect of selective logging on canopy and stand structure and tree

species composition in a lowland dipterocarp forest in peninsular Malaysia', *Forest Ecology and Management*, 175(1–3), 297-320.

Olsson, H., Naslund, B., Hagner, O. and Sylvander, R. (1991) 'Early experience on the use of satellite borne S-band SAR over Swedish forests', in *Workshop on Remote Sensing for Forestry Applications*, Copenhagen, Denmark, 13-15 November 1991, Commission of the European Communities JRC ISPRA, 223-230.

Osazuwa-Peters, O. L., Chapman, C. A. and Zanne, A. E. (2015) 'Selective logging: does the imprint remain on tree structure and composition after 45 years?', *Conservation Physiology*, 3(1), 1-12, doi:10.1093/conphys/cov012.

OSCAR (2015) 'Observing Systems Capability Analysis and Review Tool', [online], available: <http://www.wmo-sat.info/oscar/satellites/view/171> [accessed 01/10/2015].

Pagani, M., Caldeira, K., Berner, R. and Beerling, D. J. (2009) 'The role of terrestrial plants in limiting atmospheric CO₂ decline over the past 24 million years', *Nature*, 460(7251), 85-8.

Pan, Y., Birdsey, R. A., Phillips, O. L. and Jackson, R. B. (2013) 'The Structure, Distribution, and Biomass of the World's Forests', *Annual Review of Ecology, Evolution, and Systematics*, 44(1), 593-622.

Pantze, A., Santoro, M. and Fransson, J. E. S. (2014) 'Change detection of boreal forest using bi-temporal ALOS PALSAR backscatter data', *Remote Sensing of Environment*, 155, 120-128.

Perko, R., Raggam, H., Deutscher, J., Gutjahr, K. and Schardt, M. (2011) 'Forest Assessment Using High Resolution SAR Data in X-Band', *Remote Sensing*, 3(12), 792-815.

Peterken, G. F. and Game, M. (1984) 'Historical factors affecting the number and distribution of vascular plant species in the woodlands of Central Lincolnshire', *Journal of Ecology*, 72, 155-182.

Peylin, P., Bousquet, P., Le Quéré, C., Sitch, S., Friedlingstein, P., McKinley, G., Gruber, N., Rayner, P. and Ciais, P. (2005) 'Multiple constraints on regional CO₂ flux variations over land and oceans', *Global Biogeochemical Cycles*, 19(1), GB1011.

- Phillips, O. L. and Lewis, S. L. (2014) 'Recent changes in tropical forest biomass and dynamics' in Coomes, D. A., Burslem, D.F.R., Simonson, P.W.D., ed. *Forests and Global Change*, Cambridge University Press.
- Piao, S., Sitch, S., Ciais, P., Friedlingstein, P., Peylin, P., Wang, X., Ahlström, A., Anav, A., Canadell, J. G., Cong, N., Huntingford, C., Jung, M., Levis, S., Levy, P. E., Li, J., Lin, X., Lomas, M. R., Lu, M., Luo, Y., Ma, Y., Myneni, R. B., Poulter, B., Sun, Z., Wang, T., Viovy, N., Zaehle, S. and Zeng, N. (2013) 'Evaluation of terrestrial carbon cycle models for their response to climate variability and to CO₂ trends', *Glob Chang Biol*, 19(7), 2117-2132.
- Piao, S., Tan, J., Chen, A., Fu, Y. H., Ciais, P., Liu, Q., Janssens, I. A., Vicca, S., Zeng, Z., Jeong, S.-J., Li, Y., Myneni, R. B., Peng, S., Shen, M. and Penuelas, J. (2015) 'Leaf onset in the northern hemisphere triggered by daytime temperature', *Nature Communication*, 6.
- Podest, E. and Saatchi, S. (2002) 'Application of multiscale texture in classifying JERS-1 radar data over tropical vegetation', *International Journal of Remote Sensing*, 23, 1487-1506.
- Potapov, P., Hansen, M. C., Stehman, S. V., Loveland, T. R. and Pittman, K. (2008a) 'Combining MODIS and Landsat imagery to estimate and map boreal forest cover loss', *Remote Sensing of Environment*, 112(9), 3708-3719.
- Potapov, P., Yaroshenko, A., Turubanova, S., Dubinin, M., Laestadius, Thies, C., Aksenov, D., Egorov, A., Yesipova, Y., Glushkov, I., Karpachevskiy, M., Kostikova, A., Manisha, A., Tsybikova, E. and Zhuravleva, I. (2008b) 'Mapping the world's intact forest landscapes by remote sensing', *Ecology and Society*, 13(2), 51.
- Prentice, I. C., Farquhar, G. D. and Fasham, M. J. R. (2001) 'The carbon cycle and atmospheric carbon dioxide. In: Climate Change 2001: The Scientific Basis (eds Houghton JT, Ding Y, Griggs DJ, Noguera M, Van Der Linden PJ, Xiaosu D). ', *Cambridge University Press, Cambridge*.
- Putz, F. E. and Redford, K. H. (2010) 'The importance of defining 'Forest': Tropical forest degradation, deforestation, long-term phase shifts, and further transitions', *Biotropica*, 42, 10-20.
- Qin, Y., Xiao, X., Dong, J., Zhang, G., Shimada, M., Liu, J., Li, C., Kou, W. and Moore III, B. (2015) 'Forest cover maps of China in 2010 from multiple approaches and data sources: PALSAR, Landsat, MODIS, FRA, and NFI', *ISPRS Journal of Photogrammetry and Remote Sensing*, 109, 1-16.

- Qiu, F., Berglund, J., Jensen, J. R., Thakkar, P. and Ren, D. (2004) 'Speckle noise reduction in SAR imagery using a local adaptive Median filter ', *GIScience and Remote Sensing*, 41 244-266.
- Rahman, M. M., Moran, M. S., Thoma, D. P., Bryant, R., Holifield Collins, C. D., Jackson, T., Orr, B. J. and Tischler, M. (2008) 'Mapping surface roughness and soil moisture using multi-angle radar imagery without ancillary data', *Remote Sensing of Environment*, 112(2), 391-402.
- Ranson, K. J. and Sun, G. (1997) 'An evaluation of AIRSAR and SIR-C/X-SAR images for mapping northern forest attributes in Maine, USA', *Remote Sensing of Environment*, 59(2), 203-222.
- Rauste, Y. (2005) 'Multi-temporal JERS SAR data in boreal forest biomass mapping', *Remote Sensing of Environment*, 97(2), 263-275.
- Rauste, Y., Hame, T., Pulliainen, J., Heiska, K. and Hallikainen, M. (1994) 'Radar-based forest biomass estimation', *International Journal of Remote Sensing*, 15(14), 2797-2808.
- Reiche, J., Souza, C. M., Hoekman, D. H., Verbesselt, J., Persaud, H. and Herold, M. (2013) 'Feature Level Fusion of Multi-Temporal ALOS PALSAR and Landsat Data for Mapping and Monitoring of Tropical Deforestation and Forest Degradation', *IEEE JOURNAL OF SELECTED TOPICS IN APPLIED EARTH OBSERVATIONS AND REMOTE SENSING*, 6(5), 2159-2173.
- Rignot, E. J., Zimmermann, R. and van Zyl, J. J. (1995) 'Spaceborne Applications of P Band Imaging Radars for Measuring Forest Biomass', *I.E.E.E. Transactions on Geoscience and Remote Sensing*, 33, 1162-1169.
- Rosenqvist, Å. (1996) 'Evaluation of JERS-1, ERS-1 and Almaz SAR backscatter for rubber and oil palm stands in West Malaysia', *International Journal of Remote Sensing* 17, 3219-3231.
- Rosenqvist, Å., Milne, A. K., Lucas, R., Imhoff, M. and Dobson, C. (2003) 'A review of remote sensing technology in support of the Kyoto Protocol', *Environmental Science & Policy*, 6(5), 441-455.
- Rosenqvist, Å., Shimada, M., Chapman, B., Freeman, A., De Grandi, G., Saatchi, S. and Rauste, Y. (2000) 'The Global Rain Forest Mapping project - A review', *International Journal of Remote Sensing*, 21(6-7), 1375-1387.

- Rosenqvist, Å., Shimada, M., Chapman, B., McDonald, K., De Grandi, G., Jonsson, H., Williams, C., Rauste, Y., Nilsson, M., Sango, D. and Matsumoto, M. (2004) *An overview of the JERS-1 SAR Global Boreal Forest Mapping (GBFM) project*, translated by 1033-1036 vol.2.
- Rosenqvist, Å., Shimada, M. and Milne, A. K. (2007) 'The ALOS Kyoto & Carbon Initiative', in *IEEE International Geoscience and Remote Sensing Symposium, 2007*, 3614-3617.
- Ryan, C. M., Hill, T., Woollen, E., Ghee, C., Mitchard, E., Cassells, G., Grace, J., Woodhouse, I. H. and Williams, M. (2012) 'Quantifying small-scale deforestation and forest degradation in African woodlands using radar imagery', *Glob Chang Biol*, 18(1), 243-257.
- Saatchi, S. S., Harris, N. L., Brown, S., Lefsky, M., Mitchard, E. T., Salas, W., Zutta, B. R., Buermann, W., Lewis, S. L., Hagen, S., Petrova, S., White, L., Silman, M. and Morel, A. (2011a) 'Benchmark map of forest carbon stocks in tropical regions across three continents', *Proc Natl Acad Sci U S A*, 108(24), 9899-904.
- Saatchi, S. S., Houghton, R. A., Dos Santos Alvalá, R. C., Soares, J. V. and Yu, Y. (2007) 'Distribution of aboveground live biomass in the Amazon basin', *Glob Chang Biol*, 13(4), 816-837.
- Saatchi, S. S., Marlier, M., Chazdon, R. L., Clark, D. B. and Russell, A. E. (2011b) 'Impact of spatial variability of tropical forest structure on radar estimation of aboveground biomass', *Remote Sensing of Environment*, 115(11), 2836-2849.
- Saatchi, S. S., Mascaro, J., Xu, L., Keller, M., Yang, Y., Duffy, P., Espírito-Santo, F., Baccini, A., Chambers, J. Q. and Schimel, D. (2015) 'Seeing the forest beyond the trees', *Global Ecology and Biogeography*, 24(5), 606-610.
- Saatchi, S. S., Nelson, B., Podest, E. and Holt, J. (2000) 'Mapping land cover types in the Amazon Basin using 1 km JERS-1 mosaic', *International Journal of Remote Sensing*, 21(6-7), 1201-1234.
- Saatchi, S. S., Soares, J. V. and Alves, D. S. (1997) 'Mapping deforestation and land use in Amazon rainforest by using SIR-C imagery', *Remote Sensing of Environment*, 59, 191-202.
- Sader, S. A. (1987) 'Forest Biomass, Canopy Structure, and Species Composition Relationships with Multipolarization L-Band Synthetic Aperture Radar Data', *Photogrammetric Engineering and Remote Sensing*, Vol. 53 (No.2,), 193-202.

- Sandberg, G., Ulander, L. M. H., Fransson, J. E. S., Holmgren, J. and Le Toan, T. (2011) 'L- and P-band backscatter intensity for biomass retrieval in hemiboreal forest', *Remote Sensing of Environment*, 115 2874–2886.
- Santoro, M., Beaudoin, A., Beer, C., Cartus, O., Fransson, J. E. S., Hall, R. J., Pathe, C., Schmullius, C., Schepaschenko, D., Shvidenko, A., Thurner, M. and Wegmüller, U. (2015) 'Forest growing stock volume of the northern hemisphere: Spatially explicit estimates for 2010 derived from Envisat ASAR', *Remote Sensing of Environment*, 168, 316-334.
- Santoro, M., Beer, C., Cartus, O., Schmullius, C., Shvidenko, A., McCallum, I., Wegmüller, U. and Wiesmann, A. (2011) 'Retrieval of growing stock volume in boreal forest using hyper-temporal series of Envisat ASAR ScanSAR backscatter measurements', *Remote Sensing of Environment*, 115(2), 490-507.
- SCBD (2001) *Secretariat of the Convention on Biological Diversity. Assessment, Conservation and Sustainable Use of Forest Biodiversity.* , Montreal, SCBD.
- Schlund, M., von Poncet, F., Hoekman, D. H., Kuntz, S. and Schmullius, C. (2014) 'Importance of bistatic SAR features from TanDEM-X for forest mapping and monitoring', *Remote Sensing of Environment*, 151, 16-26.
- Sheldon, S., Xiao, X. and Biradar, C. M. (2012) 'Mapping evergreen forests in the Brazilian Amazon using MODIS and PALSAR 500-m mosaic imagery', *ISPRS Journal of Photogrammetry and Remote Sensing*, 74, 34-40.
- Shi, J., Wang, J., Hsu, A. Y., O'Neill, P. E. and Engman, E. T. (1997) 'Estimation of bare surface soil moisture and surface roughness parameter using L-band SAR image data', *IEEE TRANSACTIONS ON GEOSCIENCE AND REMOTE SENSING*, 35(5), 1254-1266.
- Shimabukuro, Y. E., Almeida-Filho, R., Kuplich, T. M. and de Freitas, R. M. (2007) 'Quantifying optical and SAR image relationships for tropical landscape features in the Amazônia', *International Journal of Remote Sensing*, 28(17), 3831-3840.
- Shimada, M., Itoh, T., Motohka, T., Watanabe, M., Shiraishi, T., Thapa, R. and Lucas, R. (2014) 'New global forest/non-forest maps from ALOS PALSAR data (2007–2010)', *Remote Sensing of Environment*.
- Shupe, S. M. and Marsh, S. E. (2004) 'Cover- and density-based vegetation classifications of the Sonoran Desert using Landsat TM and ERS-1 SAR imagery', *Remote Sensing of Environment*, 93(1–2), 131-149.

- Shvidenko, A., Barber, C. V. and Persson, R. (2005) 'Forests and woodland systems. Chapter 21' in Hassan, R., Scholes, R. and Ahs, N., eds., *Ecosystems and human well-being: current state and trends*, Washington: Island Press, 585-621.
- Sieber, A. J. and Noack, W. (1986) 'Results of an airborne SAR experiment over a SIR-B test Site in Germany', *ESA Journal*, 10, 291-310
- Siegert, F. and Ruecker, G. (2000) 'Use of multitemporal ERS-2 SAR images for identification of burned scars in south-east Asian tropical rainforest', *International Journal of Remote Sensing*, 21(4), 831-837.
- Simard, M., Grandi, G. D., Saatchi, S. and Mayaux, P. (2002) 'Mapping tropical coastal vegetation using JERS-1 and ERS-1 radar data with a decision tree classifier', *International Journal of Remote Sensing*, 23(7), 1461-1474.
- Simard, M., Saatchi, S. S. and De Grandi, G. D. (2000) 'The Use of Decision Tree and Multiscale Texture for Classification of JERS-1 SAR Data over Tropical Forest', *I.E.E.E. Transactions on Geoscience and Remote Sensing*, 38(5), 2310-2321.
- Sitaula, B. K., Sankhayan, P. L., Bajracharya, R. M. and Singh, B. R. (2005) 'A systems analysis of soil and forest degradation in a mid-hill watershed of Nepal using a bio-economic model', *Land Degradation & Development*, 16(5), 435-446.
- Sitch, S., Friedlingstein, P., Gruber, N., Jones, S. D., Murray-Tortarolo, G., Ahlström, A., Doney, S. C., Graven, H., Heinze, C., Huntingford, C., Levis, S., Levy, P. E., Lomas, M., Poulter, B., Viovy, N., Zaehle, S., Zeng, N., Arneth, A., Bonan, G., Bopp, L., Canadell, J. G., Chevallier, F., Ciais, P., Ellis, R., Gloor, M., Peylin, P., Piao, S., Le Quéré, C., Smith, B., Zhu, Z. and Myneni, R. (2013) 'Trends and drivers of regional sources and sinks of carbon dioxide over the past two decades', *Biogeosciences Discuss.*, 10(12), 20113-20177.
- Slik, J. W. F., Verburg, R. W. and Keßler, P. J. A. (2002) 'Effects of fire and selective logging on the tree species composition of lowland dipterocarp forest in East Kalimantan, Indonesia', *Biodiversity & Conservation*, 11(1), 85-98.
- Soja, M. J., Sandberg, G. and Ulander, L. M. H. (2013) 'Regression-Based Retrieval of Boreal Forest Biomass in Sloping Terrain Using P-Band SAR Backscatter Intensity Data ', *I.E.E.E. Transactions on Geoscience and Remote Sensing*, 51, 2646-2665.
- Souza Jr, C. M., Roberts, D. A. and Cochrane, M. A. (2005) 'Combining spectral and spatial information to map canopy damage from selective logging and forest fires', *Remote Sensing of Environment*, 98(2-3), 329-343.

- Steininger, M. K. (2000) 'Satellite estimation of tropical secondary forest above-ground biomass: Data from Brazil and Bolivia', *International Journal of Remote Sensing*, 21, 1139–1157.
- Sun, G. and Ranson, K. J. (1995) 'A three-dimensional radar backscatter model of forest canopies', *I.E.E.E. Transactions on Geoscience and Remote Sensing*, 33 372-382.
- Sun, G., Simonett, D. S. and Strahler, A. H. (1991) 'A radar backscattering model for discontinuous coniferous forests', *I.E.E.E. Transactions on Geoscience and Remote Sensing*, 29.
- Sun, Q., Zhang, F., Shao, Y., Liu, L., Wang, G., Bian, Z. and Li, K. (2012) 'S-band backscattering analysis of wheat using tower-based scatterometer', in *IEEE IGARSS*, 4621- 4624.
- Suzuki, R., Kim, Y. and Ishii, R. (2013) 'Sensitivity of the backscatter intensity of ALOS/PALSAR to the above-ground biomass and other biophysical parameters of boreal forest in Alaska', *Polar Science*, 7(2), 100-112.
- Sykes, J. M. and Lane, A. M. J. (1996) *The United Kingdom Environmental Change Network: Protocols for Standard Measurements at Terrestrial Sites*, The Stationery Office, London.
- Takeuchi, S., Suga, Y., Oguro, Y. and Konishi, T. (2000) 'Monitoring of new plantation development in tropical rain forests using JERS-1 SAR data', *Advances in Space Research*, 26(7), 1151-1154.
- Tanase, M. A., Santoro, M., de la Riva, J., Perez-Cabello, F. and Le Toan, T. (2010) 'Sensitivity of X-, C-, and L-Band SAR Backscatter to Burn Severity in Mediterranean Pine Forests', *I.E.E.E. Transactions on Geoscience and Remote Sensing*, 48(10), 3663-3675.
- Tansey, K. J., Luckman, A. J., Skinner, L., Balzter, H., Strozzi, T. and Wagner, W. (2004) 'Classification of forest volume resources using ERS tandem coherence and JERS backscatter data', *International Journal of Remote Sensing*, 25(4), 751-768.
- Thapa, R. B., Itoh, T., Shimada, M., Watanabe, M., Takeshi, M. and Shiraishi, T. (2014) 'Evaluation of ALOS PALSAR sensitivity for characterizing natural forest cover in wider tropical areas', *Remote Sensing of Environment*, 155, 32-41.

- Thiel, C., Drezet, P., Weise, C., Quegan, S. and Schmullius, C. (2006) 'Radar remote sensing for the delineation of forest cover maps and the detection of deforestation', *Forestry*, 79(5), 589-597.
- Townshend, J. R., Justice, C. O., Li, W., Gurney, C. and McManus, J. (1991) 'Global land cover classification by remote sensing: present capabilities and future possibilities', *Remote Sensing of Environment*, 35(2), 243-255.
- Trisasonkho, B. H. (2010) 'The Use of Polarimetric SAR Data for Forest Disturbance Monitoring', *Sensing and Imaging: An International Journal*, 11(1), 1-13.
- Tucker, C. J., Slayback, D. A., Pinzon, J. E., Los, S. O., Myneni, R. B. and Taylor, M. G. (2001) 'Higher northern latitude normalized difference vegetation index and growing season trends from 1982 to 1999', *International Journal of Biometeorology*, 45(4), 184-190.
- Ulaby, F. T., McDonald, K., Sarabandi, K. and Dobson, M. C. (1988a) 'Michigan microwave canopy scattering model', *Proceedings of IGARSS 88 Symposium, Winburgh, Scotland, Re\$ ESA SP-284 (IEEE 88CH24W-6)*.
- Ulaby, F. T., Moore, R. K. and Fung, A. K. (1986) 'Microwave Remote Sensing: Active and Passive, Vol 3: From the Theory to Applications. Artech House, Norwood, MA, USA', 1-2162.
- Ulaby, F. T., Sarabandi, K., McDonald, K., Whitt, M. and Dobson, M. C. (1988b) *Michigan microwave canopy scattering model (MIMICS). University of Michigan Radiation Laboratory, Report 022486-T-1*.
- Ulaby, F. T., Sarabandi, K., McDonald, K., Whitt, M. and Dobson, M. C. (1990) 'Michigan microwave canopy scattering model', *International Journal of Remote Sensing*, 11(7), 1223-1253.
- Ulander, L. M. H., Gustavsson, A., Flood, B., Murdin, D., Dubois-Fernandez, P., Depuis, X., Sandberg, G., Soja, M. J., Eriksson, L. E. B., Fransson, J. E. S., Holmgren, J. and Wallerman, J. (2011) *BioSAR 2010 technical assistance for the development of airborne SAR and geophysical measurements during the BioSAR 2010 experiment: final report*.
- UNEP, FAO and UNFF (2009) *Vital forest graphics*.
- UNFCCC (2008) *Report on the workshop on methodological issues relating to reducing emissions from deforestation and forest degradation in developing countries.*, FCCC/SBSTA/2008/11, FCCC/SBSTA/2008/11.

- Valentini, R., Matteucci, G., Dolman, A. J., Schulze, E. D., Rebmann, C., Moors, E. J., Granier, A., Gross, P., Jensen, N. O., Pilegaard, K., Lindroth, A., Grelle, A., Bernhofer, C., Grunwald, T., Aubinet, M., Ceulemans, R., Kowalski, A. S., Vesala, T., Rannik, U., Berbigier, P., Loustau, D., Gumundsson, J., Thorgeirsson, H., Ibrom, A., Morgenstern, K., Clement, R., Moncrieff, J., Montagnani, L., Minerbi, S. and Jarvis, P. G. (2000) 'Respiration as the main determinant of carbon balance in European forests', *Nature*, 404(6780), 861-865.
- van Beijma, S., Comber, A. and Lamb, A. (2014) 'Random forest classification of salt marsh vegetation habitats using quad-polarimetric airborne SAR, elevation and optical RS data', *Remote Sensing of Environment*, 149, 118-129.
- van der Sanden, J. J. and Hoekman, D. H. (1999) 'Potential of Airborne Radar To Support the Assessment of Land Cover in a Tropical Rain Forest Environment', *Remote Sensing of Environment*, 68(1), 26-40.
- van Lierop, P., Lindquist, E., Sathyapala, S. and Franceschini, G. (2015) 'Global forest area disturbance from fire, insect pests, diseases and severe weather events', *Forest Ecology and Management*, 352, 78-88.
- Verolme, H. J. H. and Moussa, J. (1999) *Addressing the Underlying Causes of Deforestation and Forest Degradation - Case Studies, Analysis and Policy Recommendations. Biodiversity Action Network, Washington, DC, USA.*
- Wagner, W., Luckman, A., Vietmeier, J., Tansey, K. J., Balzter, H., Schmullius, C., Davidson, M. W. J., Gaveau, D., Gluck, M., Le Toan, T., Quegan, S., Shvidenko, A., Wiesmann, A. and Yu, J. J. (2003) 'Large-scale mapping of boreal forest in SIBERIA using ERS tandem coherence and JERS backscatter data', *Remote Sensing of Environment*, 85(2), 125-144.
- Wang, Y., Davis, F. W. and Melack, J. M. (1993a) 'Simulated and Observed Backscatter at P-, L-, and C-Bands from Ponderosa Pine Stands', *I.E.E.E. Transactions on Geoscience and Remote Sensing*, 31, 871-879.
- Wang, Y., Day, J. and Sun, G. (1993b) 'Santa Barbara microwave backscattering model for woodlands', *International Journal of Remote Sensing*, 14(8), 1477-1493.
- Wang, Y. and Imhoff, M. L. (1993) 'Simulated and observed L-HH radar backscatter from tropical mangrove forests', *International Journal of Remote Sensing*, 14(15), 2819-2828.
- Whitt, M. W. and Ulaby, F. T. (1994) 'Radar response of periodic vegetation canopies', *International Journal of Remote Sensing*, 15, 1813-1848.

- Willcock, S., Phillips, O. L., Platts, P. J., Balmford, A., Burgess, N. D., Lovett, J. C., Ahrends, A., Bayliss, J., Doggart, N., Doody, K., Fanning, E., Green, J., Hall, J. E., Howell, K. L., Marchant, R., Marshall, A. R., Mbilinyi, B., Munishi, P. K. T., Owen, N., Swetnam, R. D., Topp-Jorgensen, E. J. and Lewis, S. L. (2012) 'Towards Regional, Error-Bounded Landscape Carbon Storage Estimates for Data-Deficient Areas of the World', *PLoS ONE*, 7(9), e44795.
- Woodhouse, I. H. (2006a) *Introduction to Microwave Remote Sensing*, Taylor & Francis, A CRC Press Book, 6000 Broken Sound Parkway NW, Suite 300, Boca Raton, FL 33487-2742.
- Woodhouse, I. H. (2006b) 'Predicting backscatter-biomass and height-biomass trends using a macroecology model', *I.E.E.E. Transactions on Geoscience and Remote Sensing*, 44, 871-877.
- Woodhouse, I. H., Marino, A. and Cameron, I. (2011) 'A standard index of spatial resolution for distributed targets in synthetic aperture radar imagery', *International Journal of Remote Sensing*, 32(23), 7929-7938.
- Woodhouse, I. H., Mitchard, E. T. A., Brolly, M., Maniatis, D. and Ryan, C. M. (2012) 'Radar backscatter is not a 'direct measure' of forest biomass', *Nature Climate Change*, 2(8), 556-557.
- Wright, S. J. (2005) 'Tropical forests in a changing environment', *Trends in Ecology & Evolution*, 20(10), 553-560.
- Wright, S. J. (2010) 'The future of tropical forests', *Annals of the New York Academy of Sciences*, 1195(1), 1-27.
- Yatabe, S. M. and Leckie, D. G. (1995) 'Clearcut and forest-type discrimination in satellite SAR imagery', *Canadian Journal of Remote Sensing*, 21, 455-467.
- Yueh, S. H., Kong, J. A., J.K., J., Shin, R. T. and Le Toan, T. (1992) 'Branching Model for Vegetation', *I.E.E.E. Transactions on Geoscience and Remote Sensing*, 30, 390-402.
- Zhenghou, S. and Fung, K. B. (1994) 'A Comparison of Digital Speckle Filters', *Proceedings of IGARSS*, 2129-2133.
- Zhuravleva, I., Turubanova, S., Potapov, P., Hansen, M. C., Tyukavina, A., Minnemeyer, S., Laporte, N., Goetz, S., Verbelen, F. and Thies, C. (2013) 'Satellite-based primary forest degradation assessment in the Democratic

Republic of the Congo, 2000–2010', *Environmental Research Letters*, 8(2), 024034.

Zianis, D., Muukkonen, P., Mäkipää, R. and Mencuccini, M. (2005) 'Biomass and stem volume equations for tree species in Europe', *Silva Fennica Monographs*, 4, 4-63.

Zimmermann, M. H. and Brown, C. L. (1971) *Trees: Structures and Function*, New York Springer-Verlag Berlin Heidelberg.